

**Branching of Polypropylene Through Reactive Extrusion**

**By**

**Xiao Chuan Wang**

**A thesis  
presented to the University of Waterloo  
in fulfilment of the  
thesis requirement for the degree of  
Doctor of Philosophy  
in  
Chemical Engineering**

**Waterloo, Ontario, Canada, 1996**

**© Xiao Chuan Wang, 1996**



**National Library  
of Canada**

**Acquisitions and  
Bibliographic Services**

395 Wellington Street  
Ottawa ON K1A 0N4  
Canada

**Bibliothèque nationale  
du Canada**

**Acquisitions et  
services bibliographiques**

395, rue Wellington  
Ottawa ON K1A 0N4  
Canada

*Your file Votre référence*

*Our file Notre référence*

**The author has granted a non-exclusive licence allowing the National Library of Canada to reproduce, loan, distribute or sell copies of his/her thesis by any means and in any form or format, making this thesis available to interested persons.**

**The author retains ownership of the copyright in his/her thesis. Neither the thesis nor substantial extracts from it may be printed or otherwise reproduced with the author's permission.**

**L'auteur a accordé une licence non exclusive permettant à la Bibliothèque nationale du Canada de reproduire, prêter, distribuer ou vendre des copies de sa thèse de quelque manière et sous quelque forme que ce soit pour mettre des exemplaires de cette thèse à la disposition des personnes intéressées.**

**L'auteur conserve la propriété du droit d'auteur qui protège sa thèse. Ni la thèse ni des extraits substantiels de celle-ci ne doivent être imprimés ou autrement reproduits sans son autorisation.**

0-612-21396-X

The University of Waterloo requires the signatures of all persons using or photocopying this thesis. Please sign below, and give address and date.

## ABSTRACT

Long chain branched polypropylenes (PPs) have been produced by reactive extrusion (REX) and the thermal, rheological and molecular properties of the modified PPs have been fully characterized. For the long chain branched samples, it is found that there is good agreement among the results from GPC, thermal properties, apparent elongational viscosity, flow activation energy, and linear viscoelastic properties.

The work consists of two parts: a) the reactive extrusion of an acrylic acid grafted PP with hexadecylamine, and b) the reactive extrusion of PP with a combination of Lupersol 101 and pentaerythritol triacrylate (PETA). In the first route, model branched polypropylenes were produced by the reaction of acrylic acid grafted PP with hexadecylamine in solution and REX. It was found that the attachment of the alkyl chains lowers the glass transition, melting and crystallization temperatures of PP, and increases the moduli and shear viscosity.

Two stages were involved in the REX experiments of the second route. Stage 1 involved preliminary experiments to search for the possibility of producing branches on PP and suitable concentrations of Lupersol 101 and PETA for further experiments. Based on the results of stage 1, REX experiments were carried out in the second stage, using stabilized linear PP with very low concentrations of peroxide (50 - 200 ppm) and PETA (0 - 3 wt.%). The products have very low levels of macrogels and the majority of macrogel formed during REX is PETA homopolymer. The sols of these modified PPs have higher thermal stabilities than linear PPs, indicating the coexistence of crosslinking structures. Generally, the sols from the PETA/peroxide modified PPs have higher melting and crystallization temperatures than those of linear PPs.

GPC-viscometry analysis shows that there is virtually no long chain branching in linear PPs. For the long chain branched PP produced, the average LCB frequency for the whole samples is estimated to be from 0.01 to 0.05 LCB/1000C, which corresponds to about

0.2 to 0.8 branches per weight average molecule. The change in the molecular weight averages with PETA and peroxide concentration in the PETA/peroxide reaction system seems nonmonotonic and it depends on PETA/peroxide relative concentrations. It is found that all the PETA/peroxide modified PPs have smaller  $\bar{M}_n$  and  $\bar{M}_w$  than those of virgin PP but some samples have  $\bar{M}_z$ s similar to that of the virgin PP. There is some broadening in the high molecular weight end in some long chain branched samples. Experimental results also suggest that there is a certain relationship between the inverse MFI and  $\bar{M}_w$  for linear polypropylenes. However, this does not apply for their long chain branched counterparts.

Apparent elongational viscosity and flow activation energy results seem consistent with the GPC results. Most of the PETA/peroxide modified PPs produced in the second stage have higher flow activation energies at constant shear stresses and higher elongational viscosities than linear PPs, which has been attributed to the existence of LCB.

Linear viscoelastic properties of these branched PPs produced are also in agreement with the GPC results and apparent elongational viscosity ( $\eta_0$ ). The  $\eta_0$ s of all PETA/peroxide modified PPs are considerably larger than the equivalent linear PPs at a similar  $\bar{M}_w$ , suggesting the existence of LCB in these polymers. For linear PPs, the relationship between the  $\eta_0$  and  $\bar{M}_w$  can be described by the general equation for linear polymers but this is not the case for branched PPs.

Due to the introduction of long chain branching, some of these modified PPs show larger storage moduli at low frequencies and slower relaxations than linear PPs. The increase in the long chain branches per weight average molecule seems to result in an increase in rheological polydispersity in most branched materials produced.

Three molecular-weight-independent plots, i.e., a) modified Cole-Cole plot, b) plots of loss tangent ( $\tan\delta$ ) versus complex modulus ( $G^*$ ), and c) storage compliance ( $J'$ ) versus storage modulus ( $G'$ ), have been constructed in order to detect the effects of MWD and LCB.

In the case of the a) plot, the broadening of MWD will shift the plot to higher  $G'$  at a constant  $G''$  for linear PPs. Roughly, for branched PPs, the increasing extent of LCB will shift the plot to higher  $G'$  storage modulus at a constant  $G''$ . The b) and c) plots seem to have a better discrimination sensitivity than the a) plot. In the case of b) plot, for linear PPs, the broadening of MWD shifts the curve to lower values of  $\tan\delta$  at constant values of  $G^*$ . For branched PPs, the increase of branching will shift the curve to lower values of  $\tan\delta$  at constant values of  $G^*$ . The c) plot has very similar characteristics to the b) plot. For these three representations, however, lower angular frequency data should be considered for better discrimination sensitivity to the differences among branched PPs.

## **ACKNOWLEDGEMENTS**

I would like to express my deepest appreciation to my supervisors Professor C. Tzoganakis and Professor G. L. Rempel for their guidance, interest and financial support during the course of my research work.

The financial support of Ontario Centre for Materials Research (OCMR) and Natural Sciences and Engineering Research Council of Canada (NSERC) is gratefully acknowledged.

I wish to express my sincere thanks to Mr. Frank Wassmer for his help in twin-screw extruder, and Mr. M. Thompson and J. D. Kim for their training in the operation of GPC and helpful discussions.

Special thanks to my wife Ting Juan for her patience, encouragement and unquestioned support during the years of this work, to my daughters Jia Ning and Jia Yuan for their love, and to my parents for their constant support. To them I dedicate this thesis.

To Ting Juan, my wife  
To Jia Ning and Jia Yuan, my daughters



## TABLE OF CONTENTS

	Page
<b>Abstract</b> .....	iv
<b>Acknowledgements</b> .....	vii
<b>List of Tables</b> .....	xiii
<b>List of Figures</b> .....	xv
<b>Nomenclature</b> .....	xxix
<b>CHAPTER 1 INTRODUCTION AND OBJECTIVES</b>	
1.1 Introduction .....	1
1.2 Objectives and Scope of the Thesis .....	2
1.3 Outline of Thesis .....	3
<b>CHAPTER 2 LITERATURE SURVEY</b>	
2.1 Reactive Extrusion (REX) .....	5
2.2 Effect of Branching on Polymer Properties .....	16
2.2.1 Introduction .....	16
2.2.2 Effect of Branching on Polymer Properties .....	17
2.3 Crosslinking and Branching of Polypropylene .....	25
2.3.1 Irradiation Method .....	25
2.3.2 Chemical Method .....	26
<b>CHAPTER 3 REACTIVE EXTRUSION OF ACRYLIC ACID GRAFTED POLYPROPYLENE WITH HEXADECYLAMINE</b>	
3.1 Introduction .....	30
3.2 Experimental .....	31
3.2.1 Materials .....	31
3.2.2 Solution Experiments .....	31
3.2.3 Reactive Extrusion Experiments .....	32
3.2.4 Characterization .....	32

3.3	Results and Discussion .....	35
3.3.1	Solution Reaction .....	35
3.3.2	Reactive Extrusion .....	40
3.4	Conclusions .....	51

## **CHAPTER 4 CHEMICAL MODIFICATION OF PP WITH PEROXIDE/PETA THROUGH REACTIVE EXTRUSION**

4.1	Introduction .....	53
4.2	Postulated Reaction Scheme .....	55
4.3	Experimental .....	57
4.3.1	Materials .....	57
4.3.2	Reactive Extrusion .....	59
4.3.3	Methods .....	60
4.4	Results and Discussion .....	63
4.4.1	Reactive Extrusion of Stage 1 .....	63
4.4.1.1	Flow Curve .....	63
4.4.1.2	Melt Flow Index (MFI) .....	67
4.4.1.3	Gel Content .....	67
4.4.1.4	FTIR Analysis of the Sols .....	69
4.4.1.5	DSC Analysis of the Sols .....	72
4.4.1.6	Conclusions .....	81
4.4.2	Reactive Extrusion of Stage 2 .....	82
4.4.2.1	Background .....	82
4.4.2.2	Effect of the Stabilizer (Irganox 1010) .....	82
4.4.2.3	Analysis of Macrogels .....	87
4.4.2.4	FTIR Spectra of the Sols .....	92
4.4.2.5	Shear Viscosity and Melt Flow Index .....	95
4.4.2.6	A Comparison of Stage 1 and Stage 2 Results ..	101
4.4.2.7	Conclusions .....	104

## **CHAPTER 5 CHARACTERIZATION OF LONG CHAIN BRANCHING (LCB) BY GEL PERMEATION CHROMATOGRAPHY (GPC)**

5.1	Introduction .....	105
5.2	Theoretical Background .....	106
5.3	GPC Operating Principles .....	110
5.3.1	Determination of Intrinsic Viscosity (IV) .....	110
5.3.2	Absolute Molecular Weight Average Determination ..	112
5.4	Experimental .....	112
5.5	Results and Discussion .....	113

5.5.1	Montell Branched PP, Virgin PP and Degraded PPs . . .	113
5.5.2	PETA/Peroxide Modified PPs . . . . .	125
5.5.3	Average $\eta_w$ and $\lambda$ for the Whole Polymers . . . . .	167
5.5.4	The Equal Hydrodynamic Volume Concept . . . . .	169
5.5.5	Relationship between MFI and $M_w$ . . . . .	169
5.6	Concluding Remarks . . . . .	174

## CHAPTER 6 EVALUATIONS OF APPARENT ELONGATIONAL VISCOSITY AND VISCOUS FLOW ACTIVATION ENERGY

6.1	Apparent Elongational Viscosity of the Whole Polymers . . . . .	178
6.1.1	Introduction . . . . .	178
6.1.2	Experimental . . . . .	181
6.1.3	Results and Discussion . . . . .	182
6.2	Viscous Flow Activation Energy . . . . .	208
6.2.1	Introduction . . . . .	208
6.2.2	Experimental . . . . .	211
6.2.3	Results and Discussion . . . . .	212
6.3	Conclusions . . . . .	220

## CHAPTER 7 THERMAL PROPERTIES OF THE SOLS

7.1	Simultaneous Thermogravimetric Analysis (TGA) and Differential Thermal Analysis (DTA) . . . . .	221
7.1.1	Introduction . . . . .	221
7.1.2	Experimental . . . . .	222
7.1.3	Results and Discussion . . . . .	222
7.2	Differential Scanning Calorimetry (DSC) . . . . .	233
7.2.1	Experimental . . . . .	233
7.2.2	Results and Discussion . . . . .	234
7.3	Concluding Remarks . . . . .	250

## CHAPTER 8 LINEAR VISCOELASTIC PROPERTIES

8.1	Introduction . . . . .	251
8.2	Experiments . . . . .	254
8.3	Results and Discussion . . . . .	255
8.3.1	Complex Viscosity ( $\eta^*$ ) and the Relationship Between $\eta_0$ and $M_w$ . . . . .	255
8.3.2	Storage Modulus ( $G'$ ), Loss Modulus ( $G''$ ) and	

	Various Correlations .....	265
8.3.3	Modified Cole-Cole Plot .....	285
8.3.4	Loss Tangent Versus Frequency ( $\tan\delta - \omega$ ) and Loss Tangent Versus Complex Modulus ( $\tan\delta - G^*$ ) ..	295
8.3.5	Dynamic Storage Compliance versus Storage Modulus ( $J' - G'$ ) .....	301
8.4	Conclusions .....	312
 <b>CHAPTER 9 CONCLUSIONS AND RECOMMENDATIONS .....</b>		<b>314</b>
 <b>APPENDIX A</b>		
	Chemical Structures of Lupersol 101, Pentaerythritol Triacrylate and Irganox 1010 .....	318
 <b>APPENDIX B</b>		
	Molecular Weight Averages and Mark-Houwink Constants ( $K$ and $\alpha$ ) Measured by GPC for Virgin PP and Peroxide-degraded PPs .....	319
 <b>REFERENCES .....</b>		<b>321</b>

## LIST OF TABLES

Table		Page
3.1	<b>T<sub>g</sub> of the REX Products Produced at 200°C.</b>	45
3.2	<b>Estimates of Carreau Model Parameters.</b>	47
3.3	<b>DSC Analysis of the Model Branched PPs.</b>	51
4.1	<b>Results of Gel Content Measurements.</b>	67
4.2	<b>Effects of PETA and Peroxide Concentrations on the Thermal Behaviour of the Sols.</b>	77
4.3	<b>Description of the Modified Polypropylenes.</b>	83
4.4	<b>Results of Gel Content Measurements.</b>	87
4.5	<b>DSC Analyses of the Macrogels of the Modified PPs.</b>	88
4.6	<b>Relative Intensity of A<sub>1740</sub>/A<sub>841</sub> of the Sols.</b>	95
4.7	<b>Comparison of Melt Flow Index for the Materials from Stage 1 and Stage 2 (200 ppm L101 Series).</b>	103
4.8	<b>FTIR Relative Intensity Comparison of Materials from Stage 1 and Stage 2 (200 ppm L101 series).</b>	103
5.1	<b>Molecular Parameters of the Montell PP and Peroxide-Degraded PPs.</b>	114
5.2	<b>Molecular Parameters of the Samples in the 50 ppm Peroxide Series.</b>	125
5.3	<b>Molecular Parameters of the Samples in 100 ppm Peroxide Series.</b>	142
5.4	<b>Molecular Parameters of the Samples in 150 ppm Peroxide Series.</b>	145
5.5	<b>Molecular Parameters of the Samples in 200 ppm Peroxide Series.</b>	152
5.6	<b>Average LCB Frequency <math>\lambda</math> (LCB/1000C) and Mean Number of Branches Per Weight Average Molecule (<math>n_w</math>) for the Whole Samples.</b>	168
6.1	<b>Summary of Molecular Parameters of the Samples.</b>	183

6.2	Flow Activation Energy at a Constant Apparent Shear Rate ( $50 \text{ s}^{-1}$ ).	213
6.3	Flow Activation Energy at Constant Apparent Shear Stresses.	218
7.1	Decomposition Temperatures of the Modified PPs.	223
7.2	DSC Results For the Sols of the Modified PPs.	245
8.1	$\eta_0$ Estimated by Ellis Model.	262
8.2	$\eta_0$ Estimated by Bueche Model.	262
8.3	Slopes of $G'$ of Modified PPs at Low Frequencies.	278
8.4	Slopes of $G''$ of Modified PPs at Low Frequencies.	278
8.5	Relaxation Time Constant ( $\Lambda$ ) of Polypropylenes.	280
8.6	Cross-over Frequency ( $\omega_c$ ) of Modified PPs (rad/s).	280
8.7	Cross-over Modulus ( $G_c$ ) of Modified PPs.	281
8.8	Polydispersity Index (PI) of Modified PPs.	281
8.9	Polydispersity Measures of Modified PPs.	283

## LIST OF FIGURES

Figure		Page
Fig. 3-1	Screw configuration of the corotating intermeshing twin screw extruder.	33
Fig. 3-2	Extruder line used for the reaction of Polybond-1002 and hexadecylamine.	34
Fig. 3-3a	FTIR spectra from 600 to 2000 $\text{cm}^{-1}$ of the virgin material and products reacted for different times in refluxing xylene. A: Polybond-1002; B: Polybond-1002 heated in xylene for 12 hours; C: 2 hours reaction time; D: 4 hours reaction time; E: 8 hours reaction time; F: 10 hours reaction time; G: 12 hours reaction time.	38
Fig. 3-3b	FTIR spectra from 1500 to 2000 $\text{cm}^{-1}$ of the virgin material and products reacted for different times in refluxing xylene. A: Polybond-1002; B: Polybond-1002 heated in xylene for 12 hours; C: 2 hours reaction time; D: 4 hours reaction time; E: 8 hours reaction time; F: 10 hours reaction time; G: 12 hours reaction time.	39
Fig. 3-4a	FTIR spectra from 600 to 2000 $\text{cm}^{-1}$ of the REX products reacted at different molar ratios of $[-\text{NH}_2]/[-\text{COOH}]$ . H: Polybond-1002 extruded at 200 $^{\circ}$ C; I: product at molar ratio of 0.3; J: product at molar ratio of 0.5; K: product at molar ratio of 1.	41
Fig. 3-4b	FTIR spectra from 1500 to 2000 $\text{cm}^{-1}$ of the REX products reacted at different molar ratios of $[-\text{NH}_2]/[-\text{COOH}]$ . H: Polybond-1002 extruded at 200 $^{\circ}$ C; I: product at molar ratio of 0.3; J: product at molar ratio of 0.5; K: product at molar ratio of 1.	42
Fig. 3-5	Nitrogen content elemental analysis results of the reactive extrusion products.	44
Fig. 3-6	Shear viscosities of Polybond-1002 and the REX products at 200 $^{\circ}$ C.	46
Fig. 3-7	Frequency dependence of storage and loss moduli of Polybond-1002 and the reactive extrusion product at a $[-\text{NH}_2]/[-\text{COOH}]$ molar ratio of 1.7 (200 $^{\circ}$ C).	48

Fig. 3-8	DSC melting endotherms of the virgin Polybond-1002 and reactive extrusion products at different [-NH <sub>2</sub> ]/[-COOH] molar ratios. 1: virgin Polybond; 2: extruded Polybond; 3: product at the ratio of 0.3; 4: product at the ratio of 0.5; 5: product at the ratio of 1.0; 6: product at the ratio of 1.7.	49
Fig. 3-9	DSC crystallization exotherms of the virgin Polybond-1002 and reactive extrusion products at different [-NH <sub>2</sub> ]/[-COOH] molar ratios. 1: virgin Polybond; 2: extruded Polybond; 3: product at the ratio of 0.3; 4: product at the ratio of 0.5; 5: product at the ratio of 1.0; 6: product at the ratio of 1.7.	50
Fig. 4-1	Possible reactions between PP, PETA and peroxide.	56
Fig. 4-2	Possible Molecular Structures of the Products. A: Linear, B: Branched, C: Branched-Crosslinked (Loose Network), D: Tight Network.	58
Fig. 4-3	Extruder line used for the PETA/peroxide modification of polypropylene by REX (Stage 1).	61
Fig. 4-4	Extruder line used for the PETA/peroxide modification of polypropylene by REX (Stage 2).	61
Fig. 4-5a	Effect of PETA and peroxide concentration on the shear viscosity of the whole polymers (200 ppm peroxide series).	64
Fig. 4-5b	Effect of PETA and peroxide concentration on the shear viscosity of the whole polymers (600 ppm peroxide series).	65
Fig. 4-5c	Effect of PETA and peroxide concentration on the shear viscosity of the whole polymers (1000 ppm peroxide series).	66
Fig. 4-6	Effect of PETA and peroxide concentration on the melt flow index (MFI) of the whole polymers. The MFI is expressed as the mean plus/minus one standard deviation.	68
Fig. 4-7	FT-IR spectra (600-2000 cm <sup>-1</sup> ) of the sols at different PETA concentrations (200 ppm peroxide series). 1: 0.00 wt.% PETA, 2: 0.64 wt.% PETA, 3: 1.80 wt.% PETA, 4: 2.80 wt.% PETA, 5: 5.00 wt.% PETA.	70
Fig. 4-8	Effect of the PETA concentration on the relative intensity of	



	the bands at 1740 cm <sup>-1</sup> and 841 cm <sup>-1</sup> in the FTIR spectra of the sols. The relative intensity of A <sub>1740</sub> /A <sub>841</sub> is expressed as the mean plus/minus one standard deviation.	71
Fig. 4-9	Effect of the PETA concentration on the DSC melting endotherms of the sols at 200 ppm peroxide level. 1: virgin PP, 2: 0.00 wt.% PETA, 3: 0.64 wt.% PETA, 4: 1.80 wt.% PETA, 5: 2.80 wt.% PETA, 6: 5.00 wt.% PETA.	74
Fig. 4-10	Effect of the PETA concentration on the DSC melting endotherms of the sols at 600 ppm peroxide level. 1: 0.00 wt.% PETA, 2: 0.64 wt.% PETA, 3: 1.80 wt.% PETA, 4: 2.80 wt.% PETA, 5: 5.00 wt.% PETA.	75
Fig. 4-11	Effect of the PETA concentration on the DSC melting endotherms of the sols at 1000 ppm peroxide level. 1: 0.00 wt.% PETA, 2: 0.64 wt.% PETA, 3: 1.80 wt.% PETA, 4: 2.80 wt.% PETA, 5: 5.00 wt.% PETA.	76
Fig. 4-12	Effect of the PETA and peroxide concentration on the crystallization temperature (T <sub>c</sub> ) of the sols.	80
Fig. 4-13	Effect of stabilizer concentration on the MFI of virgin PP. The MFI is expressed as the mean plus/minus one standard deviation.	84
Fig. 4-14	Effect of the extrusion temperature on the shear viscosity of unstabilized PP.	85
Fig. 4-15	Effect of the extrusion temperature on the shear viscosity (at 230°C) of stabilized PP with 1.0 wt.% of Irganox 1010.	86
Fig. 4-16	DSC melting endotherm of the virgin PP having same thermal history as the macrogels.	89
Fig. 4-17	DSC melting endotherms of the PETA homopolymer and the macrogels in the polypropylenes produced at 50 and 100 ppm L101 levels.	90
Fig. 4-18	DSC melting endotherms of the macrogels in the polypropylenes produced at 150 and 200 ppm L101 levels.	91
Fig. 4-19	FTIR spectra (700-2000 cm <sup>-1</sup> ) of the sols at different PETA concentrations (50 ppm peroxide series). 1: 0.5 wt.% PETA,	

	2: 1.0 wt.% PETA, 3: 2.0 wt.% PETA, 4: 3.0 wt.% PETA.	93
Fig. 4-20	FTIR spectra (700-2000 $\text{cm}^{-1}$ ) of the sols at different PETA concentrations (200 ppm peroxide series). 1: 0.5 wt.% PETA, 2: 1.0 wt.% PETA, 3: 2.0 wt.% PETA, 4: 3.0 wt.% PETA.	94
Fig. 4-21	Effect of the peroxide concentrations on the shear viscosities of the degraded polypropylenes.	96
Fig. 4-22	Effect of the PETA and peroxide concentrations on the shear viscosities of the whole polymers (50 ppm peroxide series).	97
Fig. 4-23	Effect of the PETA and peroxide concentrations on the shear viscosities of the whole polymers (100 ppm peroxide series).	98
Fig. 4-24	Effect of the PETA and peroxide concentrations on the shear viscosities of the whole polymers (150 ppm peroxide series).	99
Fig. 4-25	Effect of the PETA and peroxide concentrations on the shear viscosities of the whole polymers (200 ppm peroxide series).	100
Fig. 4-26	Effect of the PETA and peroxide concentrations on the melt flow index of the whole polymers. The MFI is expressed as the mean plus/minus one standard deviation.	102
Fig. 5-1	Effect of peroxide concentration on the molecular weight distribution of PP.	115
Fig. 5-2	Molecular weight distribution curves of the repeated samples of virgin PP.	116
Fig. 5-3	Molecular weight distribution curves of the repeated samples of 100PP.	117
Fig. 5-4	Molecular weight distribution curves of the repeated samples of Montell PP.	119
Fig. 5-5	Viscosity law plots of the repeated samples of virgin PP.	120
Fig. 5-6	Viscosity law plots of the repeated samples of 100PP.	121
Fig. 5-7	Viscosity law plots of the repeated samples of Montell PP.	122

Fig. 5-8	Viscosity law plots of the virgin PP, peroxide degraded PPs and Montell PP.	123
Fig. 5-9	$g'$ distributions across the whole molecular weight of virgin PP, peroxide degraded PPs and Montell PP.	124
Fig. 5-10	Long chain branching frequency per 1000 C ( $\lambda$ ) of Montell PP.	126
Fig. 5-11a	Long chain branching frequency per 1000 C ( $\lambda$ ) of virgin PP.	127
Fig. 5-11b	Long chain branching frequency per 1000 C ( $\lambda$ ) of 50PP.	128
Fig. 5-11c	Long chain branching frequency per 1000 C ( $\lambda$ ) of 100PP.	129
Fig. 5-11d	Long chain branching frequency per 1000 C ( $\lambda$ ) of 150PP.	130
Fig. 5-11e	Long chain branching frequency per 1000 C ( $\lambda$ ) of 200PP.	131
Fig. 5-11f	Long chain branching frequency per 1000 C ( $\lambda$ ) of 400PP.	132
Fig. 5-11g	Long chain branching frequency per 1000 C ( $\lambda$ ) of 600PP.	133
Fig. 5-12	Effect of the PETA and peroxide concentration on the molecular weight distribution of the modified PP (50 ppm peroxide series).	135
Fig. 5-13	Viscosity law plots of virgin PP and samples in the 50 ppm peroxide series.	136
Fig. 5-14	$g'$ distributions across the whole molecular weight of virgin PP, 50PP and samples in 50 ppm peroxide series.	137
Fig. 5-15a	Long chain branching frequency per 1000 C ( $\lambda$ ) of the SPT505 sample.	138
Fig. 5-15b	Long chain branching frequency per 1000 C ( $\lambda$ ) of the SPT510 sample.	139
Fig. 5-15c	Long chain branching frequency per 1000 C ( $\lambda$ ) of the SPT520 sample.	140
Fig. 5-15d	Long chain branching frequency per 1000 C ( $\lambda$ ) of the SPT530 sample.	141

Fig. 5-16	Effect of the PETA and peroxide concentration on the molecular weight distribution of the modified PP (100 ppm peroxide series).	144
Fig. 5-17	Viscosity law plots of virgin PP and samples in 100 ppm peroxide series.	146
Fig. 5-18	g' distributions across the whole molecular weight of virgin PP, 100PP and samples in 100 ppm peroxide series.	147
Fig. 5-19a	Long chain branching frequency per 1000 C ( $\lambda$ ) of the SPT1005 sample.	148
Fig. 5-19b	Long chain branching frequency per 1000 C ( $\lambda$ ) of the SPT1010 sample.	149
Fig. 5-19c	Long chain branching frequency per 1000 C ( $\lambda$ ) of the SPT1020 sample.	150
Fig. 5-19d	Long chain branching frequency per 1000 C ( $\lambda$ ) of the SPT1030 sample.	151
Fig. 5-20	Effect of the PETA and peroxide concentrations on the molecular weight distribution of the modified PP (150 ppm peroxide series).	153
Fig. 5-21	Viscosity law plots of virgin PP and samples in 150 ppm peroxide series.	154
Fig. 5-22	g' distributions across the whole molecular weight of virgin PP, 150PP and some samples in 150 ppm peroxide series.	155
Fig. 5-23a	Long chain branching frequency per 1000 C ( $\lambda$ ) of the SPT1505 sample.	156
Fig. 5-23b	Long chain branching frequency per 1000 C ( $\lambda$ ) of the SPT1510 sample.	157
Fig. 5-23c	Long chain branching frequency per 1000 C ( $\lambda$ ) of the SPT1530 sample.	158
Fig. 5-24	Effect of the PETA and peroxide concentrations on the molecular weight distribution of the modified PP (200 ppm peroxide series).	159
Fig. 5-25	Viscosity law plots of virgin PP and samples in 200 ppm	

	<b>peroxide series.</b>	160
Fig. 5-26	<b>g' distributions across the whole molecular weight of virgin PP, 200PP and samples in 200 ppm peroxide series.</b>	161
Fig. 5-27a	<b>Long chain branching frequency per 1000 C (<math>\lambda</math>) of the SPT2005 sample.</b>	162
Fig. 5-27b	<b>Long chain branching frequency per 1000 C (<math>\lambda</math>) of the SPT2010 sample.</b>	163
Fig. 5-27c	<b>Long chain branching frequency per 1000 C (<math>\lambda</math>) of the SPT2020 sample.</b>	164
Fig. 5-27d	<b>Long chain branching frequency per 1000 C (<math>\lambda</math>) of the SPT2030 sample.</b>	165
Fig. 5-28	<b>Summary of the viscosity law plots of the samples of virgin PP, SPT510, SPT1005, SPT1030 and Montell PP.</b>	170
Fig. 5-29	<b>Plot of logarithmic intrinsic viscosity versus elution volume for the samples of virgin PP, SPT510, SPT1005, SPT1030 and Montell PP.</b>	171
Fig. 5-30	<b>Plot of logarithmic molecular weight versus elution volume for the samples of virgin PP, SPT510, SPT1005, SPT1030 and Montell PP.</b>	172
Fig. 5-31	<b>Plot of logarithmic hydrodynamic volume versus elution volume for the samples of virgin PP, SPT510, SPT1005, SPT1030 and Montell PP.</b>	173
Fig. 5-32	<b>Plot of the reciprocal of melt flow index (MFI) versus weight average molecular weight of linear and branched PPs produced by reactive extrusion.</b>	175
Fig. 5-33	<b>Plot of the reciprocal of melt flow index (MFI) versus weight average molecular weight of linear and branched PPs (data published by Montell).</b>	176
Fig. 6-1	<b>Bagley plot of virgin PP.</b>	184
Fig. 6-2	<b>Bagley plot of 50PP (produced with 50 ppm L101).</b>	185

Fig. 6-3	Bagley plot of SPT510 (produced with 50 ppm L101 and 1.0 wt.% PETA).	186
Fig. 6-4	Bagley plot of SPT530 (produced with 50 ppm L101 and 3.0 wt.% PETA).	187
Fig. 6-5	Bagley plot of 100PP (degraded with 100 ppm L101).	188
Fig. 6-6	Bagley plot of SPT1005 (produced with 100 ppm L101 and 0.5 wt.% PETA).	189
Fig. 6-7	Bagley plot of SPT1010 (produced with 100 ppm L101 and 1.0 wt.% PETA).	190
Fig. 6-8	Bagley plot of SPT1020 (produced with 100 ppm L101 and 2.0 wt.% PETA).	191
Fig. 6-9	Bagley plot of SPT1030 (produced with 100 ppm L101 and 3.0 wt.% PETA).	192
Fig. 6-10	Bagley plot of Montell branched PP.	193
Fig. 6-11	Bagley correction coefficient of virgin PP and Degraded PPs.	194
Fig. 6-12	Bagley correction coefficient of virgin PP, Montell PP and the samples in the 50 ppm peroxide series.	195
Fig. 6-13	Bagley correction coefficient of the samples in the 100 ppm peroxide series.	196
Fig. 6-14	Bagley correction coefficient of the samples in the 150 ppm peroxide series.	197
Fig. 6-15	Bagley correction coefficient of the samples in the 200 ppm peroxide series.	198
Fig. 6-16	Apparent elongational viscosity of virgin PP and a series of degraded PPs.	200
Fig. 6-17	Apparent elongational viscosity of Montell PP.	201
Fig. 6-18	Apparent elongational viscosity of the samples in 50 ppm peroxide series.	202

Fig. 6-19	Apparent elongational viscosity of the samples in 100 ppm peroxide series.	203
Fig. 6-20	Apparent elongational viscosity of the samples in 150 ppm peroxide series.	204
Fig. 6-21	Apparent elongational viscosity of the samples in 200 ppm peroxide series.	205
Fig. 6-22	Relationship between the $\eta$ and $1/T$ of virgin PP at different shear stresses.	214
Fig. 6-23	Relationship between the $\eta$ and $1/T$ of Montell PP at different shear stresses.	215
Fig. 6-24	Relationship between the $\eta$ and $1/T$ of SPT510 at different shear stresses.	216
Fig. 6-25	Relationship between the $\eta$ and $1/T$ of SPT530 at different shear stresses.	217
Fig. 6-26	Relationship between the $E_c$ (at 40 KPa) and the long chain branches per weight average molecule.	219
Fig. 7-1	Thermogravimetric analyses of virgin PP, peroxide-degraded PPs and Montell Branched PP.	225
Fig. 7-2	Thermogravimetric analyses of the sols from PETA/peroxide modified PPs (50 ppm L101 series).	226
Fig. 7-3	Thermogravimetric analyses of the sols from PETA/peroxide modified PPs (100 ppm L101 series).	227
Fig. 7-4	Thermogravimetric analyses of the sols from PETA/peroxide modified PPs (150 ppm L101 series).	228
Fig. 7-5	Thermogravimetric analyses of the sols from PETA/peroxide modified PPs (200 ppm L101 series).	229
Fig. 7-6	Plot of the decomposition temperature ( $T_d$ ) from TGA versus LCB per weight average molecule for PETA/peroxide modified PPs.	231
Fig. 7-7	Plot of the decomposition temperature ( $T_d$ ) from DTA versus LCB	

	per weight average molecule for PETA/peroxide modified PPs.	232
Fig. 7-8	Melting endotherms of linear PPs and Montell branched PP.	235
Fig. 7-9	Crystallization exotherms of linear PPs and Montell branched PP.	236
Fig. 7-10	Melting endotherms of the sols of PETA/peroxide modified PPs (50 ppm L101 series).	237
Fig. 7-11	Crystallization exotherms of the sols of PETA/peroxide modified PPs (50 ppm L101 series).	238
Fig. 7-12	Melting endotherms of the sols of PETA/peroxide modified PPs (100 ppm L101 series).	239
Fig. 7-13	Crystallization exotherms of the sols of PETA/peroxide modified PPs (100 ppm L101 series).	240
Fig. 7-14	Melting endotherms of the sols of PETA/peroxide modified PPs (150 ppm L101 series).	241
Fig. 7-15	Crystallization exotherms of the sols of PETA/peroxide modified PPs (150 ppm L101 series).	242
Fig. 7-16	Melting endotherms of the sols of PETA/peroxide modified PPs (200 ppm L101 series).	243
Fig. 7-17	Crystallization exotherms of the sols of PETA/peroxide modified PPs (200 ppm L101 series).	244
Fig. 7-18	Plot of the melting temperature ( $T_m$ ) versus LCB per weight average molecule for the PETA/peroxide modified PPs.	247
Fig. 7-19	Plot of the crystallization temperature ( $T_c$ ) versus LCB per weight average molecule for the PETA/peroxide modified PPs.	248
Fig. 7-20	Plot of the degree of undercooling ( $T_m - T_c$ ) versus LCB per weight average molecule for the PETA/peroxide modified PPs.	249
Fig. 8-1	Complex viscosities of virgin PP, peroxide-degraded PPs and Montell PP.	256
Fig. 8-2	Effects of the PETA and peroxide concentrations on the complex	



	viscosities of the products (50 ppm L101 series).	257
Fig. 8-3	Effects of the PETA and peroxide concentrations on the complex viscosities of the products (100 ppm L101 series).	258
Fig. 8-4	Effects of the PETA and peroxide concentrations on the complex viscosities of the products (150 ppm L101 series).	259
Fig. 8-5	Effects of the PETA and peroxide concentrations on the complex viscosities of the products (200 ppm L101 series).	260
Fig. 8-6	The relationship between the $\eta_0$ (estimated by Ellis model) and $\bar{M}_w$ of virgin PP, peroxide degraded PPs, Montell PP and PETA/peroxide modified PPs (solid line: the regression line for linear PPs; dash lines: the regression interval at a 95% confidence level).	263
Fig. 8-7	The relationship between the $\eta_0$ (estimated by Bueche model) and $\bar{M}_w$ of virgin PP, peroxide degraded PPs, Montell PP and PETA/peroxide modified PPs (solid line: the regression line for linear PPs; dash lines: the regression interval at a 95% confidence level).	264
Fig. 8-8	Storage moduli of virgin PP, peroxide degraded PPs and Montell PP.	266
Fig. 8-9	Loss moduli of virgin PP, peroxide degraded PPs and Montell PP.	267
Fig. 8-10	Effects of the PETA and peroxide concentrations on the storage moduli of the products (50 ppm L101 series).	269
Fig. 8-11	Effects of the PETA and peroxide concentrations on the loss moduli of the products (50 ppm L101 series).	270
Fig. 8-12	Effects of the PETA and peroxide concentrations on the storage moduli of the products (100 ppm L101 series).	271
Fig. 8-13	Effects of the PETA and peroxide concentrations on the loss moduli of the products (100 ppm L101 series).	272
Fig. 8-14	Effects of the PETA and peroxide concentrations on the storage moduli of the products (150 ppm L101 series).	273
Fig. 8-15	Effects of the PETA and peroxide concentrations on the loss moduli of the products (150 ppm L101 series).	274

Fig. 8-16	Effects of the PETA and peroxide concentrations on the storage moduli of the products (200 ppm L101 series).	275
Fig. 8-17	Effects of the PETA and peroxide concentrations on the loss moduli of the products (200 ppm L101 series).	276
Fig. 8-18	Correlation between the crossover frequency $\omega_c$ and weight average molecular weight ( $\bar{M}_w$ ) for virgin PP, peroxide degraded PPs, Montell PP and PETA/peroxide modified PPs (solid line: the regression line for linear PPs; dashed lines: the regression interval at a 95% confidence level).	282
Fig. 8-19	Correlation between the rheological PI and polydispersity by GPC for virgin PP, peroxide degraded PPs, Montell PP and PETA/peroxide modified PPs.	284
Fig. 8-20	Correlation between the rheological PI and LCB per weight average molecule for PETA/peroxide modified PPs.	286
Fig. 8-21	Correlation between the Modsep at 1000 Pa and polydispersity by GPC for linear PP.	287
Fig. 8-22	Correlation between the Modsep at 1000 Pa and rheological PI for linear PP.	288
Fig. 8-23	Modified Cole-Cole plots of virgin, peroxide degraded and Montell PP	289
Fig. 8-24	Modified Cole-Cole plots of the PETA/peroxide modified PPs (50 ppm L101 series).	290
Fig. 8-25	Modified Cole-Cole plots of the PETA/peroxide modified PPs (100 ppm L101 series).	291
Fig. 8-26	Modified Cole-Cole plots of the PETA/peroxide modified PPs (150 ppm L101 series).	292
Fig. 8-27	Modified Cole-Cole plots of the PETA/peroxide modified PPs (200 ppm L101 series).	293
Fig. 8-28	The representations of loss tangent versus frequency ( $\tan\delta-\omega$ ) for virgin PP, peroxide degraded PPs and Montell PP.	296

Fig. 8-29	The representations of loss tangent versus frequency ( $\tan\delta-\omega$ ) for the PETA/peroxide modified PPs (50 ppm L101 series).	297
Fig. 8-30	The representations of loss tangent versus frequency ( $\tan\delta-\omega$ ) for the PETA/peroxide modified PPs (100 ppm L101 series).	298
Fig. 8-31	The representations of loss tangent versus frequency ( $\tan\delta-\omega$ ) for the PETA/peroxide modified PPs (150 ppm L101 series).	299
Fig. 8-32	The representations of loss tangent versus frequency ( $\tan\delta-\omega$ ) for the PETA/peroxide modified PPs (200 ppm L101 series).	300
Fig. 8-33	The representations of loss tangent versus complex modulus ( $\tan\delta-G^*$ ) for virgin PP, peroxide degraded PPs and Montell PP.	302
Fig. 8-34	The representations of loss tangent versus complex modulus ( $\tan\delta-G^*$ ) for the PETA/peroxide modified PPs (50 ppm L101 series).	303
Fig. 8-35	The representations of loss tangent versus complex modulus ( $\tan\delta-G^*$ ) for the PETA/peroxide modified PPs (100 ppm L101 series).	304
Fig. 8-36	The representations of loss tangent versus complex modulus ( $\tan\delta-G^*$ ) for the PETA/peroxide modified PPs (150 ppm L101 series).	305
Fig. 8-37	The representations of loss tangent versus complex modulus ( $\tan\delta-G^*$ ) for the PETA/peroxide modified PPs (200 ppm L101 series).	306
Fig. 8-38	The representations of storage compliance versus storage modulus ( $J'-G'$ ) for virgin PP, peroxide degraded PPs and Montell PP.	307
Fig. 8-39	The representations of storage compliance versus storage modulus ( $J'-G'$ ) for the PETA/peroxide modified PPs (50 ppm L101 series).	308
Fig. 8-40	The representations of storage compliance versus storage modulus ( $J'-G'$ ) for the PETA/peroxide modified PPs (100 ppm L101 series).	309
Fig. 8-41	The representations of storage compliance versus storage modulus ( $J'-G'$ ) for the PETA/peroxide modified PPs (150 ppm L101 series).	310

**Fig. 8-42**      **The representations of storage compliance versus storage modulus (J'-G')** for the PETA/peroxide modified PPs (200 ppm L101 series).      311

## NOMENCLATURE

$C_i$	polymer concentration of slice i
$C$	total concentration of the sample
$E_a$	zero-shear flow activation energy, Kcal/mol
$E_{\dot{\gamma}}$	flow activation energy at constant shear rate, Kcal/mol
$E_{\tau}$	flow activation energy at constant shear stress, Kcal/mol
$G'$	storage modulus, Pa
$G''$	loss modulus, Pa
$G_c$	cross-over modulus, Pa
$G^*$	Complex Modulus, Pa
$g'$	branching index (ratio of $[\eta]_b$ over $[\eta]_l$ ), dimensionless
$g$	the ratio of the mean square radius of gyration $\langle R_G^2 \rangle$ for the branched and linear polymers with molecular weights $M_l = M_b$ , dimensionless
IV	intrinsic viscosity, dl/g
$J'$	Dynamic Storage Compliance, Pa <sup>-1</sup>
K	Mark-Houwink constant
k	constant in Zimm-Stockmayer equation, dimensionless
L101	2,5-dimethyl-2,5(t-butylperoxy) hexane
LCB	long chain branching (branches)
MWD	molecular weight distribution, dimensionless
MW	molecular weight, g/mol
$\bar{M}_n$	number average molecular weight, g/mol
$\bar{M}_w$	weight average molecular weight, g/mol
$\bar{M}_z$	z average molecular weight, g/mol
$M_l$	molecular weight of linear species, g/mol
$M_b$	molecular weight of branched species, g/mol
$M_v$	viscosity-average molecular weight, g/mol
MFI	Melt flow index, g/10 min.
n	power-law index, dimensionless
$n_b$	Bagley correction coefficient, dimensionless
$n_w$	weight average long chain branches per molecule
PI	rheological polydispersity, dimensionless
PETA	pentaerythritol triacrylate
REX	reactive extrusion
$\langle R_G^2 \rangle$	the mean square radius of gyration, m <sup>2</sup>
SCB	short chain branching (branches)
$\tan \delta$	loss tangent, dimensionless
$T_g$	glass transition temperature, °C
$T_m$	the melting temperature, °C
$T_c$	crystallization temperature, °C
$T_d$	decomposition temperature, °C
$t_{1/2}$	half-life time, s

## Greek letters

$\alpha$	Mark-Houwink constant
$\dot{\epsilon}$	the apparent elongational rate, $s^{-1}$
$\dot{\gamma}_A$	apparent shear rate, $s^{-1}$
$\eta$	viscosity of sample solution (in chapter 5), g/dl
$\eta$	viscosity of a suspension (in chapter 6), Pa.s
$\eta_s$	viscosity of the polymer (in chapter 6), Pa.s
$\eta_e$	apparent elongational viscosity, Pa.s
$\eta_a$	apparent shear viscosity, Pa.s
$\eta_0$	zero-shear viscosity, Pa.s
$\eta_\infty$	infinite-shear rate viscosity, Pa.s
$\eta^*$	complex viscosity, Pa.s
$[\eta]$	polymer intrinsic viscosity, dl/g
$[\eta]_b$	intrinsic viscosity of branched polymer, dl/g
$[\eta]_l$	intrinsic viscosity of linear polymer, dl/g
$[\eta]_i$	intrinsic viscosity of slice i, dl/g
$\eta_{inh}$	inherent viscosity, dl/g
$\eta_{red}$	reduced viscosity, dl/g
$\eta_{sol}$	viscosity of pure solvent, g/dl
$\tau_w$	wall shear stress, Pa
$\lambda$	characteristic time, s (in chapter 3)
$\lambda$	long chain branching frequency per 1000 carbon atoms (in chapter 5)
$\lambda$	relaxation time constant (in chapter 8), s
$\phi$	volume fraction of the solid filler
$\omega$	angular frequency, rad/s
$\omega_c$	cross-over frequency, rad/s
$\Delta H_m$	heat of fusion, J/g
$\Delta P_{ent}$	entrance pressure drop, Pa

# CHAPTER 1

## INTRODUCTION AND OBJECTIVES

### 1.1 Introduction

Isotactic polypropylene (PP), the homopolymer of the propylene monomer, has a relatively high melting point, excellent chemical resistance, and a relatively high tensile modulus. Such desirable properties have made it one of the most widely used thermoplastics since the Ziegler-Natta discovery in 1955. Another factor for its popularity is that it can be post-reactor modified to exhibit great diversity in performance properties. Current modification techniques involve functionalization (Chiang et al., 1988), controlled-degradation (Tzoganakis et al., 1988; Suwanda et al., 1988), crosslinking (Kim et al., 1993) and branching (Scheve et al., 1990), to name a few. Reactive extrusion (REX) processes have been applied in some of these modifications because of their efficiency and economical advantages (Xanthos, 1992).

Commercial PP is a linear architecture polymer as a direct result of its Ziegler-Natta polymerization. The absence of side branches leads to a deficiency in melt strength. As a result, its use has been limited to such applications as extrusion coating, blow moulding, profile extrusion, and thermoforming. The melt strength drawback of PP can be overcome by blending it with other polymers (Scheibelhoffer et al., 1993). However, the blend approach involving different polymers is not preferred (Scheve et al., 1990). Another approach is to introduce long chain branches on the PP backbone in a post-reactor process, and this has been reported only recently in an irradiation process of isotactic PP (Scheve et al., 1990). No publications have appeared in the open literature regarding the production of branched PP using a REX process.

## 1.2 Objectives and Scope of the Thesis

From the literature survey in Chapter 2, it may be seen that possible new opportunities may exist to produce branched PP using reactive extrusion (REX) through the following two reaction routes.

The first approach is to carry out reactions between two functionalized PPs in a REX process, where branches may be formed by grafting. Thus, the grafting reaction between a nominally linear random-functionalized PP and a terminally-functionalized PP with complementary functional groups may provide an effective means of producing branched PP. Currently, terminal functionalization of PP through REX is being studied in our laboratory (Thompson et al., 1996). Unfortunately, terminally functionalized PPs are only available in small quantities and they are not easily accessible. Hence, a long chain alkyl amine, hexadecylamine, has been used in this work as a model molecule for terminally functionalized PP and reacted with an acrylic functionalized PP in a REX process.

The second approach is the reaction of PP with peroxide and a polyfunctional monomer at low concentrations. While the use of relatively high concentrations of crosslinkers to promote highly crosslinking of PP is well known (Chapter 2), little has been done in a REX process to explore the possibility of using low concentrations of a crosslinker and a peroxide to cause desirable molecular modifications such as branching while minimizing crosslinking and degradation. This offers another new opportunity for REX. The work completed via this approach may be divided in two stages. In stage 1, preliminary experiments were carried out to identify a useful range of low peroxide and polyfunctional monomer concentrations. In stage 2, these concentrations were used to produce a series of long chain branched PPs whose properties were fully characterized.

In summary, the objectives and scope of this thesis are to study the production of branched polypropylenes by reactive extrusion (REX) processes via the above two routes and to evaluate the rheological, thermal and molecular properties of the products.



### **1.3 Outline of Thesis**

- Chapter 2:** This chapter presents a literature survey on reactive extrusion developments, crosslinking of PP and the effects of branching on polymer properties.
- Chapter 3:** The reaction between an acidic functionalized PP and a long chain alkyl amine was studied both in solution and in a REX process. The model branched polypropylenes produced were characterized in order to gain a basic understanding of the effects of branching.
- Chapter 4:** Preliminary experiments on the reactive extrusion of unstabilized linear PP with pentaerythritol triacrylate (PETA) and Lupersol 101 (L101) were carried out in stage 1. The properties of the modified PPs were measured in order to search for suitable concentrations for further REX experiments and the evidence of branching. In stage 2, further REX experiments were carried out at very low concentrations of PETA and L101 in a stabilized system. Some characterization data of the whole polymers, their sols and macrogels are presented such as macrogel content, shear viscosity and melt flow index of the whole polymers, FTIR characterization of the sols and the thermal characterization of the macrogels.
- Chapter 5:** Gel permeation chromatography (GPC) was used to evaluate the molecular weight averages, molecular weight distribution, and long chain branching in the sols of the PETA/L101 modified PPs from stage 2. Results are presented and discussed.
- Chapter 6:** Data on the thermal stabilities, melting and crystallization temperatures for the sols of the PETA/L101 modified PPs from stage 2 are presented.
- Chapter 7:** The apparent elongational viscosities and viscous flow activation energies for the whole samples of the PETA/L101 modified PPs and L101-degraded PPs from stage 2 were evaluated and the results are presented in this chapter.

- Chapter 8:** Linear viscoelastic properties such as storage moduli, loss moduli and complex viscosities for the whole samples of the PETA/L101 modified PPs and L101-degraded PPs from stage 2 were studied. Zero-shear viscosities were estimated using two models and three representations were shown for the purpose of detecting the existence of long chain branching.
- Chapter 9:** The results of this work are summarized and conclusions and recommendations are presented.

## CHAPTER 2

### LITERATURE SURVEY

#### 2.1 Reactive Extrusion (REX)

The use of extruders as continuous reactors for processes such as polymerization, polymer modification or compatibilization of polymer blends involves technologies that are gaining increasing popularity and compete with conventional operations with respect to efficiency and economics. Many papers and reviews regarding different aspects of reactive extrusion have been well summarized by Xanthos (1992). The types of chemical reactions performed by REX have been classified as bulk polymerization, grafting reactions, interchain copolymer formation, coupling/cross-linking reactions, controlled-degradation and functionalization/functional group modification.

One of the successful commercial applications of REX processes to PP is the manufacturing of controlled-rheology polypropylene. During such a process, a commercial grade PP with high molecular weight and broad molecular weight distribution may be converted into various grades of PP with relatively lower molecular weights and narrower molecular weight distributions. These relatively more expensive PP grades are more suitable for film and fibre extrusion. There have been many studies regarding this subject such as the works of Tzoganakis et al. (1988a), and Suwanda et al. (1988), while a review on the subject is given by Brown (1992). Reactive extrusion has been employed for different functionalizations of PP such as the grafting of vinyl silanes (Spielau et al., 1987), acrylic acid, acrylic esters and analogs (Chiang et al., 1988), styrene and styrene analogs (Togo et al., 1988), and maleic anhydride (Gaylord et al., 1983). PP has also been crosslinked by REX with relatively high concentration of crosslinkers in the presence of peroxides (Kim et al.,

1993), or branched in a REX process via the reactions between an acrylic acid functionalized PP and hexadecylamine (Wang et al., 1994).

Polyethylenes have also been modified using REX where low or high peroxide concentrations were employed (Suwanda, 1992). Unlike PP, PE undergoes crosslinking and endlinking reactions to increase the degree of long chain branching, molecular weight and breadth of molecular weight distribution. At low peroxide concentrations, long chain branches are produced and hence the rheological properties are modified. At high peroxide concentrations, highly crosslinked materials are produced.

Recently, there still have been intensive studies on reactive extrusion. Hallden-Abberton (1991) has carried out the imidization of acrylic polymers by REX. Hert (1992) has produced tough thermoplastic polyesters by REX with epoxy-containing copolymers. Two types of ethylene copolymers, ethylene/ethyl acrylate/glycidyl methacrylate (E/EA/GMA) and ethylene/ethyl acrylate/maleic anhydride (E/EA/MAH) copolymers, were used to toughen poly(butylene terephthalate) (PBT) and poly(ethylene terephthalate) (PET) by REX. PBT blends undergo a brittle to ductile transition by toughening with GMA copolymer between 10 and 20% of the rubbery phase. The most effective toughening could be achieved by a partial crosslinking of the rubbery particles obtained by associating GMA and MAH copolymers and a reaction catalyst.

Todd (1992) has considered the advantages and rules of thumb for REX. Abramowicz et al. (1992) have also considered REX as an alternative to reactor polymerization. Carr et al. (1992) have carried out the graft polymerization of cationic methacrylate, acrylamide and acrylonitrile onto starch by REX. Donabedian et al. (1992) have carried out plasticization and reactive extrusion. Dagli et al. (1992) have reviewed the effects of reactive extrusion variables on the characteristics of nylon-6 and polypropylene blends with potential applications in recycling.

Yong et al. (1992) have grafted acrylonitrile (AN) onto unmodified cornstarch by a

continuous REX process in a corotating, intermeshing twin-screw extruder and, for comparison, in a typical batch reaction process. The effect of AN/starch weight ratios, level of ceric ammonium nitrate initiator, starch in water concentration, reaction temperature, reaction time, and extruder screw speed in the REX process was studied. Processing times in the extruder were 2-3 minutes, and total reaction time was about 7 minutes before reaction of the extruded material was terminated, compared to a reaction time of 2 hours used in the batch procedure.

Kim et al. (1993) have crosslinked an isotactic PP in a twin-screw extruder. The whole samples of the products were characterized in terms of melt flow index, mechanical properties and DSC. It was concluded that triacrylates were the most effective among the polyfunctional monomers used. Kim and Kim (1993) have also crosslinked high density polyethylene by REX using peroxide and crosslinkers, and they have studied the rheological, thermal and mechanical properties of the products.

Michaeli et al. (1993) have produced polystyrene and styrene-isoprene copolymers by reactive extrusion. The anionic "living" *s*-butyllithium-initiated bulk polymerization was performed in a corotating intermeshing twin-screw extruder. The results of the process analysis show that living polymerization of styrene can be performed in a screw-type reactor, despite the high reaction temperatures (over 200°C) and that the polystyrene melt can be modified in bulk with comonomers or coupling reagents immediately after polymer synthesis. Polystyrene and styrene-isoprene copolymers with widely different structural characteristics and properties could be produced.

Suwanda and Balke (1993) have investigated the combined reactive extrusion and orientation of polyethylene. A continuous extrusion method for oriented polymer in forms other than fibres and films was devised. Operation of a prototype of the equipment proved it capable of providing draw ratios of greater than ten. It was found that the effect of low initiator concentrations injected during extrusion (before orientation) depended on the degree

of branching, the molecular weight, and the degree of unsaturation of the polyethylene. Large increases in molecular weight could be obtained. The formation of branched molecules drastically limited draw ratios attainable by the extrusion-orientation process. It was also found that a method involving the use of a UV sensitizer and crosslinker followed by irradiation was directly adaptable to the above process and provided significant improvements in creep resistance.

Vermeesch et al. (1993) have produced poly(styrene-co-N-maleimide) copolymers by reactive extrusion of poly(styrene-co-maleic anhydride) with ammonia under short reaction times (2 minutes). The modified materials have relatively high glass-transition temperatures compared with that of the starting materials, which is believed to result mainly from hydrogen bonding between the maleimide groups.

Coudray et al. (1994) have synthesized acrylated polyurethane prepolymers by REX and bulk reaction. In order to obtain a high reaction conversion within the extruder, tin laurate catalyst was used at 90°C. At these conditions, an appropriate radical initiator can be introduced during the extrusion without double bond polymerization. The glass transition temperatures of the oligomers and networks are -18°C and +18°C, and +8°C and +27°C for the products from bulk and reactive extrusion respectively.

Ganzeveld et al. (1994) have investigated the role of mixing and rheology in reactive extrusion. Viscosity and amount differences between the components fed to the extruder considerably influence this mixing process. The extent of their influence on the mixing and hence the reaction process was studied with a decolorization reaction in a fully intermeshing counterrotating twin screw extruder with a transparent barrel. It was found that for this type of extruder, faster mixing is achieved if one component consists of low viscous material and is present in considerable amounts. An increase in the viscosity ratio between both components leads to a decrease of the mixing length and an increase of the amount ratio results in an increase of the mixing length. The experimental results agreed well with the

theoretical analysis of the flow analysis in the mixing areas of the extruder.

Hornsby et al. (1994a) have investigated the anionic polymerization of  $\epsilon$ -caprolactam in a corotating intermeshing twin-screw extruder in terms of the materials formulation, extruder screw profile, and processing parameters such as temperature and screw speed. Using a variety of analytical characterization techniques, it is demonstrated that molecular weight, residual monomer content, and mechanical properties of the polyamide 6 are very sensitive to the reactive processing conditions employed. The microstructure of the product was also analyzed (Hornsby et al., 1994b).

Pabedinskas et al. (1994a) have presented the design and analysis of a process control strategy for a REX process of polypropylene (PP) degradation. The primary control objective is to continuously produce PP with desired properties (viscosity) despite variations in the properties of the feed material. The viscosity of the PP, measured by an in-line wedge rheometer, is controlled by manipulating the feed concentration of the peroxide. An empirical model of the reactive degradation process is developed, which describes the process dynamics and the characteristic process disturbances. Minimum variance, constrained minimum variance and pole placement controllers were evaluated and compared. Finally, a pole placement controller was implemented on the actual REX process.

Pabedinskas et al. (1994b) have further presented the development of a model for the free radical initiated PP degradation by reactive extrusion which combines a kinetic model of the PP degradation reaction with a simplified model of the melting mechanism in the extruder. The predictions of the kinetic model alone and the combined kinetic-melting model are compared with the experimentally determined molecular weight distributions and molecular weight averages for the degraded PPs. The predictions of a modified kinetic model that includes the possibility of termination by combination are also examined. It was found that the kinetic-melting model provides significantly improved predictions in comparison to the original kinetic model. A viscosity-molecular weight relationship is developed and

then used in determining the gain of the degradation process as a function of the initiator concentration from the molecular weight averages predicted by the kinetic-melting model. It was shown that such prior knowledge of the process gain can be used to significantly improve the performance of process control schemes for the degradation process.

Vermeesch et al. (1994) have carried out the chemical modification of poly(styrene-co-maleic anhydride) with primary N-alkylamines by reactive extrusion in a corotating twin-screw extruder. It was found that ring formation of the imide occurred within the residence time of the extruder, at temperature exceeding 220°C and with an excess of primary amines. The increasing chain length of grafted amine onto the SMA backbone depressed the glass transition temperature of poly(styrene-co-N-alkylmaleimides) remarkably.

Wang et al. (1994) have produced model branched polypropylenes by reacting acrylic acid grafted polypropylene with hexadecylamine by reactive extrusion. The molecular, elemental, thermal and rheological properties were studied.

Maier and Lambla (1995a) have studied the esterification reaction for the grafting of nonylphenyl-ethoxylate onto a maleated ethylene-propylene in reactive extrusion. It was found that nonylphenyl-ethoxylate could penetrate into the polymer within screw distance of less than 1.3 L/D, despite using conveying elements known for their minimal mixing capacity. Within the molten medium, it was found that obtaining the expected conversion in a product does not imply that the reactants in the product have in fact been well mixed. The authors have also carried out the grafting reaction onto maleated ethylene-propylene rubber by reactive extrusion (1995b).

Mead (1995) has modeled the homogeneous and nonhomogeneous reactive extrusion of polypropylene using random chain scission statistics coupled with the double reptation mixing rule. The evolution of both the molecular weight distribution and linear viscoelastic material properties is quantitatively predicted for the reactive extrusion-pelletization process.

Michaeli et al. (1995) have modeled twin-screw extruders for reactive extrusion by



means of the ideal reactor types “cascade of continuous stirred tank reactors (CSTRs)” and “pipe reactor”. The developed model has been tested in practice on the production of homopolymers (nylon 6 and polystyrene) and on the polymerization of copolymers (nylon block copolymers). The comparison of the calculated process parameters such as residence time, drive-energy, melt temperature, and conversion rate with the values determined from experiments was fairly good.

Polance and Jayaraman (1995) have investigated the mixing in reactive extrusion of low density polyethylene melts by comparing the melt flows of linear low-density polyethylene (LLDPE) and branched low-density polyethylene (LDPE) in a fully intermeshing co-rotating twin-screw extruder. The shear viscosity curves for LLDPE and LDPE are quite similar, but LDPE has a markedly higher apparent extensional viscosity over a wide range of stretch rates. The stagger of the paddles in the mixing zone of the extruder creates axial pressure gradients and provides a nonuniform geometry for axial flow. The resulting pressure-driven axial flow can have significant extensional strain components. Residence time distributions obtained in the melt zones of the extruder with tracer dye reveal that the LDPE has a narrower residence time distribution than the LLDPE over a wide range of operating conditions. The axial dispersion for the LDPE is significantly lower than the axial dispersion for the LLDPE, which is attributed to the greater extensional viscosity of the LDPE. During the reactive extrusion process, solid maleic anhydride and polyethylene were added at the feed port but the peroxide initiator was added only after the polymer was melted. Residence time distributions measured for LLDPE melt indicate reduced levels of axial mixing with reaction. The reduction in mixing is due to a crosslinking reaction that occurs in parallel to the grafting reaction. This change in mixing is smaller than the difference in mixing between LDPE and LLDPE.

Turcsanyi (1995) has investigated the graft modification of polyethylene with N-vinylimidazole by reactive extrusion and the compatibilization of polyethylene-

polypropylene blends via imidazol-carboxyl interactions. Yang et al. (1995) have studied the anionic ring-opening polymerization of nylon 6 in a Haake torque rheometer as the simulation of reactive extrusion in a counterrotating twin-screw extruder. Experimental results for several combinations of processing parameters are presented and general relations between processing parameters (such as torque, temperature and rotating speed), conversion ratio, and molecular weight of the product are observed. These observations can be used in the eventual scaling up of investigations to an actual twin-screw extruder.

Yoon et al. (1995) have carried out reactive extrusion of polypropylene/natural rubber blends in the presence of a peroxide, [1,3-bis(*t*-butylperoxy) benzene], and a polyfunctional monomer, trimethylolpropanetriacrylate (TMPTA). Effects of peroxide and TMPTA were studied in terms of melt index (MI), melt viscosity, morphology, thermal and mechanical properties. At a constant content of TMPTA, melt viscosity increased at a low and decreased at a high content of the peroxide. On the other hand, melt viscosity increased monotonically with the TMPTA concentration at constant peroxide content. The increase and decrease of viscosity were interpreted in terms of crosslinking and chain scission of polypropylene, which governed the rubber domain size and mechanical properties of the reactive blends.

Chen et al. (1996) have investigated the simultaneous effects of flow, diffusion and reaction kinetics involved in the simultaneous reactive extrusion (REX) and devolatilization (DV) through the monoesterification reaction of styrene-maleic anhydride copolymer with 1-octanol. It was found that there is a significant enhancement of the monoesterification reaction during the REX-DV process. The results confirmed that there are synergistic effects between reactive extrusion and devolatilization. Kye and White (1996) simulated the reactive extrusion of the polymerization of caprolactam in a corotating intermeshing twin-screw extruder using three screw configurations. It was found that the predicted conversion is well matched with experimental results.

Wong and Baker (1996) have grafted glycidyl methacrylate and styrene onto

polypropylene in a Haake mixer at 180°C. The influence of initiator type, initiator and monomer concentration, and the use of a comonomer on the degree of grafting and weight average molecular weight of the grafted modified polymer were examined. Lu et al. (1996) have grafted maleic anhydride (MAH) on polypropylene in a twin-screw extruder and investigated the effects of maleation on the rheology and surface properties of the maleated PP (MPP). It was found that the shear and elongational viscosities of MPP are lower than those of virgin PP. The surface energy of MPP is increased significantly by contacting with water either at room temperature or at 100°C. Wang et al. (1996) have modified isotactic polypropylene with pentaerythritol triacrylate in a reactive extrusion process. From the thermal and rheological properties of the products, it was concluded that the modified polypropylene may contain branched and/or crosslinked chain structures.

Increasing research activities have also been directed towards polymer compatibilization using REX. Willis et al. (1990) have compounded polystyrene-co-maleic anhydride/bromobutyl rubber blends in a corotating intermeshing twin-screw extruder. The morphology and impact properties of the blends have been studied as a function of interfacial modification and melt processing conditions. It was found that dimethylaminoethanol (DAME) serves as a reactive compatibilizing agent for these blends, and that the addition of DAME results in a five-fold reduction in the size of the dispersed phase. Impact strength measurements were shown to be dependent on the quantity of DAME and concentration of elastomer. The volume average diameter of the minor phase increases significantly as the screw speed and throughput increase.

Dharmarajan et al. (1992) have studied the impact modification of brittle styrene-maleic anhydride copolymers with primary amine functionalized ethylene propylene (EP) elastomers. The blends were examined by techniques such as FTIR, differential solvent extraction, capillary and parallel-plate viscometers. It was found that graft polymer formation does not substantially increase viscosity at high strain rates, but introduces yield stress at low

shear rates. Teh et al. (1992) have studied the direct grafting of polystyrene onto polyethylene in a twin screw extruder, in the presence of dicumyl peroxide and triallyl isocyanurate. The impact properties of the blends were enhanced at an optimum level of peroxide and coagent. Further improvement was achieved by introducing styrene monomer into the system during reactive extrusion.

Nylon alloys have been investigated intensively. Chang et al. (1991) have compounded polystyrene/nylon 6,6 blends in a counter-rotating intermeshing twin-screw extruder. Styrene-maleic anhydride and styrene-glycidyl methacrylate copolymers were used as the compatibilizers. It was demonstrated in this work that polyblends with good compatibilizers do not guarantee toughness improvement. Nishio et al. (1991) have investigated the morphology of the blends of maleic anhydride grafted PP/polyamide. Lamba et al. (1992) have studied the interfacial grafting and crosslinking by free radical reactions in immiscible LDPE/polyamide-11 blends. Liang et al. (1992) have studied the dynamic mechanical properties of PP/polyamide blends. Padwa (1992) studied polyamide-6/polyethylene alloy using maleic anhydride functionalized polyethylene as a compatibilizer. It was found that in blends containing 50% nylon 6, the melt viscosity of the alloy increases exponentially as the ratio of the compatibilizer to polyethylene increases. High ratios of compatibilizer to polyethylene are desired for toughness. Alloys containing lesser amounts of compatibilizer exhibit better processability. The balance of toughness and processability is shown to be affected by the molecular weight of the compatibilizer. Takeda et al. (1992) have investigated the effect of polyamide functionality on the morphology and toughness of blends with a functionalized triblock copolymer. Armat et al. (1993) have studied the effect of compatibilizing PE and nylon-6 on the morphology and mechanical properties of their blends. Hagberg et al. (1996) have recycled the components of a nylon face fibre carpet via reactive extrusion in a counter-rotating, non-intermeshing twin-screw extruder. Using compatibilizers, fillers and/or additives, post-consumer carpets can be extruded into

thermoplastic pellets useful for injection molding.

Xanthos et al. (1991) and Liu et al. (1992a) have reviewed the compatibilization of polymer blends by reactive processing and on-line rheometry has been applied to reactive compounding in a single-screw extruder by Xanthos (1995). Sundararaj et al. (1995) have compared the dispersions of both reactive and nonreactive polymer-polymer blends in three different mixers, i.e., an industrial scale twin-screw extruder, a laboratory internal mixer and a miniature cup and rotor mixer. It was found that the morphology development in the three mixers is remarkably similar and there is a significant effect of quenching time on the blend morphology.

Yu et al. (1996) have blended polyethylene terephthalate (PET) and polybutylene terephthalate (PBT) in a Brabender extruder. The glass transition and crystallization behaviour were studied by differential scanning calorimetry. It was found that the crystallization behaviour is strongly influenced by the residence time in the extruder. Kimura et al. (1996) have also blended PET and ethylene vinyl alcohol in a reactive extrusion process using epoxide compounds as the coupling agents. With the addition of coupling agents, the viscosity, melt strength and molecular weight of the blends increased, indicating the existence of crosslinks in the blends.

Sun et al. (1996) have investigated the effects of processing parameters on the in-situ compatibilization of polypropylene and polybutylene terephthalate (PBT) blends by one-step reactive extrusion in a co-rotating intermeshing twin-screw extruder. The processing parameters examined were feed rate (Q), screw speed (N) and specific throughput (Q/N). It was found that elongation at break and impact strength of the blends increased with a decrease in Q or N. Kim et al. (1996) have produced polypropylene/ethylene-propylene-diene terpolymer/high density polyethylene ternary blends by reactive extrusion. The effects of peroxide and coagent concentrations and screw speed were studied in terms of rheological, morphological, thermal and mechanical properties of the blends.

## **2.2 Effect of Branching on Polymer Properties**

### **2.2.1 Introduction**

Typical model branched polymers are star molecules (Rocheffort et al., 1979), comb molecules (Fujimoto et al., 1970), and randomly branched molecules (Masuda et al., 1972). Star and comb branched polymers have branches of equal length. However, commercial branched polymers usually do not have branches of equal length, nor are they likely to have randomly structured branching because the manufacturing conditions are often biased rather than completely random. In practice, many nominally linear polymers may contain some branch points due to secondary reactions occurring during chain polymerization.

It has been widely accepted that long chain branches (LCB) are usually of the same order of length as the main chain while short chain branches (SCB) are of a size up to that of only a few repeating units. SCB influences the morphology and solid state properties of semicrystalline polymers, whereas LCB has a remarkable effect on solution viscosity and melt rheology.

The universal method for the determination of long side chains in a polymer is based on the fact that the branched molecule has a smaller coil dimension than a linear molecule of the same molecular weight and the same chemical composition (Schröder et al., 1989). The molecular contraction is a quantity that can be determined experimentally. A measure of that is the contraction factor  $g$  which is defined as the ratio of the radii of gyration of the branched and linear molecules of the same molecular weight and same polymer in solution. The branching index  $g'$ , the ratio of intrinsic viscosities of the branched and linear polymers of the same molecular weight, is also a measure of the amount of branching in a polymer. Up to now, the most documented commercial polymer in terms of branching is branched polyethylenes (PE). For PE, besides the above universal method, GPC (Pang et al., 1993),  $^{13}\text{C}$ -NMR (Bugada et al., 1987), FTIR (Usami et al., 1984), pyrolysis gas chromatography (Haney et al., 1983) and radiolysis (Bowmer et al., 1977) have also been used to determine

branching. Current  $^{13}\text{C}$ -NMR analyses usually measure polyethylene branches of 6 carbons or larger as long branches (Pang et al., 1993). In GPC analysis, branches of 6 carbons or less in length are measured as short while 12 carbon branches appear as long branches and the minimum length for long branches is then between 6 and 12 carbons (Rudin et al., 1984). GPC assessments of long branches in polyethylene are based on comparisons of molecular weights at equivalent hydrodynamic volume. For PE, most GPC calculations assume that the polymer is randomly branched and that it contains trifunctional branching points (Pang et al., 1993). Depending on the type of a particular polymer, other methods such as the determination of number average molecular weight (for polyvinyl acetate), the ozonolysis followed by hydrolysis (for polydienes) may also be used to determine branching in polymers (Meares, 1965).

Recently, a new technique called temperature-rising elution fractionation (TREF), has been used to analyze the branching of polymers such as polyethylenes (Defoor et al., 1992a). The principle of TREF is the selective crystallization of the polymer chains as a function of their branching degree during a slow and controlled cooling of a dilute polymer solution, followed by elution of the polymer as the temperature is subsequently raised. Using a calibration curve of elution temperature vs. branching content, the experimental elution temperature can be translated to the average branching content. However, much experimental time is needed in carrying out TREF.

Although many techniques have been developed to characterize branched polymers, complete analysis of branching in a polymer as apparently simple as polyethylene has proved to be rather difficult and it has been recognized that rheological measurements often provide better alternatives for assessing the extent of branching in polymers.

### **2.2.2 Effect of Branching on Polymer Properties**

The most important rheological feature of polymers, both in the molten and solid

states, is that they exhibit viscoelastic properties, i.e., properties of both a viscous liquid and an elastic solid. Studies of rheological properties of polymer systems have proven to be of considerable practical value in predicting resin end-use properties, particularly processability. The complete rheological descriptions must provide measures of both viscosity and elasticity.

Shear viscosity is a measure of the internal friction that resists the change of shape of a fluid. It is defined as the ratio of shear stress to shear rate acting on the fluid. A rheogram is frequently used to illustrate the viscosity dependence on the shear rate which is usually a plot of log (melt viscosity) versus log (shear rate). Elongational viscosity is a similar measure of resistance to a change of shape of a fluid, but under normal stresses. Elongational viscosity generally has limited application but it is very important in processes where drawing and spinning are involved. Elasticity refers to the resistance to the change of shape of a solid material, or the amount of energy stored relative to its equilibrium state.

From a structural point of view, it is generally understood that different rheological properties are the consequence of different molecular structures existing in materials, i.e., molecular weight (MW), molecular weight distribution (MWD) and molecular architectures such as long chain branching. Apart from its use as an indicator of relative breadth of MWD, there have been some exploitations of rheology as a structural tool trying to define resin structures, particularly the nature and degree of LCB. Significant progress has been made in elucidating the effects of molecular architecture upon the rheological behaviour of certain model (such as star branched) polymer systems which contain well-defined branch frequency, branch length, and narrow MWD (Rochefort et al., 1979; Rachapudy et al., 1979; Raju et al., 1979). However, it has been argued that the molecular architecture and hence the viscoelastic properties of commercial branched polymers may not be well represented by these model systems (Bersted, 1985).

Generally, an increase in MW increases shear viscosity, elongational viscosity and elasticity. However, elucidation of the effects of molecular branching upon the melt viscosity



and elasticity of polymers has not been straightforward (Münstedt and Laun, 1981). One of the difficulties is to define in a quantitative manner the variations in the types and distributions of branches existing in most polymers. Another difficulty is to separate the effects of MWD from those of branching. Therefore, it is worthwhile to elucidate the effects of MWD on the melt viscosity and melt elasticity of the polymers for systems of similar weight average molecular weight and molecular architecture before the effects of long chain branches of polymers on the rheological properties will be discussed.

The analysis of MWD from rheological information is based upon the concept that the low shear rate viscosity reveals relaxation processes of the larger molecules whereas the high shear rate viscosity is dominated by relaxation processes associated with the smaller molecules and segments of larger molecules. Studies of polyethylene indicate that the low shear rate viscosities of broad MWD samples are higher than those of narrow MWD samples (Guillet et al., 1965; Chartoff et al., 1969). However, the high shear rate viscosity decreases as MWD broadens, leading to crossovers in the shear viscosity-shear rate curves for samples of varying MWD. Similar results have been obtained for polystyrene (Thomas et al., 1969). Generally, the change in elongational viscosity is similar to that in shear viscosity when MWD is changed.

The melt elasticity (such as die swell and pressure losses) is also affected by MWD (Guillet et al., 1965; Combs et al., 1969; Han et al., 1978) and changes in MWD have also been detected by melt elasticity (Guillet et al., 1965; Combs et al., 1969). It has been reported that melt elasticity (which especially means die swell) increases as the molecular weight distribution broadens. These authors found that the index  $n$  in the power-law model decreases as the molecular distribution broadens. The broadening of MWD is also accompanied by increases in exit pressure loss (Han et al., 1978). Following is a brief summary on the effects of branching on the rheological and other properties of polymers.

### Shear and Elongational Viscosity

Bueche (1964) has attempted to explain theoretically the effect of branching on viscosity, and developed models to predict a viscosity reduction due to branching. This has been verified experimentally in a number of instances. However, it has also been shown experimentally that branched polymers may have higher viscosity than linear polymers of the same molecular weight at very low rates of deformation. For example, Kraus and Gruver (1965) studied the relationship between the branch architecture and shear rate dependent viscosity of polybutadiene. The major feature of this relationship is that the zero shear rate viscosity ( $\eta_0$ ) of a polymer having branches of molecular weight  $M_b$  less than 3-4 times  $M_e$  (the characteristic molecular weight above which chain entanglement becomes important), is less than that of a linear polymer of similar  $\bar{M}_w$ . For cases in which  $M_b$  of the branches exceeds 3-4 times  $M_e$ , then  $\eta_0$  of the branched polymer exceeds that of the linear polymer. This was later described as  $\eta_0$  enhancement. A further observation was that the high shear rate non-Newtonian viscosities of the branched systems were lower than those of the linear counterparts, even though viscosity enhancement was observed at low shear rates. This is also the case for branched and linear polyethylene (PE) of similar molecular weight. The extensive work of Graessley and co-workers (Rocheffort et al., 1979; Rachapudy et al., 1979; Raju et al., 1979) with monodispersed linear and star polybutadienes and their hydrogenated products supports the earlier observations by Kraus and Gruver (1965). In general, low density polyethylene (LDPE) materials have greatly diminished melt viscosities relative to the linear high density polyethylene (HDPE) at constant weight average molecular weight. However, dramatic viscosity enhancement at low shear rates ( $\eta_0$ ) has also been observed (Mendelson et al., 1970; Wild et al., 1976; Graessley et al., 1977) when LCB is present at low concentrations.

Therefore, branching can either increase or decrease zero shear rate viscosity ( $\eta_0$ ), depending on the length of the branches. LCB usually increases the shear viscosity at low

shear rates, but decreases the viscosity at high shear rates, i.e., increasing the negative slope of the rheogram.

Branching also influences elongational viscosity and hence strain hardening. For example, Nakajima (1979) and Scheve et al. (1990) showed that the strain hardening is the result of increased chain entanglement due to long chain branches. Münstedt and Laun (1981) found that low density polyethylenes show a maximum of the steady state elongational viscosity while high density polyethylenes do not exhibit this behaviour or are less pronounced. Laun and Schuch (1989) further suggested that long chain branching is much more effective than molecular weight distribution in producing a pronounced maximum in the steady state elongational viscosity. Hingmann and Marczinke (1994) also found that long chain branched polypropylene shows the above behaviour and the pronounced strain hardening in experiments at constant strain rate. Recently, Ramsey et al. (1996) investigated the effects of branching, molecular weight and molecular topology on the elongational stress growth function of atactic polystyrene (aPS) at 150°C. The elongational stress growth function is the ratio of the stress ( $\sigma$ ) on the specimen at time  $t$  ( $\sigma_t$ ) to the strain ( $\epsilon$ ) rate ( $d\epsilon/dt$ ). It should be noted that the elongational stress growth function becomes the true elongational viscosity once the steady state stress is achieved. Three topologies of aPS with very narrow molecular weight distributions were used, i.e., linear, H-shaped and three-arm star. The molecular weight has a dominant effect on the elongational stress growth function independent of the molecular topology (either linear or three-arm star), i.e., the value of this function increasing with increases molecular weight. With similar  $\bar{M}_w$ s, the H-shaped material exhibited the elongational stress growth function value slightly higher than that for the three arm star material, but still less than that for the linear material.

### **Melt Elasticity**

Melt elasticity increases with increasing degree of branching. Bagley (1961) found

that branched polyethylene (PE) has much higher values of end correction compared to those for linear PE and that branched PE exhibits a more pronounced melt elasticity than linear counterpart. Guillet et al. (1965) reported that PE fractions with a high degree of long-chain branching exhibit high die swell, while linear PE fractions show a relatively low die swell, which is independent of molecular weight over the wide range tested. Wild et al. (1976) suggested that melt elastic properties such as die swell may provide a measure of average molecular size and can be used as a measure of the degree of LCB for LDPE polymers with similar melt index values. Han et al. (1978) have found that die swell and pressure losses in the entrance and exit regions of capillary flow geometries significantly increase with degree of branching.

### **Viscous Flow Activation Energy**

Branched polymers usually have higher flow activation energy. For example, Porter et al. (1968) reviewed the studies on branched PE and proposed that the large increase in the flow activation energy of a branched PE may be due to the existence of LCB. Combs et al. (1969) found that  $E_r$  (flow activation energy at a constant shear stress) and melt viscosity increase with increasing the number of short-chain branches (0-10 carbon atoms in side chain) in polyolefins. Raju et al. (1979) have shown that the flow activation energy for star-branched hydrogenated polybutadienes is primarily a function of branch length. Romanini et al. (1980) have found that long-chain branched LDPE have a higher flow activation energy than that of linear PE. Bersted (1985) also has observed that the very low levels of LCB in PE increase both flow activation energy and viscosity at low rates and that the flow activation energy increases with branching level. Laun (1987) has also suggested that long chain branches are responsible for the high flow activation energy of LDPE compared to HDPE, and a growing number of the branches increases the flow activation energy. This conclusion was made based on the following flow activation energy values: 28 kJ/mol for HDPE, 33

kJ/mol for LLDPE, 54 kJ/mol for a long chain branched LDPE melt with 15 CH<sub>3</sub>-end groups per 1000 C-atoms, 60 kJ/mol for the one with 30 CH<sub>3</sub>-end groups per 1000 C-atoms. Scheve et al. (1990) have also found that long chain branched PP has a higher flow activation energy than linear PP.

### **Viscoelastic Properties**

Folt (1969) found that the relative degree of long chain branching in polybutadiene and polyisoprene could be assessed by the magnitude of stress oscillation encountered in capillary flow measurements. It was found that the magnitude of the stress oscillation decreased with increasing long chain branching. Nakajima et al. (1982) found that the solution concentration dependence of viscoelastic properties was significantly affected by the presence of long branches. The long-chain branched polymer not only produced different shift factors in the concentration superposition but also deviated from the master curve at semidilute concentration. Harrell et al. (1984) prepared a series of ethylene-propylene copolymer samples in which the degree of branching was systematically varied. Time-temperature superposition was employed to obtain master curves of storage modulus ( $G'$ ), loss modulus ( $G''$ ) and complex viscosity ( $\eta^*$ ). It was found that  $G'$  response relative to that of the  $G''$  is significantly enhanced as long chain branching increases. A modified Cole-Cole plot, in which the axes are expressed as the logarithms of  $G'$  and  $G''$ , was used for assessment of molecular architecture. Changes in the long-branch architecture were readily detected as systematic variations in shape and displacement of the modified Cole-Cole plot. It should be pointed out that this method seems useful for the comparison of materials with similar molecular weight distributions, yet exhibiting different molecular architectures.

### **Other Properties**

Brady et al. (1988) have investigated the effect of short chain branching on the

morphology of oriented linear low density polyethylene thin films. For similar branching distributions, the average melting temperature generally decreased as branch content increased, which could be correlated to the decrease in crystal thickness as revealed by transmission electron microscopy. Dynamic mechanical analysis showed the presence of a beta peak in branched samples only. Moreover, the alpha transition temperature shifted to lower temperatures as branch content increased.

Wooster et al. (1989) have investigated the effect of SCB distribution (SCBD) on the stress intensity factor for a series of LLDPEs at strain rates of  $11.3\text{s}^{-1}$ . It was suggested that fracture toughness correlated with spherulite morphology which was influenced by the existence of branches and the effect of SCBD on crystallization. Huang and Brown (1990) have found that the rate of slow crack growth decreases by a factor of  $10^4$  when the density of *n*-butyl branches in an ethylene-hexane copolymer increases from 0 to 4.6 butyls/1000 C. It is the number of tie molecules and whether they are pinned that control the rate of crack growth which involves the disentanglement of the fibrils in the craze. Branching increases the number of tie molecules by decreasing the lamella thickness.

Defoor et al. (1992a) have fractionated a 1-octene linear low-density polyethylene (LLDPE) with a bimodal short-chain branching (SCB) distribution with respect to the SCB content using preparative temperature-rising elution fractionation (PTREF). They found that fractions exhibited a broad single melting endotherm in contrast to the multiple melting endotherms of the unfractionated copolymer. Defoor et al. (1992b) have also investigated the lamellar morphology of the above LLDPE and its fractions by using transmission electron microscopy and observed that branches of sufficient size restrict the formation of thick lamellae. It was found that branching content was the major factor determining the lamellar thickness, while the morphological structure of the lamellae depends both on the branching content and the molecular weight.

Channell et al. (1992) have studied the effects of SCB and MW on the impact fracture

toughness of PE. It was proposed that the increased toughness of LLDPE is due to the effect of SCB on the morphology and tie-molecule concentration. Liu and Baker (1992b) have investigated the effect of the length of the short chain branch on the impact properties of linear low density polyethylene. The impact strength, ductility and impact fatigue life were observed to increase with increasing branch length.

Showaib et al. (1995) have studied the effect of SCB on the viscoelastic behaviour during fatigue fracture of several medium density ethylene copolymers. It was hypothesized that the variance in the nature of chain entanglements associated with the respective branch type might be accountable for the observed differences of viscoelastic behaviour.

### **2.3 Crosslinking and Branching of Polypropylene**

For the sake of clarity in this thesis, the term "crosslinker" is referred to both polyfunctional monomers and other compounds called coagents, which are all capable of crosslinking PP.

#### **2.3.1 Irradiation Method**

There have been many publications on the radiation chemistry of PP. Only a brief outline of this field is given here since it is irrelevant to the objectives of this thesis.

Part of the interest in PP is derived from its being intermediate in structure between PE, which predominantly crosslinks, and polyisobutylene, which only degrades when subjected to ionizing radiation. Interest is also derived from the fact that PP can be obtained in three stereospecific forms and degrees of crystallinity. However, most of research efforts are concentrated on the irradiation of atactic and isotactic PP.

Under high-energy irradiation, PP is readily degraded by a radical mechanism and exhibits a ratio of chain scission to crosslinking, which varies from 0.8 to 1.0 (Salovey et al., 1963). This crosslinking efficiency for PP is much lower than that for polyethylene, where

the ratio of scission to linking could reach 0.2 to 0.3 (Chapiro, 1962). However, the presence of certain additives, usually polyfunctional monomers (O dian et al., 1968; Nojiri et al., 1985), can improve the crosslinking efficiency.

Several studies have been carried out on the properties of irradiated PP. Nedkov et al. (1991a) investigated the morphology of gamma-irradiated PP gels crystallized from xylene solutions. The insoluble part consisted of micro- and macrogel of crosslinked PP with low and irregular crosslinking density and it was found that the spherulites and crystallites had a high defect density. It has been shown that the rate of primary nucleation increases sharply at about 0.1 MGy and then remains constant, while the rates of secondary nucleation and lamellar growth decrease sharply with dose. It has been suggested that the number of the radiation defects is one of the factors affecting the rates of primary and secondary nucleation. Nedkov et al. (1991b) also studied the kinetics of melting and crystallization of the gamma-irradiated PP by means of DSC.

Recently, Scheve et al. (1990) have been able to produce the free-end long chain branched polypropylene by subjecting a high molecular weight, solid, linear polypropylene to ionizing radiation at an appropriate dose in a nitrogen environment. This product shows greatly enhanced elongational viscosity and characteristics of strain hardening which is usually believed to be particular to long chain branching.

### **2.3.2 Chemical Method**

The modification of polyolefins by peroxide including crosslinking, branching and degradation has become a powerful technology to control the physical and rheological properties of these polymers. However, different polyolefins exhibit different molecular structure changes when exposed to peroxides. At relatively high concentrations of peroxide, a tight network of crosslinked molecules may be formed in PE or PP. For PE, at relatively low concentrations of peroxide, the reactive modification will result in increased molecular



weight, broadening of the MWD and increased degree of long chain branching (Suwanda, 1992). On the other hand, for PP, the addition of relatively low concentrations of peroxide will only cause reduction in molecular weight and narrowing of the MWD. No branching reaction has been reported in this case.

The mechanism of the degradation in polypropylene is generally explained by the chain scission of unstable tertiary alkyl macroradicals (Beta-scission), while the crosslinking, branching and chain extension in polyethylene are due to the recombination of more stable secondary alkyl macroradicals. Therefore, at relatively low peroxide concentrations branched polyethylene chains may also be formed during the recombination.

Similarly, the addition of crosslinkers together with peroxides to PP can enhance remarkably the recombination reactions. One type of crosslinker commonly used is a polyfunctional monomer which converts some of the degradative tertiary macroradicals of PP to more stable secondary macroradicals, then acting as active sites for trapping other macroradicals (Borsig et al., 1981). When relatively high crosslinker concentrations are used, crosslinking will dominate the recombination reactions and a highly crosslinked structure will be formed.

Robinson (1966) studied the cross-linking of atactic polypropylene and atactic ethylene-propylene copolymer by dicumyl peroxide or di-tert-butyl peroxide. The cross-linking process was enhanced by the presence of a crosslinker such as diallyl phthalate, pentaerythritol triallyl ether, triallyl cyanurate and divinylbenzene.

Intensive studies on crosslinked PP have been done by Kunert and coworkers. NMR techniques have been used to compare chemically crosslinked PE and PP (Kunert et al., 1980). They have measured the mechanical properties of crosslinked LDPE and crosslinked PP (Kunert et al., 1981a), and also have investigated some physical and mechanical properties of the isotactic PP crosslinked by peroxides and quinone (Kunert et al., 1981b). The effect of time and temperature on the crosslinking of polypropylene with quinone was

studied by NMR (Kunert et al., 1983). Kunert (1982) also has used a Weissenberg rheogoniometer to investigate the dynamic mechanical behaviour of crosslinked LDPE (XLPE) and crosslinked PP (XLPP). The author found that by using very small strain amplitudes, the storage moduli of crosslinked LDPE and crosslinked PP as a function of crosslinking compound concentration showed very distinct extrema, which could be attributed to several different structures in these polymers.

Chodák and his coworkers have also done intensive studies on crosslinked PP. They studied the crosslinking efficiency of isotactic polypropylene as a function of the initiator and reaction temperature (Chodák et al., 1982). The decomposition rate of the initiator was found to be of prime importance for attaining the gel point. The overall efficiency of the process is strongly influenced also by the type of the primary radicals formed and the reaction temperature. Chodák et al. (1984) studied the crosslinking of polypropylene initiated by radicals formed either by thermal or by ultra violet decomposition of dicumyl peroxide. Chodák et al. (1986a) also studied the peroxide-initiated crosslinking of PP in the presence of p-benzoquinone. They found that the efficiency of benzoquinone is about 5 times higher than those of polyfunctional monomers. The thermo-oxidative stability of crosslinked PP was also studied (Chodák et al., 1986b). Chodák et al. (1991) studied the crosslinking of polypropylene initiated by peroxide in the presence of thiourea and it was found that longer heating times and higher temperatures led to smaller gel fractions. Increasing the amount of thiourea to 3% also decreased the degree of crosslinking, especially at higher temperatures and short reaction times.

Borsig et al. (1981) found that the efficiency of chemical crosslinking of isotactic polypropylene was dependent on the peroxide used. The presence of a polyfunctional monomer (pentaerythritol tetraallyl ether) enhanced the crosslinking efficiency. Jurkiewicz et al. (1982) used proton NMR in the solid state to characterize highly quinone-crosslinked PPs with the gel fraction varying between 70 and 90%. Using four spin probes, Hlouskova

et al. (1984) studied the isotactic PP crosslinked by dicumyl peroxide in sealed glass ampoules in an inert atmosphere. The crosslinked i-PP was found to contain 20-78 wt.% gel.

De Candia et al. (1990) have studied the drawing of crosslinked PP. Isotactic PP were crosslinked by tert-butyl perbenzoate and hydroquinone, and the materials were characterized by X-ray and DSC. It was found that structural and topological features play a significant role in drawing behaviour. The yielding, necking phenomenon, stress and strain at fracture, could be correlated with the sample structure.

Borsig et al. (1990) studied the crosslinking of isotactic polypropylene by thiourea and its derivatives in the presence of peroxide. They found that the crosslinking efficiency was significantly dependent on the ratio of peroxide to thiourea, and that thiourea derivatives used were less efficient than thiourea. Borsig et al. (1993) also studied the crosslinking of atactic polypropylene with molecular weight of 12,000 by pentaerythritol tetraallyl ether in the presence of peroxide.

In all studies reviewed up to this point, crosslinking experiments were performed mainly in glass ampoules. Recently, Thitiratsakul (1991) used a batch mixer to react isotactic PP with different polyfunctional monomers or coagents in the presence of peroxides. Pentaerythritol triacrylate (PETA), a polyfunctional monomer, was found to be superior to any other crosslinkers examined. Kim et al. (1993) also crosslinked isotactic polypropylene in a twin screw extruder by using peroxide and polyfunctional monomers using reactive extrusion and it was concluded that triacrylates (including PETA) were the most effective among the polyfunctional monomers used.

In summary, as indicated from this literature review, commercial branched PP has only been produced using an irradiation process. Chemical crosslinking of PP using crosslinkers in the presence of initiators leads to the formation of highly crosslinked materials due to the use of relatively high crosslinker and initiator concentrations, and most of these crosslinking processes have been completed using ampoules or other static methods.

## **CHAPTER 3**

### **REACTIVE EXTRUSION OF ACRYLIC ACID GRAFTED POLYPROPYLENE WITH HEXADECYLAMINE**

#### **3.1 Introduction**

As mentioned in Chapter 1, branched PP may be produced by the reaction between two functionalized linear PPs containing complementary functional groups. In this reaction, one of the functionalized PPs could be a linear material on which the functional groups are distributed randomly along the PP backbone, while the other PP with the complementary functional groups could be a terminally functionalized one. Randomly functionalized PPs have been commercially available for years and most of them contain acidic functionalities. Terminally functionalized PPs have been prepared either by using a living polymerization system (Doi et al., 1986), chain-transfer reactions (Shiono et al., 1992), or by the modification of the terminal vinylidene groups of PP which are prepared by special catalyst systems (Shiono et al., 1993). There have been terminally aluminated, boronated, hydroxylated, halogenated and aminated polypropylenes and some of them have been used in the synthesis of block copolymers (Doi et al., 1986). In principle, some of them can also be used to prepare branched PP through grafting reactions. Currently, terminal functionalization of PP through REX is being studied in our laboratory (Thompson et al., 1996). Unfortunately, all these terminally functionalized PPs are only available in small quantities and they are not easily accessible.

In this chapter, efforts to produce a branched PP by using a model system are described. This system involves a PP randomly functionalized with acrylic acid (PP-g-AA) along with a long chain alkyl amine used as a model molecule for terminally functionalized PP. Hexadecylamine was chosen because of two reasons: a) it has an amine group at one end

and the chain structure is close to the PP backbone, and b) it has a high boiling point. Reactions were carried out in solution and subsequently in the melt in a twin-screw extruder, and some properties of the materials produced were evaluated.

Polymers with acidic functionalities have been reacted with amines in the past. However, the objective of these studies was different from that of this study. In two patents (Kopchik, 1981; Hallden-Abberton et al., 1988), poly(methyl methacrylate) has been imidized through reactions with several short chain amines in twin screw extruders. In this reaction, the final product contained nitrogen in the form of 2,6-piperidinedione (glutarimide) units formed by ring closure of adjacent carboxylic acid units in the chain. No catalyst was used in this process. Diamines have also been reacted with acidic functionalized polymers in a rheomixer to produce crosslinked structures and the reactivity of primary, secondary and tertiary diamines has been studied (Song et al., 1992).

## **3.2 Experimental**

### **3.2.1 Materials**

The acidic functionalized polypropylene (Polybond-1002, melt index = 20, from BP Chemicals) was used as received and it contained 6 wt.% acrylic acid groups grafted on the polymer backbone. Hexadecylamine (boiling point = 322.5°C/760 mm Hg, obtained from Aldrich) was also used as received.

### **3.2.2 Solution Experiments**

To obtain a basic understanding of the reaction, experiments were first carried out in solution according to the following procedure. In a three-necked round bottom flask having a N<sub>2</sub> inlet and equipped with a stirrer and a condenser, Polybond-1002 was reacted with hexadecylamine in refluxing xylene at equal molar ratio of [-NH<sub>2</sub>]/[-COOH]. After the reaction, the solution was poured into four times its volume of hot tetrahydrofuran (THF)

under vigorous stirring and the precipitate was filtered and washed. This purification procedure was repeated three times. Then the product was dried in a vacuum oven at about 60°C for 48 hours. The previous purification procedure was considered to be adequate for the removal of the unreacted amine since no bands could be detected in the FTIR spectra of the purified polymers at 3330 and 3381  $\text{cm}^{-1}$ , which are due to the symmetric and asymmetric stretching vibrations of  $-\text{NH}_2$ .

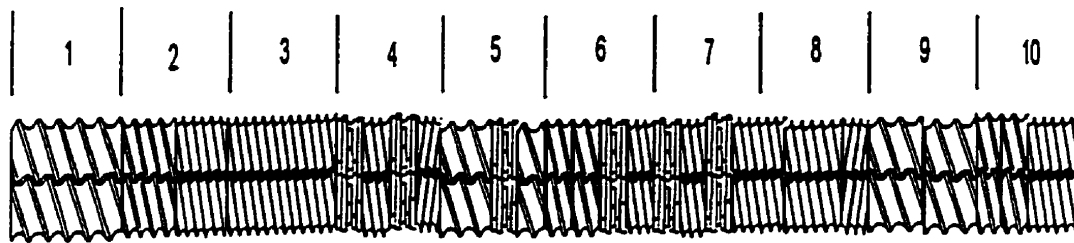
### 3.2.3 Reactive Extrusion Experiments

REX experiments were carried out in a Leistritz LSM 30.34 co-rotating intermeshing twin-screw extruder (ten zones plus a die) which was equipped with a Ktron LWFD5-200 loss-in-weight solids feeder and vacuum capacity (30 in. Hg vacuum). Possible volatile products and solvent were removed through a vent port at zone nine. The temperature at the first zone was kept low (about 70°C) by water cooling while the temperatures of the other zones were controlled at 200°C. The experiments were carried out at a screw speed of 100 rpm and a throughput of 24 g/min. The screw configuration and the extruder line are shown in Figs. 3-1 and 3-2.

Polybond-1002 pellets were fed into the extruder at the feed port. The hexadecylamine was dissolved in hot tetrahydrofuran (45%wt.) and injected into the extruder at the first conveying element of the fifth zone (open port) using a metering pump. Experiments were performed using molar ratios of  $[-\text{NH}_2]$  to  $[-\text{COOH}]$  in the range of 0 to 1.7. The pelletized products were dissolved in boiling xylene, poured into hot THF, and then filtered. The purification procedure was the same as the one used in the solution experiments.

### 3.2.4 Characterization

For FTIR spectroscopic analysis, films were obtained by dissolving the purified reaction products in chlorobenzene at the same concentration and casting similar amounts



- Zone 1: Solid feed of mixture of polymer powders or granules; conveying element
- Zone 2: Conveying and melting; conveying elements for moderate and high pressure generations
- Zone 3: Conveying and melting; conveying element for high pressure generation
- Zone 4: Shear mixing, conveying and creating back pressure for melt seal; kneading blocks, conveying and reverse elements
- Zone 5: Conveying and shear mixing; conveying elements and kneading blocks, feed of hexadecylamine in hot THF
- Zone 6: Conveying and shear mixing; conveying elements and kneading blocks, more pressure generated than in Zone 5
- Zone 7: Shear mixing and conveying; kneading blocks and conveying elements
- Zone 8: Conveying and creating back pressure for melt seal; conveying and reverse elements
- Zone 9: Devolatilization and conveying to remove gaseous products by vacuum
- Zone 10: Conveying elements
- Zone 11: Die exit. Not shown.

Fig. 3-1 Screw configuration of the corotating intermeshing twin screw extruder.

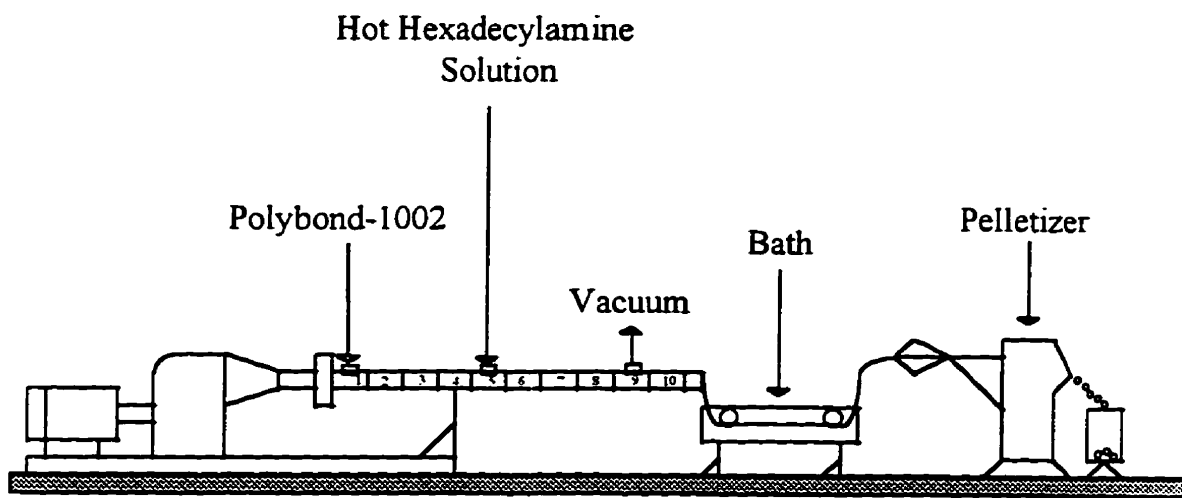


Fig. 3-2 Extruder line used for the reaction of Polybond-1002 and hexadecylamine.



of solution onto NaCl disks. These films were dried at 60°C in a vacuum oven for 24 hours and subsequently stored in a desiccator over phosphorus pentoxide. FTIR spectra were obtained on a Nicolet 520 FTIR Spectrometer with a resolution of 2 cm<sup>-1</sup>. Elemental analysis for nitrogen of the purified products was also performed by Guelph Chemical Laboratories Ltd. to obtain the nitrogen content in the products.

Shear viscosities of the virgin material and purified products were measured at 200°C using a Kayeness Galaxy V capillary rheometer with a die of L/D = 40. Linear viscoelastic properties were measured on a Rheometrics Mechanical Spectrometer at 200°C under 10% strain with parallel plate geometry (12.5 mm diameter and 2 mm thickness).

The glass transition temperatures ( $T_g$ ) were measured on a Perkin Elmer dynamic mechanical analyzer (DMA-7). Temperature scans were performed at 1.0 Hz from -120°C to 150°C by using the parallel plate measuring mode and a heating rate of 20°C/min. Before the temperature scans, the specimens were conditioned by heating to 140°C and holding at this temperature for 15 minutes. Thermal analysis on the purified samples from the reactive extrusion products was carried out with a TA Instruments thermoanalyzer equipped with a 2920 differential scanning calorimetric (DSC) cell under a helium environment. The DSC was calibrated with indium as the standard. Specimens were scanned from -60°C to 200°C, held at 200°C for 3 minutes, and then cooled to 40°C. The heating and cooling rates were 20°C/min and the sample weight used was around 2-4 mg. The first heating/cooling cycle was used to condition the samples and hence only the data of the second cycle are reported here. The information obtained from the DSC runs consists of a) the heat of fusion ( $\Delta H_m$ ), b) the melting temperature ( $T_m$ ), and c) the crystallization temperature ( $T_c$ ).

### **3.3 Results and Discussion**

#### **3.3.1 Solution Reaction**

The chemical composition of the reaction products was studied by FTIR

spectroscopy. The spectra of the virgin material and those of the solution reaction products are shown in Figs. 3-3a and 3-3b. There is a very strong band around  $1710\text{ cm}^{-1}$  in the spectrum of the virgin Polybond material (A), which is due to the carbonyl stretching vibrations of the acid groups. The band at  $841\text{ cm}^{-1}$  is due to the  $\text{CH}_3$  rocking vibrations mixed with C-C stretch vibrations on the PP backbone and can be used as an internal reference to compensate for the differences in sample thicknesses when comparing different spectra (Watanabe et al., 1989). Curve B corresponds to the virgin functionalized PP after heating in xylene for 12 hours without any hexadecylamine. It was found that the relative intensity of the bands at  $1710\text{ cm}^{-1}$  and  $841\text{ cm}^{-1}$  ( $A_{1710}/A_{841}$ ) did not change, indicating that there was no dehydration of the acid groups under the temperature used in the reaction experiments.

After the reaction, the band at  $1710\text{ cm}^{-1}$  almost disappeared in the spectra of all products, suggesting a very high consumption of the carboxyl groups. The spectrum of sample C (2 hours reaction time) shows a broad peak at around  $1717\text{ cm}^{-1}$  and a small shoulder at  $1700\text{ cm}^{-1}$  (Fig. 3-3b). The  $1717\text{ cm}^{-1}$  band is generally attributed to a carbonyl group that is hydrogen-bonded but not dimerized (Colthup et al., 1990), and in this case, it may be due to the interaction between the unreacted carboxyl group and the amide and/or imide formed. The small shoulder at  $1700\text{ cm}^{-1}$  is due to the carboxylic acid dimer band of the unreacted acrylic acids (Colthup et al., 1990). The presence of these two bands indicates that the acrylic acid groups had not been reacted completely. The small sharp bands at around  $1653\text{ cm}^{-1}$  due to the carbonyl vibration (amide I band) and at  $1540\text{ cm}^{-1}$  which is mainly due to bending mode of N-H mixed with the stretching vibration of C-N (amide II band), indicate the formation of the secondary amide (Nakanishi et al., 1977). The shoulder at about  $1733\text{ cm}^{-1}$ , and bands at around  $1696$  and  $1506\text{ cm}^{-1}$  indicate the formation of imide (Colthup et al., 1990). However, the band at  $738\text{ cm}^{-1}$  which is due to the NH wagging vibration of the imide, can not be observed in this spectrum, suggesting that the quantity of imide formed was

very small. The reactions between Polybond and hexadecylamine can be further confirmed by the presence of the characteristic band at around  $720\text{ cm}^{-1}$  which is due to the  $(\text{CH}_2)_n$  ( $n>4$ ) rocking mode introduced by hexadecylamine.

In spectrum D (4 hours reaction time), the band at around  $1717\text{ cm}^{-1}$  has become a weak shoulder. Meanwhile, a much more defined band at about  $1733\text{ cm}^{-1}$  (due to the carbonyl stretching vibration of imide) and the appearance of a weak band at  $738\text{ cm}^{-1}$  suggest that a larger amount of imide was formed. It was also noted that a small band appears at  $1675\text{ cm}^{-1}$  which may be due to the six-membered cyclic imide formed by the ring closure of adjacent homopolymerized acrylic acid units present in the acid grafted PP. The possible form of this cyclic imide is 2,6-piperidinedione (glutarimide) group similar to the product reported in the literature (Kopchik, 1981).

In the spectrum E (8 hours reaction time), the bands around the carbonyl region are similar to those in the spectrum D. However, the appearance of a shoulder at around  $1272\text{ cm}^{-1}$ , which may be mainly due to the C-N stretching vibration mixed with the bending vibration of N-H (amide III band), suggests an increase in the amount of amide formed. With longer reaction times up to 10 hours (spectrum F), the shoulder at  $1717\text{ cm}^{-1}$  has disappeared. Higher reaction conversions can also be inferred from the more significant bands at  $1272$ ,  $738$  and  $720\text{ cm}^{-1}$ .

The reactions between the acrylic acid grafted PP and hexadecylamine can approach equilibrium and reverse reactions may occur, if water (the by-product of the amidation and imidation reactions) is not removed from the system. This could be seen from the spectrum of a 12-hour product (spectrum G). It is found that the band at  $1717\text{ cm}^{-1}$  appears again and the band at  $1700\text{ cm}^{-1}$  becomes more significant. Meanwhile, the three bands at  $1272$ ,  $738$  and  $720\text{ cm}^{-1}$  become less significant or even disappear. This is an indication of the reversal of the reaction. Owing to the structure of the amine used, the imide groups formed do not contain N-H bonds. Hence, the absence of a strong band at  $3300\text{ cm}^{-1}$ , which is due to the

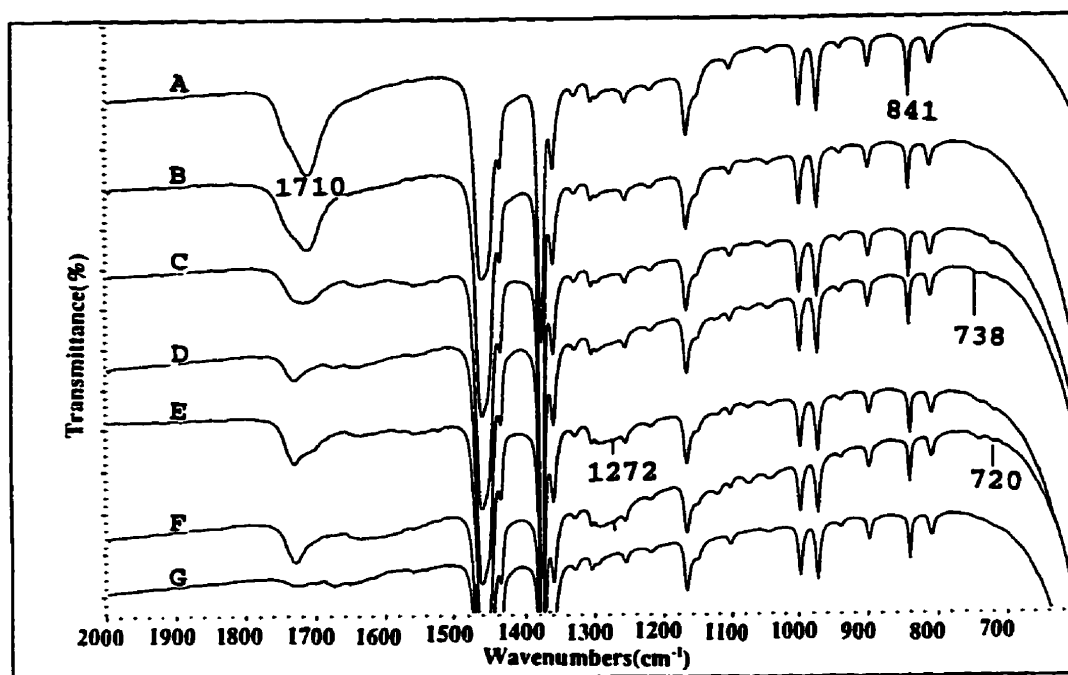


Fig. 3-3a FTIR spectra from 600 to 2000 cm<sup>-1</sup> of the virgin material and products reacted for different times in refluxing xylene. A: Polybond-1002; B: Polybond-1002 heated in xylene for 12 hours; C: 2 hours reaction time; D: 4 hours reaction time; E: 8 hours reaction time; F: 10 hours reaction time; G: 12 hours reaction time.

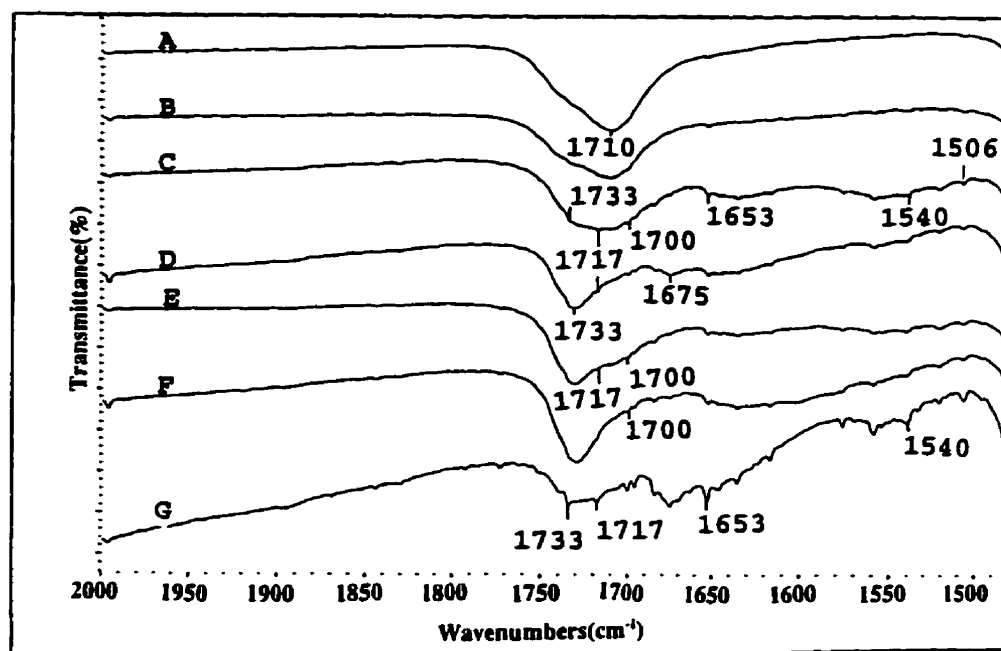


Fig. 3-3b FTIR spectra from 1500 to 2000 cm<sup>-1</sup> of the virgin material and products reacted for different times in refluxing xylene. A: Polybond-1002; B: Polybond-1002 heated in xylene for 12 hours; C: 2 hours reaction time; D: 4 hours reaction time; E: 8 hours reaction time; F: 10 hours reaction time; G: 12 hours reaction time.

N-H stretching vibrations, suggests that the concentration of amide groups is relatively low.

In summary, the reaction between acrylic acid functionalized PP and hexadecylamine in refluxing xylene at equal molar ratio of  $[-NH_2]/[-COOH]$  is a reversible reaction. Both amide and imide products could be formed in this case. To complete this reaction, water, the by-product of imidation and amidation reactions, should be removed out of the reaction system and this process can be assisted by the high temperatures and vacuum capacity of the extruder used.

### 3.3.2 Reactive Extrusion

#### FTIR Analysis

The spectra of the REX products are shown in Figs. 3-4a and 3-4b. The virgin acrylic acid functionalized PP was also extruded and analysed by FTIR (spectrum H). It was found that the relative intensity of  $A_{1710}/A_{841}$  decreased slightly after the extrusion. This suggests that the extrusion process may cause slight thermal dehydration of the acrylic acid groups. However, there were no significant peaks at 1858 and 1780  $cm^{-1}$  that are due to the carbonyl stretching vibration of the anhydride. This means that the quantity of anhydride formed was very small.

In the spectrum of the material produced at  $[-NH_2]/[-COOH]$  molar ratio of 0.3 (spectrum I), there is a strong broad band around 1717  $cm^{-1}$ , indicating that carboxylic acid groups had not been reacted completely. Again, the shoulder at 1733  $cm^{-1}$  and bands at 1696 and 1506  $cm^{-1}$  indicate the presence of a small quantity of imide. The presence of the bands at 1653 and 1540  $cm^{-1}$  are also indicative of the amide formation. At a molar ratio of 0.5 (spectrum J), it was found that the band at 1717  $cm^{-1}$  becomes weaker. Meanwhile the bands at 1653 and 1540  $cm^{-1}$  for amide seemed to be stronger. With further increasing the molar ratio to 1 (spectrum K), the band at 1717  $cm^{-1}$  becomes a weak shoulder and the band at 1733  $cm^{-1}$  becomes much more significant. These changes in the spectra suggest that the reaction

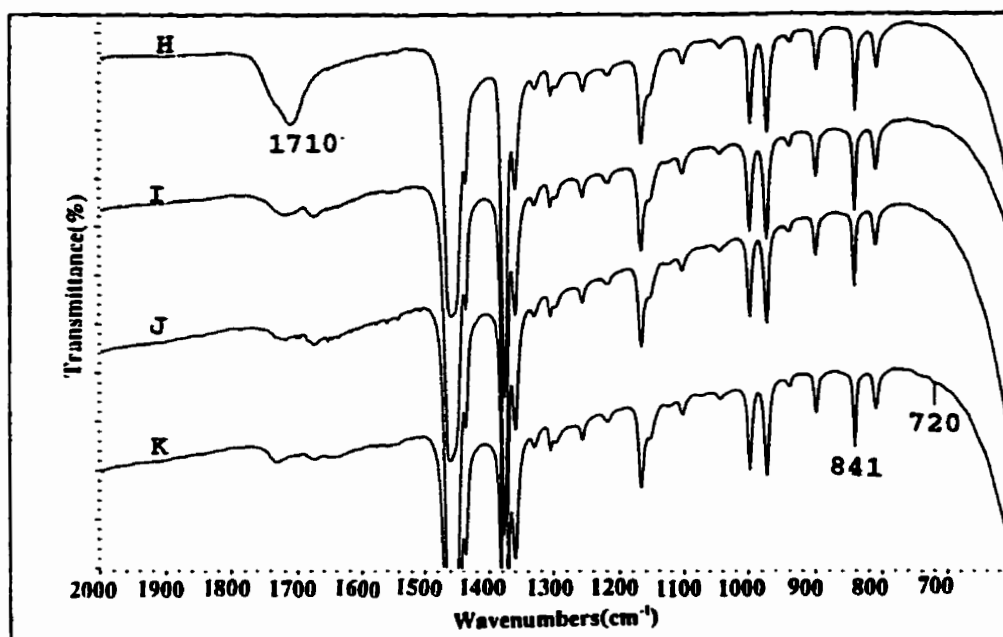


Fig. 3-4a FTIR spectra from 600 to 2000 cm<sup>-1</sup> of the REX products reacted at different molar ratios of [-NH<sub>2</sub>]/[-COOH]. H: Polybond-1002 extruded at 200°C; I: product at molar ratio of 0.3; J: product at molar ratio of 0.5; K: product at molar ratio of 1.

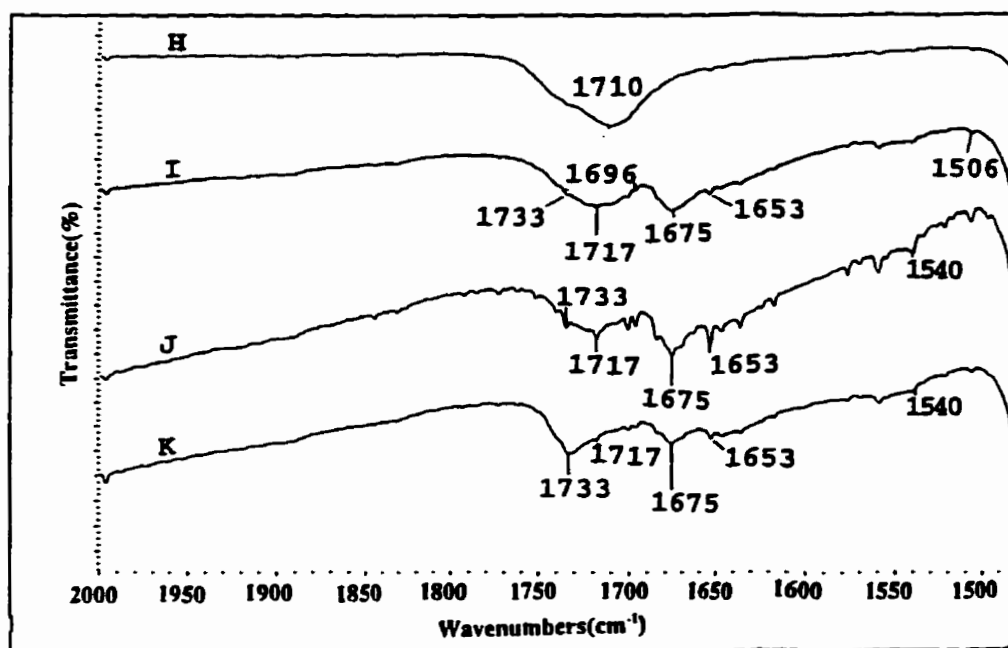


Fig. 3-4b FTIR spectra from 1500 to 2000 cm<sup>-1</sup> of the REX products reacted at different molar ratios of [-NH<sub>2</sub>]/[-COOH]. H: Polybond-1002 extruded at 200°C; I: product at molar ratio of 0.3; J: product at molar ratio of 0.5; K: product at molar ratio of 1.



between acrylic acid grafted on the PP backbone and hexadecylamine has proceeded to a higher extent. A similar spectrum was observed for the product at the molar ratio of 1.7 although it is not shown here. There is always a strong band at  $1675\text{ cm}^{-1}$  in the spectra of all the REX products even when the molar ratio used is very small. This may suggest that higher reaction temperature and the removal of the by-product in the reactive extrusion enhance the cyclic imidation of the carboxyl groups of the grafted polyacrylic acid chains. Another phenomenon observed in spectrum K is that there is not a band at about  $1272\text{ cm}^{-1}$ , which is due to the amide III band. This suggests that the reactive extrusion products contain more imide than amide compared with the solution reaction ones. Finally, as in the solution reaction results, there are no significant bands detected at around  $3300\text{ cm}^{-1}$ .

### Elemental Analysis

Results of elemental analysis on the purified products are shown in Fig. 3-5. It can be observed that initially the nitrogen content increases with the  $[-\text{NH}_2]/[-\text{COOH}]$  molar ratio, and it reaches a constant value at a molar ratio of about one. This phenomenon is consistent with the FTIR results.

### DMA Measurements

DMA measurements were carried out for the samples produced at  $200^\circ\text{C}$  and the results are summarized in Table 3.1. The attachment of small amount of alkyl chains appears to lower the  $T_g$  when the molar ratio of  $[-\text{NH}_2]/[-\text{COOH}]$  varies from 0 to 1.0. However, the  $T_g$  is almost unchanged when the ratio is further increased to 1.7. The decrease in  $T_g$  can be explained by a) the higher concentration of the chain ends due to the attachment of alkyl chains and the associated increased free volume, and b) the less polar environment resulting from the reaction, which may weaken the interactions between the chains and hence would favour the motion of the PP segment.

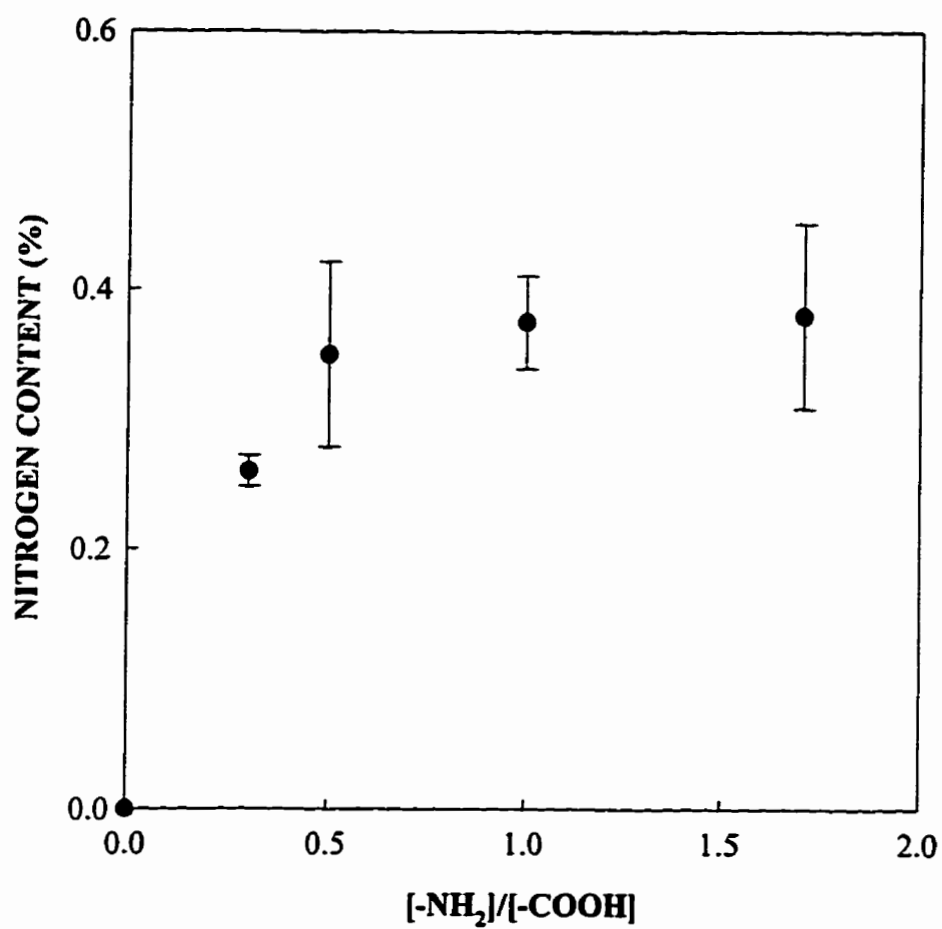


Fig. 3-5 Nitrogen content elemental analysis results of the reactive extrusion products.

**TABLE 3.1:  $T_g$  of the REX Products Produced at 200°C**

Sample	[-NH <sub>2</sub> ]/[-COOH] Molar Ratio	$T_g$ (°C)
Polybond	0.0	16.0
PB6	0.3	14.5
PB5	0.5	9.0
PB1	1.0	6.5
PB7	1.7	7.0

### Shear Viscosity

Results from the shear viscosity measurements are shown in Fig. 3-6 for the samples produced at 0, 0.5 and 1.7 [-NH<sub>2</sub>]/[-COOH] molar ratios. At low shear rates the viscosity increases with an increase in the concentration of the alkyl amine. This seems reasonable since the attachment of the alkyl chain to the polymer backbone is favoured at higher amine concentrations, as suggested by the FTIR results. These data suggest that the zero-shear viscosity ( $\eta_0$ ) increases as the reaction progresses. A Carreau model

$$\frac{\eta - \eta_\infty}{\eta_0 - \eta_\infty} = [1 + (\lambda \dot{\gamma})^2]^{\frac{n-1}{2}} \quad (3-1)$$

was fitted to the data and Table 3.2 lists the estimated values of the model parameters. It can be seen that although the power-law index ( $n$ ) and the infinite-shear rate viscosity ( $\eta_\infty$ ) remain almost constant, the zero-shear rate viscosity ( $\eta_0$ ) and the characteristic time ( $\lambda$ ) increase with the amine concentration in the feed as expected.

### Viscoelastic Measurements

The storage and loss moduli of the virgin material and the sample produced at 1.7 of

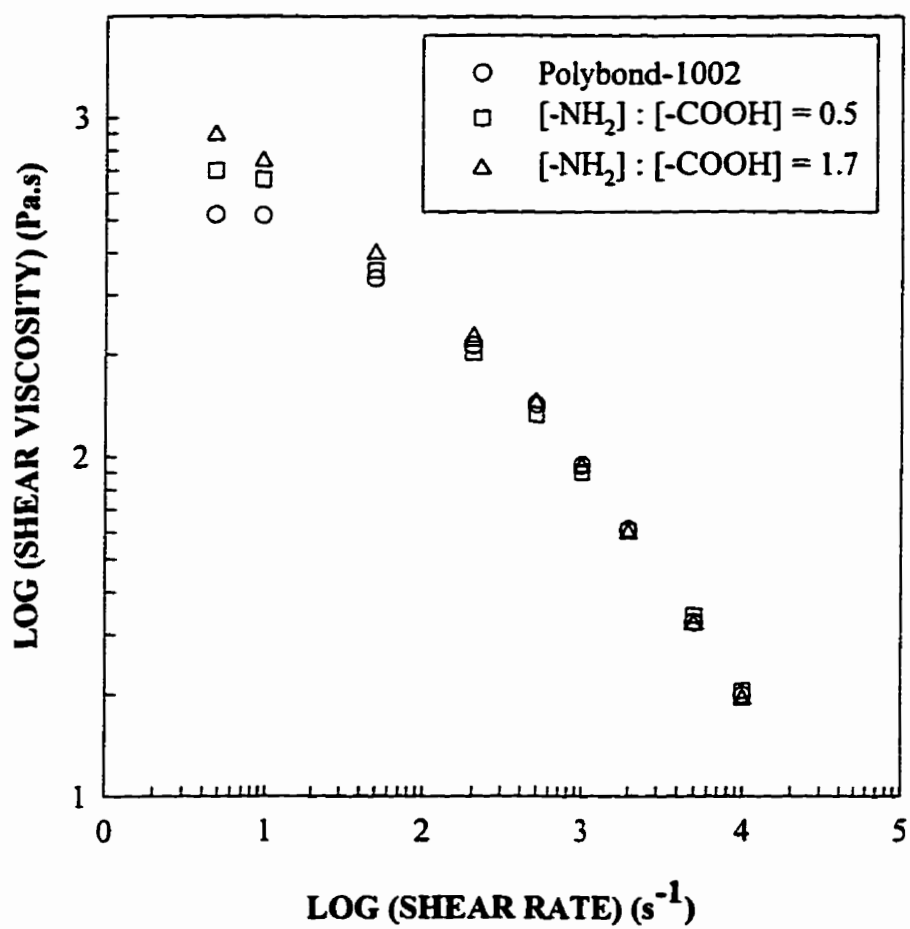


Fig. 3-6 Shear viscosities of Polybond-1002 and the REX products at 200°C.

**TABLE 3.2: Estimates of Carreau Model Parameters**

$[-NH_2]/[-COOH]$ molar ratio	$\eta_0$ (Pa.s)	$\eta_∞$ (Pa.s)	$\lambda$ (s)	n
0.0	530	$5.0 \times 10^{-7}$	0.05	0.56
0.5	730	$1.7 \times 10^{-7}$	0.08	0.53
1.7	970	$4.0 \times 10^{-7}$	0.15	0.55

the  $[-NH_2]/[-COOH]$  molar ratio are shown in Fig. 3-7. It can be seen that as a result of the attachment of the alkyl side chains, the moduli of the reacted material are higher than those of the virgin one. This result might be attributed to the attachment of branches.

### DSC Analysis

Fig. 3-8 shows the DSC melting endotherms of the virgin Polybond, extruded Polybond and the REX products. It can be seen that there is a single melting peak and a small shoulder in the DSC traces of the virgin Polybond and its extrudate. The peak is due to the melting of the PP crystals while the shoulder may be due to the melting of the less crystallizable PP species generated by the grafting of acrylic acid units (monomeric and/or polymeric). The grafted polyacrylic acid chains, if any, are non-crystallizable and hence there should not be a melting peak for it in the DSC traces. In contrast to the relatively linear virgin materials, there are two sharp melting peaks  $T_{m1}$  (the higher melting peak) and  $T_{m2}$  (the lower melting peak) in the DSC traces of all the model branched PPs. Since the alkyl chains with 16 carbon atoms are able to crystallize, the presence of  $T_{m2}$  is mainly due to the introduced alkyl branches. Only a single crystallization peak ( $T_c$ ) is observed for the virgin material, its extrudate and model branched PPs in their crystallization thermograms (Fig. 3-9).

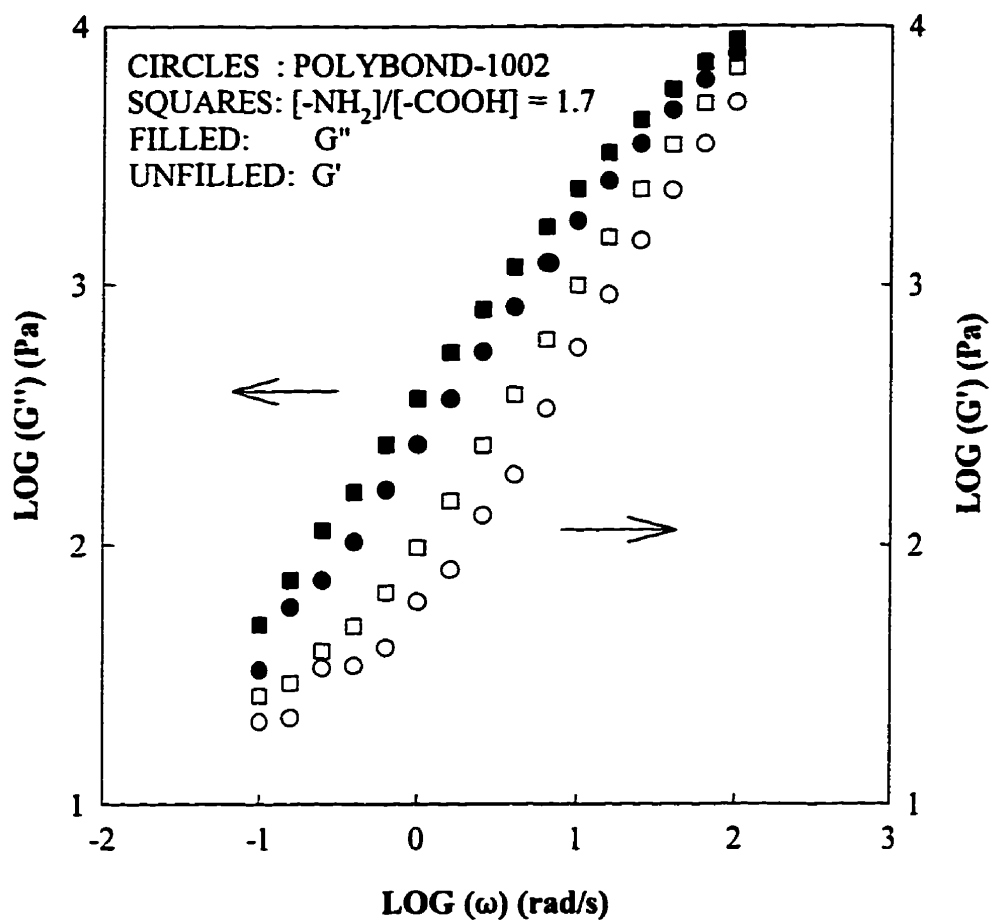


Fig. 3-7 Frequency dependence of storage and loss moduli of Polybond-1002 and the reactive extrusion product at a  $[-NH_2]/[-COOH]$  molar ratio of 1.7 (200°C).

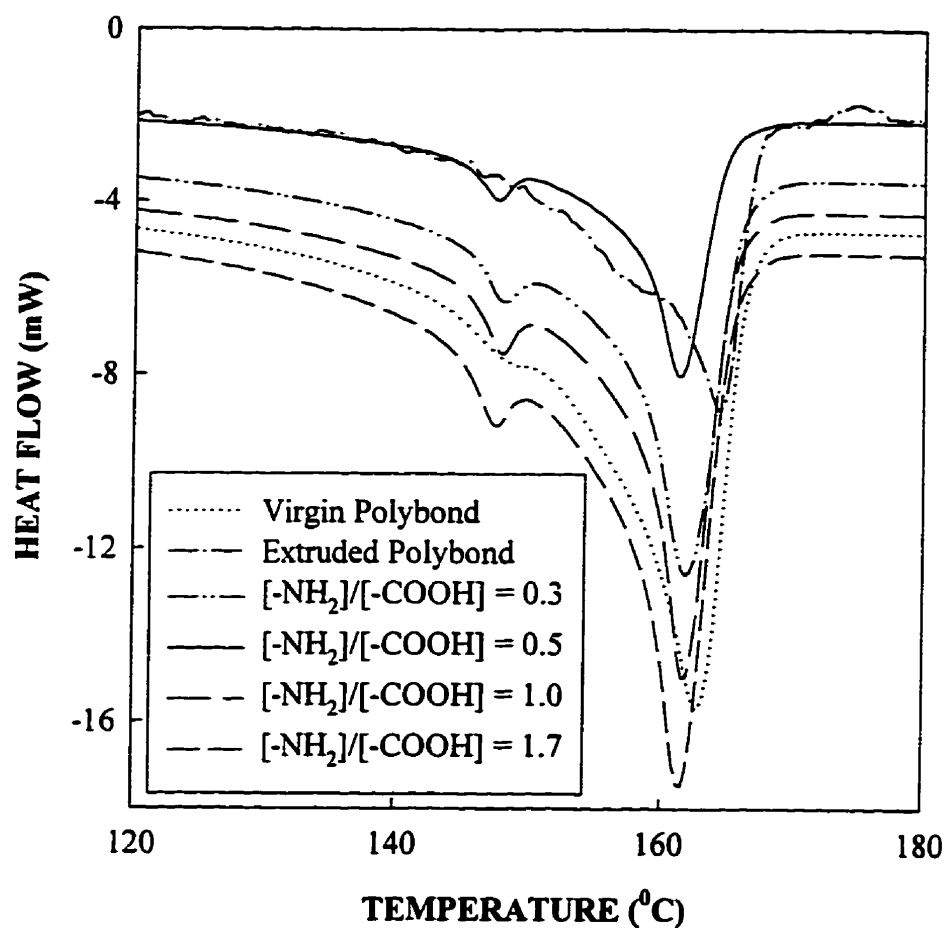


Fig. 3-8 DSC melting endotherms of the virgin Polybond-1002 and reactive extrusion products at different  $[-\text{NH}_2]/[-\text{COOH}]$  molar ratios. 1: virgin Polybond; 2: extruded Polybond; 3: product at the ratio of 0.3; 4: product at the ratio of 0.5; 5: product at the ratio of 1.0; 6: product at the ratio of 1.7.

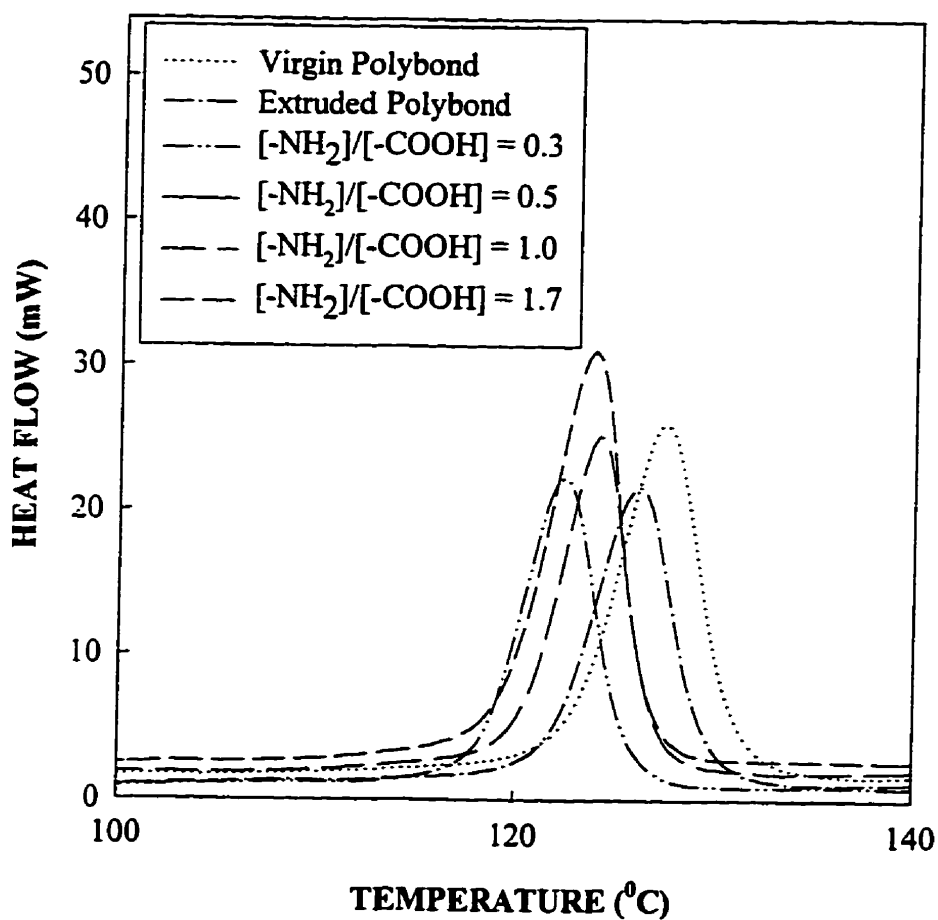


Fig. 3-9 DSC crystallization exotherms of the virgin Polybond-1002 and reactive extrusion products at different  $[-\text{NH}_2]/[-\text{COOH}]$  molar ratios. 1: virgin Polybond; 2: extruded Polybond; 3: product at the ratio of 0.3; 4: product at the ratio of 0.5; 5: product at the ratio of 1.0; 6: product at the ratio of 1.7.



The DSC analyses are summarized in Table 3.3. The  $T_{m1}$  and  $\Delta H_{m1}$ s of the branched PPs seem to be slightly lower than those of the virgin Polybond and its extrudate and this is consistent with the observation for linear and branched polyethylenes (Mark et al., 1993). The differences in  $T_{m1}$ s are small due to the relatively short branches attached. The effect of introducing branches can also be reflected in the decrease of  $T_{m2}$ . The  $T_c$ s of the branched PPs are lower than those of the virgin Polybond and its extrudate, which is in agreement with the observation of Borsig et al. (1989). The sensitive response of  $T_c$  to the change in molecular structures is similar to observations in the literature (Foreman et al., 1996).

**TABLE 3.3: DSC Analysis of the Model Branched PPs<sup>1</sup>**

Sample	[-NH <sub>2</sub> ]/[-COOH] molar ratio	T <sub>m</sub> (°C)		ΔH <sub>m</sub> (g/J)		T <sub>c</sub> (°C)
		T <sub>m1</sub>	T <sub>m2</sub>	ΔH <sub>m1</sub>	ΔH <sub>m2</sub>	
Polybond	0.0	162.84	149.46 <sup>2</sup>	112.3	---	127.40
EPB <sup>3</sup>	0.0	162.11	---	112.1	---	125.96
PB6	0.3	161.99	148.15	111.40	1.58	122.47
PB5	0.5	161.47	147.41	108.20	2.82	123.27
PB1	1.0	161.68	147.70	114.90	2.35	123.95
PB7	1.7	161.79	147.53	111.40	2.07	123.86

1: All the data in Table 3.3 represent the average value of two DSC samples

2: Shoulder temperature

3: Extruded Polybond-1002 under the reaction conditions

### 3.4 Conclusions

Analysis of the FTIR spectra of the samples produced in the solution experiments at an equal molar ratio of [-NH<sub>2</sub>]/[-COOH] without catalyst addition and without removal of the by-product, revealed that the formation of imide was increased with increasing the

reaction time up to 10 hours, while a further increase in reaction time resulted in a reversal of the reaction. In the REX experiments, FTIR analysis showed that imide formation increased with the  $[-\text{NH}_2]/[-\text{COOH}]$  molar ratio. At a molar ratio of one, more imide was present in the REX product than in the solution one. Elemental analysis suggested that the nitrogen content in the products initially increased with  $[-\text{NH}_2]/[-\text{COOH}]$  molar ratio and then reached an almost constant value at a molar ratio value of about unity. The glass transition temperature ( $T_g$ ) was measured by dynamic mechanical analysis (DMA), and it was found that the attachment of the alkyl chains caused a reduction in  $T_g$  of the products. Finally, rheological measurements showed that the zero-shear viscosity of the products increased with the amine/carboxyl molar ratio and that their moduli were enhanced probably due to the attachment of the alkyl side chains. Two melting peaks were detected in the DSC traces of the model branched PPs and their crystallization temperatures were lower than that of the starting material.

## CHAPTER 4

### CHEMICAL MODIFICATION OF PP WITH PEROXIDE/PETA THROUGH REACTIVE EXTRUSION

#### 4.1 Introduction

In Chapter 3, model branched PPs were produced by reacting a randomly functionalized PP and hexadecylamine. However, the branches introduced are considered short in terms of the long chain branching (LCB) concept, which usually regards long branches to be of the same order of length as the main chain. A very low level of long chain branching will have a significant effect on the rheological properties of polymers.

As mentioned in Chapter 2, Scheve et al. (1990) produced long chain branched PP by irradiating a solid, high molecular weight linear PP in a nitrogen environment and the product exhibited melt strain hardening behaviour. Another route to branching PP may be through the recombination reactions in which PP molecules react with a polyfunctional monomer in the presence of a peroxide. This approach is based on the fact that for PP/peroxide systems, and at relatively low concentration of a peroxide, primary radicals generated by a peroxide will abstract preferentially the tertiary hydrogens from the PP backbone, forming tertiary PP macroradicals which are unstable and degrade through  $\beta$ -scission (Borsig et al., 1981; Xanthos, 1992). However, addition of a polyfunctional monomer to such a system can convert some of the tertiary macroradicals to the more stable secondary macroradicals which tend to undergo recombination rather than scission (Borsig et al., 1981; Borsig et al, 1993). During this process, in addition to degradation PP chains may be extended, branched or even crosslinked simultaneously.

As discussed in Chapter 2, much work has been done on extensive crosslinking of PP by using polyfunctional monomers or coagents in glass ampoules. Recently, Thitiratsakul

(1991) reacted isotactic PP with different polyfunctional monomers or coagents in a batch mixer mainly at 175°C using various peroxides. Peroxides were used at three relatively high concentrations (1000, 5000 and 10000 ppm) and from the torque data during the reactions, pentaerythritol triacrylate (PETA) was found to be superior to any other crosslinkers examined. It was concluded qualitatively from gel permeation chromatography (GPC) that PP was branched during the reactions. However, no other properties of either the whole polymers or their sols were studied. Kim et al. (1993) also crosslinked an isotactic PP at 230°C using a twin-screw extruder and four crosslinkers respectively, in the presence of 1,3-bis(t-butylperoxy-isopropyl) benzene. No separation of gels was performed in this work and the whole products were analyzed in terms of melt flow index (MFI), mechanical properties and differential scanning calorimetry (DSC). It was concluded that triacrylates (including PETA) were the most effective among the polyfunctional monomers tested.

In this thesis, pentaerythritol triacrylate (PETA) and 2,5-dimethyl-2,5-di(t-butylperoxy) hexane (Lupersol 101 or L101) were used in an effort to produce a long chain branched PP via reactive extrusion. The objectives were to study the effects of the PETA/peroxide relative concentrations on material properties and to characterize the existence of long chain branching (LCB) in the modified PPs. It was hoped that this approach could be applied to commercial PP where stabilizers are usually present. The branched PP produced by Montell (designated as Montell PP) as described by Scheve et al. (1990) was also analyzed as a benchmark material.

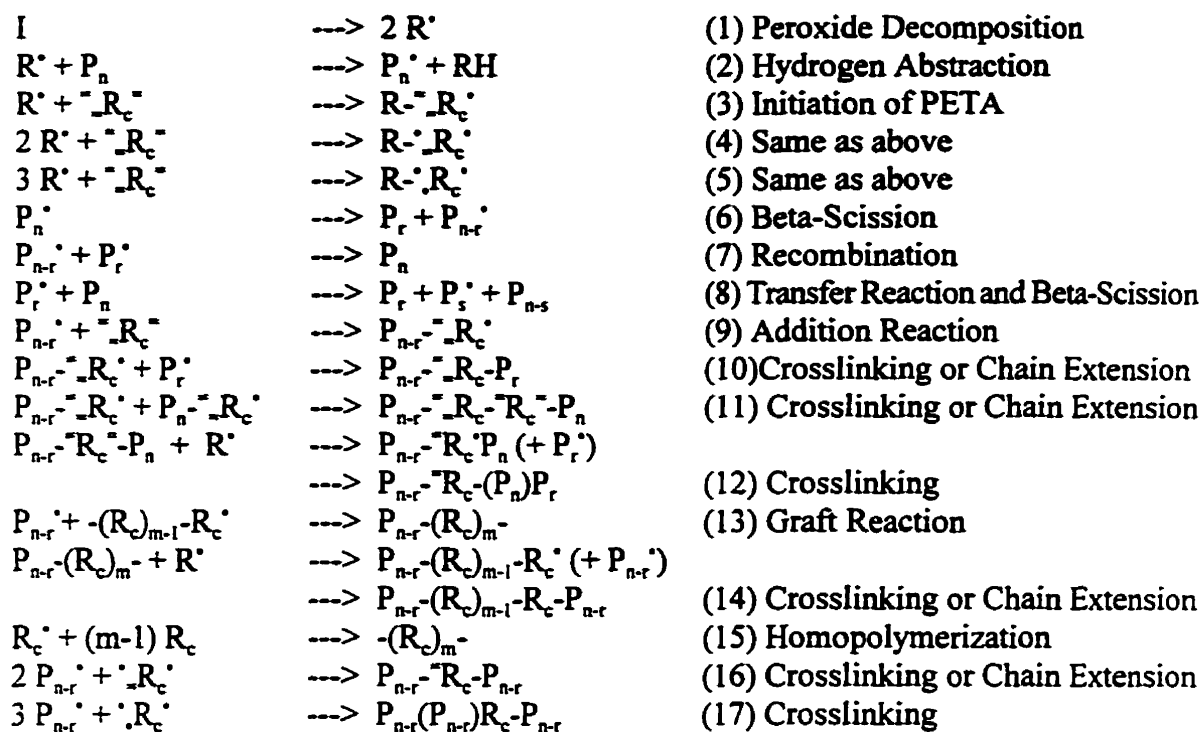
The development of long chain branched PP was composed of two stages. In stage 1, preliminary experiments were carried out on the reactive extrusion of unstabilized isotactic PP with PETA and L101. The unstabilized system was chosen at this stage in an attempt to avoid the possible interference of the stabilizers with the reactions. The objectives of this stage were to search for a suitable REX process and PETA/L101 concentrations that lead to branching. Based on the results of stage 1, further REX experiments in stage 2 were carried

out at very low concentrations of PETA and L101 in a stabilized system using a new REX process. Some characterization results of the whole polymers, their sols and macrogels are presented in this chapter. More characterization data for the thermal, molecular and rheological properties of the whole polymers or sols will be given in Chapters 5, 6, 7 and 8.

Finally, "crosslinking" of PP in this work refers to the trifunctional long chain branching resulting from a recombination of two PP macroradicals. The modified PPs with limited degree of crosslinking, are actually highly branched but still soluble polypropylenes. In this system, besides the insoluble highly crosslinked PP possibly formed, the PETA monomer may also form an insoluble homopolymer. Thus, the term "macrogel" refers to any insoluble portion which may consist of insoluble highly crosslinked PP and/or the homopolymer of the PETA monomer. "Chain extension" occurs when the terminal radicals of two macromolecules recombine.

#### **4.2 Postulated Reaction Scheme**

The postulated reactions between PP macromolecules, PETA and peroxide radicals are shown in Fig. 4-1. Two primary radicals ( $R^{\cdot}$ ) are formed in the initiation step (reaction 1) which can abstract tertiary hydrogen atoms from the PP backbone and form tertiary PP macroradicals (reaction 2). They can also initiate PETA molecules and hence result in PETA monomer radicals. Due to the molecular structure of PETA, several kinds of monomer radicals could be formed (reactions 3-5). The tertiary PP macroradicals are unstable and as a result a  $\beta$ -scission reaction takes place which leads to the production of shorter polymer chains (reaction 6). The PP macroradicals could also recombine together (reaction 7), or transfer to another PP chain (reaction 8). Simultaneously, a PETA molecule may add to the tertiary PP macroradical to form a more stable secondary radical (reaction 9). The recombination of the secondary macroradicals with tertiary PP macroradicals leads to crosslinking or chain extension (reaction 10). Secondary macroradicals may also combine



### Descriptions

$I$ & $R^{\cdot}$	Peroxide and primary radical respectively
$=$	A double bond of PETA
$P_n, P_r$ or $P_{n-s}$	PP macromolecule of n,r or n-s monomer units
$P_n^{\cdot}, P_{n-r}^{\cdot}$ or $P_s^{\cdot}$	Tertiary PP macroradical of n,n-r or s monomer units
$\text{---}R_c\text{---}$ or $R_c$	PETA molecule with three double bonds
$R\text{---}R_c^{\cdot}$	PETA radical with one double bond initiated
$R\text{---}R_c^{\cdot}$ or $\text{---}R_c^{\cdot}$	PETA radical with two double bonds initiated
$R\text{---}R_c^{\cdot}$ or $\text{---}R_c^{\cdot}$	PETA radical with three double bonds initiated
$P_{n-r}\text{---}R_c^{\cdot}$	Secondary alkyl radical attached to PP backbone or at the chain ends
$R_c^{\cdot}$	All kinds of PETA monomer radicals
$\text{---}(R_c)_m\text{---}$	PETA homopolymer
$\text{---}(R_c)_{m-1}\text{---}R_c^{\cdot}$	Chain radical consisting of m PETA monomer units
$P_{n-r}\text{---}(R_c)_m\text{---}$	PP grafted with PETA chain of m monomer units
$P_{n-r}\text{---}R_c\text{---}P_n$	PP linked by PETA molecule

Fig. 4-1 Possible reactions between PP, PETA and peroxide.

together (reaction 11). The products of reaction 10 and/or 11 could further react and lead to crosslinking as shown in reaction 12.

The PETA monomer radicals may propagate to form a chain radical, which could combine with PP macroradicals to form grafted PETA homopolymer (reaction 13). The products of reaction 13 may further react as shown in step 14. PETA chain radical may also terminate without other reactions to form PETA homopolymer (reaction 15). The PETA monomer radicals in reaction 4 or 5 may recombine with PP macroradicals to form products of chain extension or crosslinking (reactions 16 and 17). Another important reaction which is not shown in Fig. 4-1, is that the peroxide radical  $R'$  can also attack the main PP backbone and/or the PP branch in any product resulting from these main reactions. This may have a significant effect on the length of the branches formed and hence the rheological properties of the products.

Based on the postulated reaction scheme, the resulting four possible molecular structures of polypropylene are represented in Fig. 4-2. It should be noted that all these four structures may be present simultaneously in the products, i.e., the system structure becomes heterogeneous after the REX step.

### **4.3 Experimental**

#### **4.3.1 Materials**

Additive-free isotactic polypropylene powder (KY6100) was supplied by Shell Canada. The MFI of this PP was 3 when measured with 1.0%wt Irganox 1010. 2,5-dimethyl-2,5-di(*t*-butylperoxy) hexane (Lupersol 101 or L101) was obtained from Elf Atochem North America, Inc., and pentaerythritol triacrylate (PETA), containing 100 ppm hydroquinone monomethyl ether as inhibitor was obtained from Aldrich company. Both L101 and PETA were used as received and their molecular structures are shown in Appendix A. Irganox 1010, which is tetrakis[methylene-3-(3',5'-di-*t*-butyl-4'-hydroxyphenyl)propionate] methane,

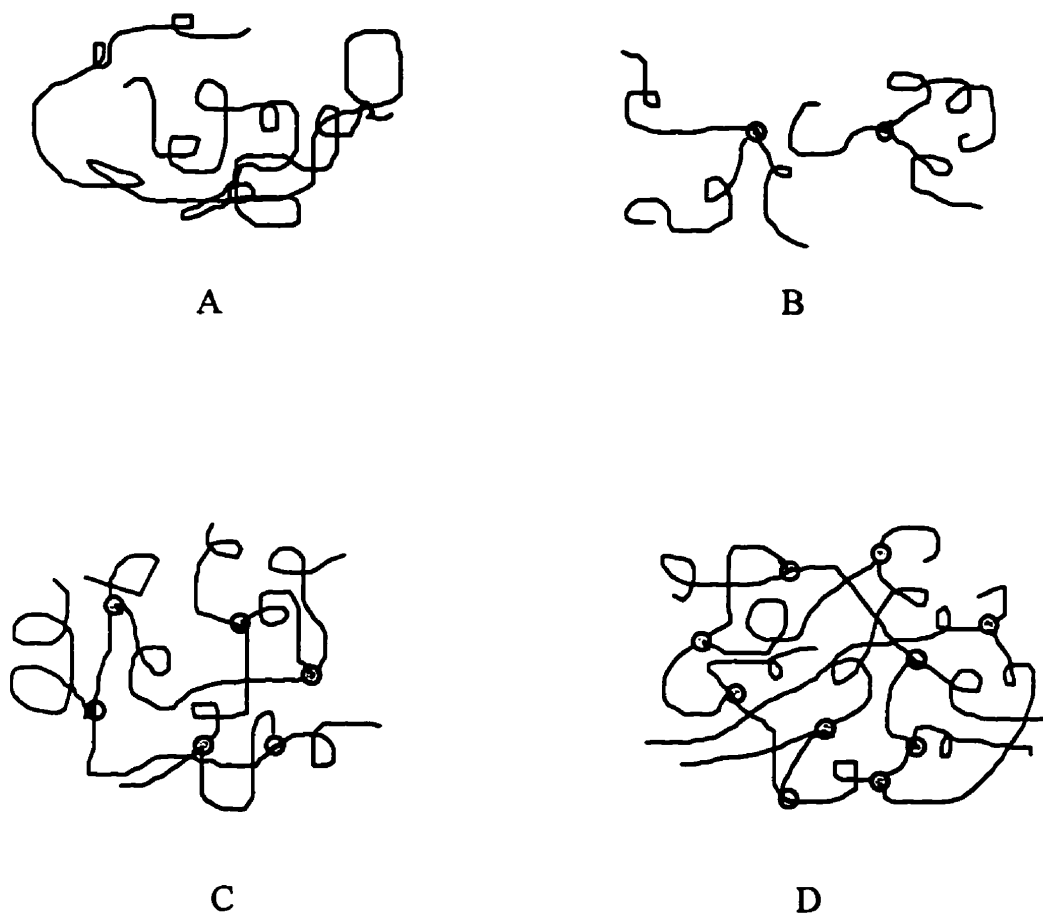


**Fig. 4-2** Possible Molecular Structures of the Products. A: Linear, B: Branched, C: Branched-Crosslinked (Loose Network), D: Tight Network.



was obtained from Ciba Geigy Co. and its molecular structure is also shown in Appendix A. Branched PP from Montell (Montell PP) was used as received and its MFI was 0.5.

#### **4.3.2 Reactive Extrusion**

The same twin-screw extruder setup presented in Chapter 3 and the configuration shown in Fig. 3-1 were used in both stages 1 and 2. Based on preliminary REX experiments at 200°C, a throughput of 1.4 kg/h and a screw speed of 60 rpm would be suitable to reduce the degradation of PP and provide sufficient mixing for the current reaction system (Wang et al., 1994). At the chosen operating conditions, the average residence time was estimated to be about 75 seconds by using a high molecular weight PP as a tracer. This average residence time was adequate for L101 used ( $t_{1/2} = 18.6$  seconds at 200°C) to complete about 95% decomposition. Throughout the two stages, the reactant solution was injected into the extruder using a FMI (Fluid Metering Inc., Oyster Bay, NY) metering pump which injects liquid reactants in a pulse mode. The precision of the injection rate was around  $\pm 1\%$  of the setpoint on an average basis within the sampling period. The homogeneity of the REX products were assured by observing the following: a) before the injection of the reactant solution, both the extruder and the feeder were run for twenty minutes under the REX conditions in order to ensure that the whole extruder system had reached a steady state, b) the samples were collected only after 15 minutes of the continuous injection of the reactants, c) during the REX runs, the injection rate was monitored at about every two minutes.

#### **Reactive Extrusion Process - Stage 1**

The extruder line in stage 1 is shown in Fig. 4-3. In this stage, the PP powder was mixed with a peroxide master batch to obtain the desired peroxide concentrations before REX runs. Three peroxide concentrations (200, 600 and 1000 ppm) were used and the PETA concentration employed was varied from 0.00 wt.% to 5.00 wt.%. PETA was dissolved in

acetone at the concentration of 20 wt.%. During the REX runs, PETA solution was injected into the extruder at the feed port using the metering pump.

### **Reactive Extrusion Process - Stage 2**

The extruder line in stage 2 is shown in Fig. 4-4. The main differences between the REX processes of stage 1 and stage 2 are: a) In stage 2, PP powder was stabilized with 1 wt.% of Irganox 1010 before REX, b) PETA and peroxide were dissolved together in acetone at the concentration of 20 wt.% and cooled in an ice bath while being injected into the extruder, c) The reactants were injected directly into the melt at the conveying element of the fifth zone, where a homogeneous PP melt may have been achieved, d) Based on the results of stage 1, very low peroxide concentrations (50, 100, 150 and 200 ppm) and low PETA concentrations (0.0 wt.%, 0.5 wt.%, 1.0 wt.%, 2.0 wt.% and 3.0 wt.%) were used in stage 2.

#### **4.3.3 Methods**

Flow properties of the whole polymers produced were measured using a Kayeness Galaxy V capillary rheometer. The melt flow index (MFI) was measured at 230°C using a load of 2.16 kg according to the ASTM D-1238-86T standard. The shear viscosity was measured at 230°C using a die of  $L/D = 40$  ( $D = 0.02''$ ) and the Rabinowitsch correction was applied to the data. In stage 2, shear viscosity was measured at 210°C using a die of  $L/D = 40$  ( $D = 0.03''$ ) and no further stabilizer was added to the samples. Again the Rabinowitsch correction was applied to the data.

In stage 1, the amount of the insoluble portion (macrogel) in the samples was determined by Soxhlet extraction in refluxing xylene containing 0.1 wt.% of hydroquinone as the antioxidant for 48 hours. In stage 2, the macrogel amount of the REX products was determined by Soxhlet extraction in refluxing xylene containing 1.0 wt.% of Irganox 1010 as the antioxidant for 72 hours. After the extraction, the hot solution was poured into four

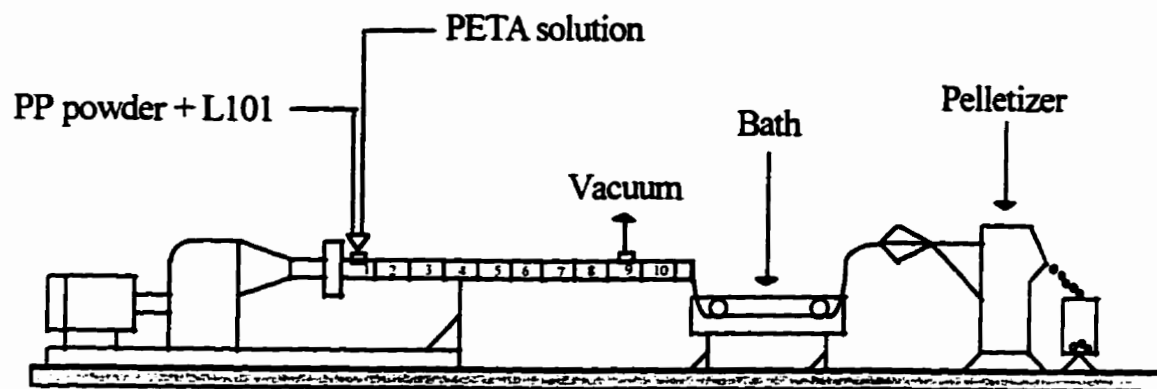


Fig. 4-3 Extruder line used for the PETA/peroxide modification of polypropylene by REX (Stage 1).

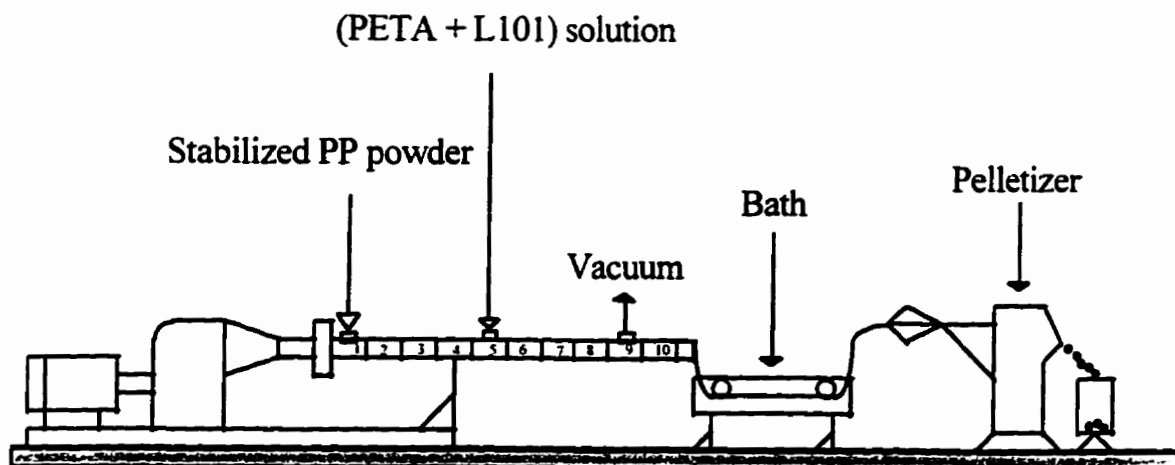


Fig. 4-4 Extruder line used for the PETA/peroxide modification of polypropylene by REX (Stage 2).

times its volume of acetone under vigorous stirring and the precipitate was filtered and washed with acetone. After drying, the sols were dissolved in xylene, precipitated and washed again. This purification procedure was repeated for three times. The purified sols were dried under vacuum at 60°C for 24 hours and consecutively used for further measurements. Montell PP was also extracted under this condition and it was found that there is no macrogel in it.

FTIR spectra of the purified sols were obtained using a Nicolet 520 FTIR spectrometer. Samples were dissolved in chlorobenzene and then cast onto NaCl disks. Films were formed by drying at 60°C under vacuum for 24 hours and then they were stored in a desiccator over phosphorus pentoxide before the measurement.

Thermal analyses on the purified sols of stage 1 were carried out with a TA Instruments thermoanalyzer equipped with a 2920 differential scanning calorimetric (DSC) cell under a helium environment. The DSC was calibrated with indium as the standard and no stabilizer was added to all the samples measured. Specimens were scanned from -60°C to 200°C, held at 200°C for three minutes, and then cooled to 40°C. The heating and cooling rates were 20°C/min and the same sample weight ( $4.12 \pm 0.02$  mg) was used throughout the DSC experiments. For all the experiments, the first heating/cooling cycle was used to condition the samples and hence only the data of the second cycle are reported here. The information obtained from the DSC runs consists of a) the heat of fusion ( $\Delta H_m$ ), b) the melting temperature ( $T_m$ ) and the melting range which is represented by the halfwidth of the melting peak (qualitative information only), and c) the crystallization temperature ( $T_c$ ).

The macrogels of stage 2 were also dried under the above similar conditions and some of them were analyzed using DSC. Again the DSC unit was calibrated with indium as the standard. All specimens were scanned from 40°C to 200°C at a heating rate of 20°C/min. Most of the sample weights ranged from 4.5 to 7.0 mg. The first heating cycle was used to condition the samples and only the data of the second cycle are reported here. The

information obtained consists of the heat of fusion ( $\Delta H_m$ ) and the melting temperature ( $T_m$ ).

In this chapter, the FTIR results for the sols of both stage 1 and stage 2 are shown. The GPC and thermal characterizations for the sols of stage 2 will be reported in Chapters 5 and 7.

## **4.4 Results and Discussion**

### **4.4.1 Reactive Extrusion - Stage 1**

#### **4.4.1.1 Flow Curve**

Degradation reactions in polypropylene are generally explained by the fragmentation of tertiary alkyl macroradicals, while the crosslinking, branching and extension reactions in polyethylene can be explained by the recombination of secondary alkyl macroradicals that have a lesser tendency to degrade. The addition of a polyfunctional monomer can stabilize tertiary PP macroradicals against scission by assisting the formation of secondary macroradicals which can subsequently lead to recombination reactions (Borsig et al., 1993). The resulting chain extension, branching and crosslinking reactions may cause the increase in molecular weight and long chain branching, and hence may increase the viscosity of the polymer melt. Thus, at a given peroxide concentration, materials produced using PETA should exhibit enhanced melt viscosities compared to the degraded PP (0.0 wt.% PETA). This behaviour can be observed in the shear viscosity data presented in Figs. 4-5a-c. It can be seen that generally the shear viscosity increases with PETA concentration and decreases with increasing peroxide concentration. In Fig. 4-5a (200 ppm peroxide level series) it can be observed that at 1.8 wt.% and 5.0 wt.% PETA concentrations, the viscosities of the materials produced are higher than that of the virgin PP. This suggests that the recombination reactions prevail over the chain scission reaction that tends to reduce the viscosity. Fig. 4-5 also shows that the chain scission reaction takes place simultaneously, suggesting that the branches, if formed, may be shortened by some of peroxide radicals. It seems that regardless

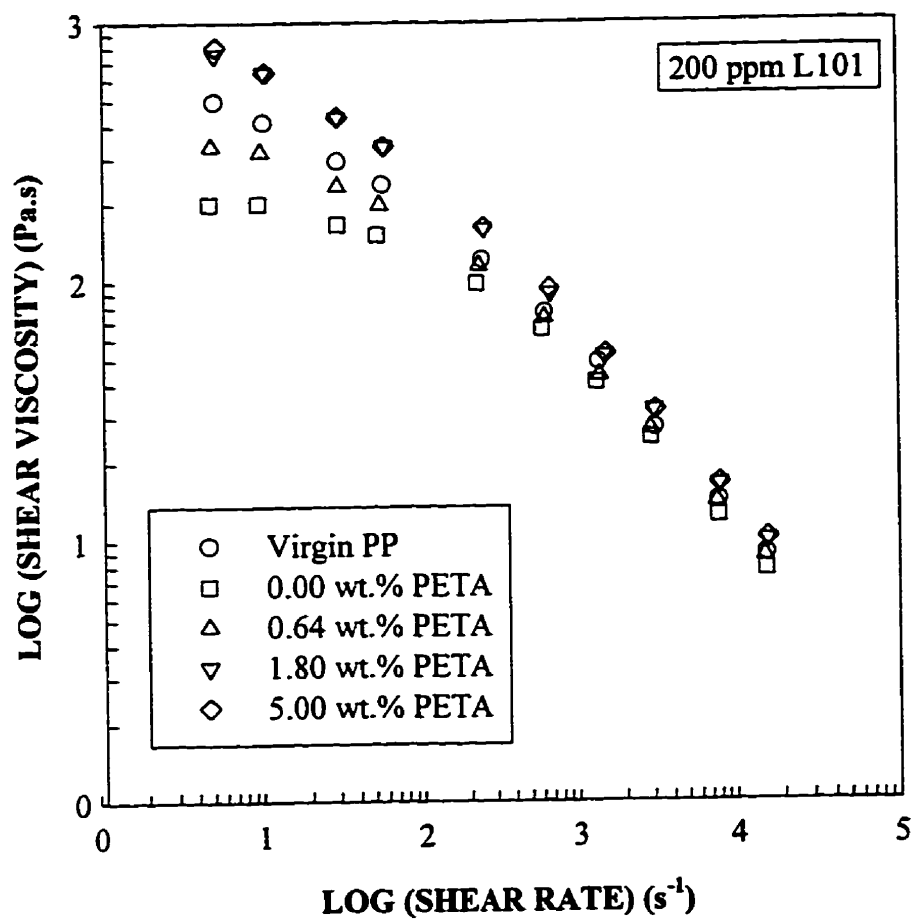


Fig. 4-5a Effect of PETA and peroxide concentration on the shear viscosity of the whole polymers (200 ppm peroxide series).

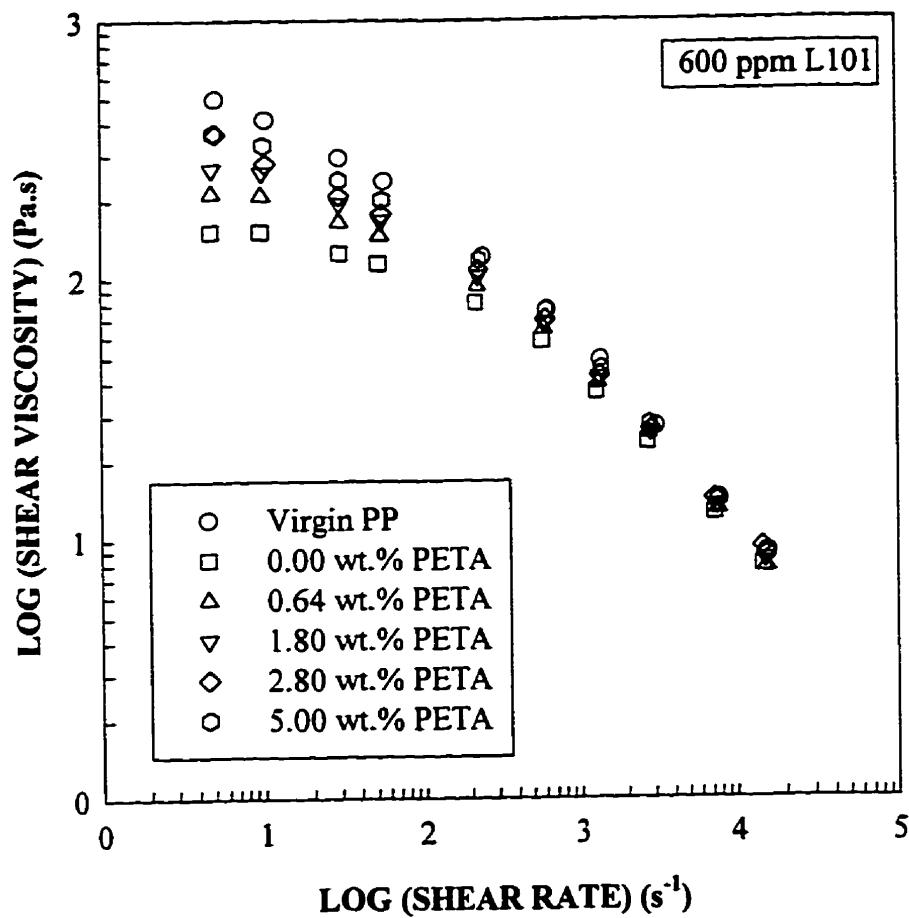


Fig. 4-5b Effect of PETA and peroxide concentration on the shear viscosity of the whole polymers (600 ppm peroxide series).

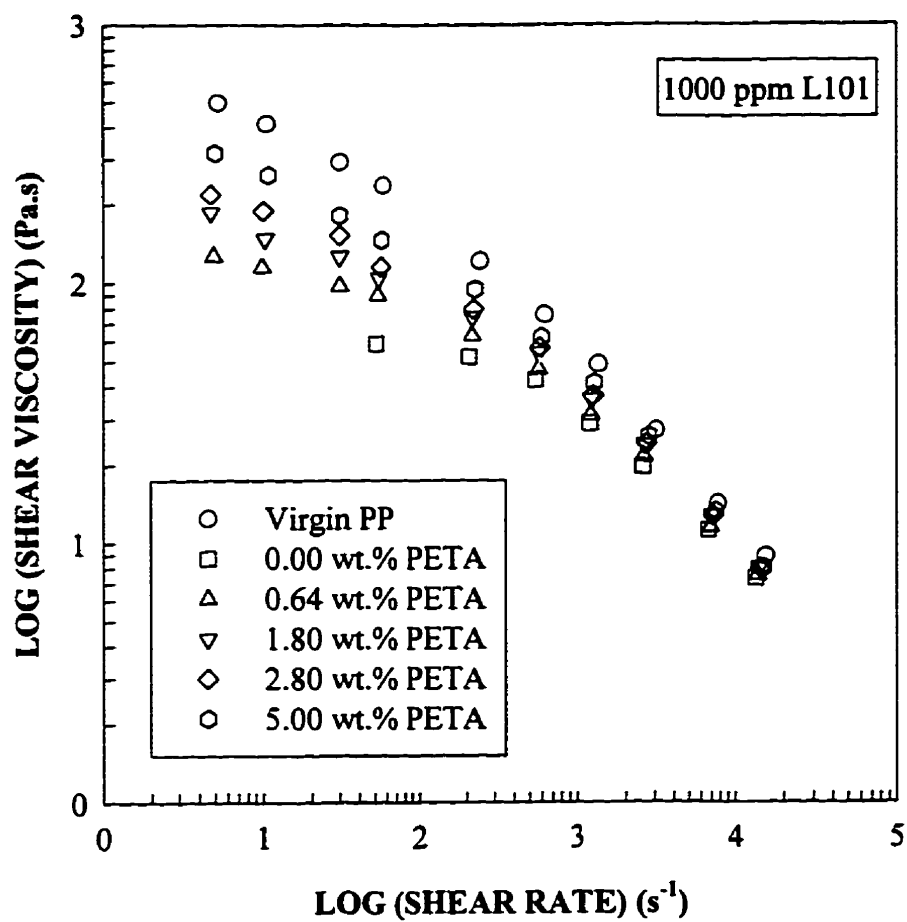


Fig. 4-5c Effect of PETA and peroxide concentration on the shear viscosity of the whole polymers (1000 ppm peroxide series).



of the peroxide concentration, the Newtonian plateau is shifted to lower shear rates as the PETA level is increased.

#### 4.4.1.2 Melt Flow Index (MFI)

The effect of PETA concentration on the MFI is shown in Fig. 4-6 and the results are consistent with the above shear viscosity data. As expected, the MFI decreases when PETA is added to the system for any peroxide concentration. However, PETA seems to have no significant effect on MFI at high concentration levels. This may be attributed to the increased PETA grafting reactions and PETA homopolymerization.

#### 4.4.1.3 Gel Content

As mentioned before, PETA molecules can form an insoluble homopolymer as well. Hence, the insoluble content should be regarded as possible mixed macrogels of highly crosslinked PP and PETA homopolymer, which are rather difficult to separate experimentally. In Table 4.1, it can be observed that overall no significant macrogel amount was formed for the concentration ranges used in this study. It is interesting to note that there

**TABLE 4.1 Results of Gel Content Measurements**

PETA wt.%	Gel Content (wt.%)		
	200 ppm L101	600 ppm L101	1000 ppm L101
0.00	0.00	0.00	0.00
0.64	0.00	0.00	0.00
1.80	0.00	0.20	0.56
2.80	0.05	0.83	1.00
5.00	0.55	1.13	2.54

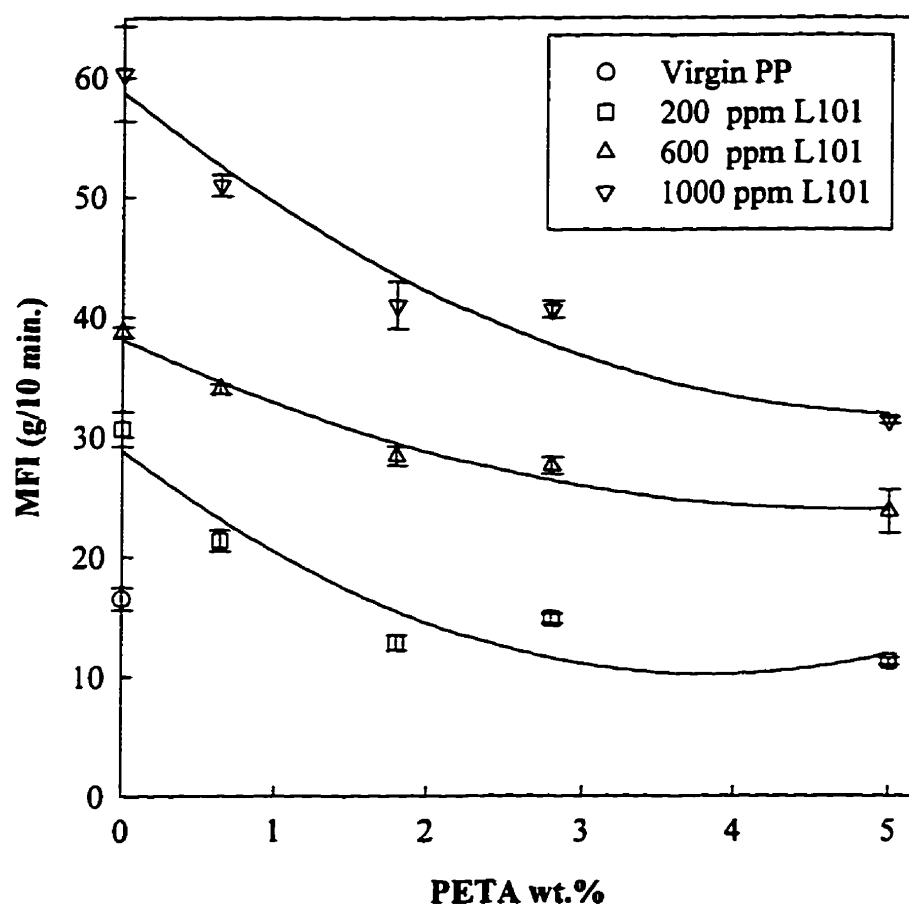


Fig. 4-6 Effect of PETA and peroxide concentration on the melt flow index (MFI) of the whole polymers. The MFI is expressed as the mean plus/minus one standard deviation.

is no significant evidence of any macrogel formation at the low PETA concentration (0.64 wt.%) regardless of the peroxide level. The onset of macrogel formation seems to occur at progressively lower PETA levels as the peroxide concentration is increased. For a given PETA concentration higher than 0.64 wt.%, the macrogel amount increases with increasing peroxide content. These results suggest that in order to minimize the formation of macrogel, low concentrations of PETA and peroxide should be used in the REX process.

#### 4.4.1.4 FTIR Analysis of the Sols

Similar FTIR spectra are obtained for the sols at all three peroxide levels and only the ones at 200 ppm peroxide level are shown in Fig. 4-7. For all the samples reacted with PETA, there are bands at around  $1740\text{ cm}^{-1}$  which are due to the stretching vibration of the carbonyl group of the ester in the PETA molecule and the intensity of this band seems to increase with PETA concentration. Similar to Chapter 3, the band at  $841\text{ cm}^{-1}$  is used as an internal reference. The relative intensity of these two bands ( $A_{1740}/A_{841}$ ) is shown in Fig. 4-8 as a function of the PETA concentration used. This intensity may serve as an indication of the extent of the recombination reactions. It should be noted, however, that there are two possible existing forms of the PETA units on the PP backbone which can contribute to this relative intensity. These include the grafted PETA units (either monomeric or polymeric) and the PETA units incorporated due to recombination reactions such as chain extension, branching or crosslinking.

In Fig. 4-8, it can be observed that generally  $A_{1740}/A_{841}$  increases with PETA concentration at all the peroxide levels, suggesting that more PETA would favour the reactions between PP and PETA. Obviously, the recombination reactions would be enhanced as indicated earlier from the viscosity and MFI data. It appears that for PETA concentrations lower than or equal to 2.80 wt.%, the peroxide level does not affect significantly this relative intensity and hence the amount of PETA incorporated into the PP chain. Within this range.

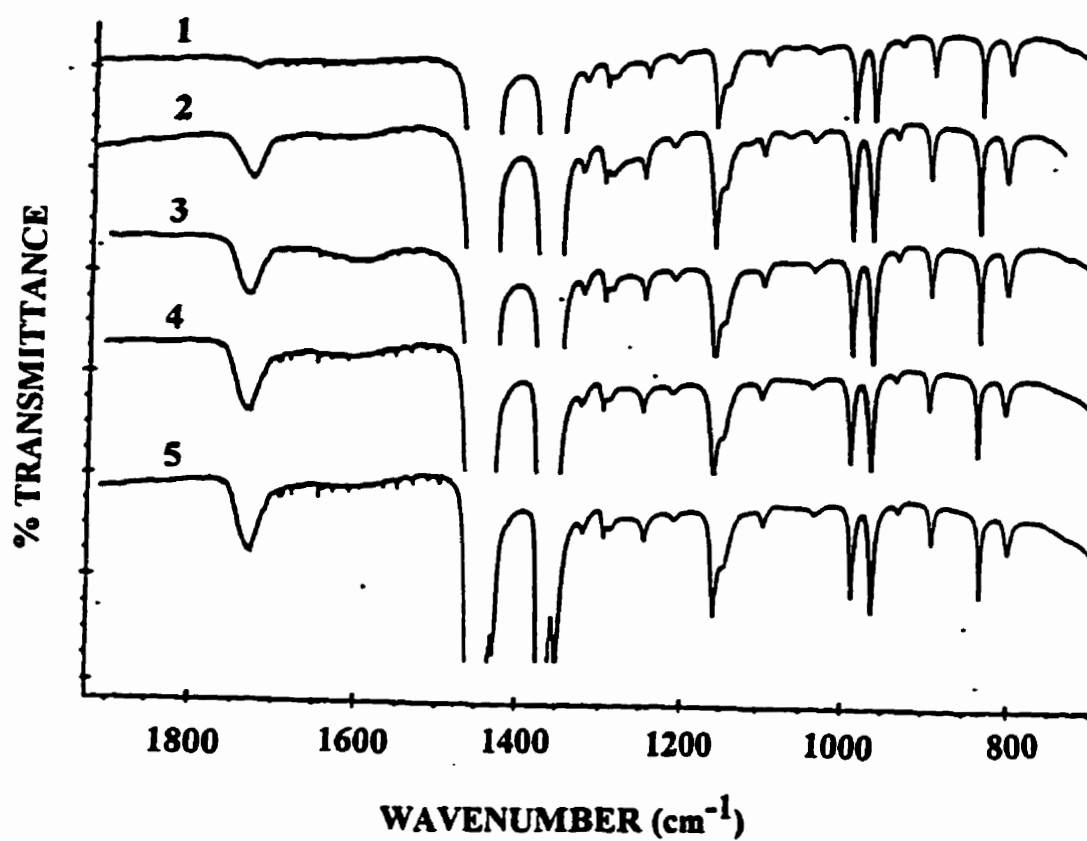


Fig. 4-7 FT-IR spectra (600-2000 cm<sup>-1</sup>) of the sols at different PETA concentrations (200 ppm peroxide series). 1: 0.00 wt.% PETA, 2: 0.64 wt.% PETA, 3: 1.80 wt.% PETA, 4: 2.80 wt.% PETA, 5: 5.00 wt.% PETA.

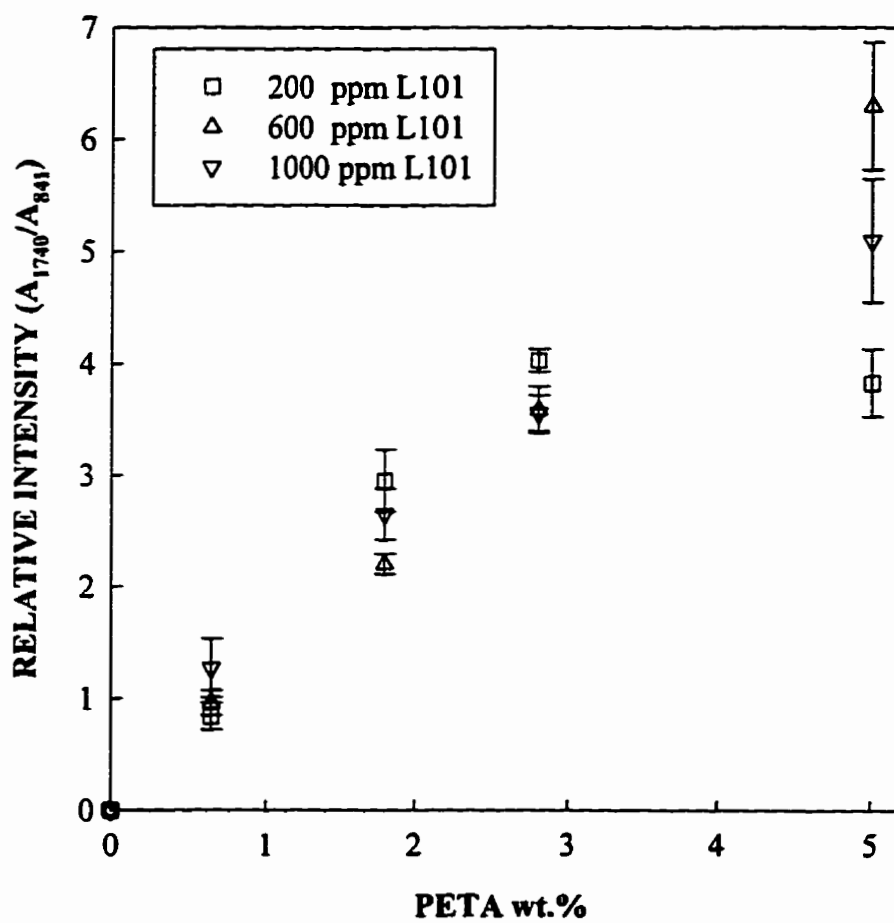


Fig. 4-8 Effect of the PETA concentration on the relative intensity of the bands at 1740  $\text{cm}^{-1}$  and 841  $\text{cm}^{-1}$  in the FTIR spectra of the sols. The relative intensity of  $A_{1740}/A_{841}$  is expressed as the mean plus/minus one standard deviation.

the relationship between  $A_{1740}/A_{841}$  and PETA concentration seems to be linear. At higher PETA levels (greater than 2.80 wt.%) and for 200 ppm peroxide level, this relative intensity appears to level off, which can be attributed to an increased consumption of primary peroxide radicals by the excess PETA rather than by PP chains (to form macroradicals), thus stabilizing the amount of the PP macroradicals generated and therefore the amount of PETA incorporated into PP chains. For the 600 and 1000 ppm peroxide cases, the system appears not to be saturated with PETA yet, and as a result increasing PETA concentration leads to higher value of relative intensity and therefore more PETA incorporated into PP chains. It should be pointed out that at 5.00 wt.% PETA, a reversal of effects between the 600 and 1000 ppm cases is observed which suggests the effect of peroxide level on the PETA amount incorporated into PP is not monotonic. This further indicates that under certain conditions (600 ppm series), the reaction between PP macroradicals and PETA is favoured over the PETA homopolymerization.

#### **4.4.1.5 DSC Analysis of the Sols**

In the present system, degradation, recombination and grafting reactions may take place simultaneously. These reactions will result in the changes of following molecular factors: (a) molecular weight and its distribution, and (b) chain irregularity due to branching/crosslinking, grafting of PETA and/or binding of peroxide radicals to the polymer chain. These microstructural differences will affect the crystallization behaviour of the sols of the modified PPs. Generally, for a given polymer and at a given crystallization temperature, the degree of crystallinity depends on the molecular weight and the structural regularity of the chain (Mark et al., 1993). For homopolymers, at higher molecular weight and hence melt viscosity, the ease of crystallization decreases and thus the final extent of crystallization is reduced. Thus, the level of crystallinity is relatively high at the lower molecular weights and then decreases monotonically with increasing molecular weights until

a limiting value is reached. The crystallinity level, which can be reflected by the heat of fusion  $\Delta H_m$ , is further reduced by the introduction of noncrystallizing structural units into the chains such as branching. Meanwhile,  $T_m$  decreases due to the introduction of chain defects (chain ends, crosslinks, branching points and non-isotactic sequences) which would act as a second component in the system. One example is that the  $T_m$  of branched PE is significantly less than that of linear PE and its melting range is broader.

Figs. 4-9,10,11 show the DSC melting endotherms of the sols of the samples prepared at 200, 600 and 1000 ppm peroxide levels and the data are summarized in Table 4-2. In Fig. 4-9, curve 1 is the DSC trace of initial PP, in which a doublet melting endotherm is observed at 154.45°C and 158.50°C. This situation is probably because of the coexistence of  $\alpha$  and  $\beta$  form crystals as observed also by Jacopy et al. (1986) on their roll milled virgin isotactic PP, although no nucleating agent for  $\beta$  form crystals was added. It may also be due to the proceeded perfection of crystal structures by recrystallization (Cheng et al., 1995). Similar to the DSC traces of the model branched PPs in Chapter 3, a main melting peak ( $T_{m1}$ ) and a second small melting peak ( $T_{m2}$ ) are also observed in most of the DSC traces. Increasing the peroxide concentration causes the appearance of  $T_{m2}$  at lower PETA concentrations. For example,  $T_{m2}$  begins to appear at 2.80 wt.% of PETA in the 200 ppm peroxide series (Fig. 4-9), at 1.80 wt.% PETA in the 600 ppm series (Fig. 4-10) and at 0.64 wt.% for the 1000 ppm series (Fig. 4-11). The presence of  $T_{m2}$  can not be attributed to the possibly grafted PETA homopolymer chains since they are not crystallizable as indicated from DSC scans of PETA homopolymer prepared by ampoule experiments. The presence of multiple melting peaks may suggest the existence of multiple molecular structures in this system. This is in agreement with similar melting characteristics observed for branched LDPE and the sols of crosslinked LDPE (Kao and Phillips, 1986). However, the branched PP species here may not be simple branched polymers such as our model branched PPs, but rather intermolecularly crosslinked and/or branched ones due to the molecular structure of the PETA used and the

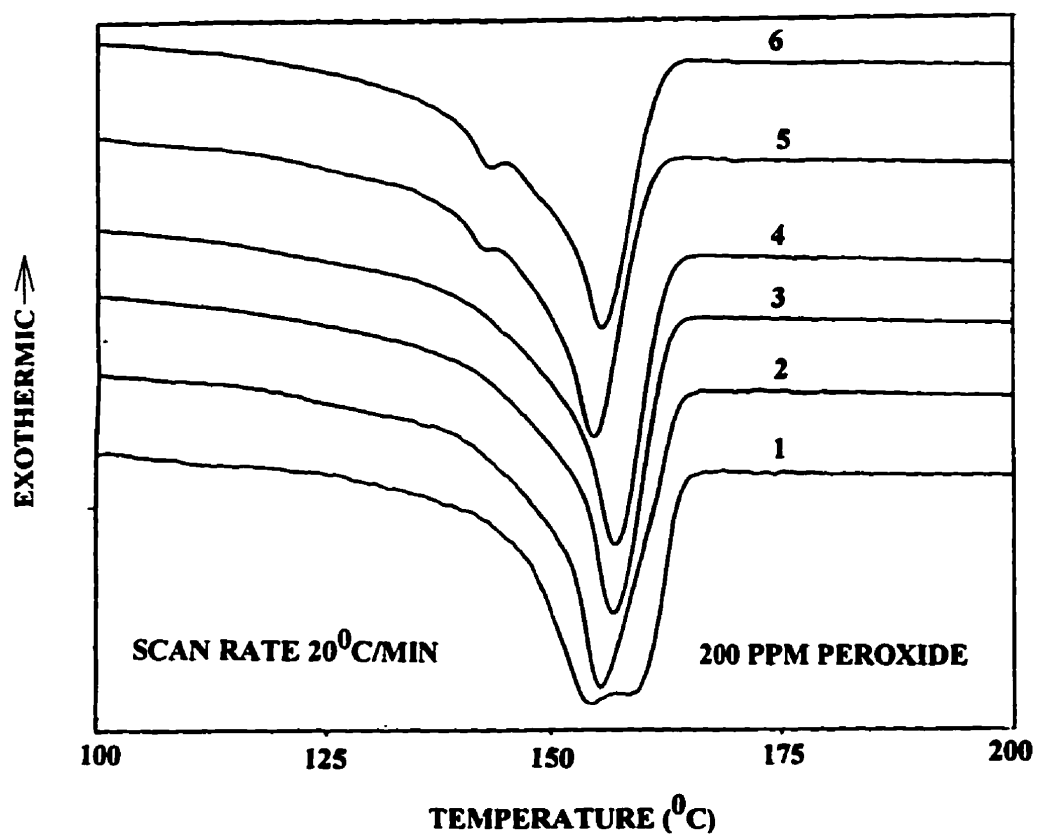


Fig. 4-9 Effect of the PETA concentration on the DSC melting endotherms of the sols at 200 ppm peroxide level. 1: virgin PP, 2: 0.00 wt.% PETA, 3: 0.64 wt.% PETA, 4: 1.80 wt.% PETA, 5: 2.80 wt.% PETA, 6: 5.00 wt.% PETA.



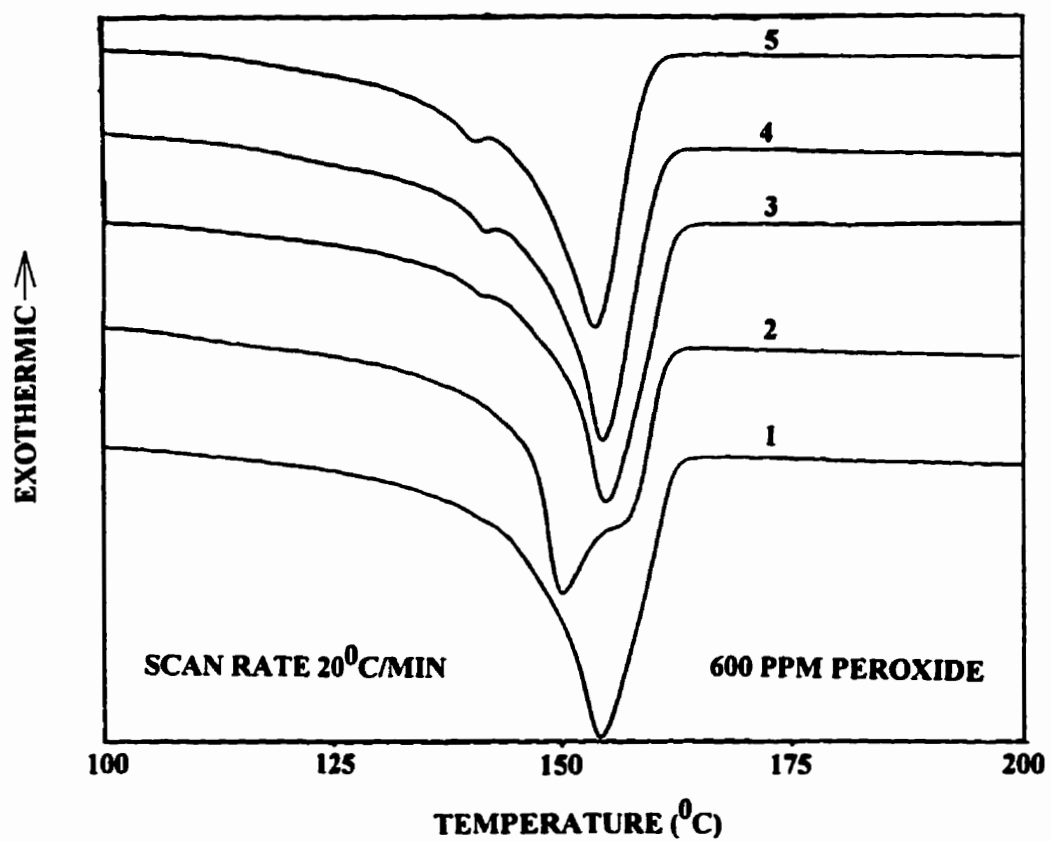


Fig. 4-10 Effect of the PETA concentration on the DSC melting endotherms of the sols at 600 ppm peroxide level. 1: 0.00 wt.% PETA, 2: 0.64 wt.% PETA, 3: 1.80 wt.% PETA, 4: 2.80 wt.% PETA, 5: 5.00 wt.% PETA.

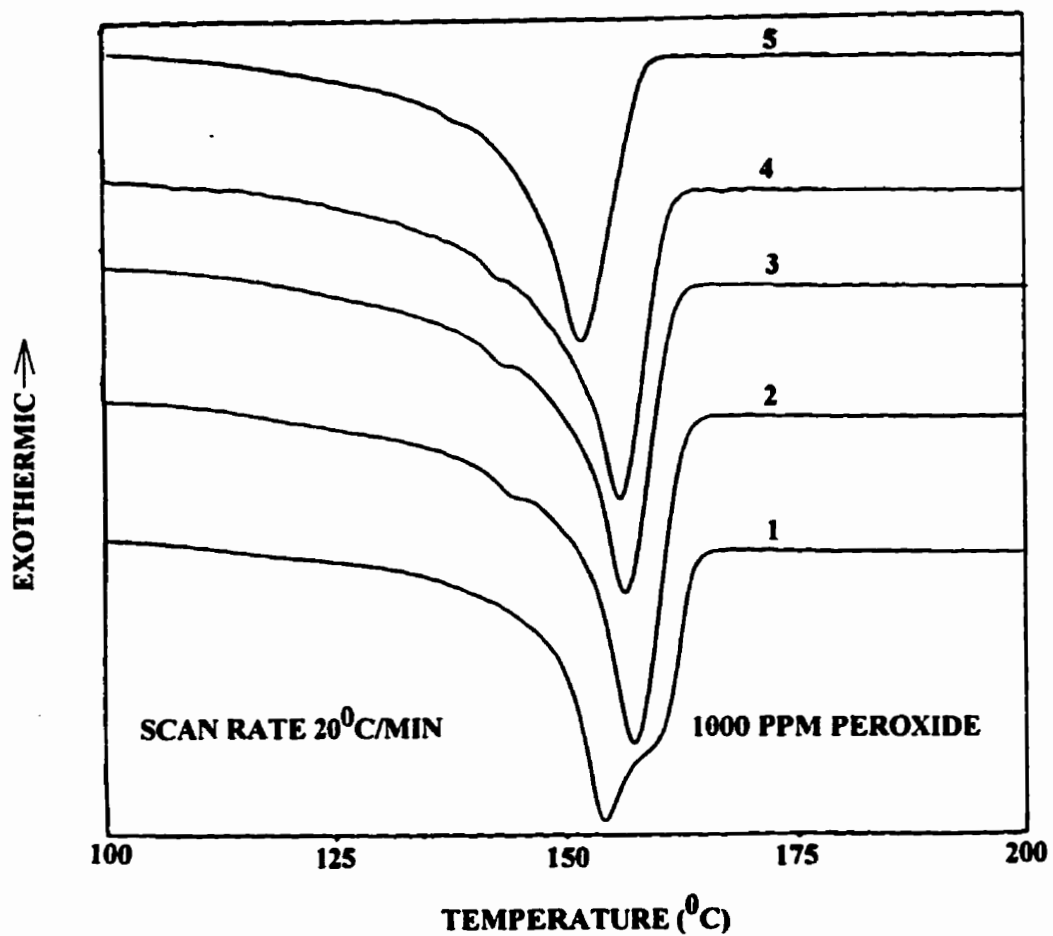


Fig. 4-11 Effect of the PETA concentration on the DSC melting endotherms of the sols at 1000 ppm peroxide level. 1: 0.00 wt.% PETA, 2: 0.64 wt.% PETA, 3: 1.80 wt.% PETA, 4: 2.80 wt.% PETA, 5: 5.00 wt.% PETA.

**TABLE 4.2 Effects of PETA and Peroxide Concentrations on the Thermal Behaviour of the Sols**

[L101] (ppm)	PETA (wt.%)	T <sub>m1</sub> (°C)	T <sub>m2</sub> (°C)	ΔH <sub>m</sub> (J/g)
200	0.00	155.75	---	96.68
200	0.64	157.16	---	97.44
200	1.80	157.16	---	91.29
200	2.80	157.56	143.60	91.29
200	5.00	155.64	143.45	93.14
600	0.00	154.34	---	95.49
600	0.64	151.15	---	94.08
600	1.80	154.70	141.64	96.30
600	2.80	154.98	142.60	95.34
600	5.00	154.00	141.50	93.45
1000	0.00	154.51	---	95.75
1000	0.64	157.88	145.75	99.05
1000	1.80	156.60	144.05	97.51
1000	2.80	156.16	143.41	96.38
1000	5.00	151.81	---	92.19
Virgin PP	---	158.50	154.45 <sup>1</sup>	95.54

<sup>1</sup> The T<sub>m2</sub> of virgin PP was detected as the main melting peak by the DSC built-in program. However, the T<sub>m1</sub>s of all the other samples were detected as the main peaks by DSC.

randomness of the recombination reactions.

In Table 4.2, for the 200 and 1000 ppm peroxide series,  $\Delta H_m$  and  $T_{m1}$  seems to increase initially with PETA concentration, reach a maximum at relatively low PETA concentrations and then decrease. The sols from 600 ppm peroxide series seem to behave differently. In this series,  $\Delta H_m$  and  $T_{m1}$  initially pass through a minimum, increase and then remain relatively constant. Kim et al. (1993) reported similar thermal behaviour on the modified PPs crosslinked by PETA and other crosslinkers. However, the multiple melting behaviour and the presence of a maximum in the change of  $T_{m1}$  in terms of the PETA concentrations were not reported in their work. In the study of the branched PPs produced by irradiation method, DeNicola et al. (1992) also found that at the same TREF elution temperatures, the  $T_m$  for the irradiated PP appears to be either higher or lower than that of the virgin linear PP. The increase in  $T_{m1}$  is contrary to the observations on our simple model branched polymers. It has been proposed (Kim et al., 1993) that the increase in  $T_m$  is due to the improved packing of polymer chains into a crystalline structure by a few crosslinking points which can properly restrict the flow of the melt. Although this is possible, some other factors may also cause the changes in  $T_{m1}$ : a) the change in the structure and size of the crystals because of the modified chain structures such as crosslinking/branching, and b) the reduction in the melting entropy  $\Delta S_m$  as a result of chemical crosslinking/branching of the chains. With intermolecular crosslinking, the conformational entropy of a polymer melt decreases (Kao and Phillips, 1986; Bershtein et al., 1994). Therefore, the  $\Delta S_m$  becomes smaller and for the crosslinked PPs the elevation of the temperature  $T_m = \Delta H_m / \Delta S_m$  can be expected if  $\Delta H_m$  is not changed very much. The modified chain structure may also lower the enthalpy of fusion  $\Delta H_m$ , especially at the higher PETA concentrations where the crosslinking density of PP chains may be very high and hence reduces the mobility of the chain. If the  $\Delta H_m$  is reduced too much, it will finally result in a decrease in the  $T_m$  despite the decrease in  $\Delta S_m$ . Finally, it is found from the observed DSC thermograms that the halfwidths (used

to represent the melting range  $\Delta T_m$ ) of some of the modified PPs are narrower than those of the virgin PP and degraded PPs. This might be due to the change in the dispersion of the lamella thicknesses caused by the crosslinks since  $\Delta T_m$  is usually related to the dispersion of the lamella thicknesses (Bershtein et al., 1994). The complicated situation in  $T_{m1}$  and  $T_{m2}$  implies that the sols of the modified polypropylenes should not be a single species of simple branched polypropylene (Wang et al., 1994), but possibly a combination of linear, branched or even lightly crosslinked (highly branched).

When the melts were cooled at a rate of 20°C/min, only one peak was observed in the crystallization endotherms of the virgin PP, degraded PPs and all the sols of the modified PPs. This suggests a co-crystallization process between a large range of different molecular structures in the sols of the modified materials. In Fig. 4-12, the crystallization temperature  $T_c$  of the virgin PP and the sols is plotted as a function of PETA amount at all three peroxide levels used. The observed  $T_c$  is about 106.5°C for our virgin linear PP, which is in agreement with literature value (DeNicola et al., 1992). Generally,  $T_c$  seems to increase and to subsequently level off at 200 and 1000 ppm peroxide concentrations. However, in the 600 ppm peroxide series  $T_c$  decreases at low PETA levels before recovering and levelling off at higher PETA values. It is also noted that almost all the sols from the materials modified with PETA have higher  $T_c$  than that of the virgin PP or the corresponding degraded PPs (0.00 wt.% PETA). The crystallization exotherm  $T_c$  is an indication of the bulk crystallization rate. The higher the  $T_c$ , the faster the polymer crystallizes. Hence, the degraded PPs have faster crystallization rates than virgin and this is in agreement with the results of Chen et al. (1994). Meanwhile, generally the sols from the modified PPs have higher crystallization rates than these degraded PPs at the same peroxide level under the present crystallization conditions. This increase in the crystallization rate may be due to the increased nucleation density because of the introduction of the crosslinks by the recombination reactions. For example, Philips et al. (Phillips and Kao, 1986; Gohil and Phillips, 1986) noted that the introduction

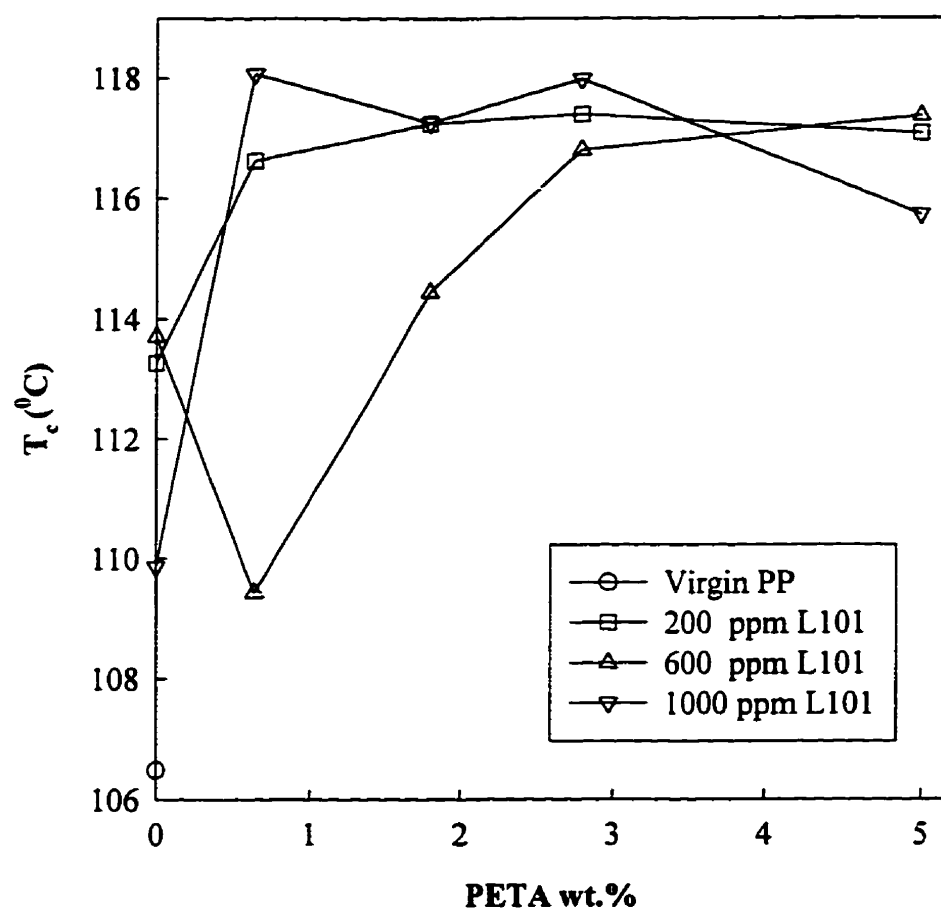


Fig. 4-12 Effect of the PETA and peroxide concentration on the crystallization temperature ( $T_c$ ) of the sols.

of a small number of crosslinks considerably increases the nucleation density of crosslinked low density branched polyethylene and that the sol crystallizes much more rapidly than the uncrosslinked polymer. DeNicola et al. (1992) also found that the  $T_c$  of the irradiated PP (branched PP) was always higher than that of the linear PP at the same TREF elution temperature and the nucleation density of the irradiated PP was much higher than that of the linear precursor. Hence, it could be inferred that the elevation of  $T_c$  in our system may be due to the increased nucleation density caused by the branching/crosslinking of the linear PP. Compared to the results in Chapter 3 for the model branched PP, the thermal behaviour of these sols suggests that the branching structures generated by the recombination reactions may not be as simple as the ones observed in the usual randomly branched polymers.

#### 4.4.1.6 Conclusions

Branched/crosslinked PP have been produced by a reactive extrusion process using a mixture of a L101 and PETA. Measurements of shear viscosity and MFI of the modified PPs indicate an enhancement of viscosity and hence an increase in the recombination reactions. The amount of macrogel in the modified PP has been found to increase with increasing PETA and L101 concentrations and it can be minimized by using low concentrations. The amount of PETA incorporated into the virgin PP may be detected through FTIR measurements and it has been found to increase with increasing PETA concentration at all peroxide levels. Two  $T_m$ s have been observed in the DSC traces of the sols in some of the modified PPs and generally,  $T_c$ s have been higher than those of the virgin and corresponding degraded PPs. These suggest that the branched structures formed, are not as simple as the ones in randomly branched polymers.

## **4.4.2 Reactive Extrusion - Stage 2**

### **4.4.2.1 Background**

In stage 1, some PETA/peroxide modified PPs have been produced with relatively low PETA and peroxide concentrations in a unstabilized system. It is found that within certain range of PETA and Lupersol 101 (L101) concentrations, there is no significant amount of macrogels formed during the REX experiments. Experimental results suggest the possible existence of branched structures in these modified PPs. However, results also indicate that degradation reactions take place simultaneously with the recombination reactions. This is due to the nature of the peroxide primary radicals that tend to react with PP chains preferentially and not with the polyfunctional monomer (Borsig et al., 1981), which may cause the shortening in both backbone chains and the branches formed. Thus, in order to produce long chain branched polypropylenes and to apply this process to commercial polypropylenes which are usually stabilized, further REX experiments were carried out using a stabilized PP and very low concentrations of L101 in a new REX process shown in Fig. 4-4. The conditions used in the stage 2 runs are given in Table 4.3.

### **4.4.2.2 Stabilizer Effect**

Irganox 1010 is a primary antioxidant, or a radical scavenger used to retard the oxidative degradation reaction, in which alkyl hydroxyl radicals are converted to hydroperoxide molecules by abstracting the reactive hydrogen atoms of Irganox 1010. Fig. 4-13 shows the effect of the amount of Irganox 1010 on the MFI of PP. It can be seen that the MFI decreases rapidly with the increasing level of stabilizer and it reaches a value of about three at 1.0 wt.% stabilizer, which is similar to the data from the resin supplier. Fig. 4-14 shows the shear viscosities of unstabilized virgin PP extruded at different temperatures. It can be seen that there is a reduction of viscosity as the temperature is increased and this may be attributed to a combination of degradation processes. The addition of Irganox 1010



**TABLE 4.3 Description of the Modified Polypropylenes**

Polymer	[PETA] wt.%	[L101] (ppm)	Polymer	[PETA] wt.%	[L101] (ppm)
50PP	0.0	50	SPT1010	1.0	100
100PP	0.0	100	SPT1020	2.0	100
150PP	0.0	150	SPT1030	3.0	100
200PP	0.0	200	SPT1505	0.5	150
400PP	0.0	400	SPT1510	1.0	150
600PP	0.0	600	SPT1520	2.0	150
SPT505	0.5	50	SPT1530	3.0	150
SPT510	1.0	50	SPT2005	0.5	200
SPT520	2.0	50	SPT2010	1.0	200
SPT530	3.0	50	SPT2020	2.0	200
SPT1005	0.5	100	SPT2030	3.0	200

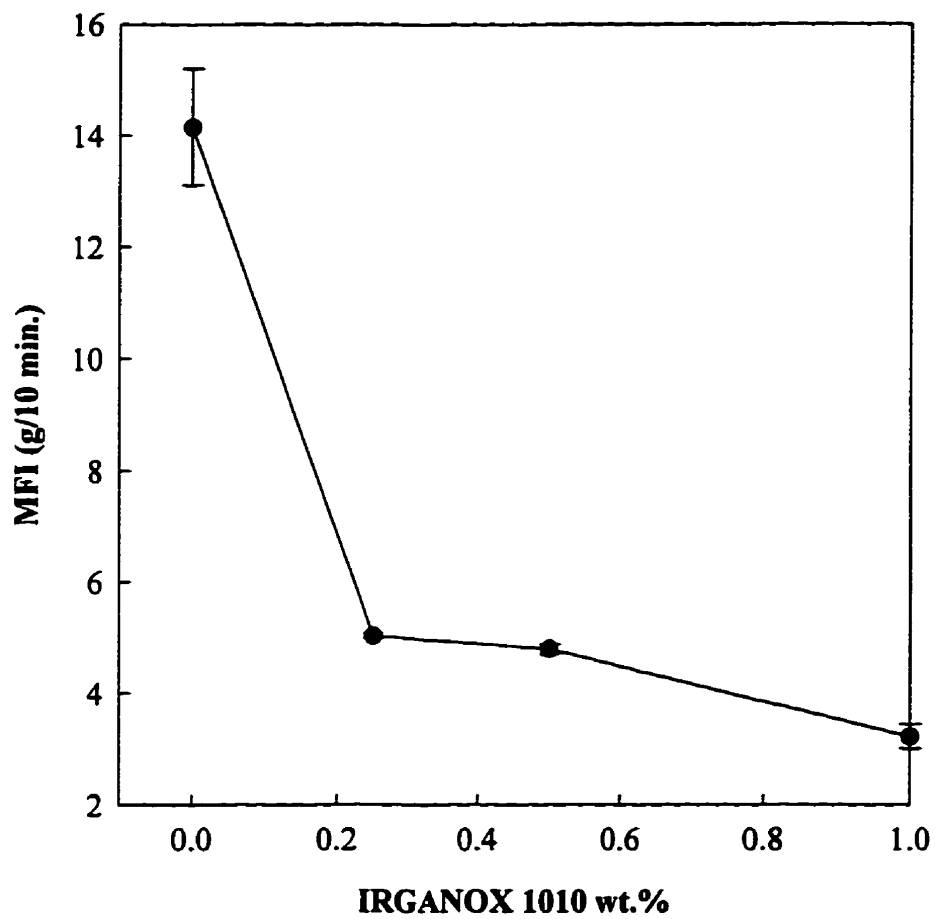


Fig. 4-13 Effect of stabilizer concentration on the MFI of virgin PP. The MFI is expressed as the mean plus/minus one standard deviation.

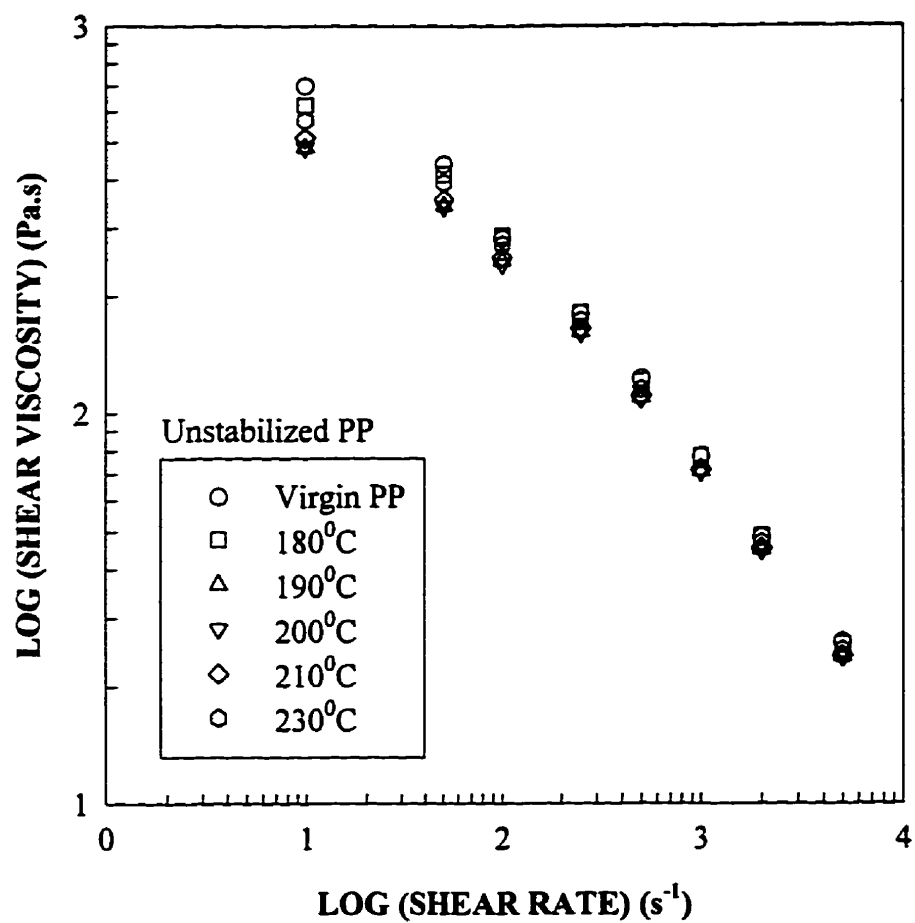


Fig. 4-14 Effect of the extrusion temperature on the shear viscosity of unstabilized PP.

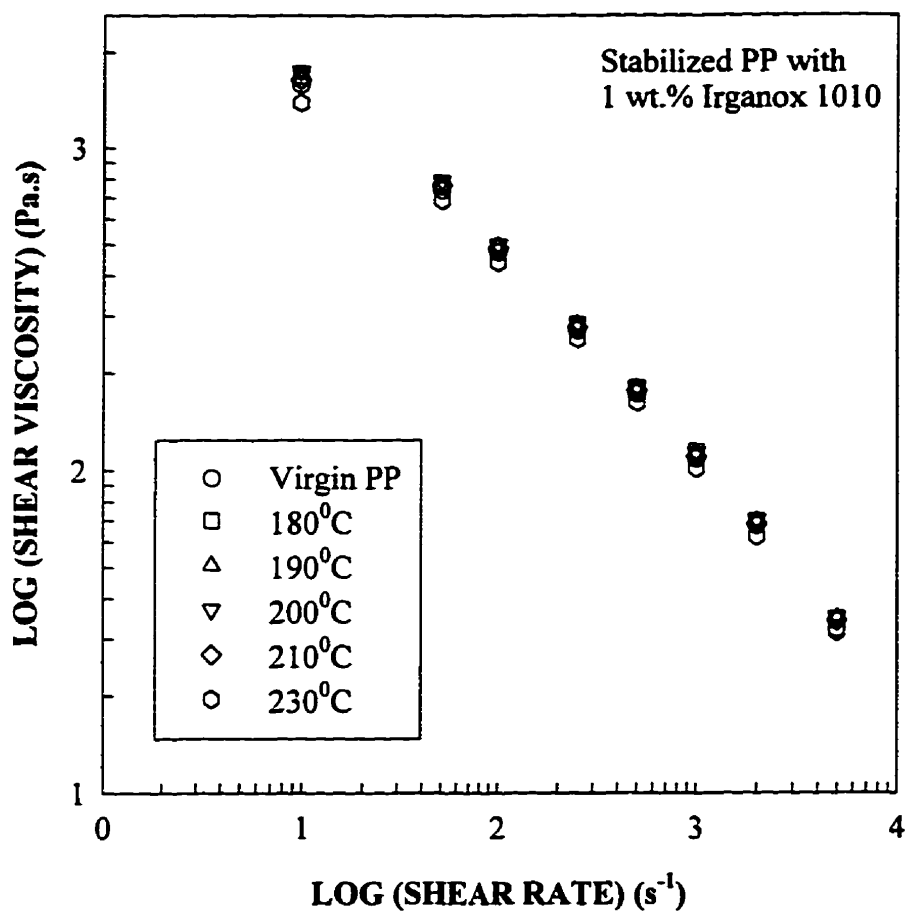


Fig. 4-15 Effect of the extrusion temperature on the shear viscosity (at 230<sup>o</sup>C) of stabilized PP with 1.0 wt.% of Irganox 1010.

increases the stability of PP (Fig. 4-15), even though a secondary antioxidant normally used to decompose the hydroperoxide molecules, was not added to the system.

#### 4.4.2.3 Analysis of Macrogels

Gel content data are summarized in Table 4.4 and overall the amounts of macrogel formed were very small. Generally, the macrogel content increases with increasing PETA and peroxide concentrations, which is consistent with the results in stage 1. Surprisingly, at the low PETA concentration (e.g., PETA concentration of 0.5 wt.%) there were very low level of macrogels detected. It is also found that at comparable PETA and peroxide concentrations, there is more macrogel formed in stage 2 than in stage 1, even in the cases where the lower PETA and peroxide concentrations were used in stage 2. The increased macrogel formation may be due to the increased PETA homopolymerization. This is partly because in stage 2, the PETA monomer and peroxide were mixed together and then injected into the extruder. Owing to the heat generated by the injection pump, the homopolymerization of PETA may take place more easily in the presence of L101 than in

**TABLE 4.4 Results of Gel Content Measurements**

PETA (wt.%)	Gel Content (wt.%)			
	50 ppm	100 ppm	150 ppm	200 ppm
	L101	L101	L101	L101
0.00	0.00	0.00	0.00	0.00
0.50	0.03	0.00	0.05	0.07
1.00	0.24	0.16	0.27	0.34
2.00	0.60	0.74	0.75	1.24
3.00	0.94	1.31	2.68	1.88

the case of stage 1, where PETA and peroxide were added into the system separately. This explanation can be supported by the fact that in the early stage of experiments, the injection pump was clogged frequently and hence a cooling-down setup for the mixed solution before injection had to be employed, which indeed reduced greatly the occurrence of the pump clogging. Another reason for this increase may be due to the pre-homopolymerization of the mixed solution within the end of the tubing which are close to the extruder and may have a high enough temperature to induce this polymerization.

The above inference was supported by the DSC analyses of the macrogels. Virgin PP was also scanned as a comparison under the same condition (Fig. 4-16). It shows two melting peaks (155.62°C and 159.96°C) that are much more significant than the case in stage 1 since their thermal conditions were different. This multi-melting is again attributed to the proceeded perfection of crystal structures by recrystallization (Cheng et al., 1995). Figs. 4-17 and 4-18 show the DSC melting traces of the macrogels and the results are summarized in Table 4.5.

It can be seen that all of macrogels exhibit very weak and broad melting peaks. Similar to some samples in stage 1, a melting peak and a shoulder are observed in the traces of the macrogels from SPT1530 and SPT2020. As speculated in stage 1, the shoulder may

**TABLE 4.5 DSC Analyses of the Macrogels of the Modified PPs**

Macrogel from sample	$T_m$ (°C)	$\Delta H_m$ (J/g)	Macrogel from sample	$T_m$ (°C)	$\Delta H_m$ (J/g)
SPT520	155.40	4.11	SPT1520	155.00	6.84
SPT530	157.00	0.67	SPT1530	147.12, 160.44	14.57
SPT1010	156.20	4.02	SPT2010	152.87	7.88
SPT1020	155.40	4.06	SPT2020	147.80, 159.26	14.65
SPT1030	156.00	4.84	SPT2030	155.80	6.74

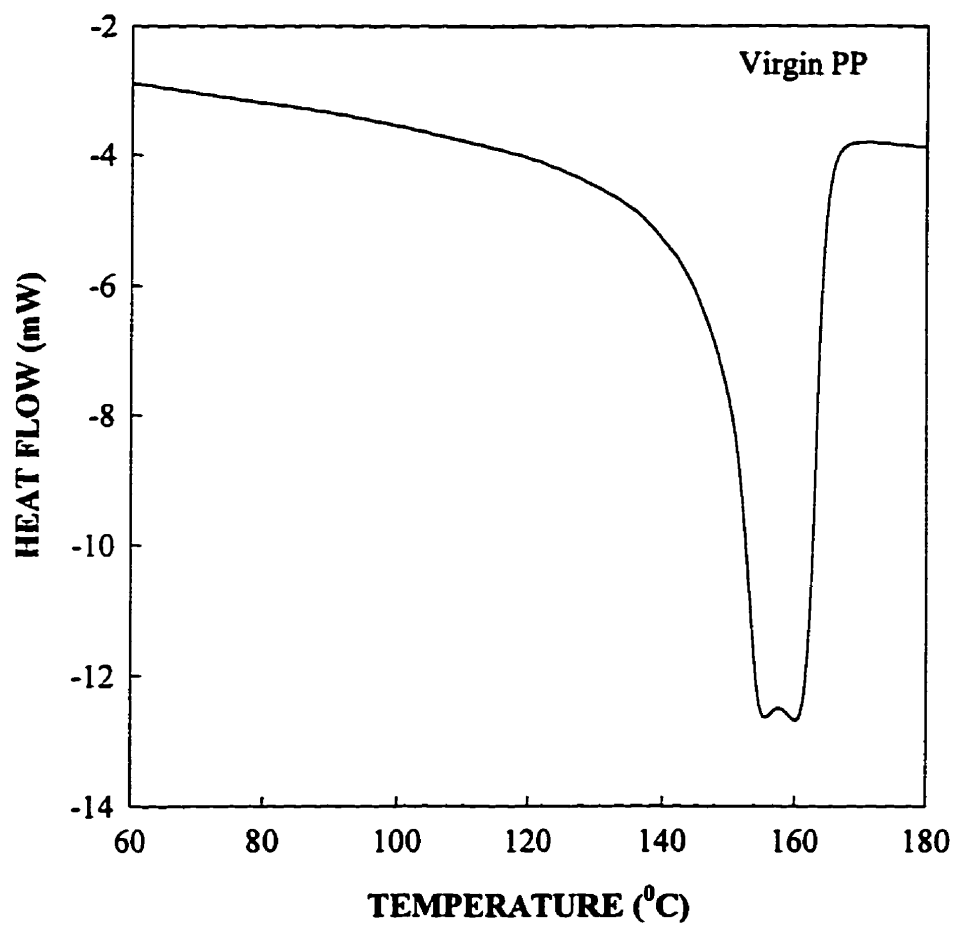


Fig. 4-16 DSC melting endotherm of the virgin PP having same thermal history as the macrogels.

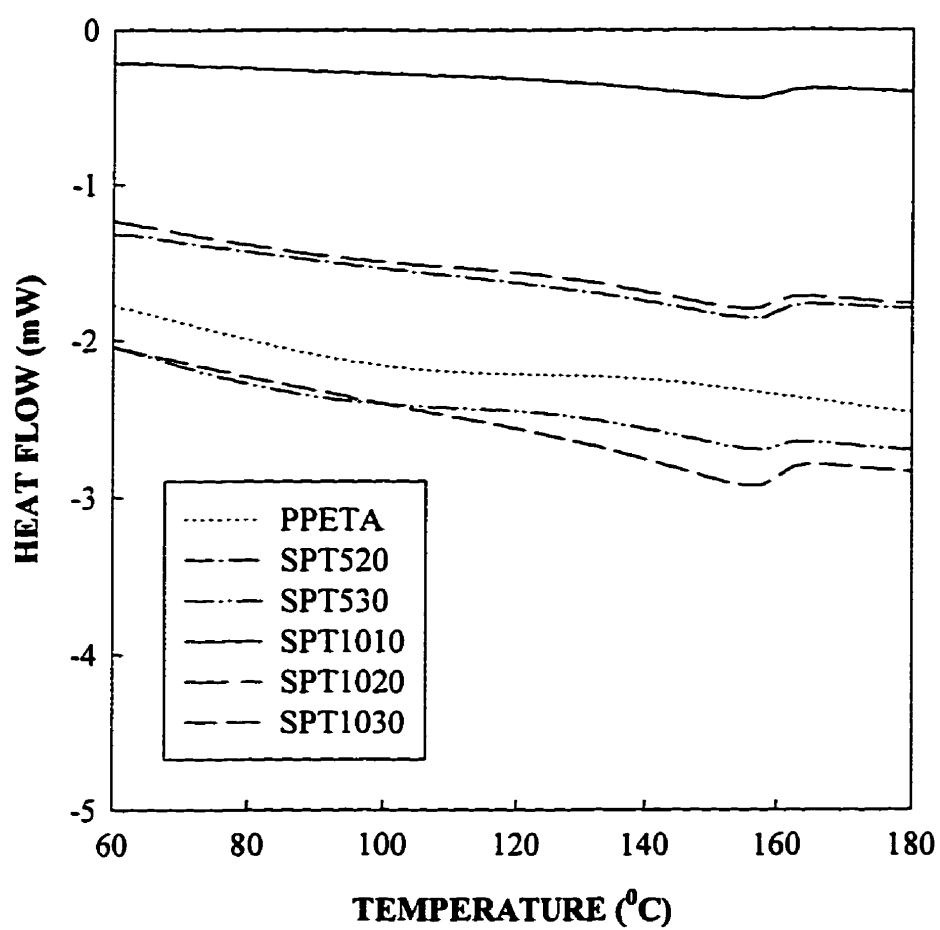


Fig. 4-17 DSC melting endotherms of the PETA homopolymer and the macrogels in the polypropylenes produced at 50 and 100 ppm L101 levels.



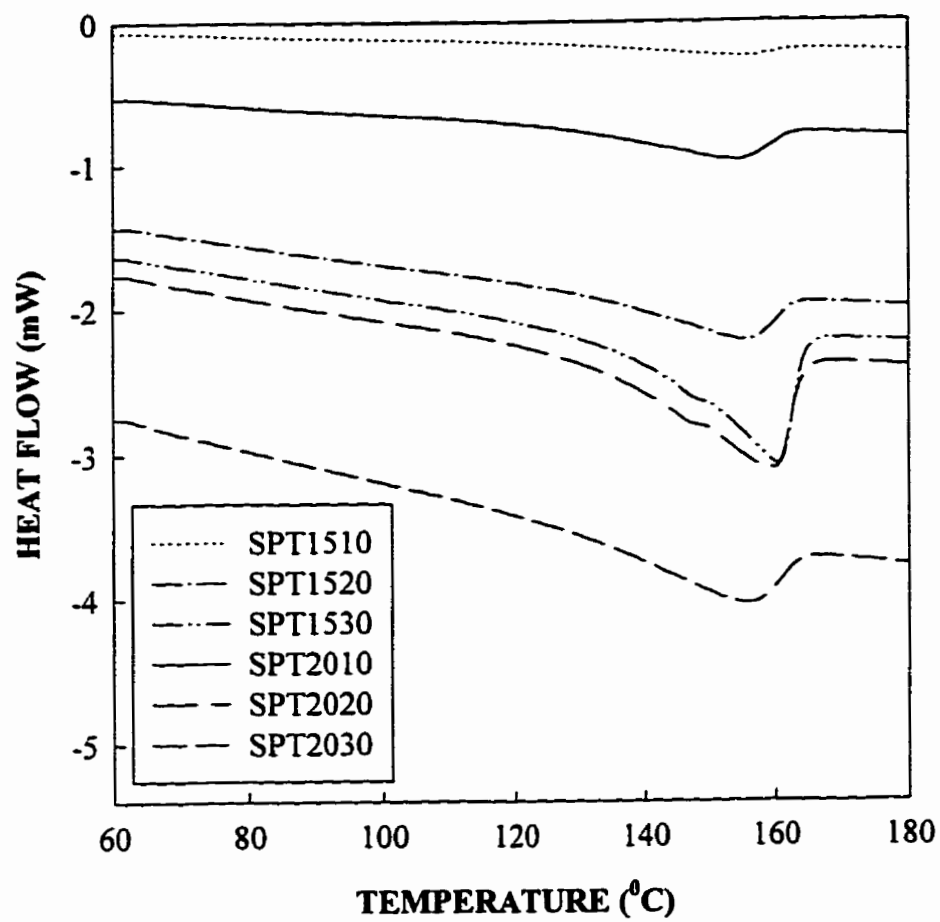


Fig. 4-18 DSC melting endotherms of the macrogels in the polypropylenes produced at 150 and 200 ppm L101 levels.

be due to the melting of highly crosslinked PP species. It is quite interesting to note that all the macrogels have quite high  $T_m$ s and they are close to the  $T_m$ s of the virgin PP. This fact suggest that the crosslinking densities of the PP macrogels are not so high. Hence, the PP chain segments between the crosslinks are long enough to form normal crystals whose structures are similar to ones formed by linear virgin PP. This may induce a further inference that the sols may most likely have branched-crosslinked molecular structures, which has been confirmed by the results in Chapters 5 and 7. The amount of PP macrogels formed should be small. The  $\Delta H_m$  observed for virgin PP at this condition is 102.00 J/g. In Table 4.5, it can be seen that all the macrogels have very low  $\Delta H_m$ s, which suggests that the majority in the macrogel formed was the non-crystallizable PETA homopolymer and hence, the content of the highly crosslinked PP macrogel was very low. This indicates that in order to reduce the macrogel formation, PETA and peroxide should be added into the system separately.

#### 4.4.2.4 FTIR Spectra of the Sols

FTIR spectra of the purified sols from different peroxide series are very similar and only the spectra from the 50 ppm and 200 ppm peroxide series are shown in Figs. 4-19 and 4-20.

Similar to the FTIR spectra in stage 1, the relative intensities of the two bands at 1740  $\text{cm}^{-1}$  and 841  $\text{cm}^{-1}$  ( $A_{1740}/A_{841}$ ) are obtained as the mean plus/minus one standard deviation and the results are shown in Table 4.6. It can be seen that generally, either PETA or peroxide level has no significant effect on this relative intensity within the level ranges examined here. This result seems close to the observation in stage 1, where it was found that for PETA concentrations lower than or equal to 2.8 wt.%, the differences in the relative intensity among those samples were not large. In stage 2, it seems that a maximum of relative intensity might exist in each series, depending on the relative PETA/peroxide concentration. Within certain concentration range, more PETA would favour the reactions between PP and PETA.

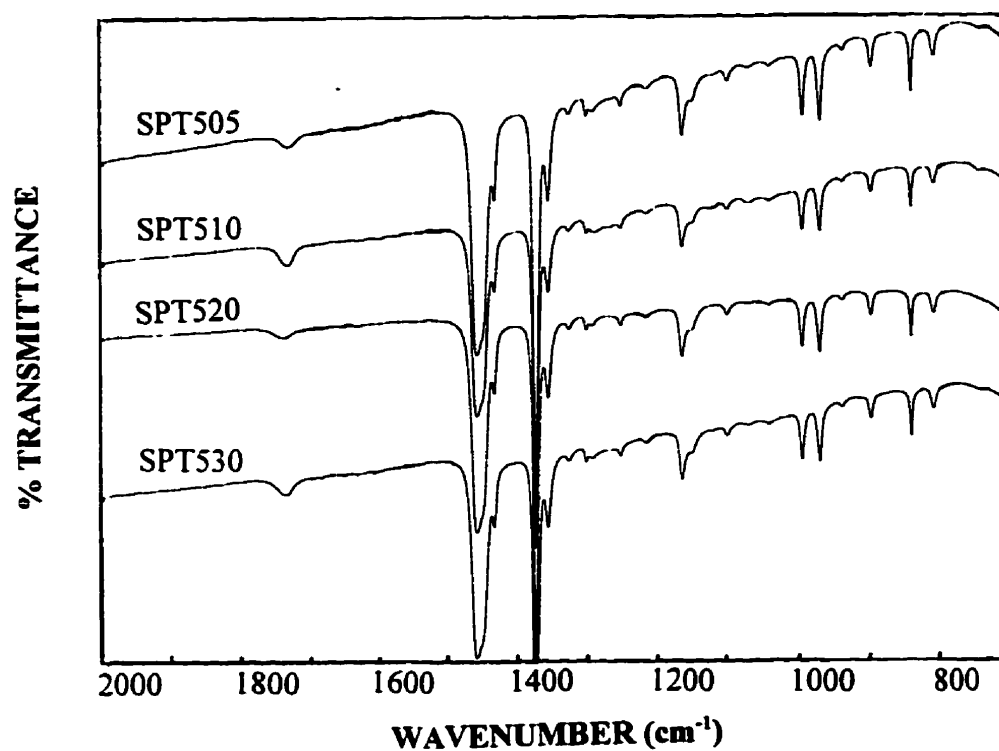


Fig. 4-19 FTIR spectra (700-2000 cm<sup>-1</sup>) of the sols at different PETA concentrations (50 ppm peroxide series). 1: 0.5 wt.% PETA, 2: 1.0 wt.% PETA, 3: 2.0 wt.% PETA, 4: 3.0 wt.% PETA.

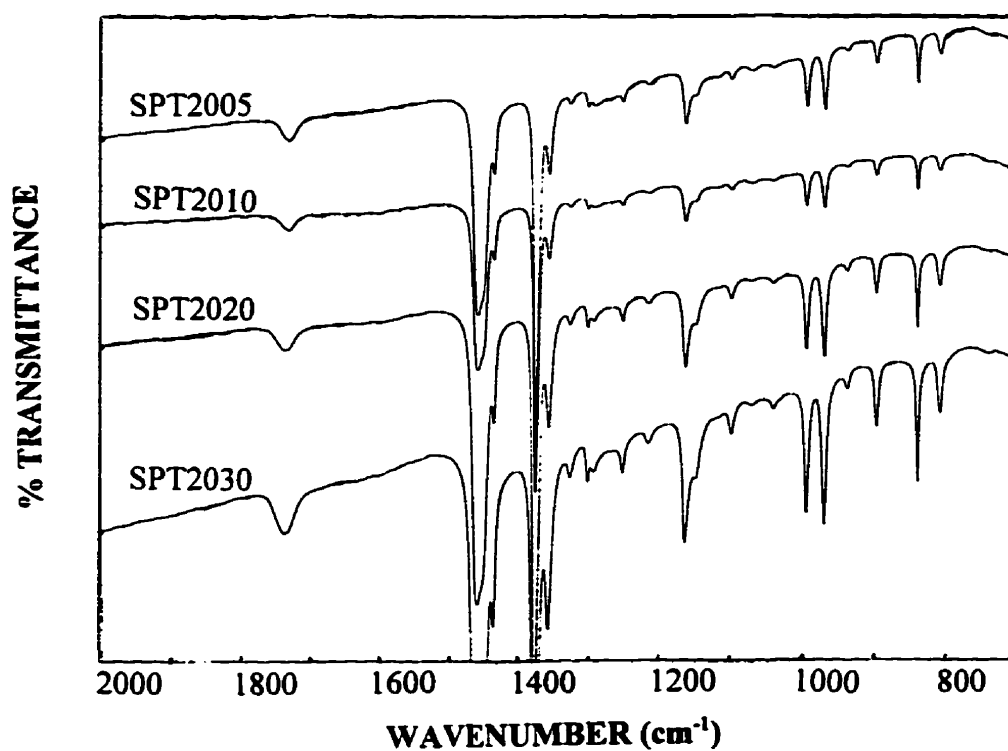


Fig. 4-20 FTIR spectra (700-2000 cm<sup>-1</sup>) of the sols at different PETA concentrations (200 ppm peroxide series). 1: 0.5 wt.% PETA, 2: 1.0 wt.% PETA, 3: 2.0 wt.% PETA, 4: 3.0 wt.% PETA.

**TABLE 4.6** Relative Intensity of  $A_{1740}/A_{841}$  of the Sols

Sample	$A_{1740}/A_{841}$	Sample	$A_{1740}/A_{841}$
SPT505	$1.54 \pm 1.03$	SPT1505	$1.17 \pm 0.84$
SPT510	$2.48 \pm 0.65$	SPT1510	$2.00 \pm 1.01$
SPT520	$2.05 \pm 0.90$	SPT1520	$2.15 \pm 0.70$
SPT530	$1.88 \pm 0.40$	SPT1530	$1.64 \pm 0.14$
SPT1005	$0.60 \pm 0.55$	SPT2005	$1.42 \pm 0.61$
SPT1010	$3.31 \pm 1.62$	SPT2010	$2.29 \pm 0.41$
SPT1020	$4.84 \pm 1.77$	SPT2020	$2.20 \pm 0.76$
SPT1030	$1.92 \pm 0.45$	SPT2030	$2.78 \pm 0.54$

#### 4.4.2.5 Shear Viscosity and Melt Flow Index

The shear viscosity data for peroxide-degraded polypropylenes (no PETA used) are shown in Fig. 4-21. Clearly, the shear viscosity of PP was reduced with increasing peroxide concentration and this can be seen even when the shear rate is relatively high. However, the PETA/peroxide modified PPs in the 50 ppm, 100 ppm peroxide series are difficult to be differentiated from each other by shear viscosity, though all these materials show enhanced viscosities than those of the virgin PP and corresponding degraded PPs (Figs. 4-22 to 4-25). The samples in 200 ppm peroxide series seem to have lower viscosities than that of virgin PP but still hard to be distinguished from each other. Thus, unlike the materials in stage 1 where relatively high peroxide concentrations were used, there are some difficulties of using shear viscosity to distinguish these PETA modified PPs in stage 2. Besides the material properties, this is also partly due to the limit of lowest shear rate which can be reached by the capillary rheometer used.

The changes in MFI with respect to the PETA and peroxide concentrations in stage

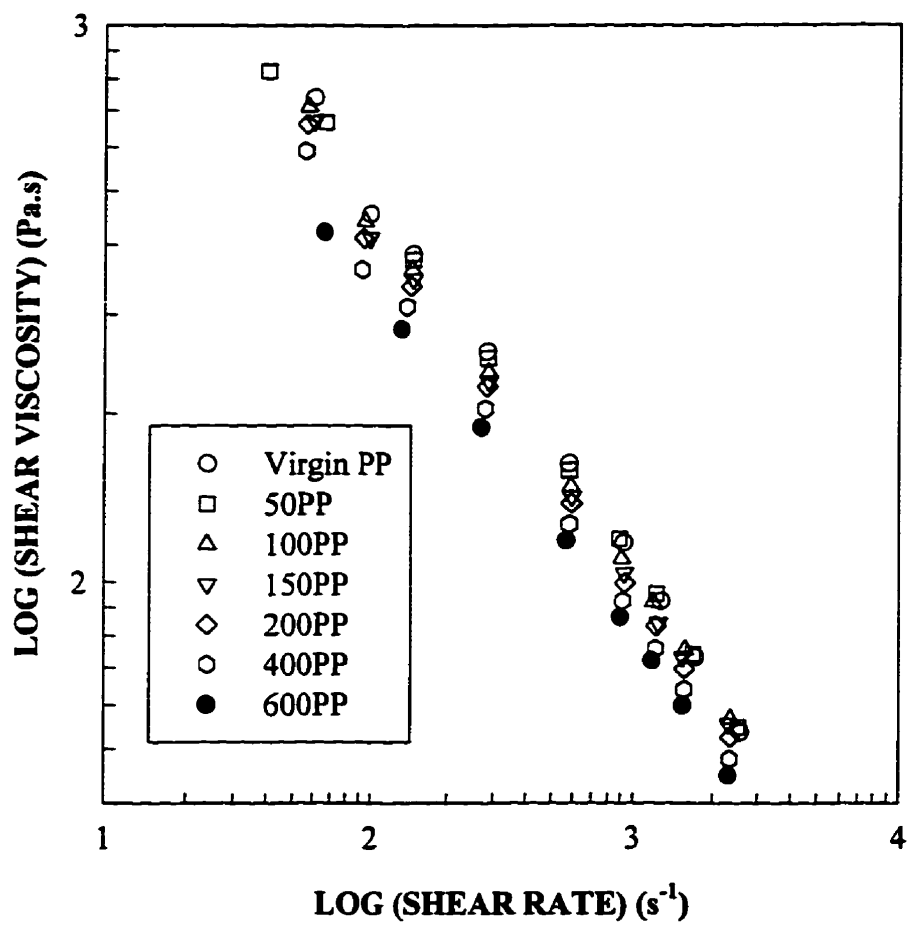


Fig. 4-21 Effect of the peroxide concentrations on the shear viscosities of the degraded polypropylenes.

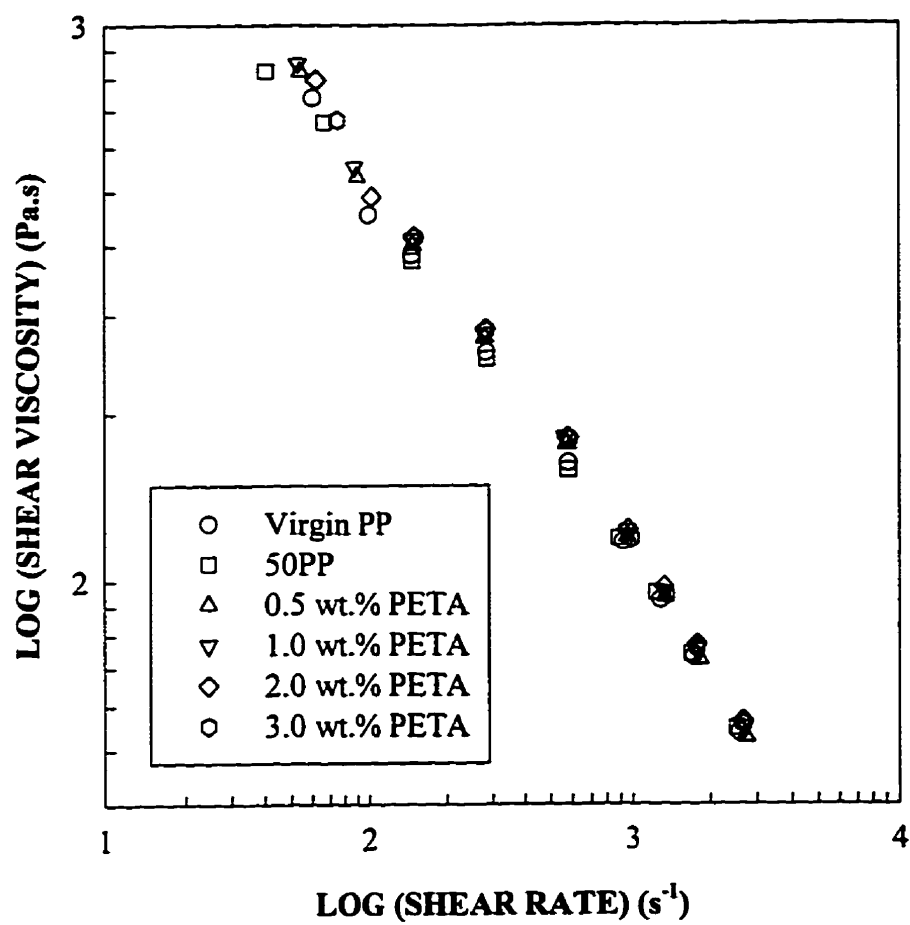


Fig. 4-22 Effect of the PETA and peroxide concentrations on the shear viscosities of the whole polymers (50 ppm peroxide series).

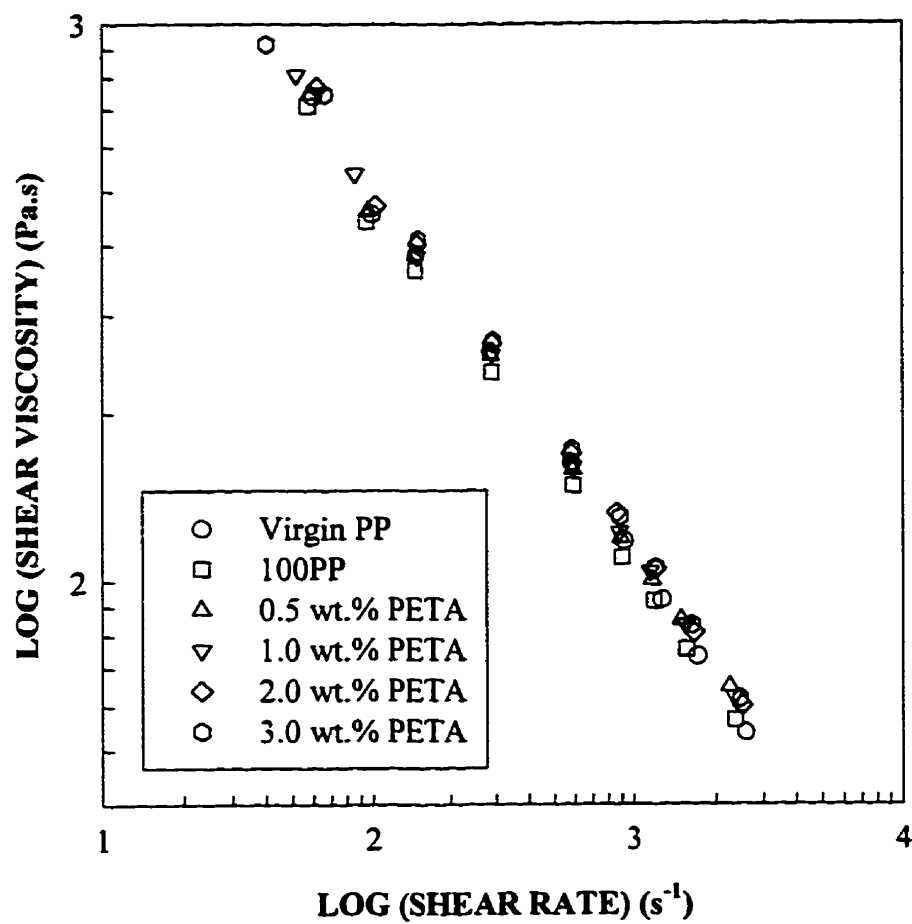


Fig. 4-23 Effect of the PETA and peroxide concentrations on the shear viscosities of the whole polymers (100 ppm peroxide series).



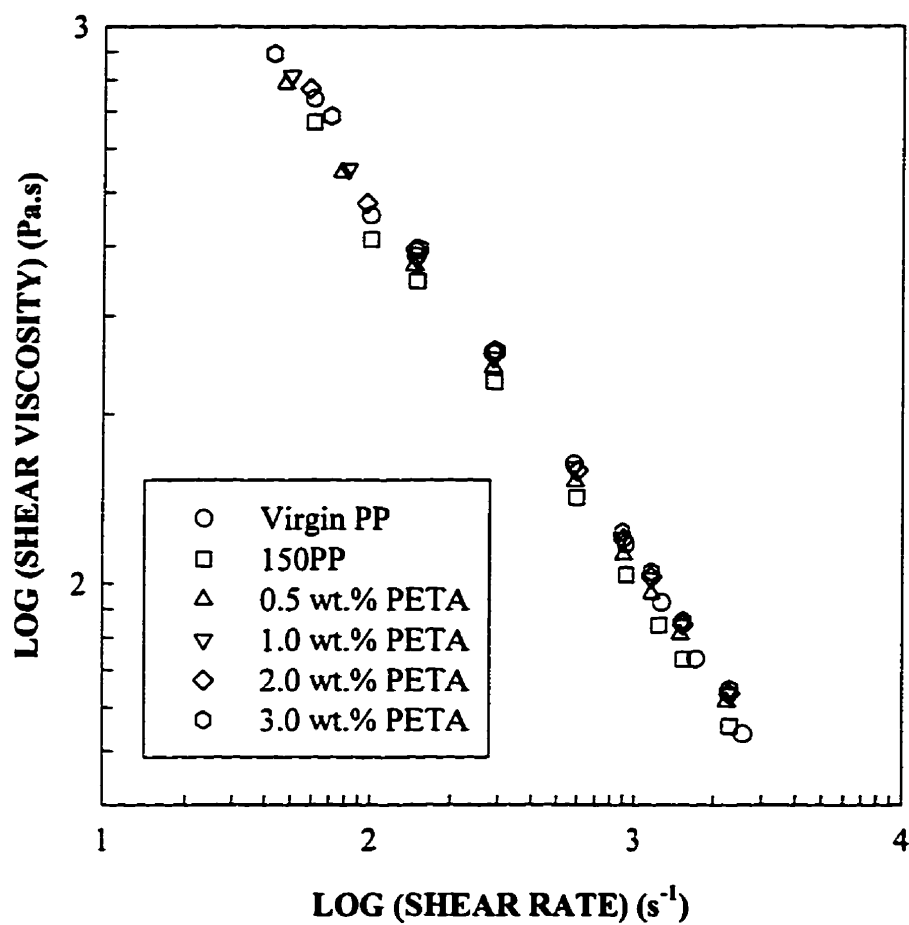


Fig. 4-24 Effect of the PETA and peroxide concentrations on the shear viscosities of the whole polymers (150 ppm peroxide series).

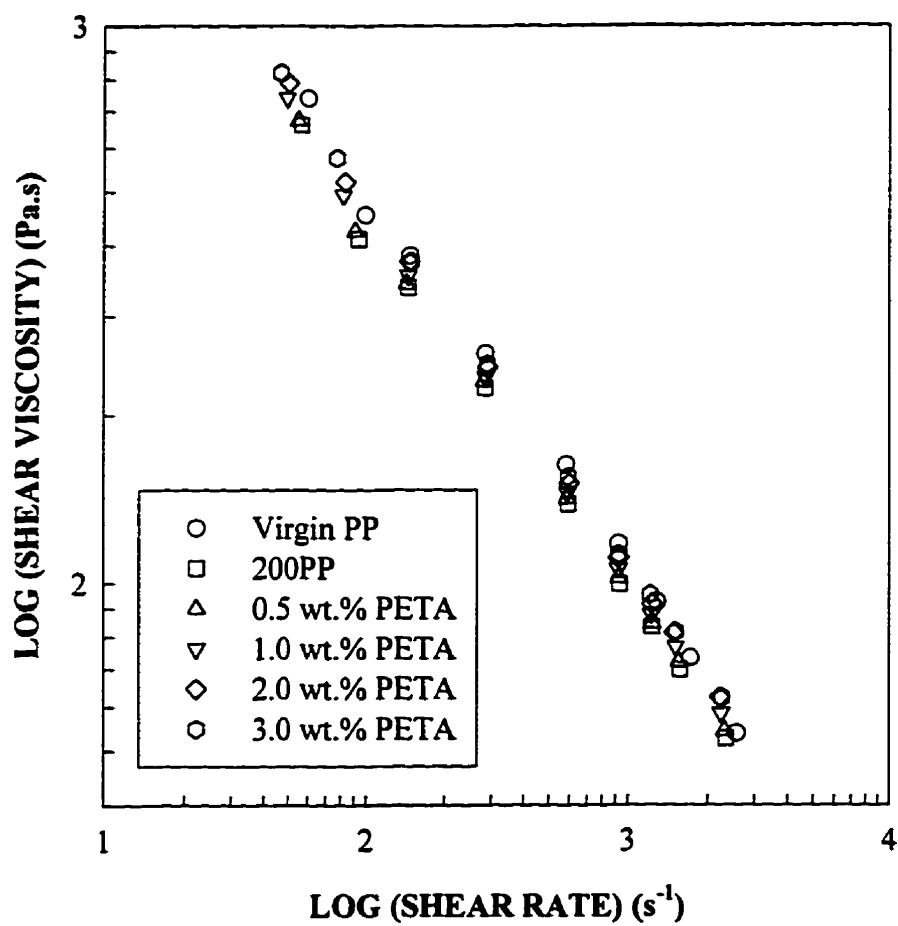


Fig. 4-25 Effect of the PETA and peroxide concentrations on the shear viscosities of the whole polymers (200 ppm peroxide series).

2 are similar to those in stage 1 and are much higher because of the use of a stabilizer (Fig. 4-26). Again, PETA seems to have no significant effect on MFI at high concentrations even when the much lower peroxide concentrations were used in stage 2 than in stage 1. It appears that MFI is able to show some differences among these modified PPs in the same peroxide series. It has also been known that for linear polypropylenes, there is a linear logarithmic relationship between the reciprocal of MFI and the weight average molecular weight, i.e., lower MFI representing the higher weight average molecular weight (Tzoganakis, 1988; Bremner et al., 1990; DeNicola et al., 1992). For branched PPs, lower MFI does not represent necessarily a higher weight average molecular weight (DeNicola et al., 1992) and this will be seen in the discussions of Chapter 5. Thus, MFI data alone are not enough to distinguish the molecular differences among these materials.

#### 4.4.2.6 A Comparison of Stage 1 and Stage 2 Results

In order to compare roughly the REX processes of stage 1 and stage 2, the MFI of some samples from these two stages with comparable PETA and L101 levels (200 ppm L101 series) are summarized in Table 4.7. The MFI of the materials from stage 1 was measured after REX with the products coated with 1.0 wt.% Irganox 1010. The MFI of the materials from stage 2 was measured with no further stabilizer added. It seems that the samples in stage 2 have much lower MFIs than those in stage 1 with comparable PETA and peroxide concentrations. Several factors may contribute to this: a) the premixing of Irganox 1010 with PP reduced the attack from peroxide primary radicals, b) the more homogeneous mixing of stabilizer with PP, and c) the PETA/L101 reacted immediately with PP melt.

The FTIR relative intensities ( $A_{1740}/A_{841}$ ) of the above materials from stage 1 and stage 2 are summarized in Table 4.8. Again, the relative intensity of  $A_{1740}/A_{841}$  is expressed as the mean plus/minus one standard deviation. It can be seen that at low PETA levels, there is no significant difference between the two stages in terms of this relative intensity. At a

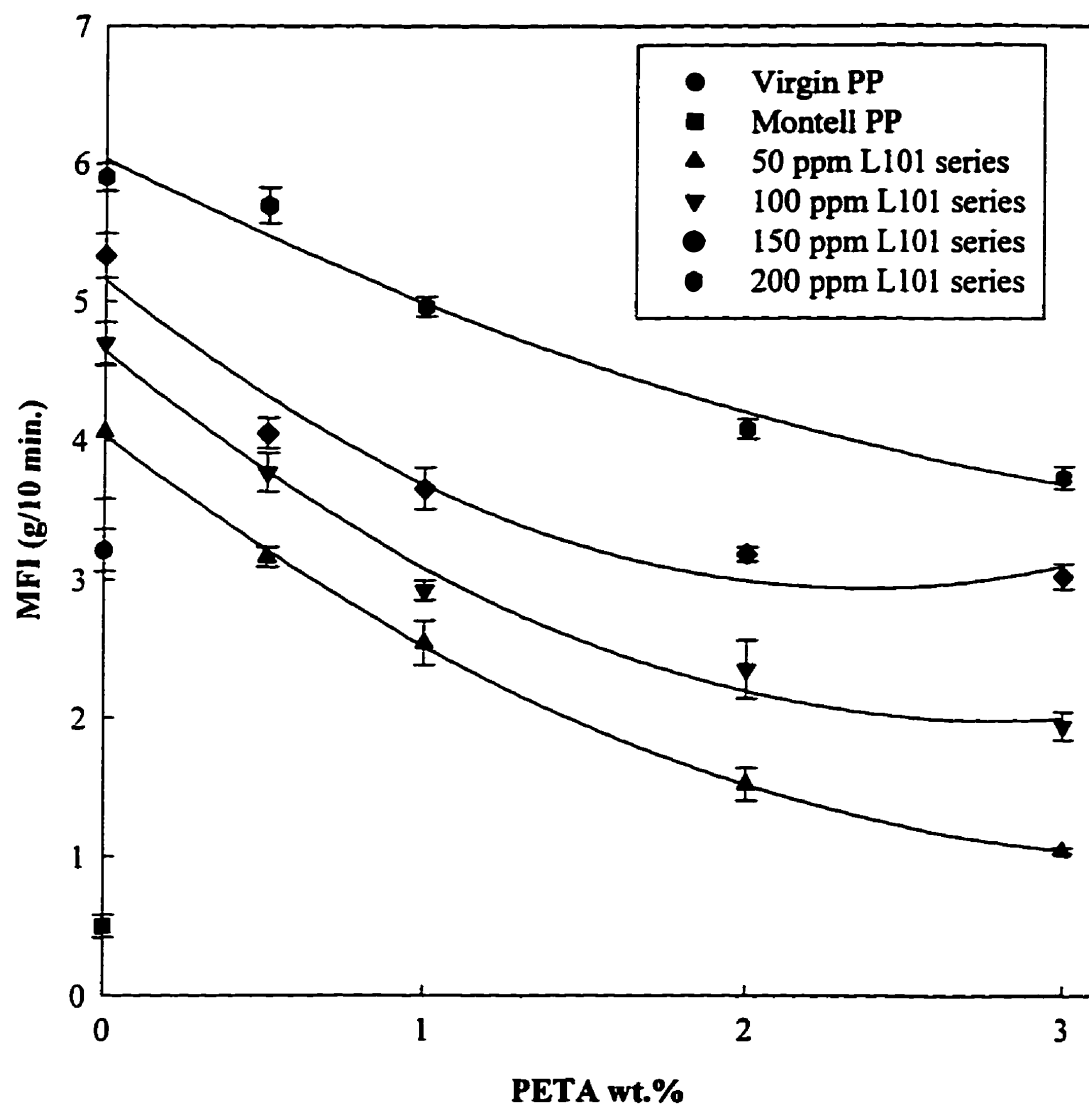


Fig. 4-26 Effect of the PETA and peroxide concentrations on the melt flow index (MFI) of the whole polymers. The MFI is expressed as the mean plus/minus one standard deviation.

relatively high PETA level,  $A_{1740}/A_{841}$  is higher in stage 1 than in stage 2. This seems consistent with the observation that at comparable PETA and peroxide levels, there are more macrogels formed in stage 2 than in stage 1, since the increased PETA homopolymerization reduces the amount of PETA reacted with PP.

**TABLE 4.7 Comparison of Melt Flow Index for the Materials from Stage 1 and Stage 2 (200 ppm L101 Series)**

Stage 1		Stage 2	
PETA wt. %	MFI with 1.0 wt. % Irganox 1010	PETA wt. %	MFI with 1.0 wt. % Irganox 1010
0.00	22.30	0.00	5.90
0.64	15.47	0.50	5.69
1.80	12.28	2.00	4.08
2.80	11.89	3.00	3.73

**TABLE 4.8 FTIR Relative Intensity Comparison of Materials from Stage 1 and Stage 2 (200 ppm L101 series).**

Stage 1		Stage 2	
PETA wt. %	$A_{1740}/A_{841}$	PETA wt. %	$A_{1740}/A_{841}$
0.64	$0.84 \pm 0.12$	0.50	$1.42 \pm 0.61$
1.80	$2.95 \pm 0.28$	2.00	$2.20 \pm 0.76$
2.80	$4.03 \pm 0.10$	3.00	$2.78 \pm 0.54$

#### 4.4.2.7 Conclusions

In stage 2, products with low amount of macrogels can be produced using very low peroxide concentrations. DSC experiments reveal that the crosslinking densities in the PP macrogels may not be so high since these macrogels show high melting points. It is also found by DSC that the majority in the macrogel formed in stage 2 is the non-crystallizable PETA homopolymer and, hence, the content of the highly crosslinked polypropylene is very low. FTIR results show that the relative intensity ( $A_{1740}/A_{841}$ ) seems to be the highest in the comparable samples of 100 ppm peroxide series and there is an optimum concentration ratio of PETA/peroxide for favouring the recombination reactions. MFI measurements show similar changes in terms of the variations of PETA and peroxide concentrations. Unlike stage 1, it is difficult in stage 2 to distinguish these PETA/peroxide modified PPs within the same peroxide series by using the shear viscosities generated by the current capillary rheometer. More techniques are required in order to better characterize these materials.

## **CHAPTER 5**

### **CHARACTERIZATION OF LONG CHAIN BRANCHING (LCB) BY GEL PERMEATION CHROMATOGRAPH (GPC)**

#### **5.1 Introduction**

Along with molecular weight and molecular weight distribution, long chain branching (LCB) is one of the fundamental parameters needed to fully describe the structure of a polymer and its melt-processing properties. In order to understand branching structures, one has to know at least some of the branching structural parameters such as a) the functionality of the branch points (e.g., trifunctional or tetrafunctional), b) the length of branches (long or short), c) the number of branch points per molecule (Schröder et al., 1989) and often d) the long chain branching frequency per 1000 carbon atoms. Elucidating the effects of branching is not easy since often these effects are confounded with that of polydispersity.

Since the fundamental work of Zimm and Stockmayer (1949), the influence of long chain branching (LCB) on the properties of polymers has been extensively studied (Meira, 1991) and it can be determined experimentally by GPC combined methods such as GPC-viscometry (Lecacheux et al., 1982; Pang et al., 1993) and GPC-LALLS (low angle laser light scattering) (Rudin et al., 1984). The basis for all GPC-related methods is the universal elution volume-hydrodynamic volume relation (universal calibration) proposed by Benoit et al. (1966). Branched molecules have a smaller hydrodynamic volume than linear ones and thus will elute in GPC with lower molecular weight linear species.

Particularly, the GPC-viscometry method has been widely used to establish the intrinsic viscosity-molecular weight relationship. Up to now, branched polyethylene has been the main polymer of interest for this LCB frequency analysis (Rudin, 1993). For long chain branched polyethylenes, it has been reported that GPC rates LCB frequency correctly and

these estimates are in reasonable agreement with the results from  $^{13}\text{C}$  NMR (Pang et al., 1993). The  $^{13}\text{C}$  NMR method is believed to be the reference method because of its inherent sensitivity to structural features, and the absence of assumptions regarding the relation between molecular structure and radius of gyration as in the case of using GPC to characterize LCB (Pang et al., 1993). On the other hand, GPC analyses are found to be not as sensitive as NMR techniques and rheological measurements (Pang et al., 1993; Dickie et al., 1990). Nonetheless, GPC, when equipped with detectors which can measure molecular weight directly, is the only current analytical technique that can provide information on the variation of LCB with molecular weight, without fractionation of the polymer (Rudin, 1993). For branched PPs, Hingmann et al. (1994) reported the estimation of the mean number of branching reactions per molecule from the applied concentration of the crosslinking agent. However, no detailed information was given regarding the reaction system. Recently, Thitiratsakul (1991) used GPC-viscometry to characterize branched PPs which were produced in a batch mixer. The molecular weight averages, molecular weight distributions and viscosity law plots were obtained. Using the difference of the area in both high and low molecular weight regions between virgin PP and reacted PP, the fractions of branching and degradation were estimated to be around 1-3.5% and 8.5-15.8% respectively. However, long chain branching frequencies for the whole polymers were not evaluated.

## 5.2 Theoretical Background

For monodisperse linear polymers in the GPC solvent, the Mark-Houwink equation relates the intrinsic viscosity to the viscosity average molecular weight ( $M_v$ ) as shown in the following equation:

$$[\eta] = KM_v^\alpha \quad (5-1)$$

where  $[\eta]$  is the polymer intrinsic viscosity for a given set of solvent/temperature conditions,



$M_v$  is the viscosity-average molecular weight, and  $K$  and  $\alpha$  are the Mark-Houwink constants. In the GPC chromatogram,  $M_v$  is replaced by  $M$  since the concern is with small, relatively monodisperse slices. Theoretically, for a linear polymer the viscosity law plot ( $\log [\eta]$  versus  $\log M$ ) is linear across the molecular weight distribution with an intercept equal to  $\log K$  and a slope equal to  $\alpha$ . However, it has been observed that intrinsic viscosity behaviour departs seriously from the Mark-Houwink equation at both low and very high molecular weights (Van Krevelen, 1990). The failure of the Mark-Houwink relationship to predict behaviour at low molecular weight is a consequence of the non-Gaussian character of short flexible chains, and due to the hydrodynamic interaction at very high molecular weights (Lovell, 1989).

The principle of universal calibration in GPC states that for given sets of solvent and temperature conditions in which a polymer sample is separated by a pure size mechanism, the logarithm of the hydrodynamic volume of a polymer molecule as a function of its elution volume (or time) is identical for all polymers, linear or branched (Drott and Mendelson, 1970). The hydrodynamic volume is defined as the product of intrinsic viscosity ( $[\eta]$ ) and molecular weight (MW). The universal calibration curve can be obtained by using one set of well characterized, narrow distribution polymer standards such as polystyrene.

Based on the concept of equal hydrodynamic volume, at equal GPC elution volume (or time) and infinite dilution, the molecular weights of linear and branched versions of the same polymer can be related by:

$$[\eta]_b M_b = [\eta]_l M_l \quad (5-2)$$

where the subscripts  $b$  and  $l$  refer to branched and linear macromolecules that have the same GPC elution volume or time.

Now consider a branched and a linear version of the same polymer, both with the same molecular weight. Since a branched polymer molecule has a more compact

conformation in solution than a linear molecule of the same molecular weight, the molecular weight of a branched molecule is greater than that of a linear molecule eluted at the same elution volume (or time). From equation 5-2, it follows that the intrinsic viscosity,  $[\eta]_b$ , of the linear polymer will be greater than that of the branched species,  $[\eta]_b$ , in the GPC solvent. The ratio of the two intrinsic viscosities is defined as the branching index:

$$g' = \frac{[\eta]_b}{[\eta]_l} \quad (5-3)$$

Also from equations 5-1 and 5-2:

$$g' = \left[ \frac{M_l}{M_b} \right]^{\alpha+1} \quad (5-4)$$

At any given elution volume or time,  $M_b$  is measured directly with a continuous viscometer (CV) or a low angle laser light scattering detector (LALLS), while  $M_l$  is calculated from the universal calibration curve of the linear polymer. The  $g'$  can be calculated at each slice across the molecular weight distribution and the average value of  $g'$  for the whole polymer can be obtained. Both of them can be used for comparison of long-chain branching among samples.

To estimate the number of branches in a molecule and hence the LCB frequency, it is necessary to assume a relationship between the branching index ( $g'$ ) and the ratio ( $g$ ) of the mean square radius of gyration  $\langle R_G^2 \rangle$  for the branched and linear polymers with molecular weights  $M_l = M_b$ :

$$g = \frac{\langle R_G^2 \rangle_b}{\langle R_G^2 \rangle_l} \quad (5-5)$$

where  $g$  is smaller than 1. The relationship between  $g'$  and  $g$  has been proposed as following (Zimm et al, 1959; Berry, 1971):

$$g' = g^k \quad (5-6)$$

The theoretical value of  $k$  is between 0.5 and 1.5 (Zimm and Stockmayer, 1949; Zimm and Kilb, 1959).  $k$  is 0.5 for randomly branched polymers (Zimm and Kilb, 1959) and this has been supported by many experimental results for various branched polymers (Drott and Mendelson, 1970). However,  $k$  is a somewhat varying value even for the same kind of branched polymers. For example, it has been found that  $k$  may not be the same for polyethylenes with different long chain concentrations (Grinsphun et al., 1986). Different values of  $k$  have been used for branched polyethylenes in the literature to evaluate the LCB frequency by GPC, i.e., 0.55-0.65 (Nordmeier et al., 1990), 0.7 (Pang and Rudin, 1993), and 0.8 (Hert et al., 1983).

In order to estimate the number of long branches per molecule in our system, several assumptions were used: i) the polymer is randomly branched, ii) the value of  $k$  is 0.5, iii) the branched PP contains trifunctional branching points, iv) the polymer solutions are  $\theta$  ones, although actually these polymers are just dissolved in a good solvent. Then, the  $g$  in equation 5-5 can be related to the weight-average number of branch points per molecule,  $n_w$ , using the Zimm-Stockmayer relation (Zimm and Stockmayer, 1949):

$$g = \frac{6}{n_w} \left\{ \frac{1}{2} \left( \frac{2+n_w}{n_w} \right)^{0.5} \ln \left[ \frac{(2+n_w)^{0.5} + n_w^{0.5}}{(2+n_w)^{0.5} - n_w^{0.5}} \right] - 1 \right\} \quad (5-7)$$

Thus, the long chain branching frequency  $\lambda$  per 1000 carbon atoms can be estimated using:

$$\lambda = \frac{n_w(14)(1000)}{M_b} \quad (5-8)$$

where  $M_b$  is the molecular weight measured for the branched species at any given elution volume or time.

### 5.3 GPC Operating Principles

In this thesis, a Waters 150 CV Plus Gel Permeation Chromatograph was used to analyze the molecular properties of the sols from stage 2. This GPC system is configured with two detectors which are connected in series: a) differential refractive index (DRI) detector or refractometer and b) a continuous differential viscometer (CV) detector (Waters, 1994a).

The refractometer is a concentration detector. It generates a signal directly proportional to the concentration of polymer in the eluent. The response chromatogram from the refractometer can be divided into many small slices. The concentration ( $C_i$ ) of the sample in any slice in the polymer region can be calculated from the refractometer data using the following equation:

$$C_i = \frac{C V A_i}{\Delta v A} \quad (5-9)$$

where  $A_i$  is the area of slice  $i$ ,  $A$  is the total area of refractometer response for the polymer sample,  $C$  is the concentration of polymer in the sample injected,  $V$  is the injection volume, and  $\Delta v$  is the volume of slice  $i$ .

The viscometer measures the viscosity of a sample in solution. This is achieved by measuring the difference in fluid pressure across a small capillary using a differential pressure transducer. The viscometer pressure transducer signal, in conjunction with the refractometer signal, is used to a) calculate the intrinsic viscosity and absolute molecular weight of a polymer, and b) determine the extent of polymer long-chain branching.

#### 5.3.1 Determination of Intrinsic Viscosity (IV)

Generally, the intrinsic viscosity (IV) can be determined from either the inherent viscosity ( $\eta_{inh}$ ) or from the reduced viscosity ( $\eta_{red}$ ):

$$\eta_{inh} = \frac{\ln(\eta/\eta_{sol})}{C} \quad (5-10)$$

$$\eta_{red} = \frac{(\eta - \eta_{sol})}{\eta_{sol} C} \quad (5-11)$$

where the  $\eta$  and  $\eta_{sol}$  are the viscosity of the sample solution and pure solvent respectively, and  $C$  is the concentration of the sample. If data from  $\eta_{inh}$  or from  $\eta_{red}$  are determined for several different concentrations of the sample in the solvent of interest, they can be used to determine the intrinsic viscosity using a linear extrapolation to zero concentration.

In the 150CV Plus system used, the viscometer generates a signal equal to the pressure drop across the viscometer capillary as described by Poiseuille's law. When no polymer sample is eluting from the columns, the viscometer measures the pressure drop ( $P_0$ ) of the pure solvent flowing through the capillary, i.e., the baseline signal. When a polymer sample is eluting, there is an increase in the pressure drop during the elution of a small slice  $i$  ( $P_i$ ). In 150CV Plus GPC, the computer data system will obtain the polymer signal by subtracting the baseline signal. Using the equation for reduced viscosity (equation 5-11), the intrinsic viscosity of the dilute solution of polymer for any slice ( $i$ ) in the viscometer signal can be calculated using the equation:

$$[\eta]_i = \frac{(P_i - P_0)}{C_i P_0} \quad (5-12)$$

where  $[\eta]_i$  is the intrinsic viscosity of slice  $i$ ,  $C_i$  is the polymer concentration in slice  $i$ ,  $P_i$  and  $P_0$  are the sample and baseline viscometer signals respectively.

Finally, the intrinsic viscosity of the whole polymer eluting from the system can be calculated as:

$$[\eta] = \frac{\sum C_i [\eta_i]}{\sum C_i} \quad (5-13)$$

where  $[\eta]$  is the polymer intrinsic viscosity,  $C_i$  is the polymer concentration of slice  $i$  and  $[\eta_i]$  is the intrinsic viscosity of slice  $i$ .

### 5.3.2 Absolute Molecular Weight Average Determination

As discussed in section 5.3.1, the viscometer data ( $P_i$ ,  $P_0$ ) in 150CV Plus system can be used to calculate the product of the concentration of the polymer ( $C_i$ ) and its intrinsic viscosity ( $[\eta_i]$ ) at any slice in the GPC chromatogram (equation 5-12). For a specific polymer sample, the viscometer data are used to calculate  $C_i[\eta_i]$  at each slice and the DRI data are used to calculate the corresponding concentration  $C_i$ . Dividing the viscometer data by the DRI data provides the intrinsic viscosity,  $[\eta_i]$ , of the polymer at each slice in the GPC chromatogram. From the universal calibration curve, the hydrodynamic volume ( $[\eta_i]M_i$ ) at each slice can be calculated. Dividing the hydrodynamic volume by  $[\eta_i]$  gives the absolute molecular weight ( $M_i$ ) of each slice. Absolute molecular weight averages can then be calculated from the concentration ( $C_i$ ) and molecular weight ( $M_i$ ) at each slice in the GPC chromatogram.

## 5.4 Experimental

A high temperature Waters 150-CV Plus gel permeation chromatograph equipped with a differential refractive index detector (DRI) and a continuous differential viscometer (CV) detector, was used in this experiment. Four columns were used and calibrated using 14 polystyrene standard samples (American Polymer Standards Corp., Ohio) with molecular weights ranging from 2500 to  $9.1 \times 10^5$ . The GPC experiments were run with a flow rate of 1.0 ml/min at 140°C. The injected polymer solution was filtered through a 0.45 micron

tetrafluoroethylene filter.

The GPC samples used are the purified sols from the samples of stage 2 produced in Chapter 4, which include the peroxide-degraded PPs, PETA/peroxide modified PPs and commercial Montell branched PP (Montell PP). The description of these materials can be found in Chapter 4. To prevent oxidative degradation of PP, Irganox 1010 (Ciba Geigy Co.) was added as the antioxidant to the eluent, 1,2,4-trichlorobenzene or TCB (chromatography grade, BDH Inc.) at a concentration of 0.5 mg/ml. All the solutions for analysis were prepared using the same solvent used as the GPC eluent. Sample concentrations were around 0.4-1.0 mg/ml. The preparation of the solution samples was based on the method suggested by Billiani et al. (1990) with a slight modification, i.e., dissolving the polymer with the above eluent at around 170°C for one hour with gentle stirring and then at 140°C for six hours with spinning. The modified method originally suggested by Grinshpun et al. (1986), i.e., dissolving the polypropylenes at 140°C for thirty to forty-five hours, was also tried though the temperature used in literature was 145°C. It was found that comparable results could be obtained using these two methods. The experimental variation in the molecular weight averages was found to be less than 12% (maximum). The  $\bar{g}'$  for the whole polymers are averaged within the good data regions which are chosen based on the procedures described in the GPC manual (Waters, 1994b). The LCB frequencies for the whole samples were obtained by averaging the LCB frequency level of each slice while accounting for the weight fraction of each slice.

## **5.5 Results and Discussion**

### **5.5.1 Montell Branched PP, Virgin PP and Degraded PPs**

Table 5.1 lists the molecular parameters for the whole polymer GPC samples of virgin PP, peroxide-degraded PPs and Montell branched PP. It can be seen that all the molecular weight averages for Montell PP are much higher than those of the virgin PP used

for experiments in the present study. As expected, the molecular weight averages of PP and polydispersity values decrease with increasing peroxide concentrations. For the sake of clarity, the actual molecular weight distribution (MWD) curves for some of these degraded PPs are shown in Fig. 5-1. It can be observed that with increasing peroxide concentration, the distribution is progressively moved to lower molecular weight, while the change in the low molecular weight end seems relatively small. This is fully in agreement with previous works (Suwanda et al., 1988; Tzoganakis et al., 1988). There are increases in the amount of macromolecules with moderate molecular weights since the peak heights increase with peroxide concentration. The MWD curves of the repeated GPC samples for virgin PP and 100PP are shown in Figs. 5-2 and 5-3 and it can be seen that the reproducibility seems good.

Reasonable results were obtained for intrinsic viscosities since generally  $[\eta]$  decreases with increasing peroxide concentration (Table 5.1). The standard deviation of  $[\eta]$

**TABLE 5.1 Molecular Parameters of the Montell PP and Peroxide-Degraded PPs**

Sample	[L101] (ppm)	$\bar{M}_n$	$\bar{M}_w$	$\bar{M}_z$	$\bar{M}_w/\bar{M}_n$	$g'$	$[\eta]$ (dl/g)
Montell PP <sup>a</sup>	--	81,500	371,800	1,217,800	4.56	0.885	1.2726
Virgin PP <sup>b</sup>	--	50,600	272,200	1,003,100	5.38	0.896	1.5235
50PP	50	49,500	266,100	935,400	5.38	0.956	1.2640
100PP <sup>c</sup>	100	46,400	237,300	835,000	5.12	0.941	1.2564
150PP	150	45,500	217,300	689,500	4.78	0.967	1.3025
200PP	200	43,800	197,400	636,500	4.51	1.040	1.2228
400PP	400	41,800	186,900	542,300	4.47	0.912	0.9673
600PP	600	37,800	154,300	448,700	4.09	0.990	1.0891

a: Average data from two GPC samples,

b: Average data from two GPC samples,

c: Average data from three GPC samples. See Appendix B for K and  $\alpha$  constants.



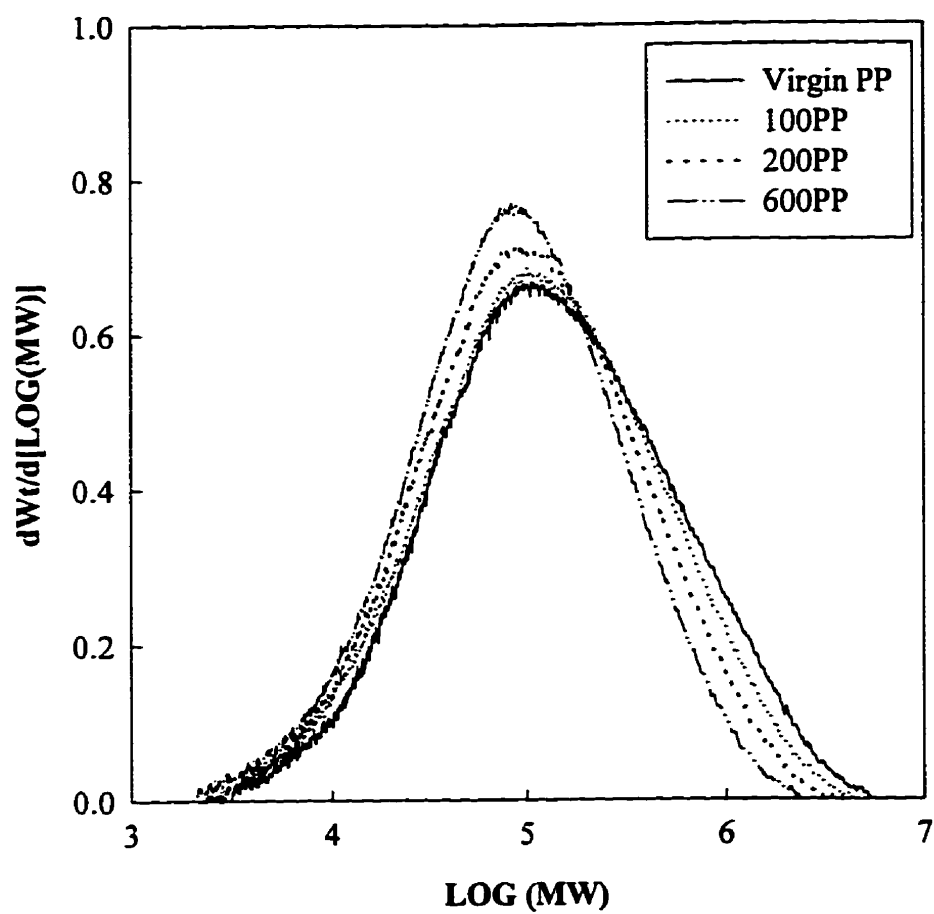


Fig. 5-1 Effect of peroxide concentration on the molecular weight distribution of PP.

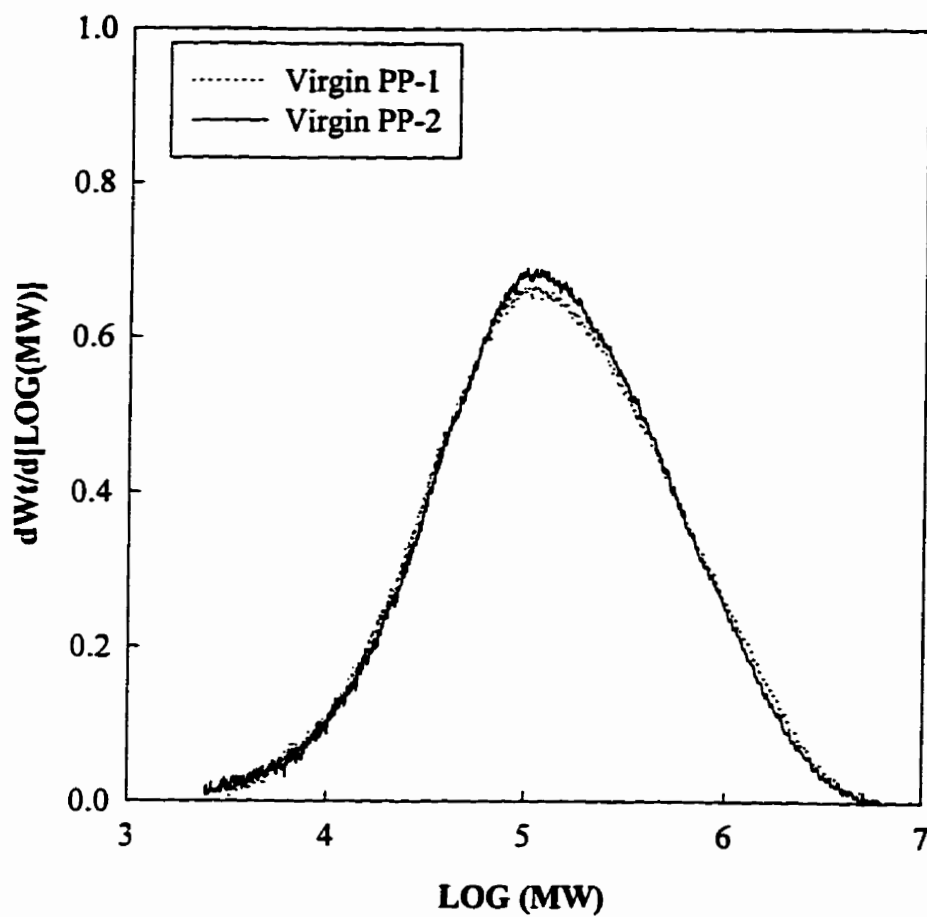


Fig. 5-2 Molecular weight distribution curves of the repeated samples of virgin PP.

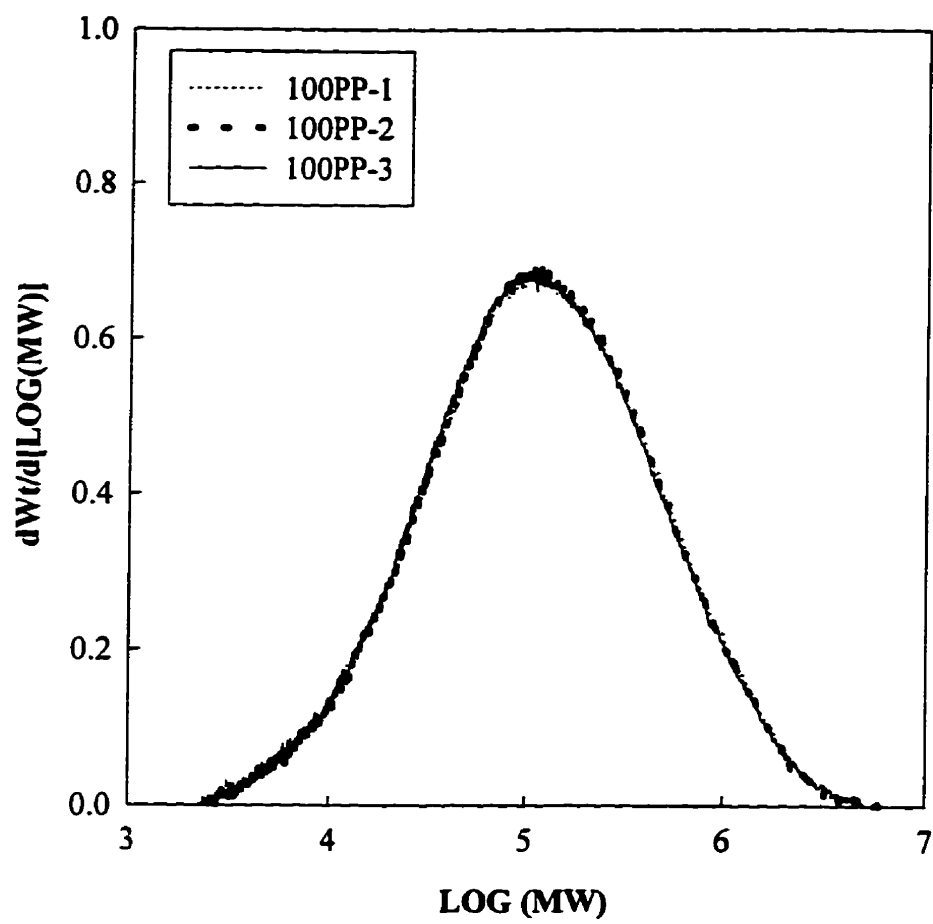


Fig. 5-3 Molecular weight distribution curves of the repeated samples of 100PP.

was found to be around 0.0512 dl/g for the repeated GPC measurements of 100PP and it is assumed to be valid for all the samples throughout this experiment.

The  $[\eta]$  of the branched Montell PP is significantly lower than that of the virgin PP or similar to those of some degraded PPs, even though its  $\bar{M}_w$  is much higher than those of these linear polymers. Fig. 5-4 shows two measurements of the Montell PP MWD and again the reproducibility is good.

Figs. 5-5, 5-6 and 5-7 show the viscosity law plots of the repeated GPC samples for virgin PP, 100PP and Montell PP, corresponding to the samples in Figs. 5-2, 5-3 and 5-4 respectively. Overall, it seems that the reproducibility of the viscosity law plots are good. The viscosity law plots for the virgin PP, some peroxide-degraded PPs and Montell PP are summarized in Fig. 5-8. All the plots of virgin PP and degraded PPs do not show curvatures at high molecular weight regions since they are all linear. It seems that the viscosity law curve for Montell PP is somewhat lower than those of the linear PPs. This is expected since Montell PP is claimed to be a branched polymer from the resin supplier. However, it is surprising to see that its viscosity law plot does not show significant curvature even at the very high molecular weight end.

The average value of  $g'$  for the whole GPC samples of all the linear polypropylenes is 0.957 with a standard deviation of 0.048. The  $g'$  for Montell PP is 0.885, which is somewhat smaller than the lower limit for the  $g'$  of all the linear PPs. The  $g'$  at each slice across the molecular weight distribution for the above linear samples and Montell PP are presented in Fig. 5-9. It can be seen that the  $g'$ s of these linear PPs are all around unity across the whole molecular weight region and there is no significant difference among them. This further supports the results for the average  $g'$  of the whole polymers in Table 5.1. It is also noted that the  $g'$  distribution of Montell PP does not deviate significantly from unity for almost the whole molecular weight region. Only within a narrow region at very high molecular weight does Montell PP show any evidence of this deviation. This may explain

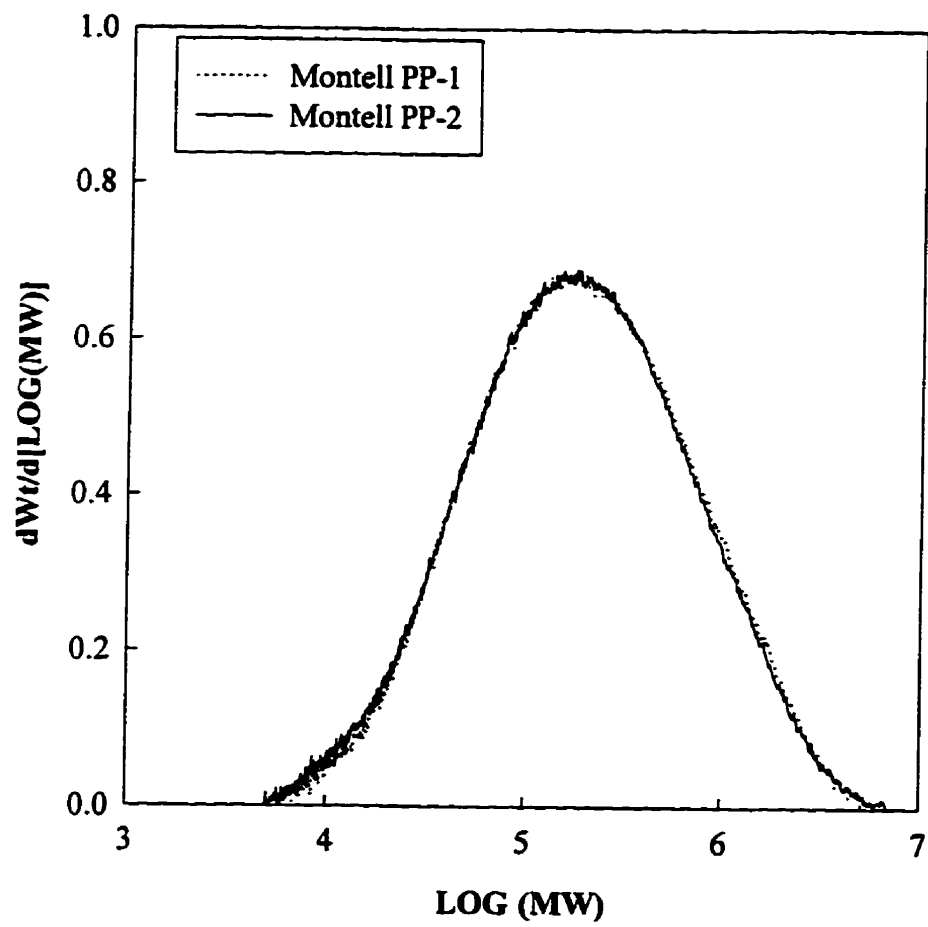


Fig. 5-4 Molecular weight distribution curves of the repeated samples of Montell PP.

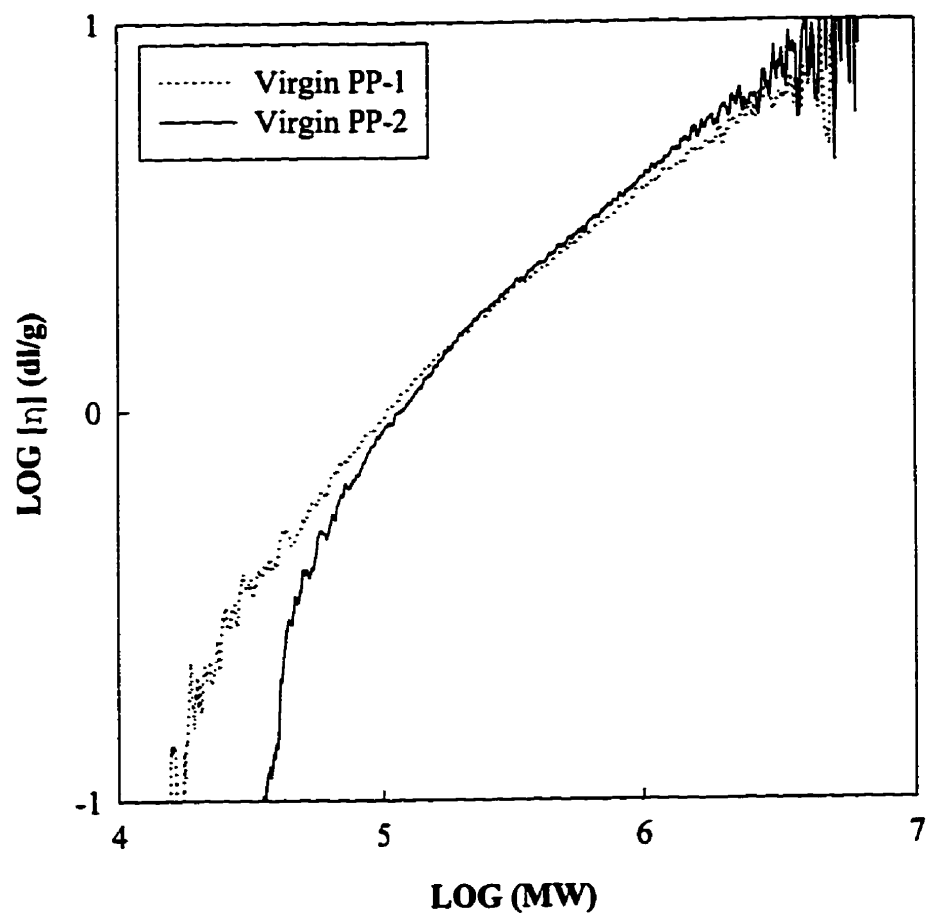


Fig. 5-5 Viscosity law plots of the repeated samples of virgin PP.

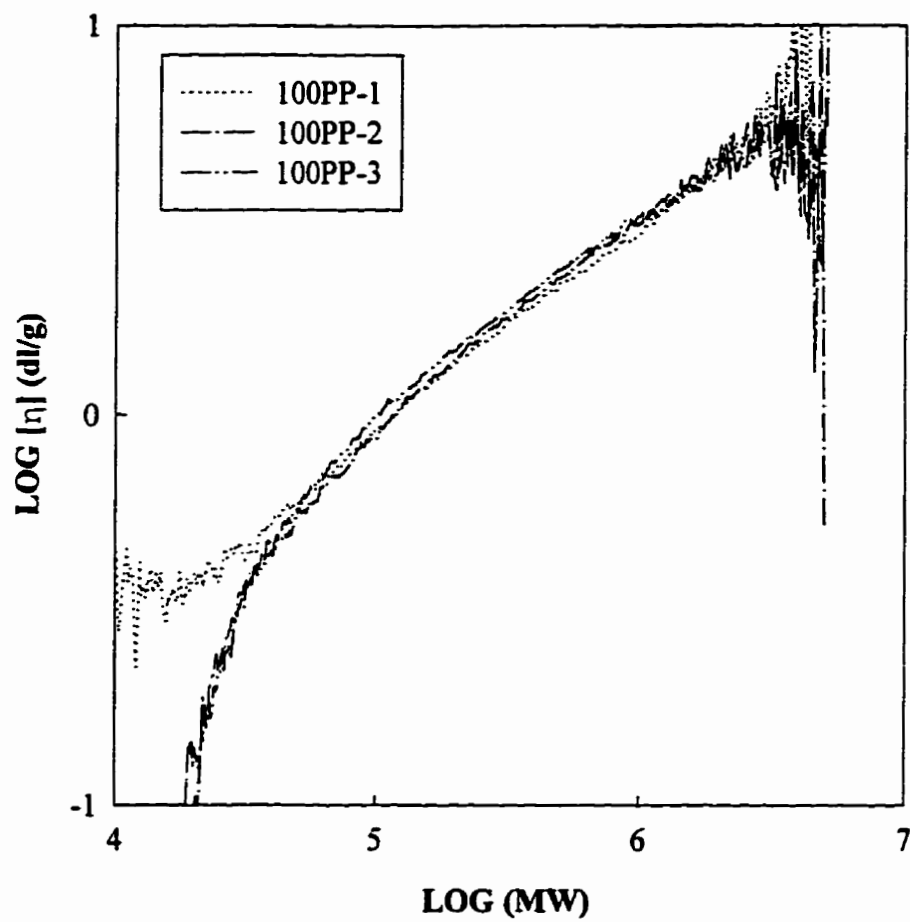


Fig. 5-6 Viscosity law plots of the repeated samples of 100PP.

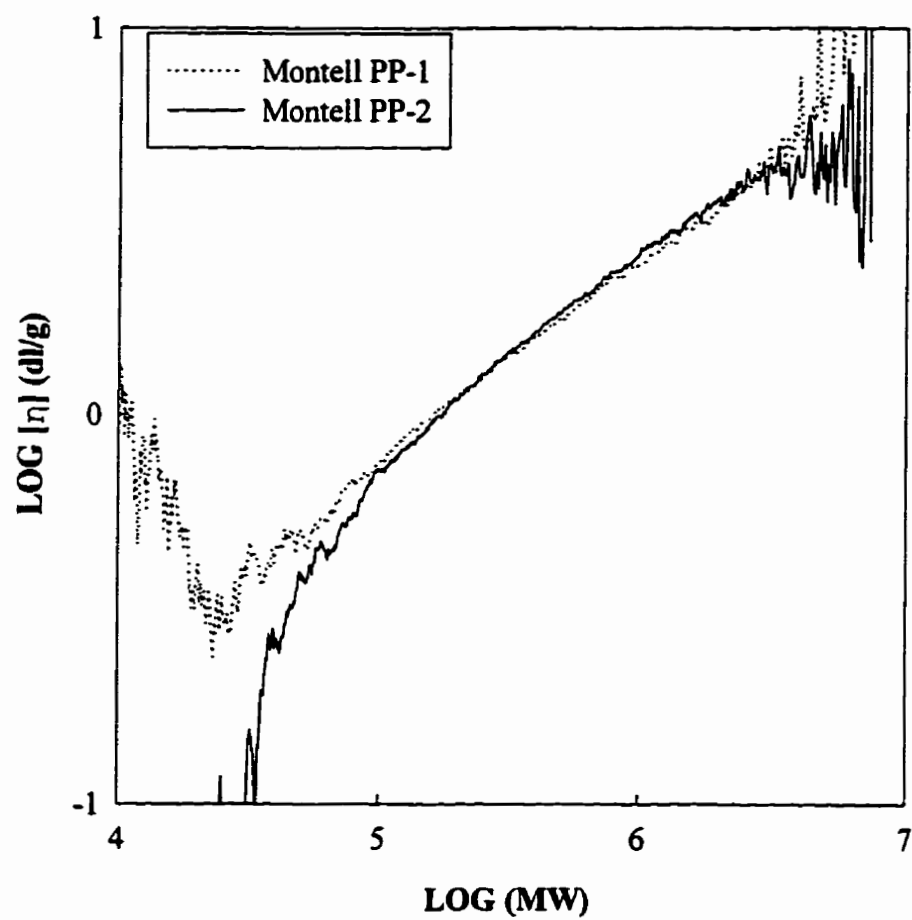


Fig. 5-7 Viscosity law plots of the repeated samples of Montell PP.



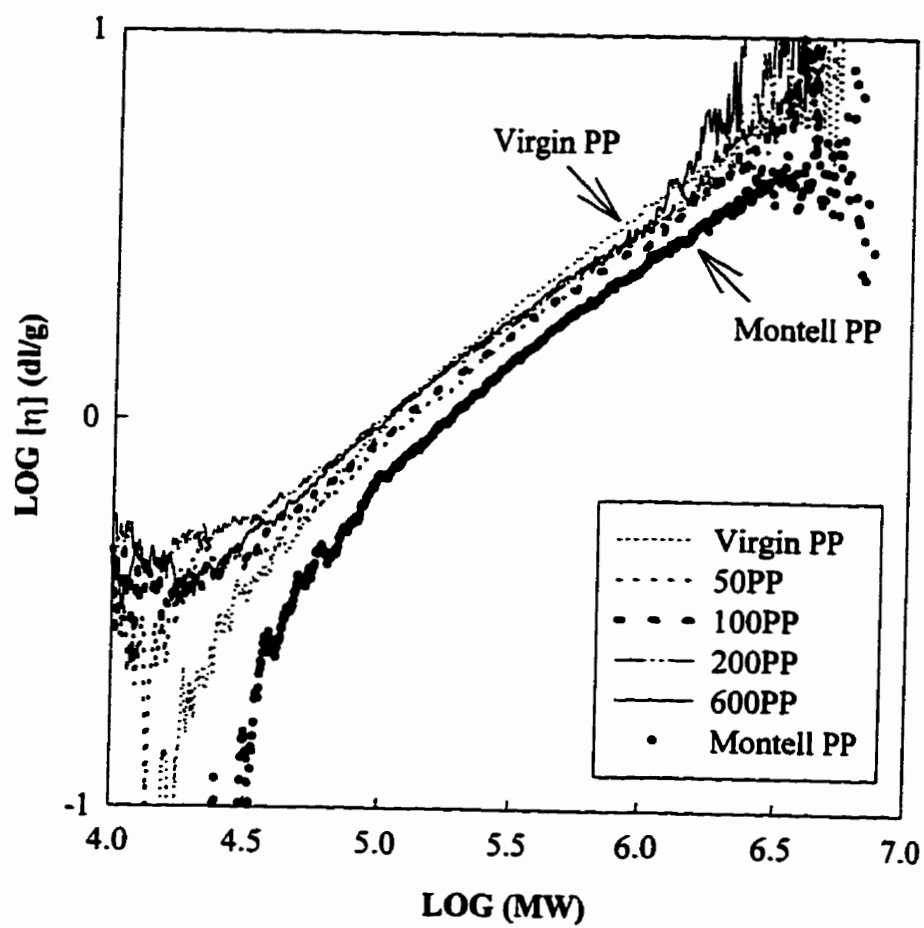


Fig. 5-8 Viscosity law plots of the virgin PP, peroxide degraded PPs and Montell PP.

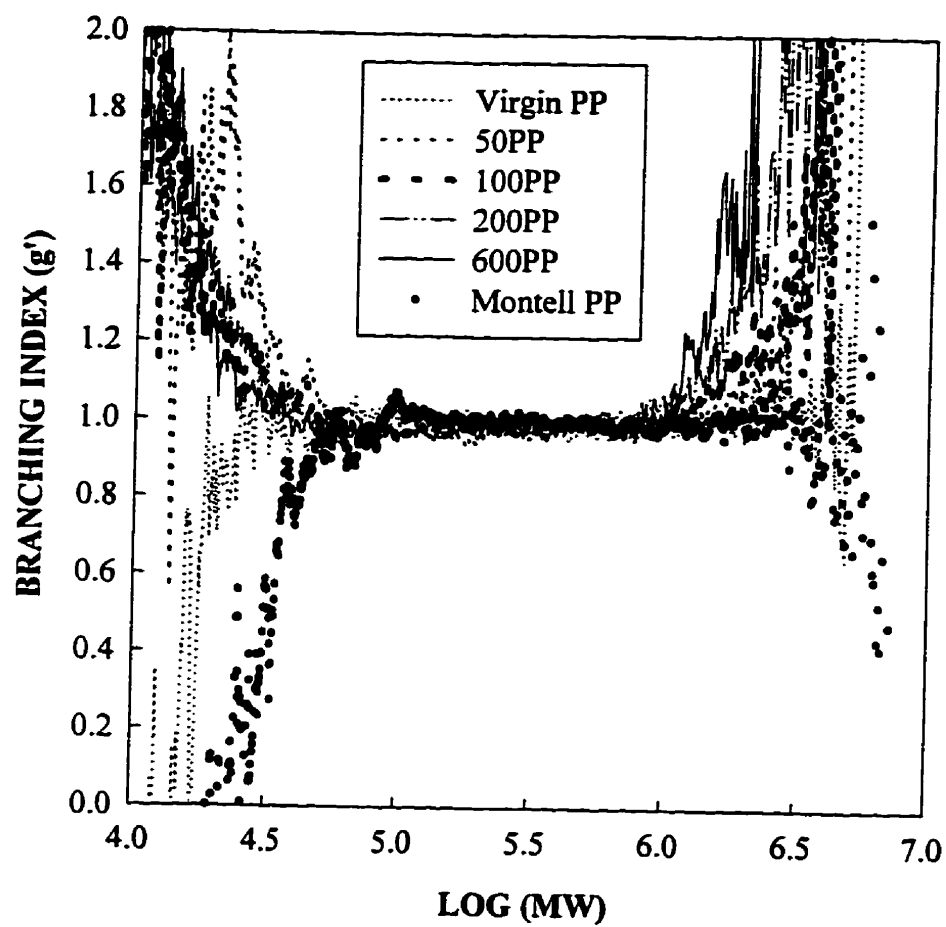


Fig. 5-9  $g'$  distributions across the whole molecular weight of virgin PP, peroxide degraded PPs and Montell PP.

why the Montell PP has a relatively high  $g'$  (compared with those of long chain branched PP shown below). From the above discussions, it can therefore be seen that the results of  $g'$  distributions of linear PPs and Montell PP seem consistent with the average  $g'$  values of their whole samples.

LCB results for Montell PP are shown in Fig. 5-10 and it seems that it contains a very low level of LCB. The long chain branching frequencies per 1000 carbon atoms ( $\lambda$ ) for the linear PPs are shown in Figs. 5-11a-g. It is clear that there is virtually no long chain branching at the high molecular weight regions in linear PPs. LCB frequency appears within the relatively low molecular weight region. Although chain branching may also occur as a result of recombination reactions, other factors may also cause the appearance of LCB in this region, such as a) the experimental noise in the detector signals, b) the Mark-Houwink relationship may not apply across the whole molecular weight range. It has also been reported that the frequently observed increase in LCB in the low molecular weight region of the chromatogram is probably fallacious due to the insensitivity of the molecular weight detectors to low molecular weight species (Mirabella and Wild, 1990).

### 5.5.2 PETA/Peroxide Modified PPs

**50 ppm peroxide series** Table 5.2 lists the molecular parameters as measured by GPC

**TABLE 5.2 Molecular Parameters of the Samples in the 50 ppm Peroxide Series**

Sample	$\bar{M}_n$	$\bar{M}_w$	$\bar{M}_z$	$\bar{M}_w/\bar{M}_n$	$g'$	$[\eta]$ (dl/g)
SPT505	32,200	175,300	614,500	5.45	0.966	1.2393
SPT510	38,100	188,100	712,500	4.94	0.779	0.9700
SPT520	40,500	212,200	809,200	5.24	0.876	1.2428
SPT530	41,800	227,300	1,093,500	5.43	0.812	1.1845

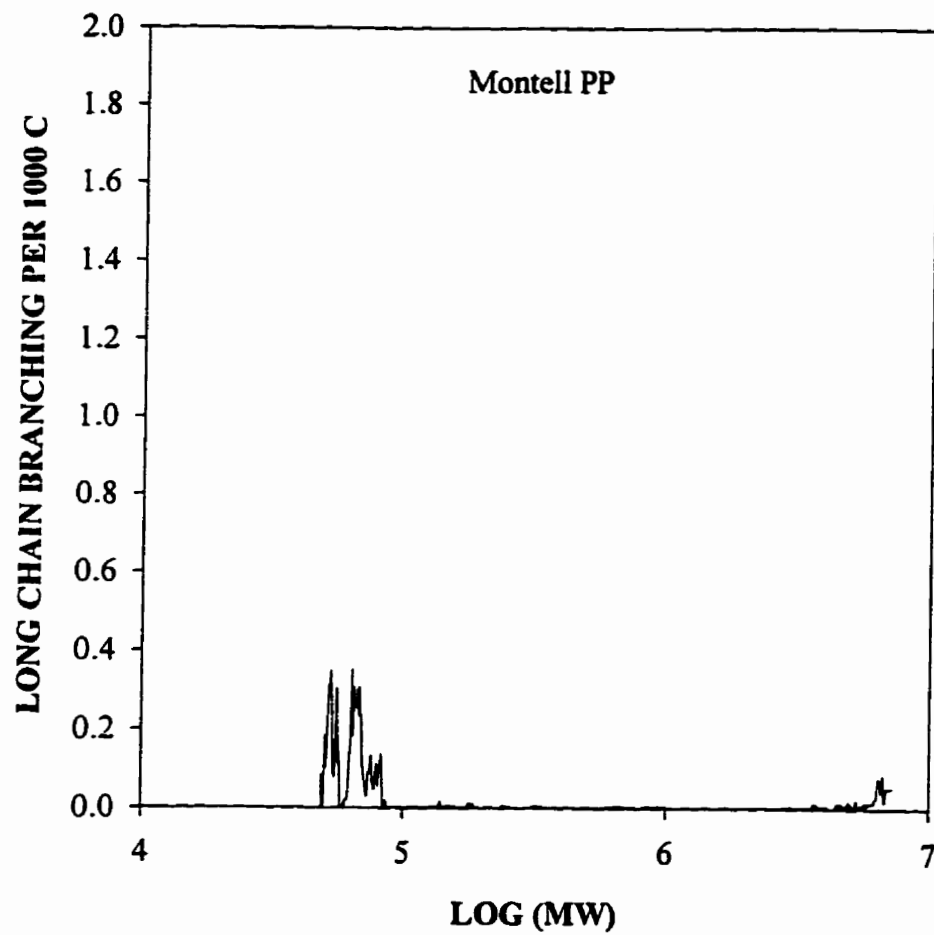


Fig. 5-10 Long chain branching frequency per 1000 C ( $\lambda$ ) of Montell PP.

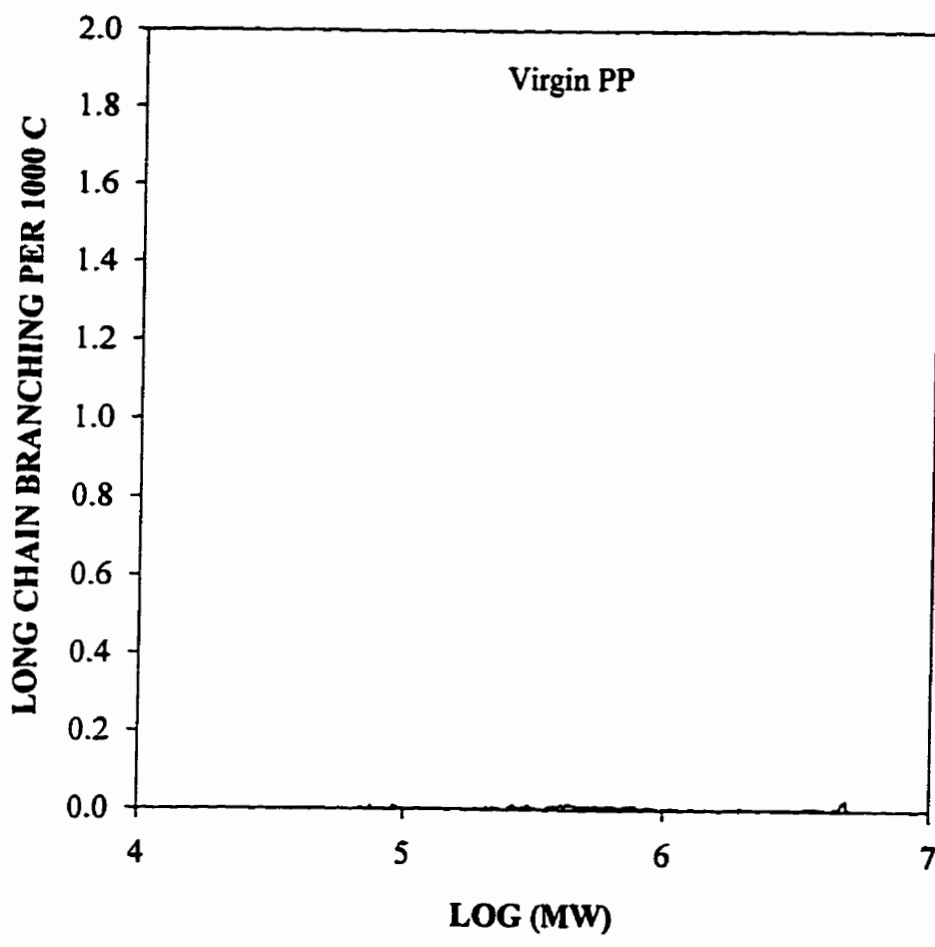


Fig. 5-11a Long chain branching frequency per 1000 C ( $\lambda$ ) of virgin PP.

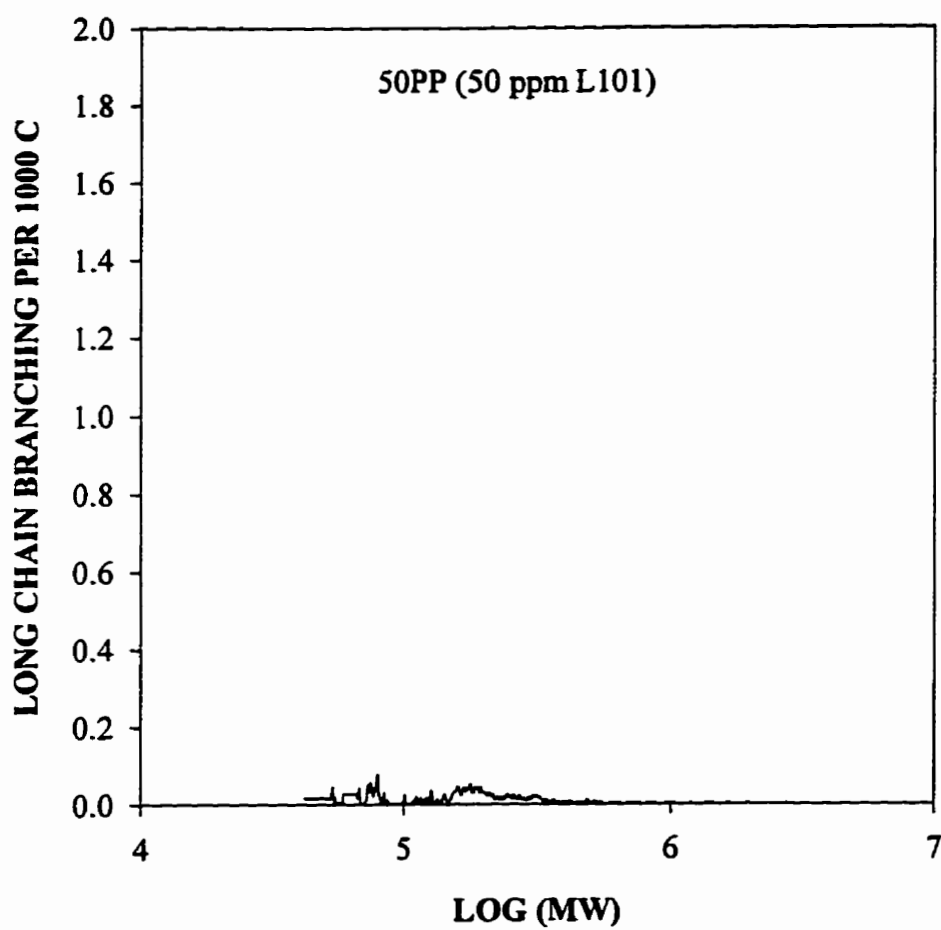


Fig. 5-11b Long chain branching frequency per 1000 C ( $\lambda$ ) of 50PP.

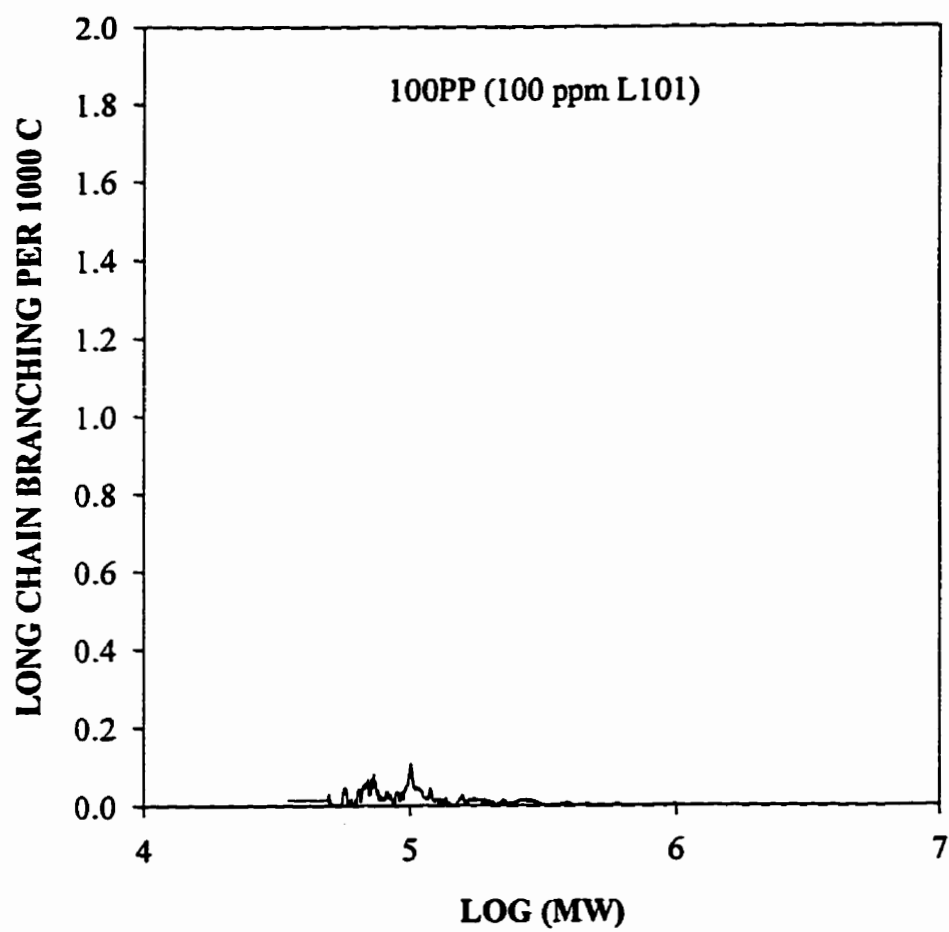


Fig. 5-11c Long chain branching frequency per 1000 C ( $\lambda$ ) of 100PP.

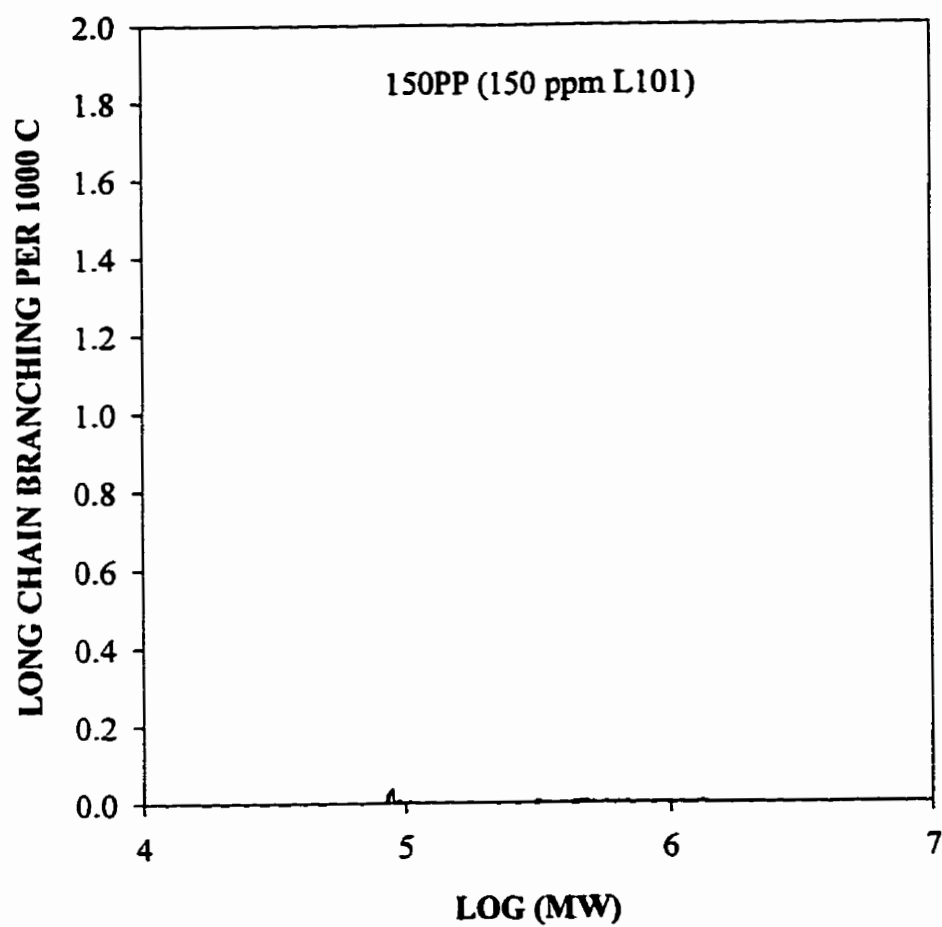


Fig. 5-11d Long chain branching frequency per 1000 C ( $\lambda$ ) of 150PP.



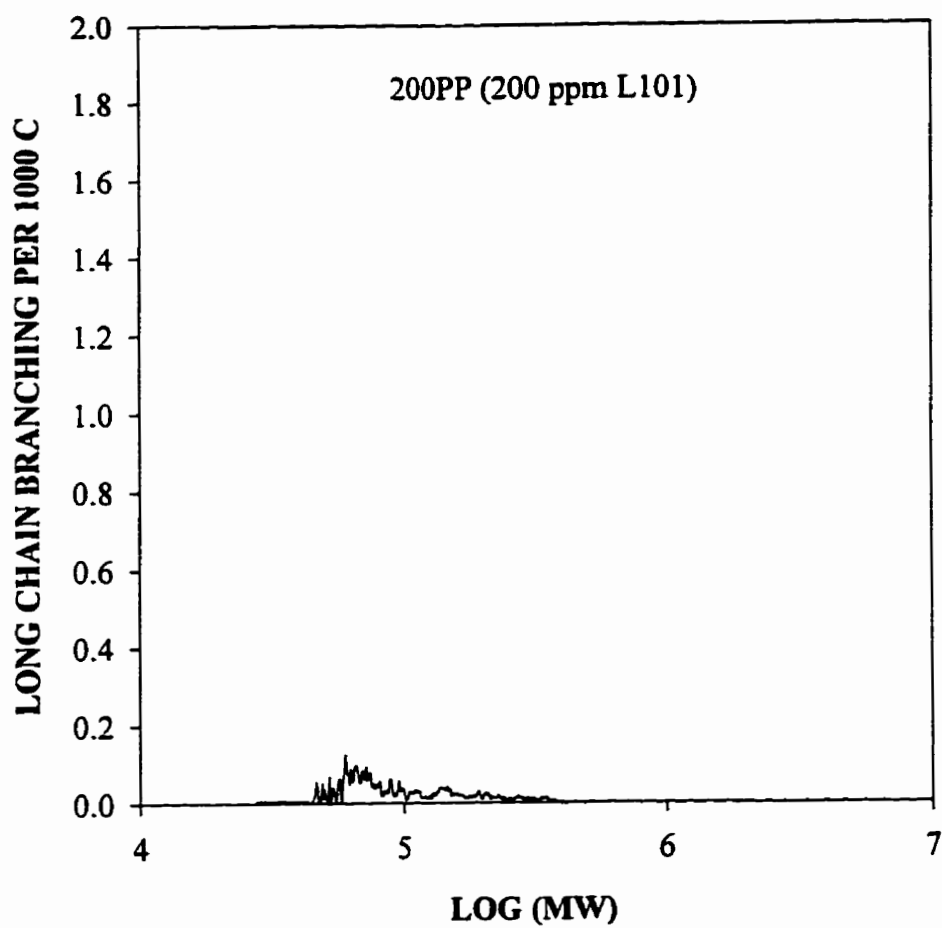


Fig. 5-11e Long chain branching frequency per 1000 C ( $\lambda$ ) of 200PP.

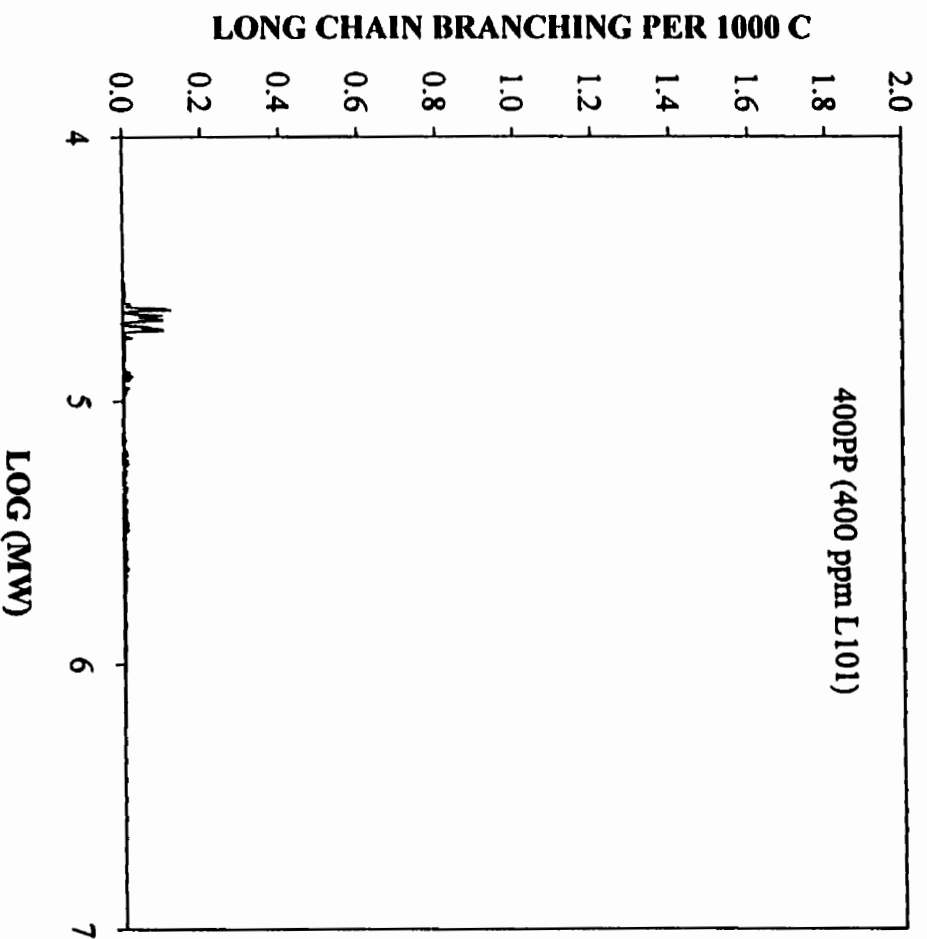


Fig. 5-11F Long chain branching frequency per 1000 C ( $\lambda$ ) of 400PP.

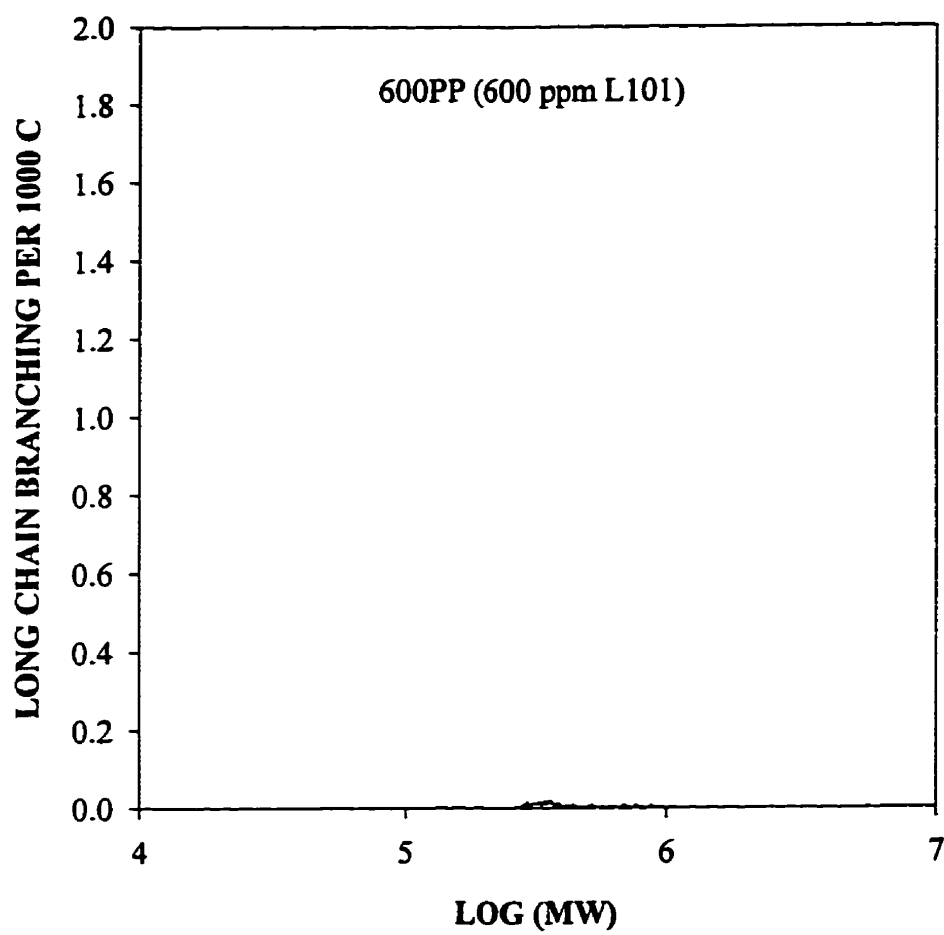


Fig. 5-11g Long chain branching frequency per 1000 C ( $\lambda$ ) of 600PP.

for the samples in the 50 ppm peroxide series. It can be seen that  $\bar{M}_n$ ,  $\bar{M}_w$ , and  $\bar{M}_z$  increase with increasing PETA concentration. However, the polydispersity values remain relatively constant. It is found that the  $\bar{M}_z$  of SPT530 has been increased close to that of virgin PP. Fig. 5-12 shows the MWD curves, where it can be seen that the high molecular weight ends of SPT510 and SPT520 have been brought close to that of virgin PP, and SPT530 seems to have a more significant high molecular weight tail. Also, it can be seen that there are a large amount of molecules with moderate molecular weight formed in SPT510.

The average  $g'$  of the whole SPT505 sample is close to unity, indicating that there is not much branching in this material. Increasing the PETA concentration to 1.0 wt.% (SPT510), the  $g'$  is significantly decreased. Further increasing PETA concentration to 2.0 wt.% (SPT520) does not reduce the  $g'$ . However, a lower  $g'$  than that of SPT520 is found for the sample of SPT530. These results on the whole samples suggest that SPT510 and SPT530 may be the most branched materials in this series. This can be confirmed by comparing the  $[\eta]$ s of the whole polymers such as SPT505 and SPT510, the two with similar  $\bar{M}_w$ . The more branched polymer (SPT510) appears to have a lower intrinsic viscosity as expected.

Fig. 5-13 shows the viscosity law plots for the materials in the 50 ppm series. In the region of relatively low molecular weight, there is no significant difference among the samples in this series. In the high molecular weight region, the viscosity law curve of the samples SPT510 shows curvature and is lower than those of linear PPs and other samples in this series. The  $g'$  distribution across molecular weight shown in Fig. 5-14. It seems that SPT510 and SPT530 may have much lower values of  $g'$  in the high molecular weight region, though it may be also due to the experimental noise in detector signals. However, when combined with the apparent elongational viscosity results in Chapter 6, it seems that the data in this high molecular weight region may contain some useful information about LCB.

The LCB frequencies ( $\lambda$ ) for the 50 ppm series are shown in Figs. 5-15 a-d. It can be

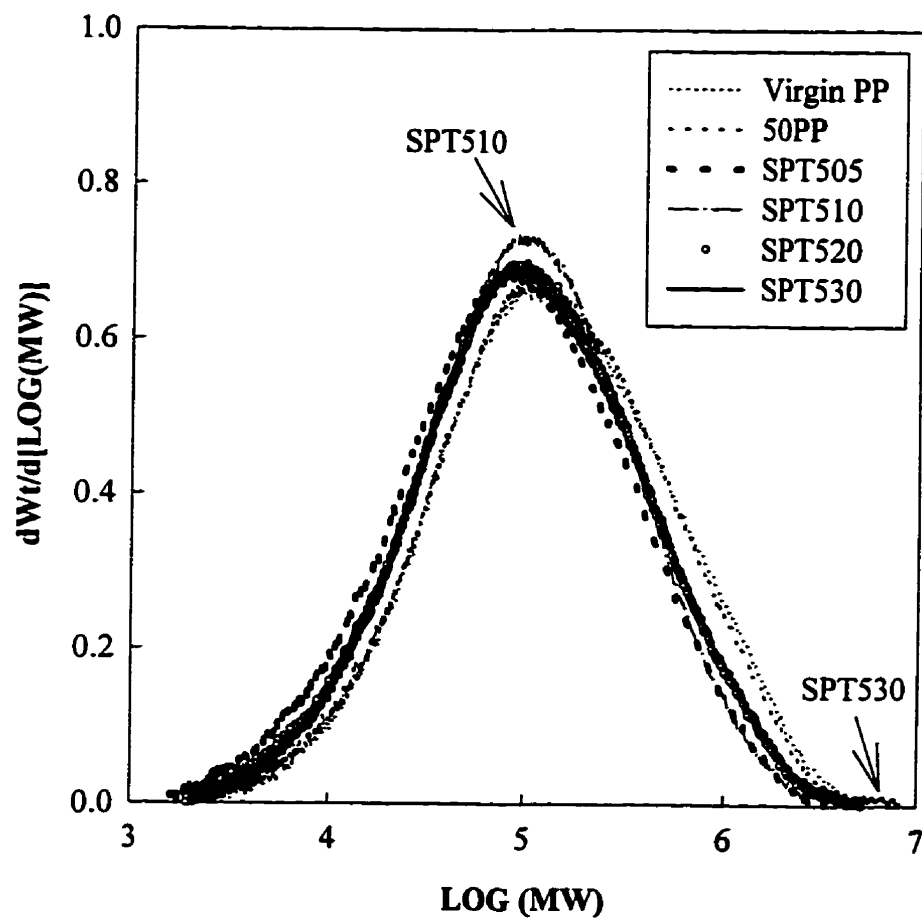


Fig. 5-12 Effect of the PETA and peroxide concentration on the molecular weight distribution of the modified PP (50 ppm peroxide series).

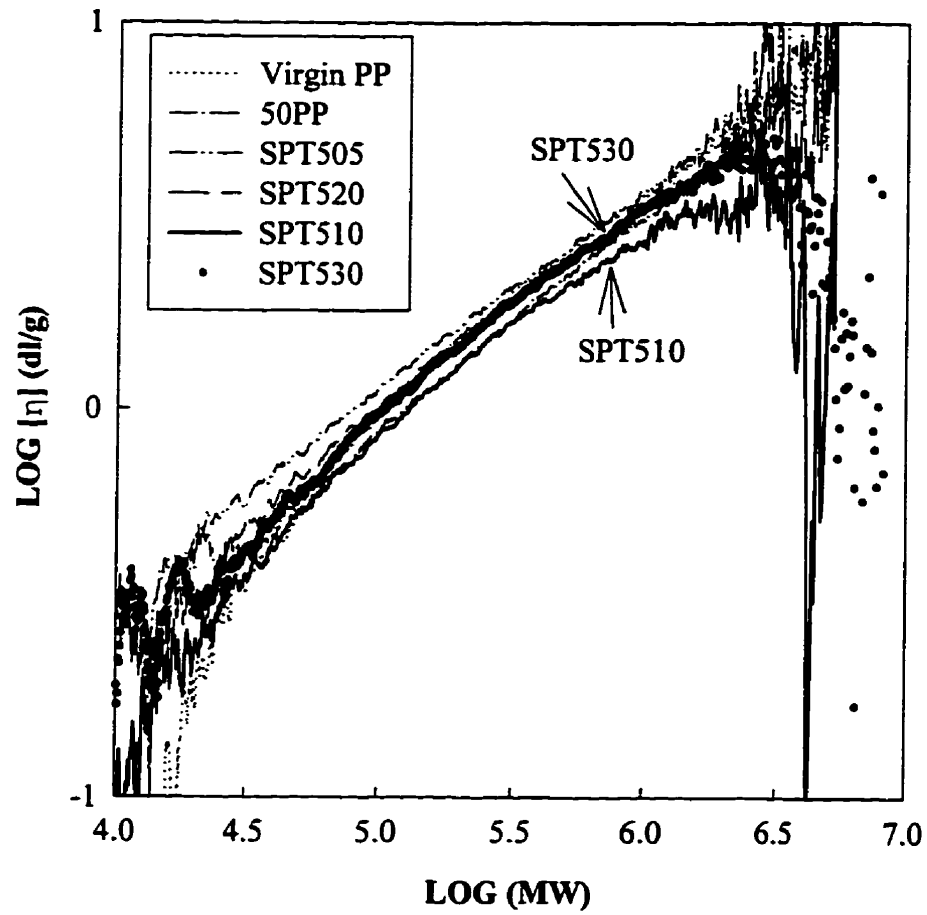


Fig. 5-13 Viscosity law plots of virgin PP and samples in the 50 ppm peroxide series.

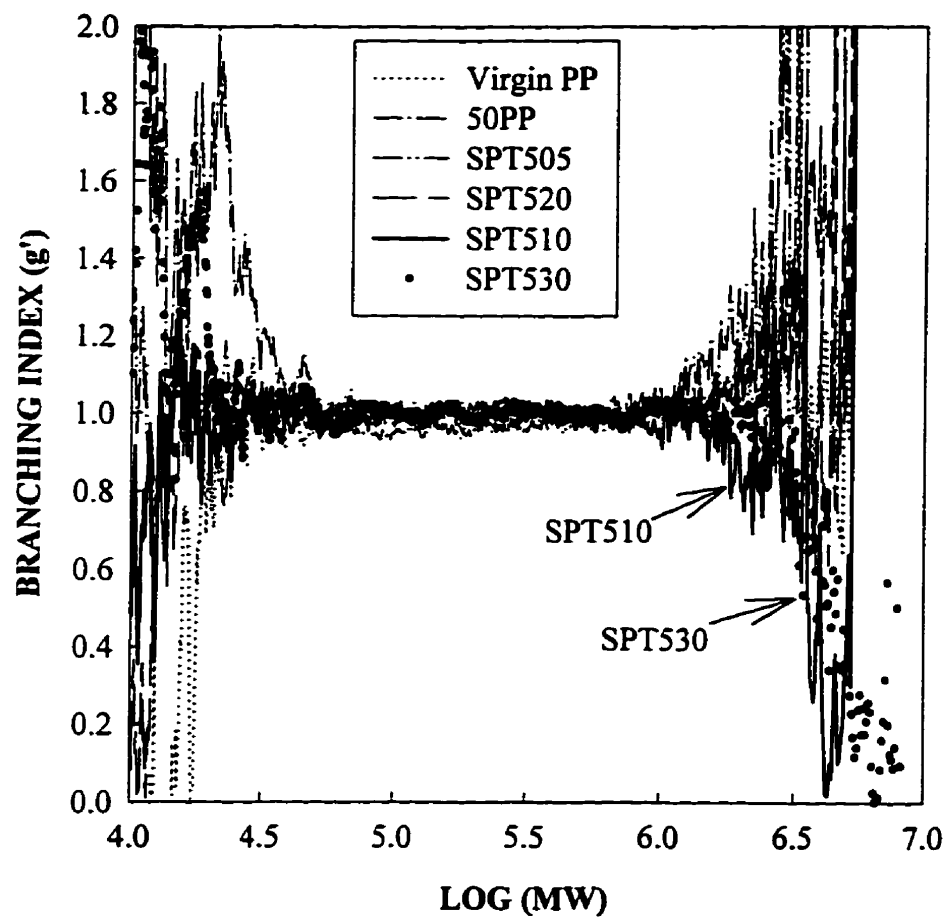


Fig. 5-14  $g'$  distributions across the whole molecular weight of virgin PP, 50PP and samples in 50 ppm peroxide series.

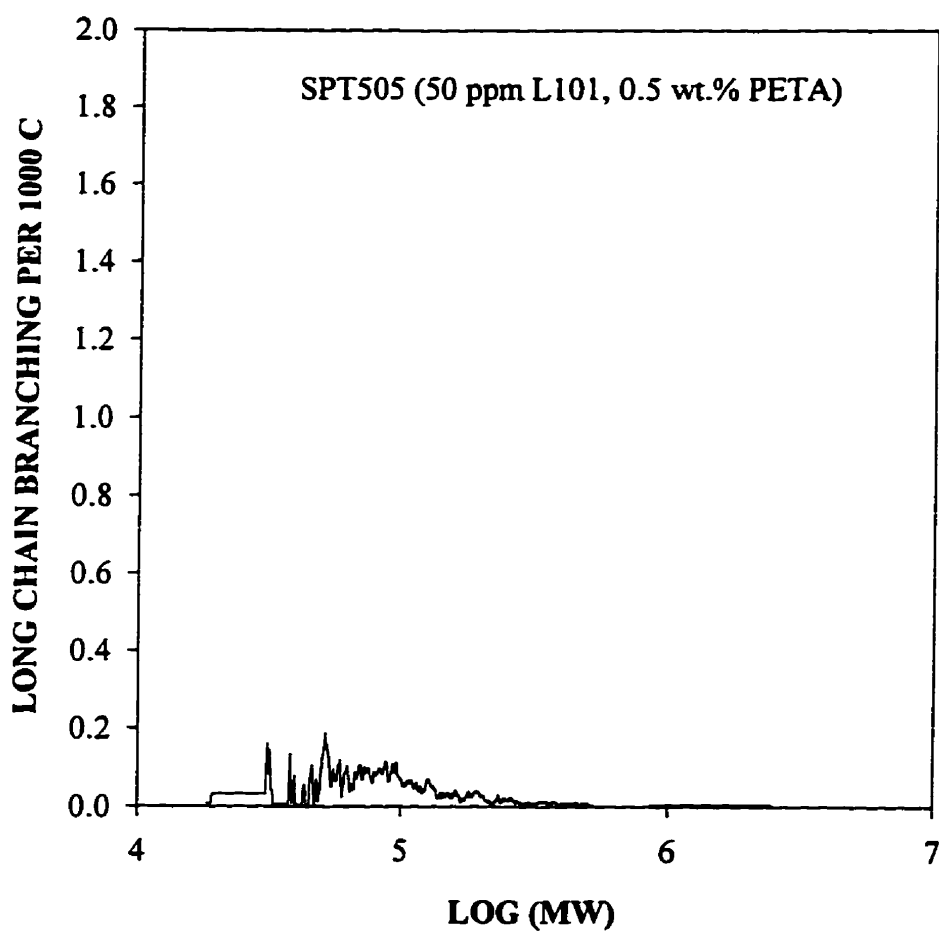


Fig. 5-15a Long chain branching frequency per 1000 C ( $\lambda$ ) of the SPT505 sample.



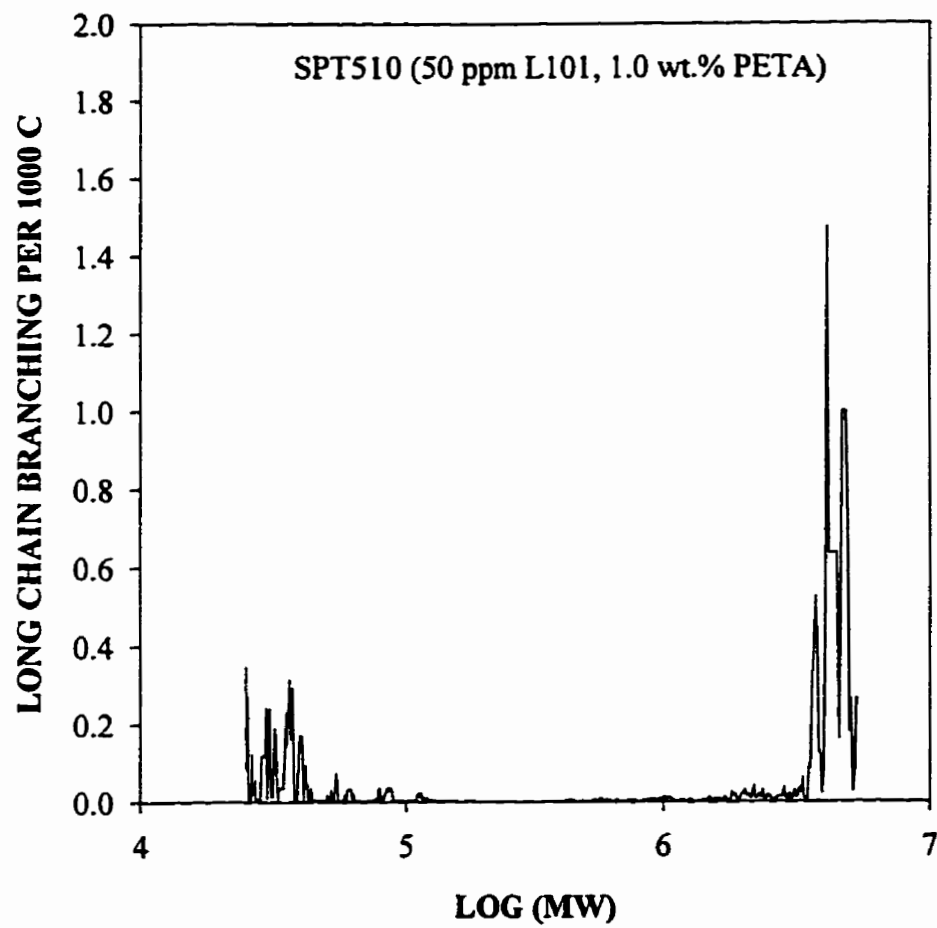


Fig. 5-15b Long chain branching frequency per 1000 C ( $\lambda$ ) of the SPT510 sample.

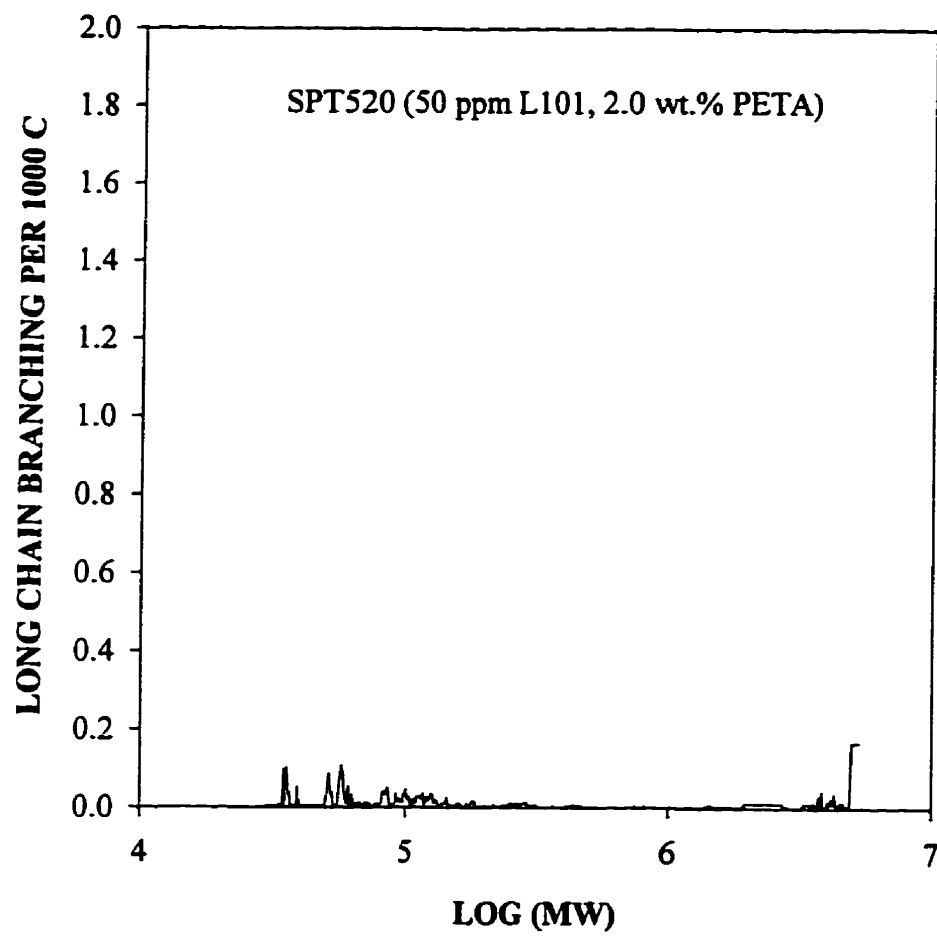


Fig. 5-15c Long chain branching frequency per 1000 C ( $\lambda$ ) of the SPT520 sample.

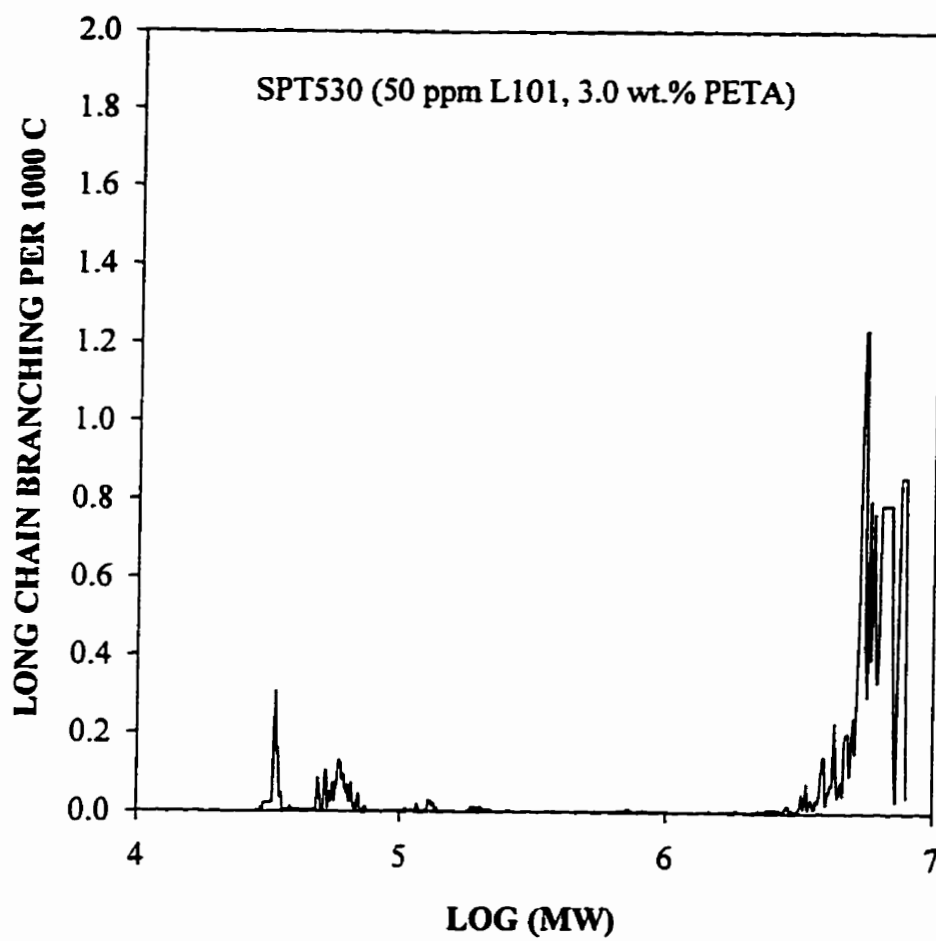


Fig. 5-15d Long chain branching frequency per 1000 C ( $\lambda$ ) of the SPT530 sample.

observed that samples SPT510 and SPT530 may have certain levels of LCB while SPT520 and SPT505 may have very low levels of LCB. From Table 5.2, Figs. 5-13, 5-14 and 5-15, it can be seen that for a highly branched polymer such as SPT510, the results from the viscosity law plot,  $g'$  distribution and LCB frequency distribution seem consistent with the average  $g'$  value of the whole polymer and GPC is able to differentiate it from other less branched or linear polymers.

**100 ppm peroxide series** The results for the samples in 100 ppm series are shown in Table 5.3. Unlike the samples in 50 ppm series,  $\bar{M}_n$  and  $\bar{M}_w$  seem to decrease with increasing PETA concentration in 100 ppm series. These results are in agreement with the work of Thitiratsakul (1991), who has observed that the  $\bar{M}_n$  and  $\bar{M}_w$  of the reacted PPs were less than

**TABLE 5.3 Molecular Parameters of the Samples in 100 ppm Peroxide Series**

Sample	$\bar{M}_n$	$\bar{M}_w$	$\bar{M}_z$	$\bar{M}_w/\bar{M}_n$	$g'$	$[\eta]$ (dl/g)
SPT1005	50,600	262,000	949,800	5.18	0.878	1.0393
SPT1010	45,300	222,800	901,700	4.92	0.761	1.1574
SPT1020	48,500	213,500	794,700	4.40	0.756	1.0186
SPT1030	40,700	205,100	1,004,300	5.04	0.794	0.9596

those of the virgin PP. In the 100 ppm series, generally the  $\bar{M}_z$  has been increased and it is higher than that of the degraded material (100PP). The samples of SPT1005 and SPT1030 actually have similar  $\bar{M}_z$ s to that of virgin linear PP. The decrease in  $\bar{M}_n$  and  $\bar{M}_w$  and increase in  $\bar{M}_z$  may suggest the simultaneous branching and degradation reactions. Also, the increase in  $\bar{M}_z$  is not so significant in our samples when compared with the results by Thitiratsakul

(1991), probably due to the much lower peroxide concentration used in our system.

The MWD curves of 100 ppm series samples are shown in Fig. 5-16. It can be seen that the high molecular weight end has been brought close to or even higher than that of virgin PP even when very low PETA concentrations are used (0.5-2.0 wt.%). A more significant tail has been created with a higher PETA concentration of 3.0 wt.%. It is also noted that large amount of molecules with moderate molecular weight were formed with the use of PETA since the peak heights have been increased.

In Table 5.3, it can be seen that all the samples in the 100 ppm series have significantly lower  $g$ 's, especially at the higher PETA concentrations (1.0-3.0 wt.% PETA). The samples produced using PETA concentrations from 1.0 wt. % to 3.0 wt.% (SPT1010, SPT1020 and SPT1030), seem to have similar  $g$ 's. This suggests that these polymers may have similar levels of LCB. It is noted that SPT1030 has a similar  $\bar{M}_w$  and average  $g'$  to those of SPT1010 and the former has a lower  $[\eta]$ . A few comments have to be made about the determination of  $g'$  for the whole polymer in GPC. Because of the experimental noise and the possible region where the Mark-Houwink relationship may not apply, GPC analyses may indicate the presence of LCB where none is present in reality and hence the average  $g'$  is underestimated. It is also possible that the average  $g'$  of the whole polymer is overestimated because of the experimental noise within the high molecular weight region so that data in this region may be excluded. In reality, however, LCB is usually found within the high molecular weight region. It has been found that GPC sometimes can not detect the existence of some very high molecular weight species (Raju et al., 1979) present at very low concentrations. However, such a high molecular weight species (either linear or branched), even at a very low concentration, has a profound effect on the rheological properties of polymers.

The viscosity law plots of the 100 ppm series are shown in Fig. 5-17. It is not surprising to see that SPT1030 exhibits significantly lower viscosity at the same molecular weight than that of the linear PP and other samples in this series. It is found that SPT1005

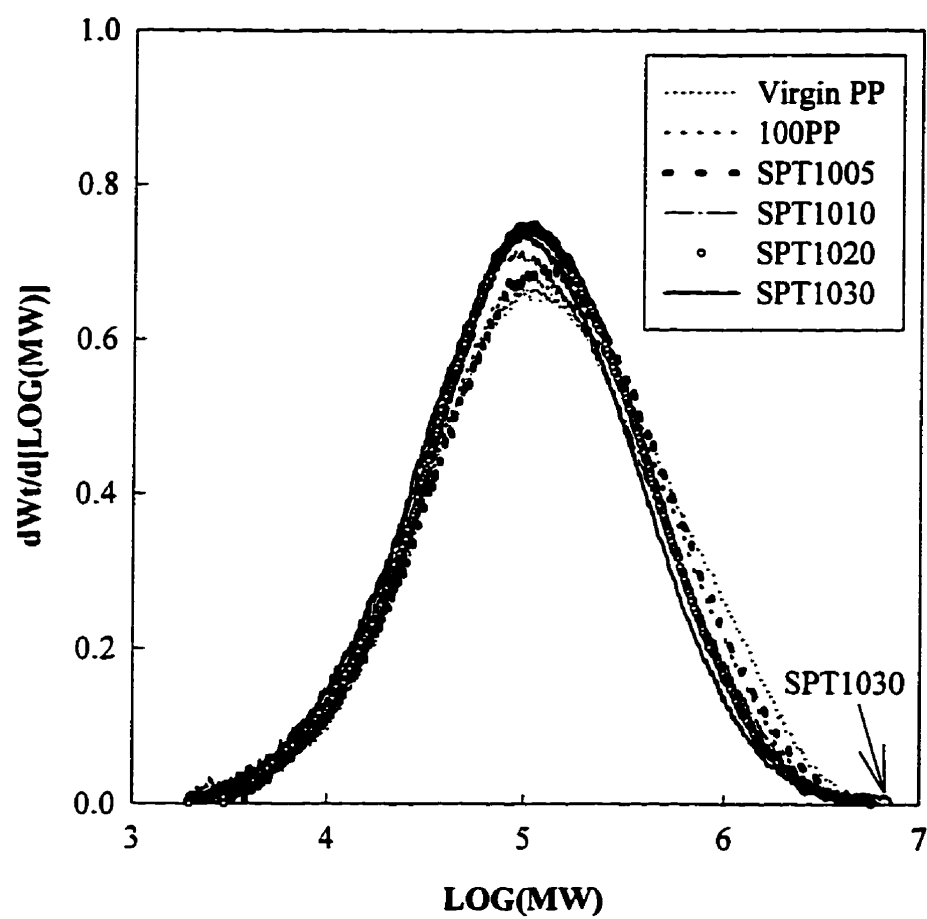


Fig. 5-16 Effect of the PETA and peroxide concentration on the molecular weight distribution of the modified PP (100 ppm peroxide series).

has a lower intrinsic viscosity curve than those of other samples and this is not consistent with the average  $g'$  and  $[\eta]$  of the whole polymer in Table 5.3. The reason for this is not clear. The  $g'$  across the molecular weight distribution (Fig. 5-18) seems to confirm the results of the average  $g'$  in Table 5.3. The  $g'$  distribution curves of SPT1010, SPT1020 and SPT1030 deviate from unity within the high molecular weight region, further indicating that LCB exists in these three samples.

Figs. 19a-d show the long chain branching frequency per 1000 carbon atoms ( $\lambda$ ) for the 100 ppm series. It seems that SPT1010, SPT1020 and SPT1030 all have some similar levels of LCB. Although SPT1005 shows the smallest level of LCB in this series, branches of moderate length may also exist in this sample. By comparing Fig. 5-18 with Fig. 5-19, the  $\lambda$  distribution across the molecular weight appears to be a better tool than the  $g'$  distribution plot to show the difference in the LCB frequencies among these samples.

**150 and 200 ppm peroxide series** The results for three samples in the 150 ppm series are shown in Table 5.4. With increasing PETA concentration, all the molecular weight averages increase but most of them are lower than those of the degraded PP (150PP). Only SPT1530 has similar values with those of 150PP. PDI values indicate that the distribution has been slightly broadened. The actual MWD curves are shown in Fig. 5-20 where it can be observed that low molecular weight molecules have been formed. The viscosity law plots are shown

**TABLE 5.4 Molecular Parameters of the Samples in 150 ppm Peroxide Series**

Sample	$\bar{M}_n$	$\bar{M}_w$	$\bar{M}_z$	$\bar{M}_w/\bar{M}_n$	$g'$	$[\eta]$ (dl/g)
SPT1505	23,900	119,900	463,700	5.01	1.06	0.9294
SPT1510	24,600	146,500	545,600	5.96	0.888	1.0802
SPT1530	35,300	182,300	654,000	5.17	0.956	1.0974

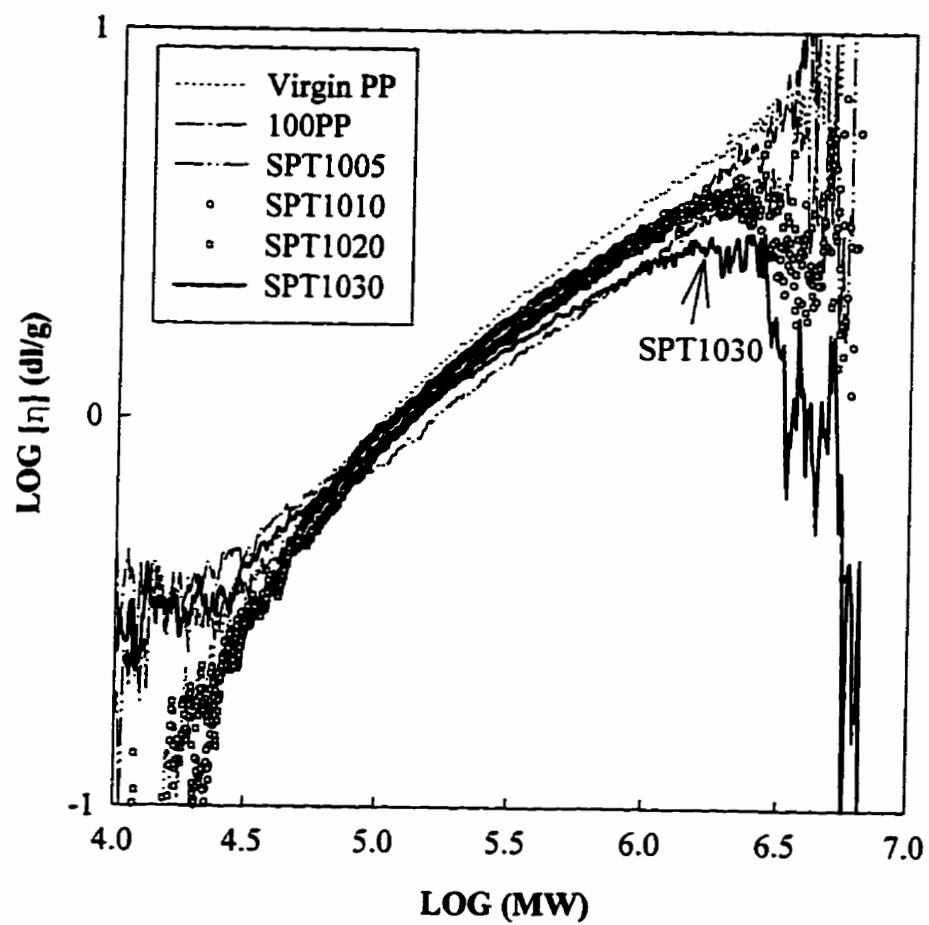


Fig. 5-17 Viscosity law plots of virgin PP and samples in 100 ppm peroxide series.



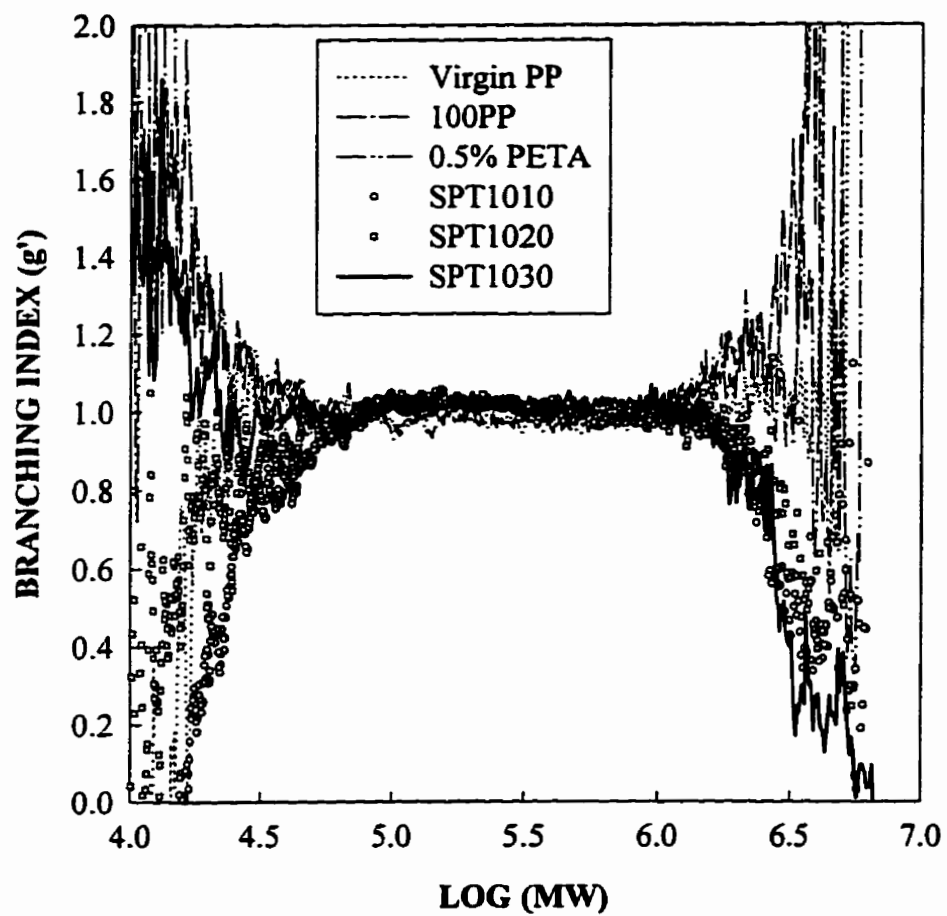


Fig. 5-18  $g'$  distributions across the whole molecular weight of virgin PP, 100PP and samples in 100 ppm peroxide series.

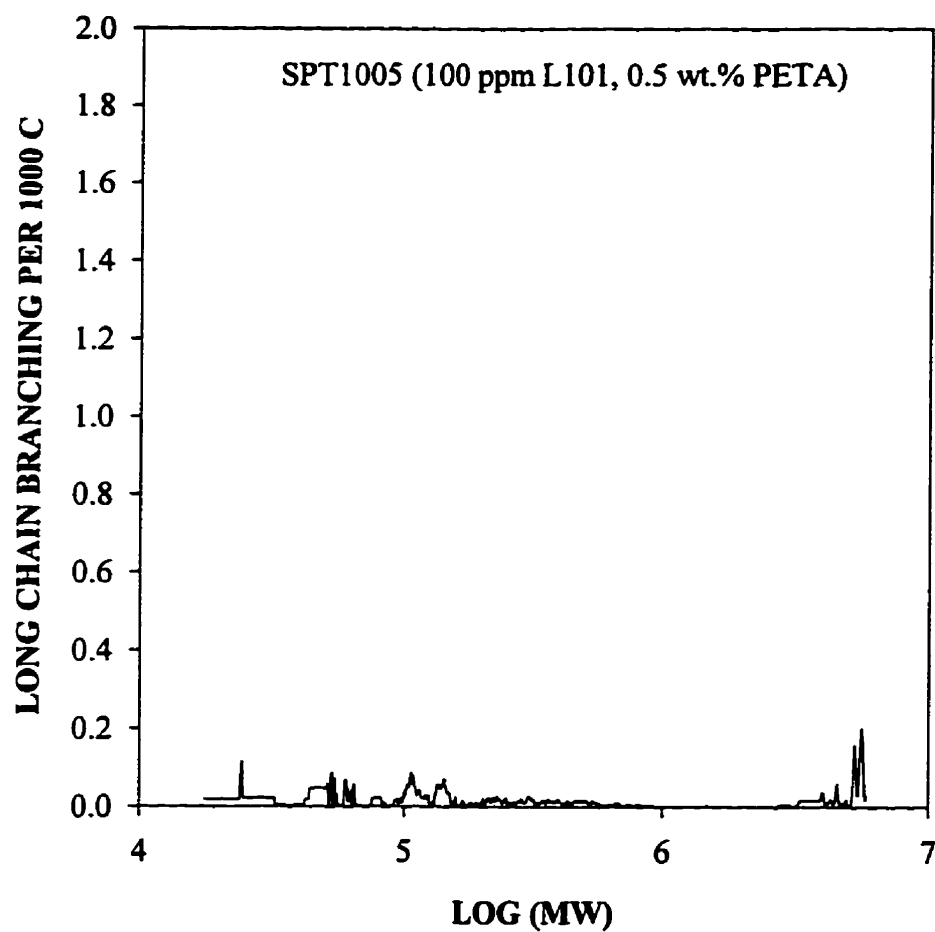


Fig. 5-19a Long chain branching frequency per 1000 C ( $\lambda$ ) of the SPT1005 sample.

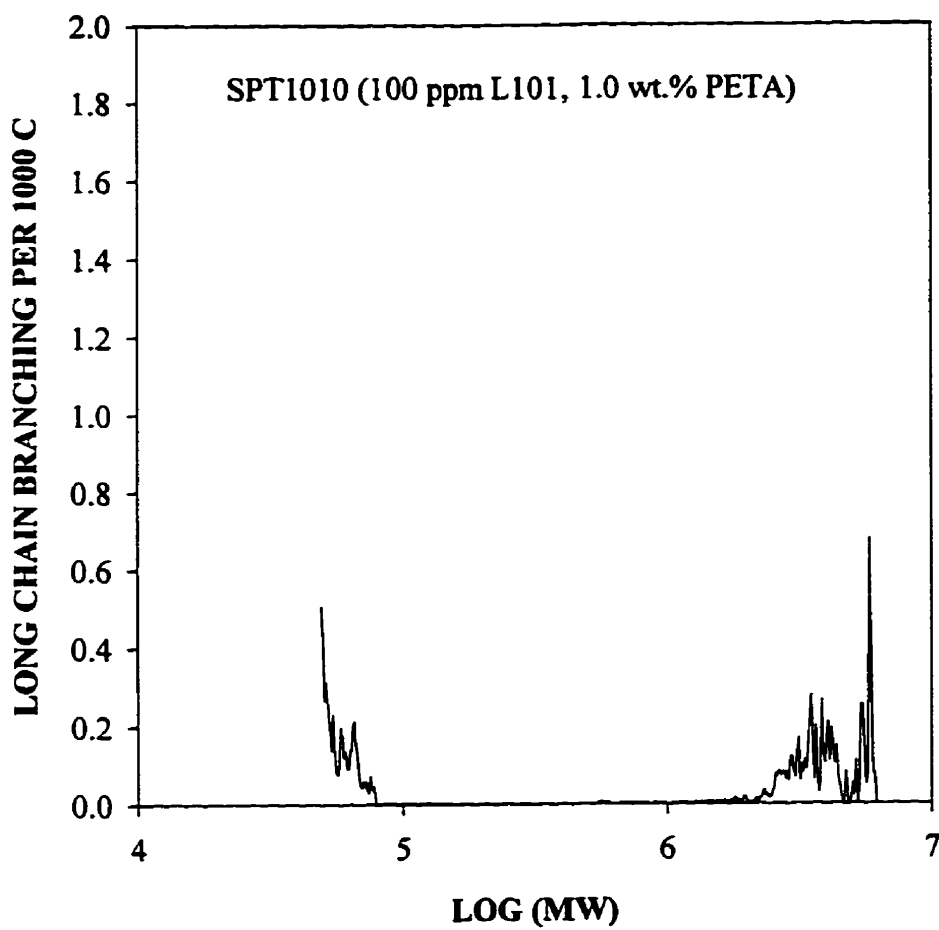


Fig. 5-19b Long chain branching frequency per 1000 C ( $\lambda$ ) of the SPT1010 sample.

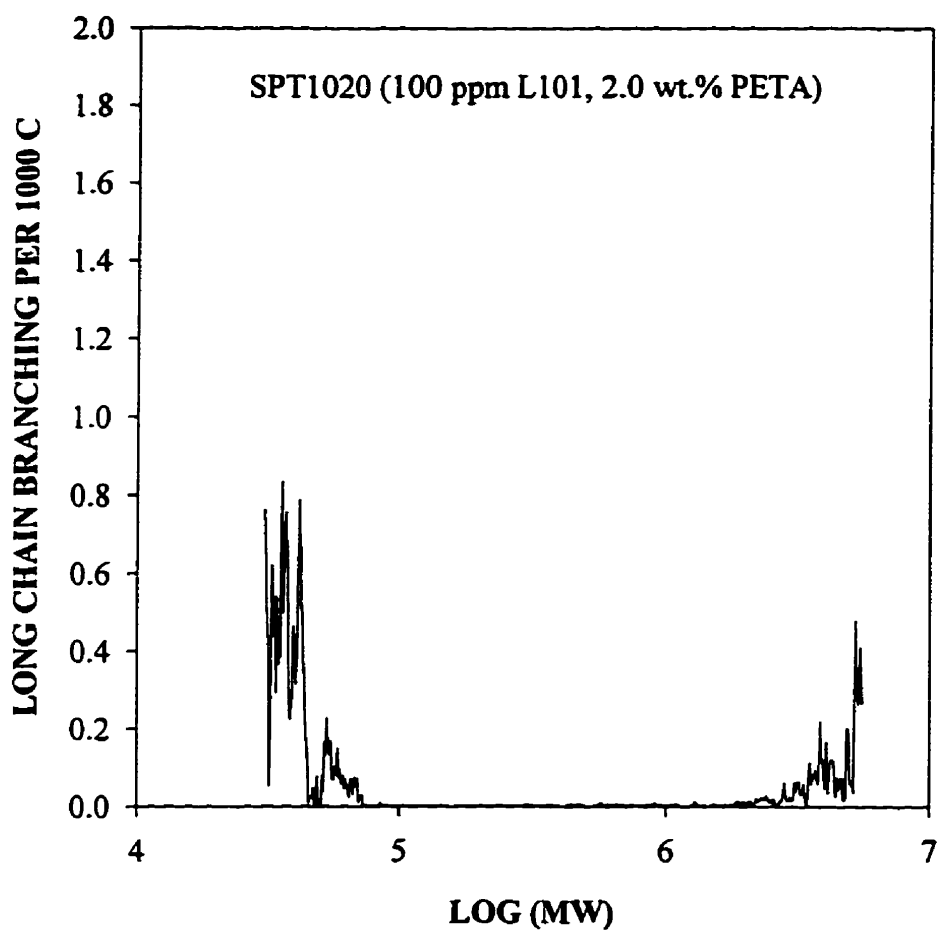


Fig. 5-19c Long chain branching frequency per 1000 C ( $\lambda$ ) of the SPT1020 sample.

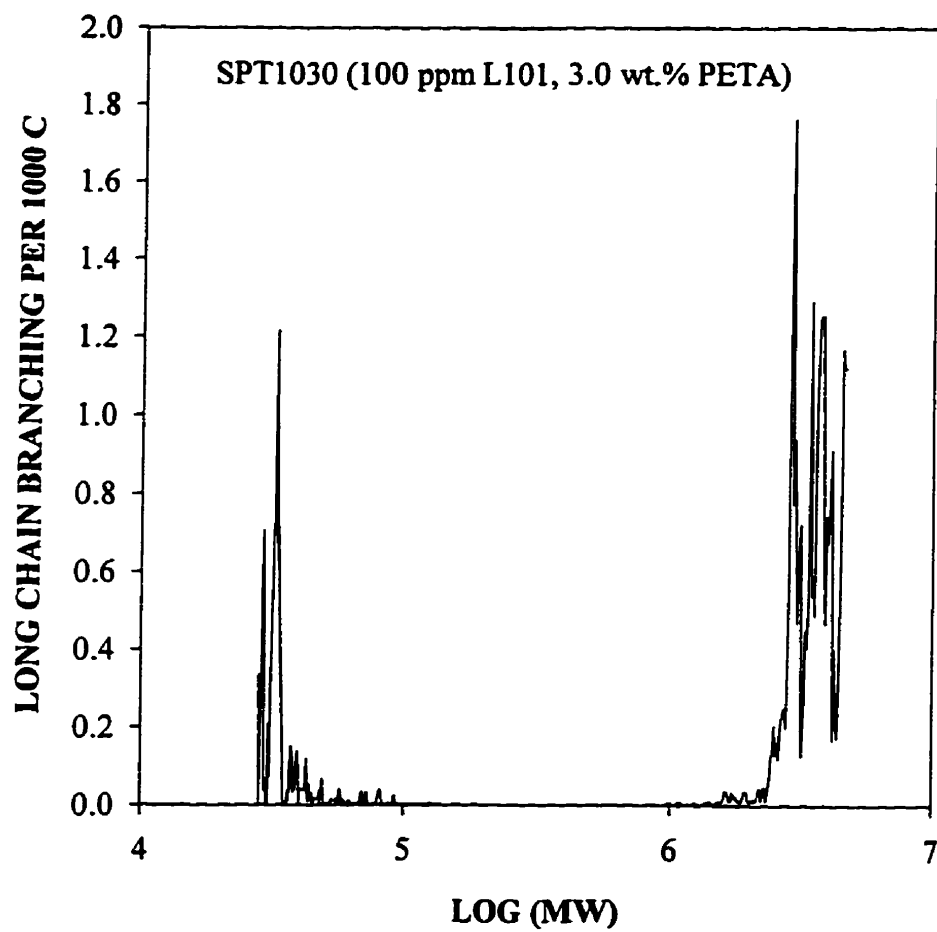


Fig. 5-19d Long chain branching frequency per 1000 C ( $\lambda$ ) of the SPT1030 sample.

in Fig. 5-21. It can be observed that none of the samples in the 150 ppm series shows significant difference from the virgin linear PP and also there is not a significant difference among them. The  $g'$  distribution curves seem to be in agreement with this result. As it can be seen in Fig. 5-22, none of them shows significant deviations from unity in the high molecular weight region. The LCB frequencies for this series is shown in Fig. 5-23a-c and it can be seen that the LCB frequencies are low in the high molecular weight regions for all the samples of this series. However, LCB might exist in relatively low molecular weight regions for these samples.

The results of the 200 ppm series are presented in Table 5.5, Figs. 5-24, 5-25, 5-26 and 5-27. The viscosity law plot of the sample SPT2030 is far from the other plots, which might be attributed to the relatively large change in chemical structure or composition. LCB frequency plots show that LCB levels in samples SPT2005, SPT2010, SPT2020 may be very low while SPT2030 might have some higher LCB levels than other samples in this series. However, the length of these branches may be shorter than those in the 50 and 100 ppm series due to the higher peroxide concentrations used.

From the results of the above four peroxide series, it can be seen that the majority of the long chain branched samples are in the 50 and 100 ppm peroxide series. This seems reasonable since with using relatively high peroxide levels, the branches, if formed, may be

**TABLE 5.5 Molecular Parameters of the Samples in 200 ppm Peroxide Series**

Sample	$\bar{M}_n$	$\bar{M}_w$	$\bar{M}_z$	$\bar{M}_w/\bar{M}_n$	$g'$	$[\eta]$ (dl/g)
SPT2005	22,200	82,300	262,400	3.70	1.077	1.0060
SPT2010	36,400	138,900	428,700	3.82	0.967	0.9470
SPT2020	34,000	135,300	409,300	3.97	1.008	0.9691
SPT2030	31,100	93,700	280,200	3.01	0.917	1.3603

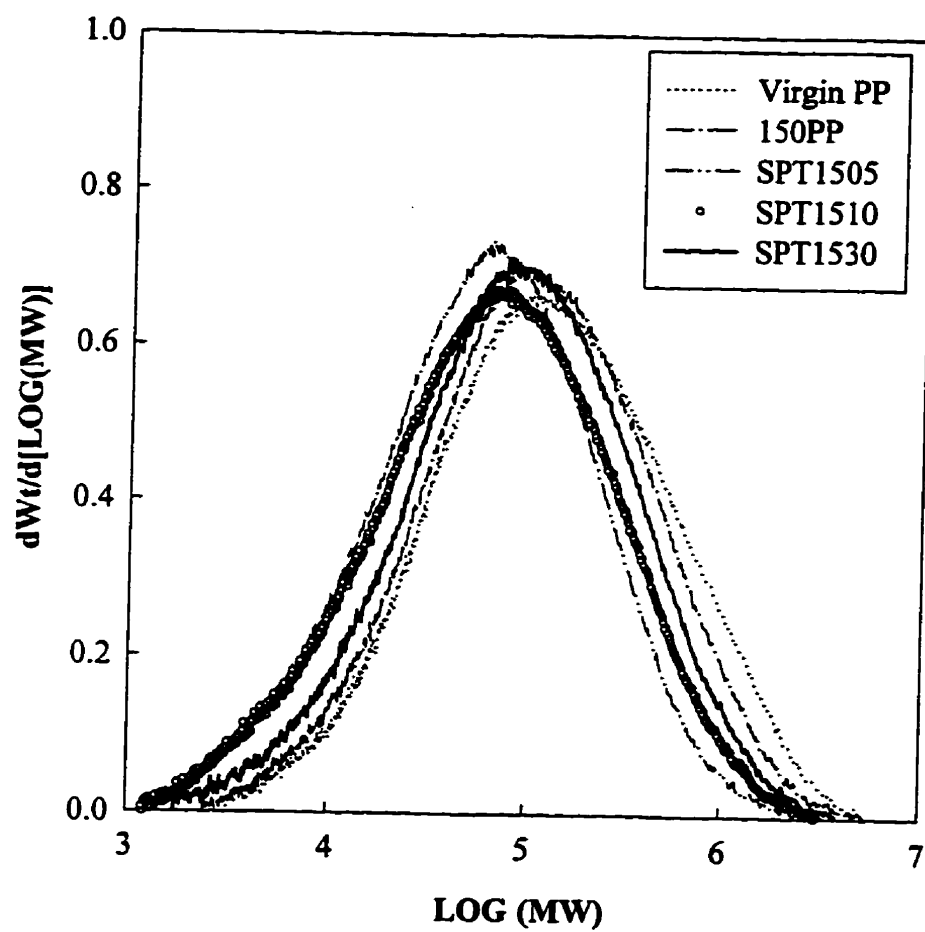


Fig. 5-20 Effect of the PETA and peroxide concentrations on the molecular weight distribution of the modified PP (150 ppm peroxide series).

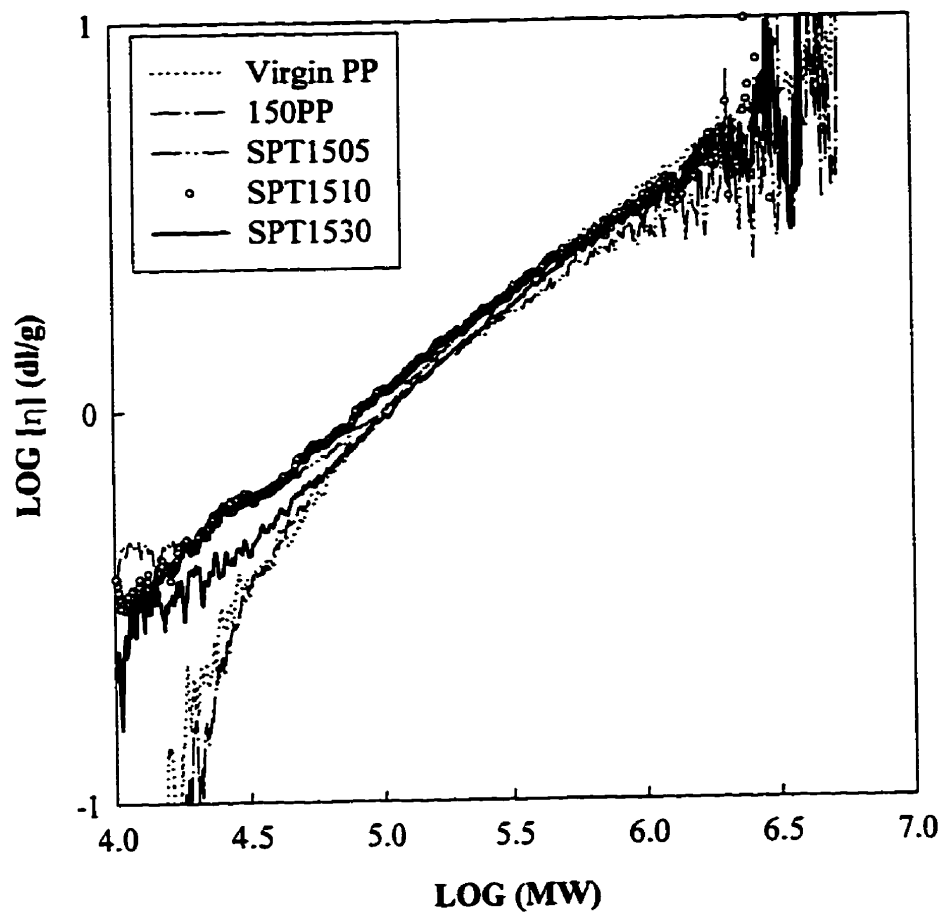


Fig. 5-21 Viscosity law plots of virgin PP and samples in 150 ppm peroxide series.



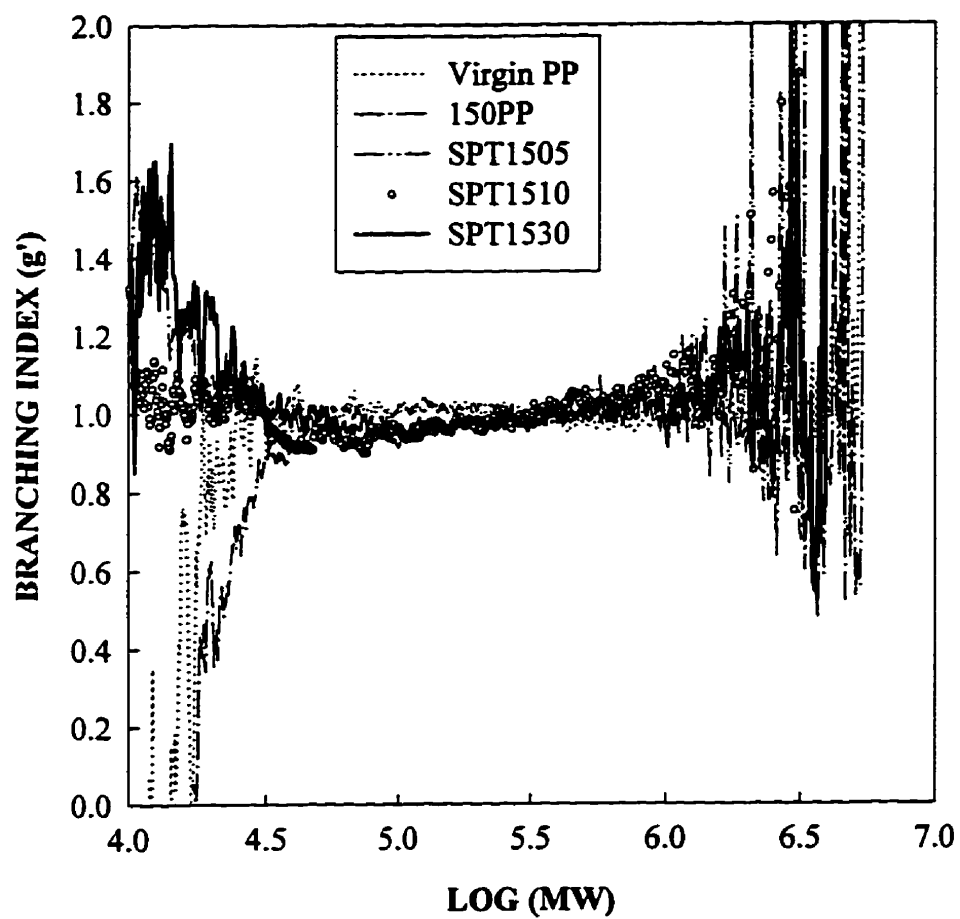


Fig. 5-22  $g'$  distributions across the whole molecular weight of virgin PP, 150PP and some samples in 150 ppm peroxide series.

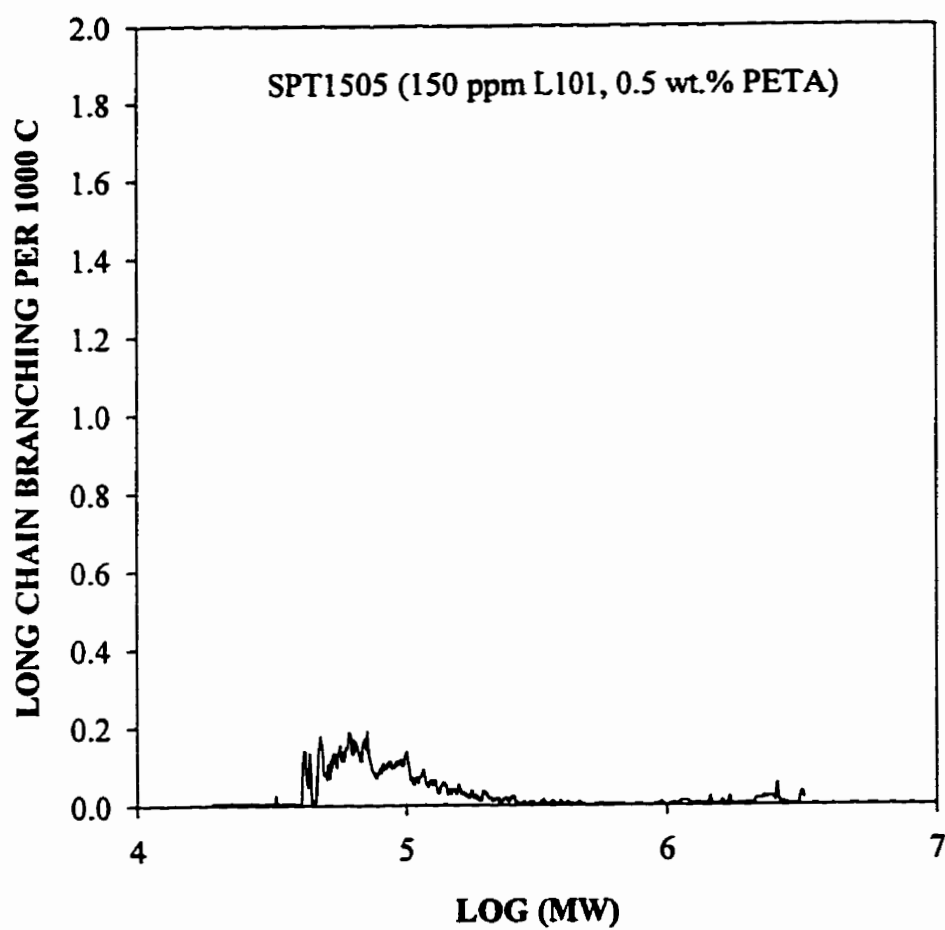


Fig. 5-23a Long chain branching frequency per 1000 C ( $\lambda$ ) of the SPT1505 sample.

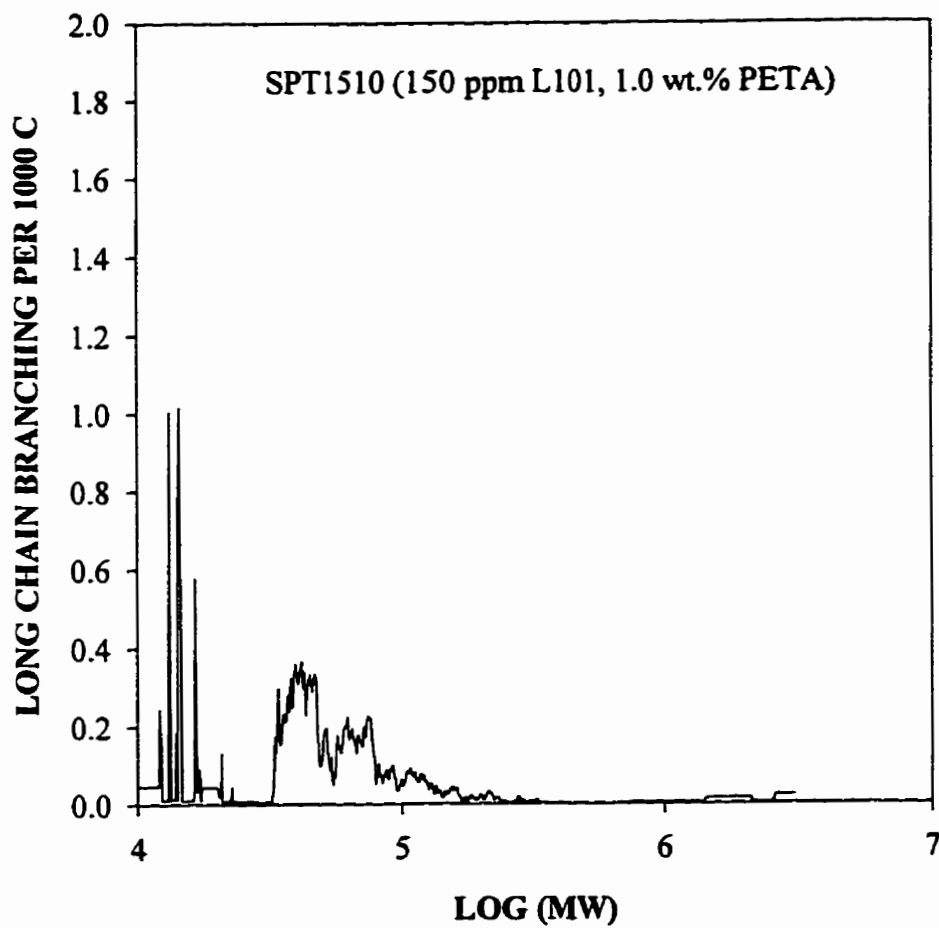


Fig. 5-23b Long chain branching frequency per 1000 C ( $\lambda$ ) of the SPT1510 sample.

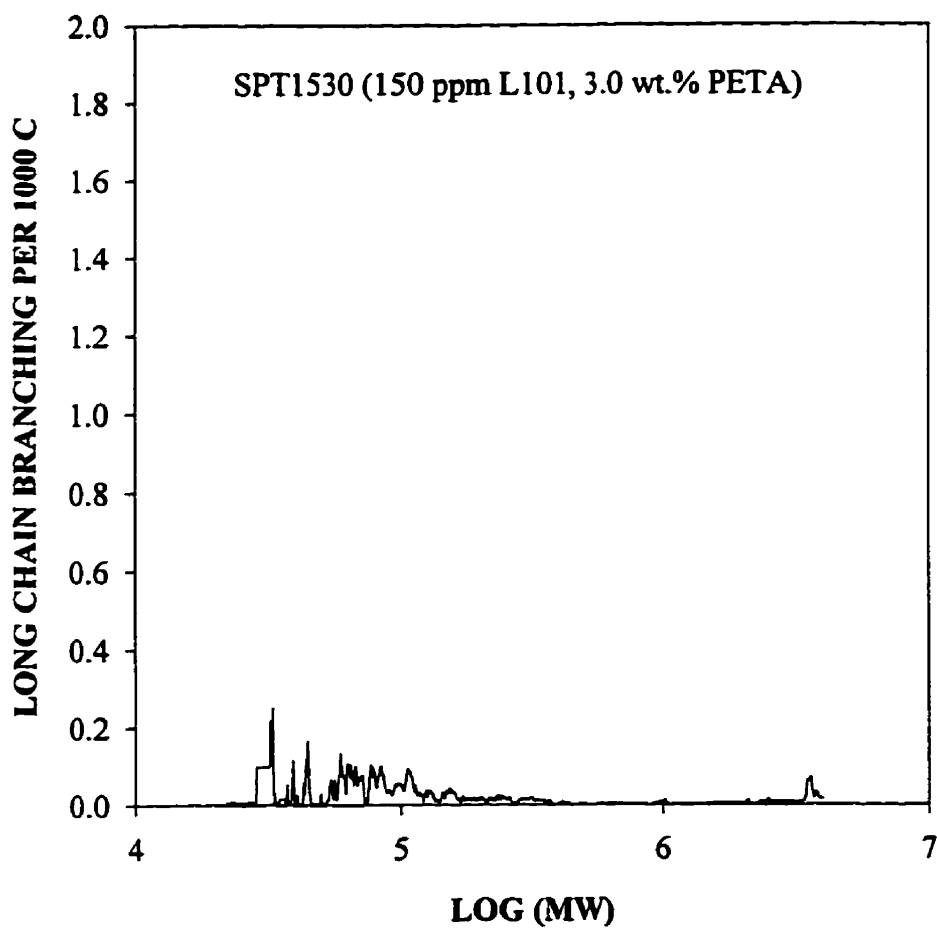


Fig. 5-23c Long chain branching frequency per 1000 C ( $\lambda$ ) of the SPT1530 sample.

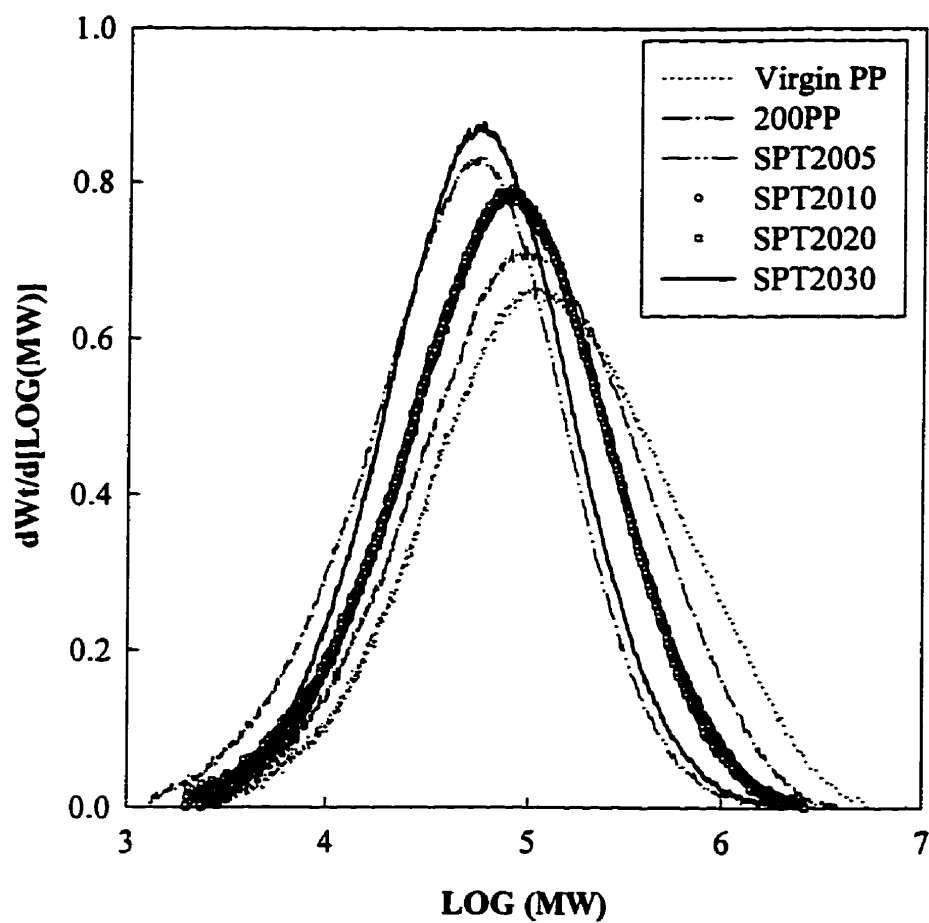


Fig. 5-24 Effect of the PETA and peroxide concentrations on the molecular weight distribution of the modified PP (200 ppm peroxide series).

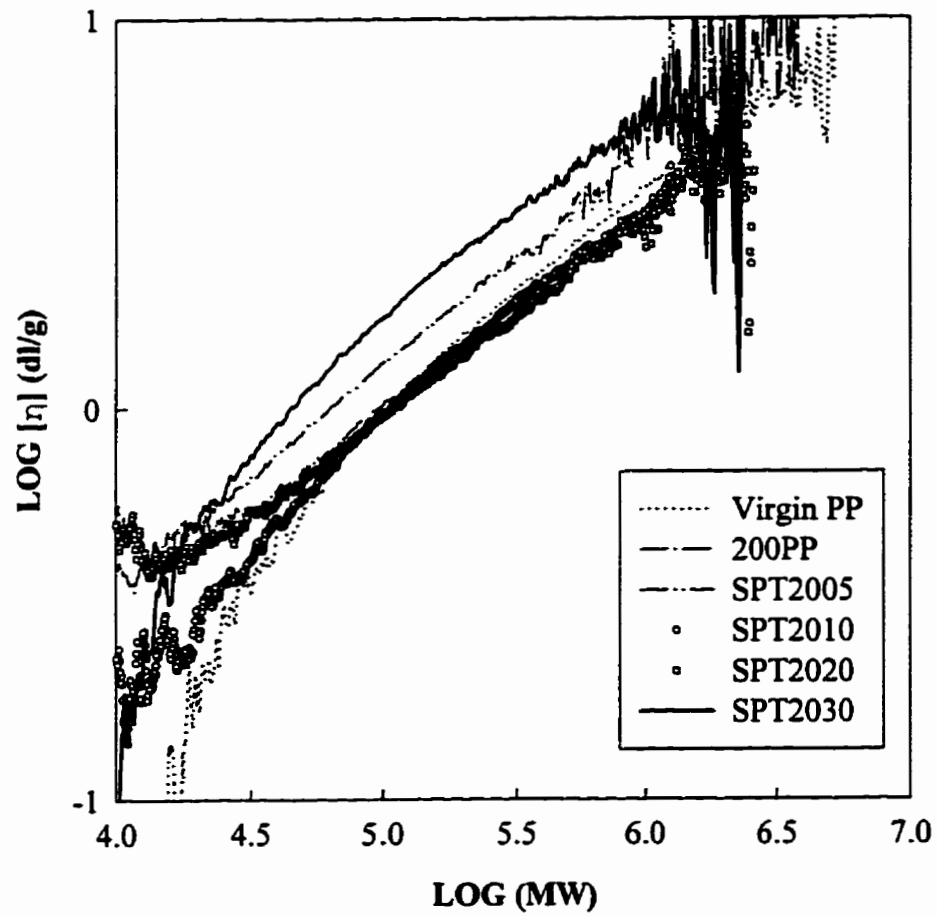


Fig. 5-25 Viscosity law plots of virgin PP and samples in 200 ppm peroxide series.

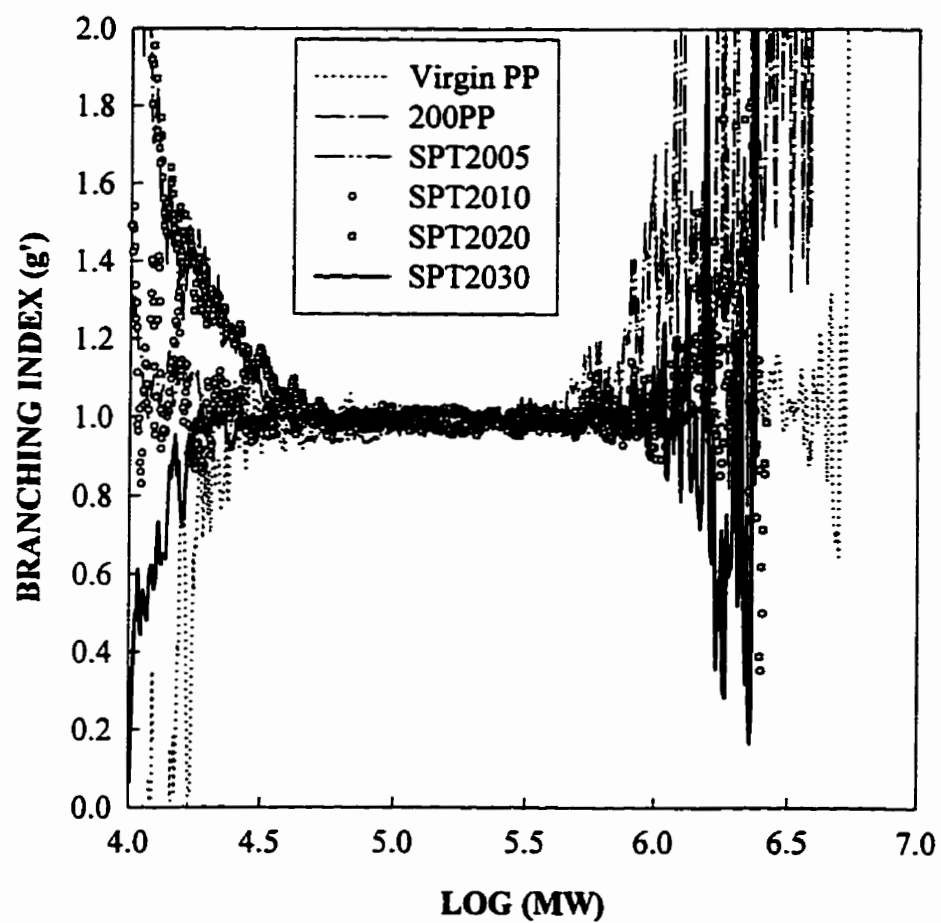


Fig. 5-26 g' distributions across the whole molecular weight of virgin PP, 200PP and samples in 200 ppm peroxide series.

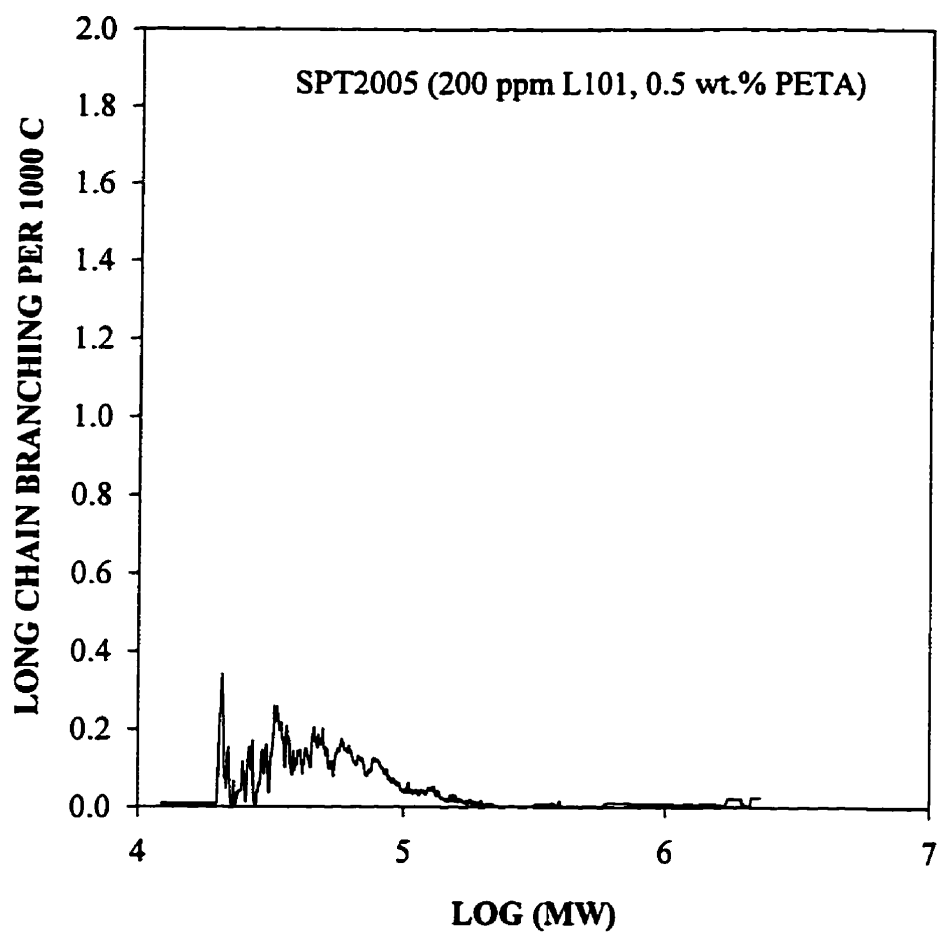


Fig. 5-27a Long chain branching frequency per 1000 C ( $\lambda$ ) of the SPT2005 sample.



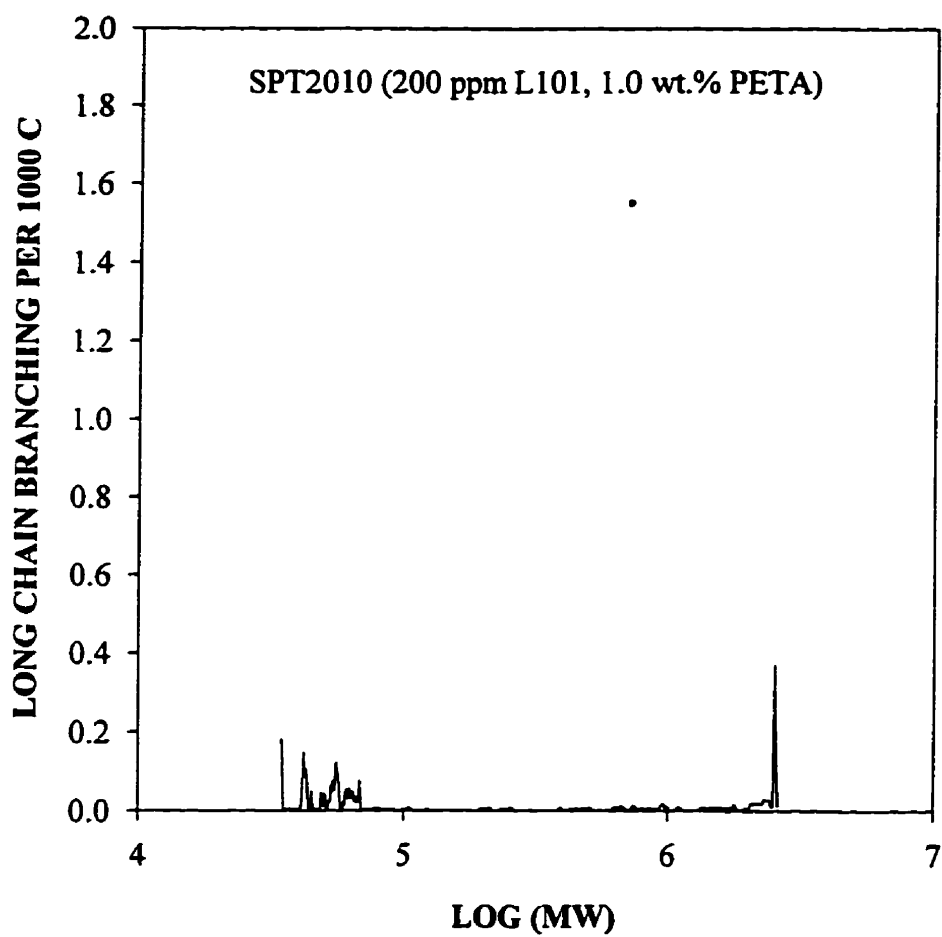


Fig. 5-27b Long chain branching frequency per 1000 C ( $\lambda$ ) of the SPT2010 sample.

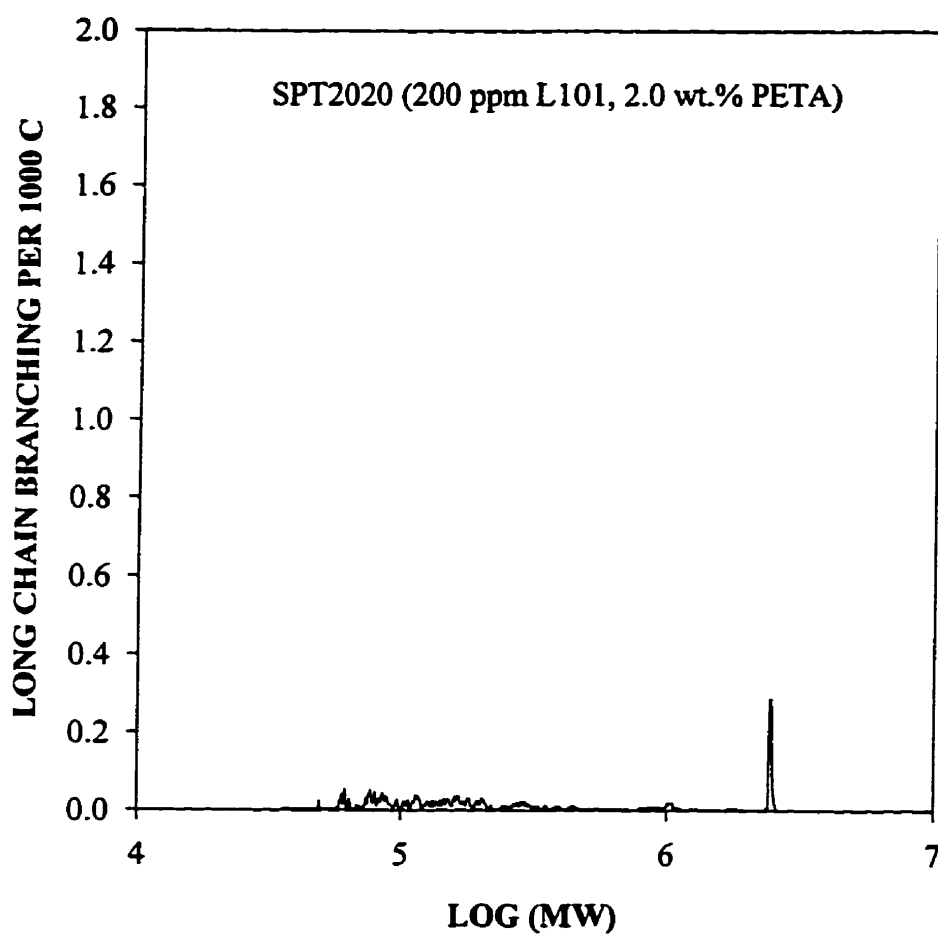


Fig. 5-27c Long chain branching frequency per 1000 C ( $\lambda$ ) of the SPT2020 sample.

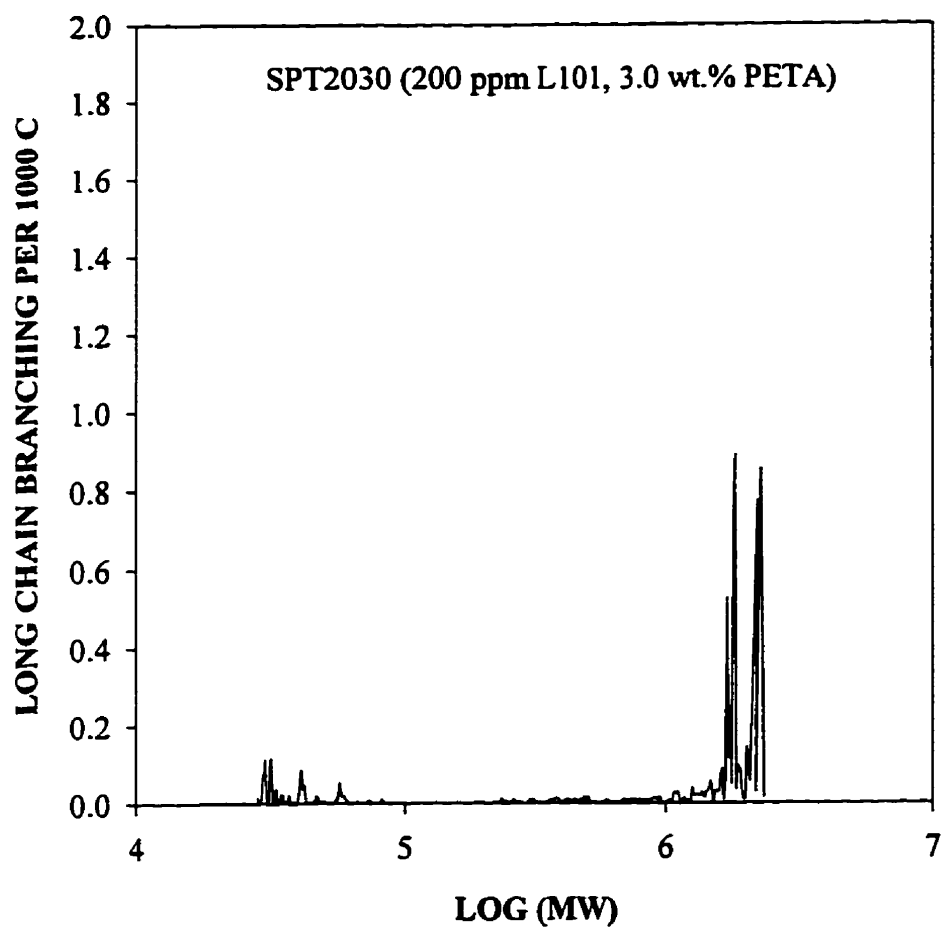


Fig. 5-27d Long chain branching frequency per 1000 C ( $\lambda$ ) of the SPT2030 sample.

shortened by the excess peroxide radicals. On the other hand, certain peroxide concentrations must be used in order to initiate the reactions between PETA and PP and hence to introduce the branching points.

In summary, the molecular weight averages in the peroxide degraded systems decrease with increasing peroxide concentration. However, the change in the molecular weight averages with PETA and peroxide concentration in the PETA/peroxide reaction system seems to be non-monotonic and it will depend on PETA/peroxide relative concentrations. It is found that all the PETA/peroxide modified PPs have smaller  $\bar{M}_n$  and  $\bar{M}_w$  than those of virgin PP but some samples have  $\bar{M}_z$ s similar to that of the virgin PP.

In our system, broadening in the high molecular weight end is observed in long chain branched samples such as SPT510, SPT530 and SPT1030. These samples seem to have high molecular weight ends close to that of virgin PP or even a more significant high molecular weight tail. The increased amount of the molecules with moderate molecular weights is also observed in many samples since the peak heights of the MWD curves are increased.

Reasonable results were obtained on a series of linear PPs, for the molecular weight and LCB information such as overall branching index, viscosity law plots, branching index distribution and LCB frequency. This suggests that the GPC analysis in our case is reliable. The analysis on the PETA/peroxide modified samples suggests that the majority of the long chain branched samples are in the 50 and 100 ppm peroxide series. Combined with the overall branching index and LCB frequency plots, it is concluded that SPT510, SPT530, SPT1005, SPT1010, SPT1020 and SPT1030 might be the long chain branched samples.

Finally, it is surprising that the analysis on Montell PP did not yield the expected results such as the curvature of the viscosity law plot in the high molecular weight region and the low overall branching index. It is not clear at this point whether or not this is due to some inherent property of this commercial material.

### 5.5.3 Average $n_w$ and $\lambda$ for the Whole Polymers

The average long chain branching frequency per 1000 carbon atoms ( $\lambda$ ) and the mean number of branches per weight average molecule ( $n_w$ ) for whole samples were estimated and the results are shown in Table 5.6.

It can be seen that the estimated LCB levels of linear PPs are very low and they are actually originated from the LCB frequencies in the relatively low molecular weight region, which was regarded probably fallacious due to the insensitivity of the molecular weight detectors to low molecular weight species (Mirabella and Wild, 1990). The existence of LCB when PP is reacted with a peroxide alone has not been reported. Hence, it can be concluded that there is no long chain branching in linear PPs and the average LCB levels for linear PPs ( $\lambda = 2.21 \times 10^{-3} \pm 1.35 \times 10^{-3}$  LCB/1000 C and  $n_w = 0.034 \pm 0.025$  LCB/molecule) could be used as a source of the experimental error.

From Table 5.6, it seems that there is certain low LCB level in Montell PP measured. For many of the PETA/peroxide modified PPs, it can be seen that the LCB frequencies and  $n_w$ s are higher than those of linear PPs, suggesting that there are some levels of LCB in these materials. However, these LCB levels are relatively low if compared with those for some commercial branched polyethylenes, whose LCB levels could be up to 2.07 to 2.58 LCB/1000C (Pang and Rudin, 1993). Specifically, the 50 and 100 ppm peroxide series may contain most of the long chain branched samples. In 50 ppm series, the GPC rates the order of LCB levels as follows: SPT510 > SPT530 > SPT520 > SPT505. The samples in 100 ppm series may contain higher LCB levels than many samples in other series and they are mainly from the LCB frequencies in the high molecular weight regions. There may be some LCB levels in SPT1510 and SPT1530 but it should be noted that these are mainly from the LCB in the relatively low molecular weight region. The LCB levels in the 200 ppm series may be very low or there are no LCB at all.

Finally, it should be pointed out that the current  $\lambda$  and  $n_w$  estimations are regarded as

**TABLE 5.6 Average LCB Frequency  $\lambda$  (LCB/1000C) and Mean Number of Branches Per Weight Average Molecule ( $n_w$ ) for the Whole Samples**

Sample	$g'$	$\lambda$	$n_w$
Montell PP	0.885	0.006	0.159
Virgin PP	0.896	0 (0.002)	0 (0.040)
50PP	0.956	0 (0.004)	0 (0.076)
100PP	0.941	0 (0.002)	0 (0.034)
150PP	0.967	0 (0.001)	0 (0.015)
200PP	1.040	0 (0.0005)	0 (0.0007)
400PP	0.912	0 (0.004)	0 (0.053)
600PP	0.990	0 (0.002)	0 (0.022)
SPT505	0.966	0.007	0.088
SPT510	0.779	0.017	0.229
SPT520	0.876	0.009	0.136
SPT530	0.812	0.012	0.195
SPT1005	0.878	0.015	0.281
SPT1010	0.761	0.022	0.350
SPT1020	0.756	0.051	0.778
SPT1030	0.794	0.026	0.381
SPT1505	1.060	0.001	0.009
SPT1510	0.888	0.035	0.366
SPT1530	0.956	0.026	0.338
SPT2005	1.077	0.006	0.035
SPT2010	0.967	0.008	0.079
SPT2020	1.008	0.009	0.087
SPT2030	0.917	0.006	0.040

tentative at this stage due to the lack of a reference method developed for branched PP. However, it is believed that the current estimations are reasonable due to the fact that, a) the LCB levels of linear PPs are evaluated by GPC reasonably, and b) generally, the LCB levels rated by GPC for the PETA/peroxide modified PPs are in agreement with the evaluation of apparent elongational viscosities in Chapter 6.

#### 5.5.4 The Equal Hydrodynamic Volume Concept

The viscosity law plots for virgin PP, SPT510, SPT1005, SPT1030 and Montell PP are summarized in Fig. 5-28. The elution volume for these samples is plotted versus the logarithm of the measured intrinsic viscosity in Fig. 5-29. At low elution volume, all these samples exhibit lower intrinsic viscosity than that of virgin PP. However, the PETA/peroxide modified PPs show higher viscosity at high elution volume. Based on equation 5-2, the above intrinsic viscosity differences should be reflected in the plot of elution volume versus molecular weight (Fig. 5-30). Indeed all the samples exhibit higher molecular weight at low elution volume while the PETA modified PPs show lower values than that of virgin PP. The hydrodynamic volumes are plotted versus elution volume and it can be seen that both branched and linear PPs form a single curve (Fig. 5-31), as stated in equation 5-2.

#### 5.5.5 Relationship between MFI and $\bar{M}_w$

The relationship between the MFI and  $\bar{M}_w$  is worth discussing here, for both linear and branched polypropylenes. It has been found that for a series of polymers including linear PP (Tzoganakis, 1988; Bremner et al., 1990), there is a relationship as follows:

$$\frac{1}{MFI} = K \bar{M}_w^x \quad (5-14)$$

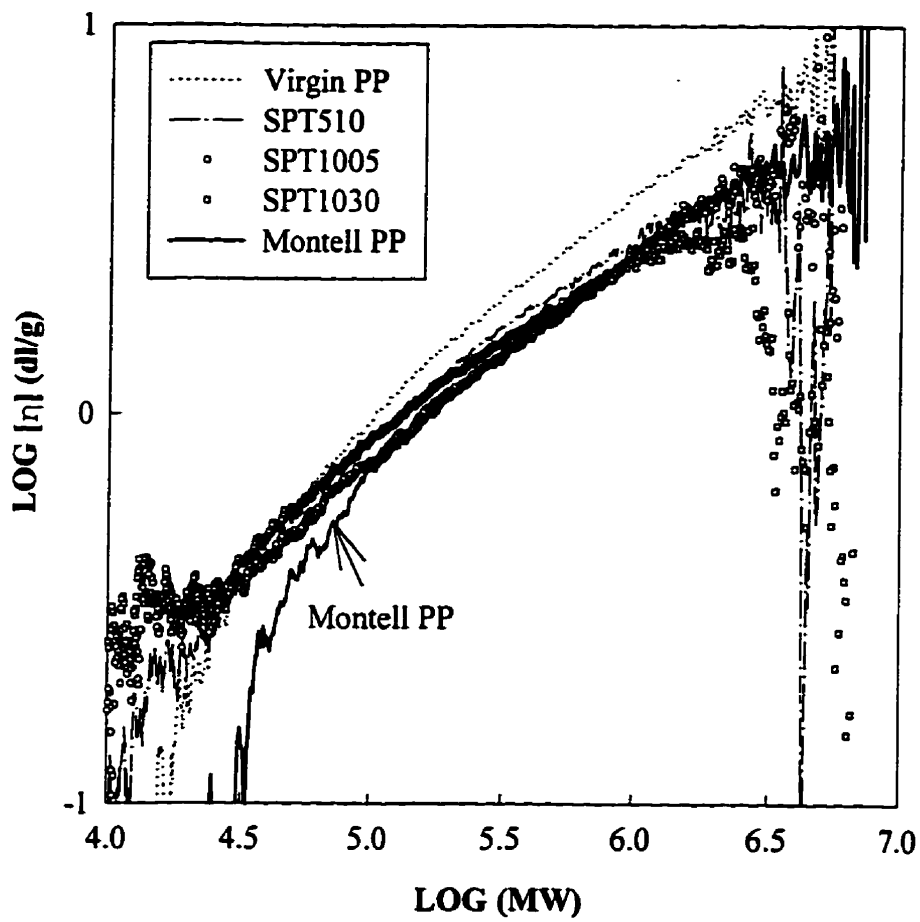


Fig. 5-28 Summary of the viscosity law plots of the samples of virgin PP, SPT510, SPT1005, SPT1030 and Montell PP.



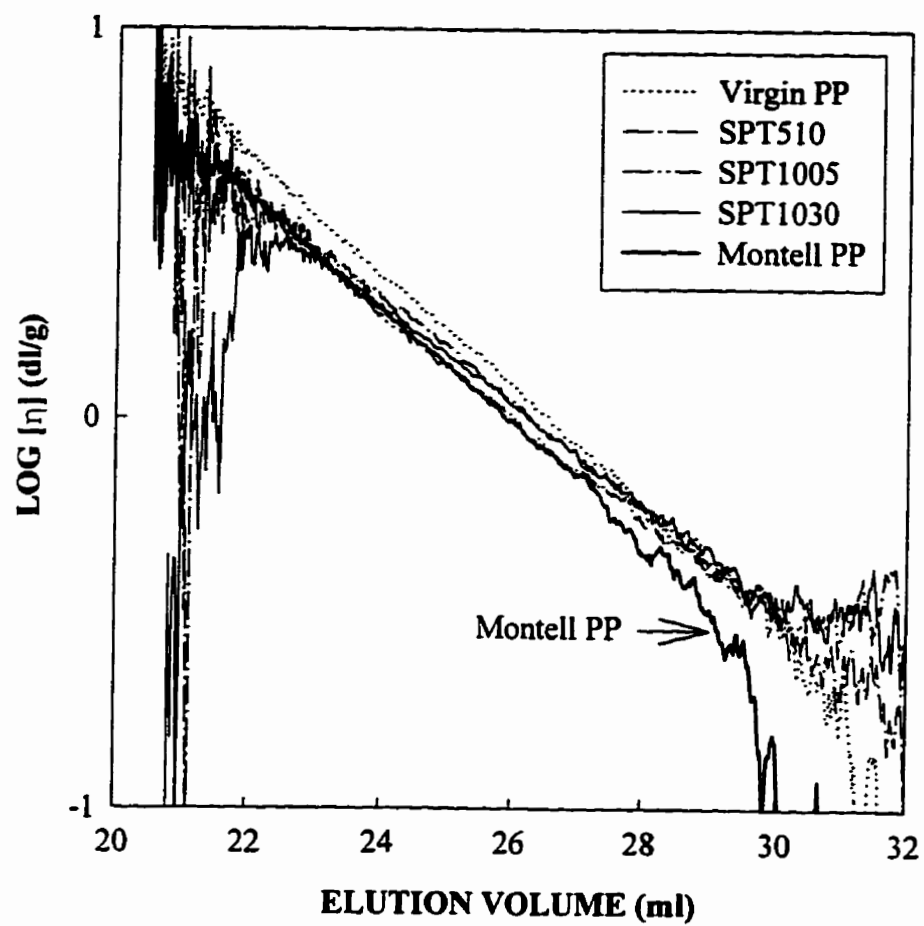


Fig. 5-29 Plot of logarithmic intrinsic viscosity versus elution volume for the samples of virgin PP, SPT510, SPT1005, SPT1030 and Montell PP.

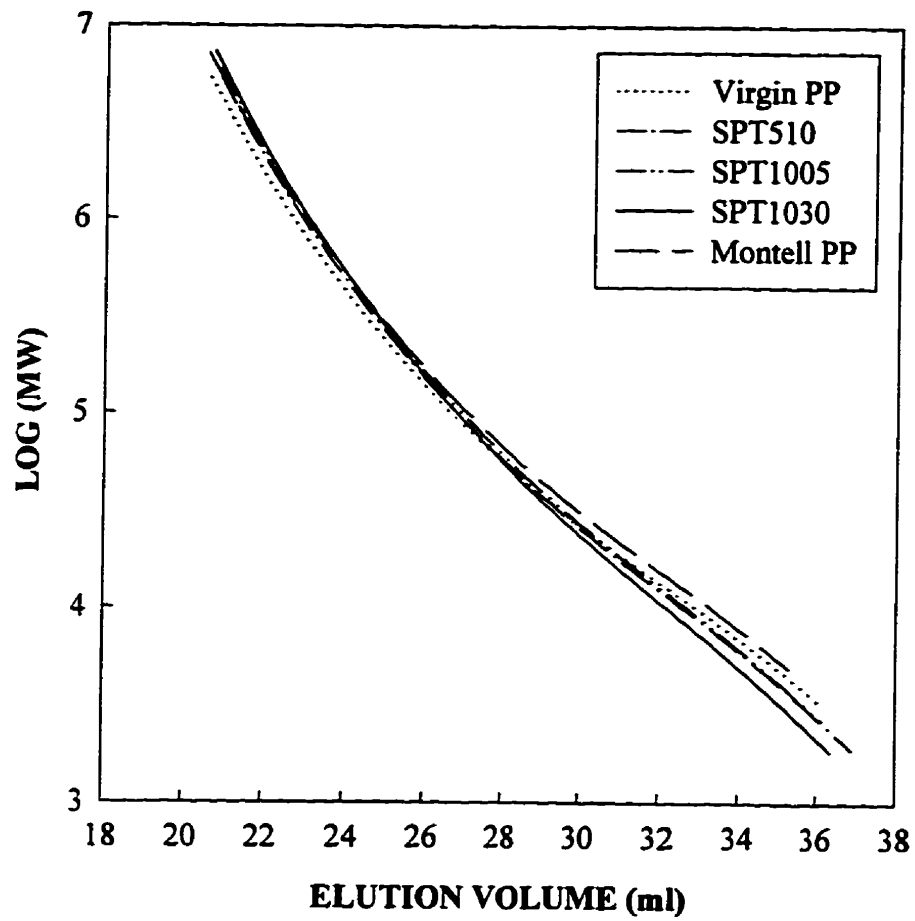


Fig. 5-30 Plot of logarithmic molecular weight versus elution volume for the samples of virgin PP, SPT510, SPT1005, SPT1030 and Montell PP.

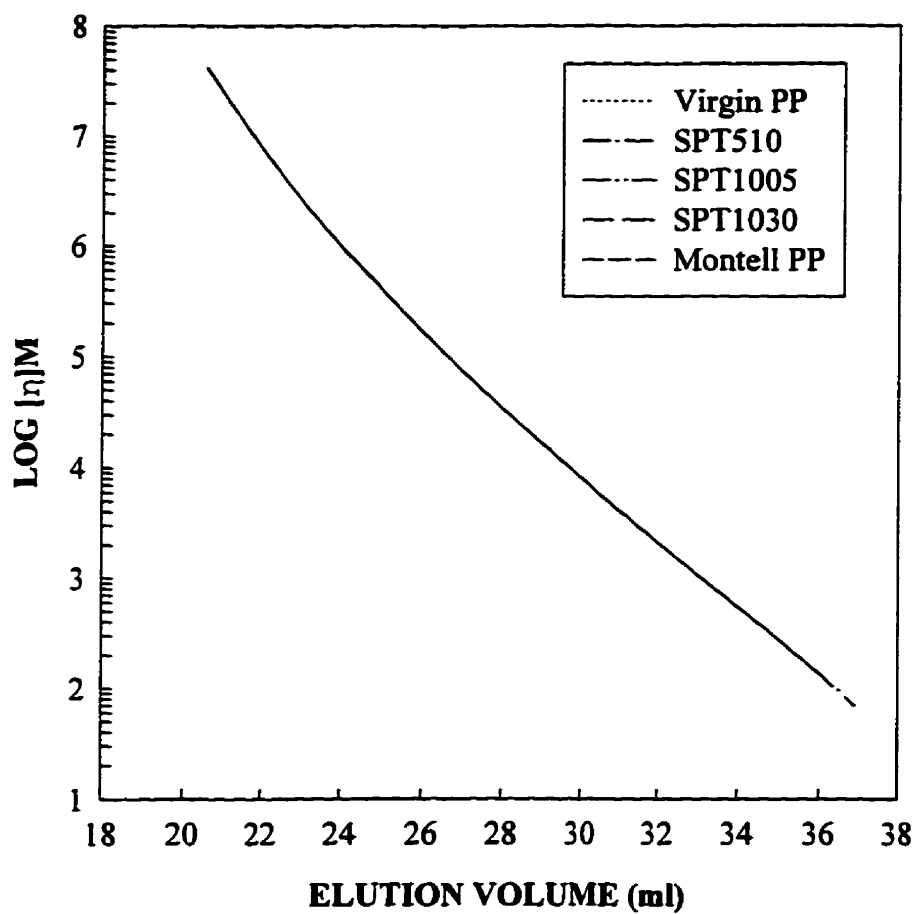


Fig. 5-31 Plot of logarithmic hydrodynamic volume versus elution volume for the samples of virgin PP, SPT510, SPT1005, SPT1030 and Montell PP.

where  $x$  is found to be 3.20 (data from Tzoganakis, 1988b) and 3.92 (data from Bremner et al.). For our system,  $x$  is found to be 2.01 (Fig. 5-32) and it can be seen that all the linear PPs (virgin and peroxide-degraded PPs) form a straight line. However, Montell PP and almost all the PETA/peroxide modified PPs lie far from this line. Data of linear and branched PPs published by Montell (DeNicola, 1992) are also plotted in Fig. 5-33 and the  $x$  is found to be 3.31. Similarly, all the linear PPs roughly form a straight line while some of the branched PPs deviate from it. The above results indicate that there is indeed a relationship between the inverse MFI and the  $\bar{M}_w$  for linear PPs. For branched species, however, there may not exist a definite relationship between these two parameters.

## 5.6 Concluding Remarks

From the combined results of average  $g'$ ,  $[\eta]$ ,  $\lambda$  and  $n_w$  of the whole GPC samples, the viscosity law plot,  $g'$  distribution, long chain branching frequency per 1000 C ( $\lambda$ ), the current GPC analysis determines that there is virtually no long chain branching in virgin linear PP and peroxide-degraded PPs as expected. The commercial branched PP has a much higher weight average molecular weight than those of all the samples in our system and may contain a low LCB level. Most of the long chain branched PPs produced by REX are found in the 50 and 100 ppm peroxide series. In 50 ppm series, the GPC rates the order of LCB levels as follows: SPT510 > SPT530 > SPT520 > SPT505. The LCB levels of the samples in 100 ppm peroxide series may be similar and higher than those of many samples in other series. There may be some LCB levels in samples SPT1510 and SPT1530. The LCB levels in 200 ppm series may be very low or there are no LCB at all. For the long chain branched PP produced in our work, the average LCB frequency for the whole sample is estimated to be from 0.01 to 0.05 LCB/1000C, which corresponds to about 0.2 to 0.8 branches per weight average molecule.

The molecular weight averages in peroxide-degraded polypropylenes decrease with

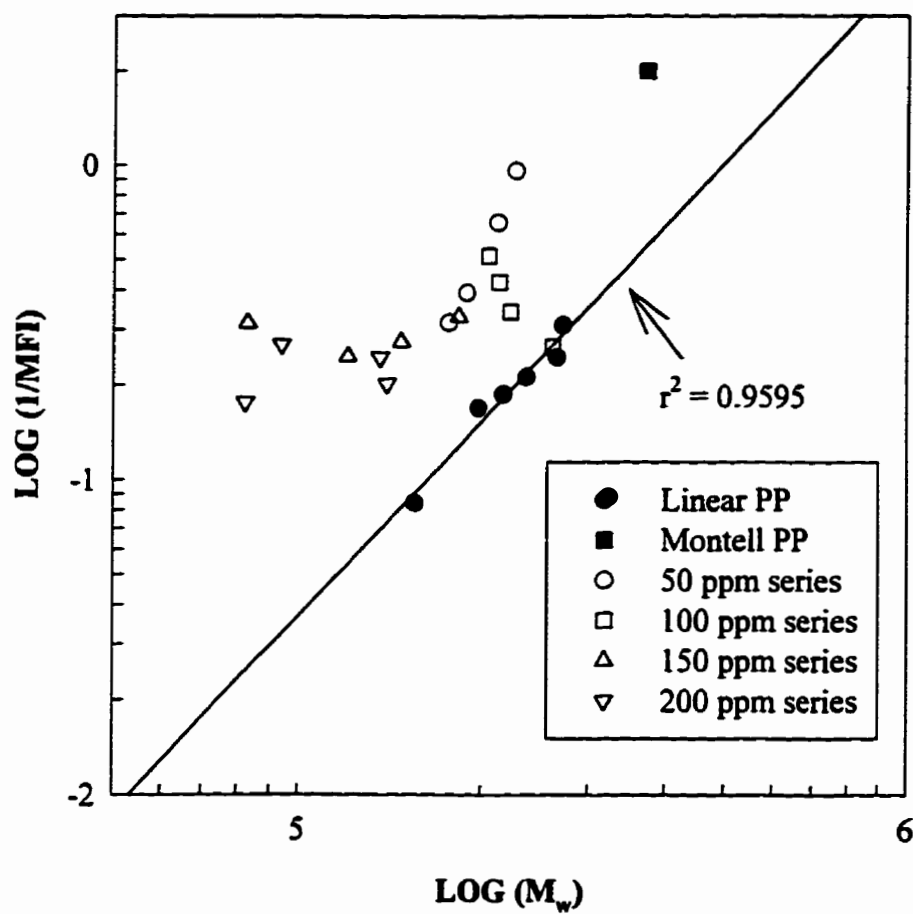


Fig. 5-32 Plot of the reciprocal of melt flow index (MFI) versus weight average molecular weight of linear and branched PPs produced by reactive extrusion.

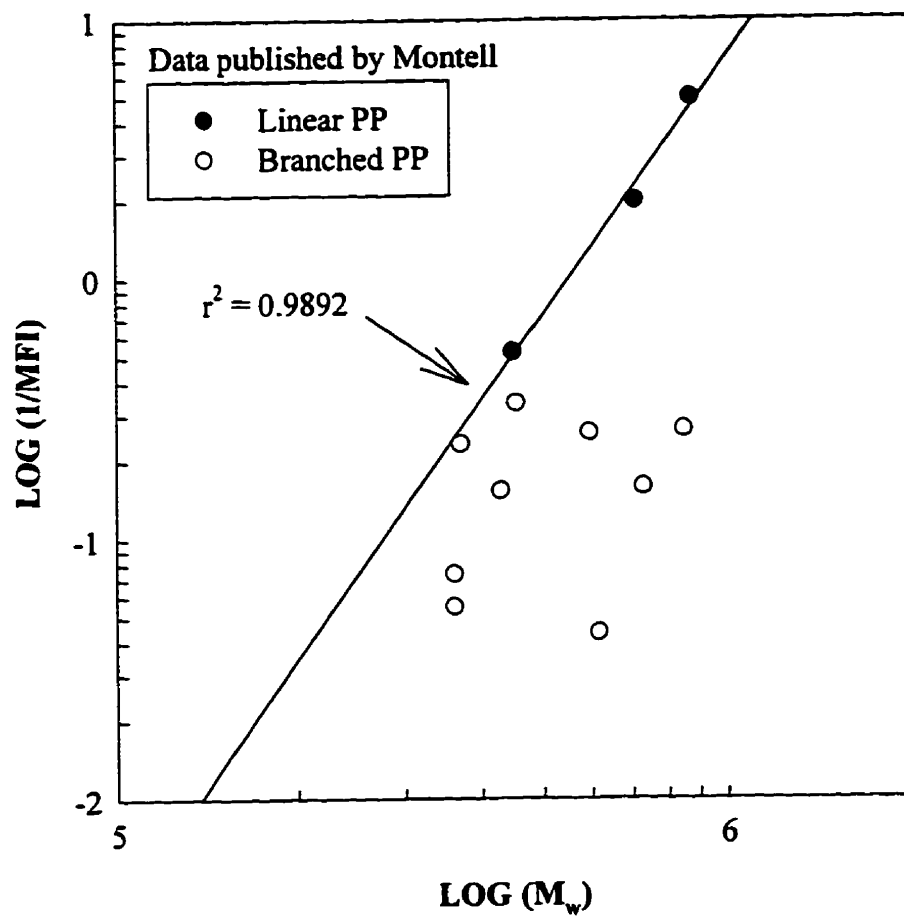


Fig. 5-33 Plot of the reciprocal of melt flow index (MFI) versus weight average molecular weight of linear and branched PPs (data published by Montell).

increasing peroxide concentration as expected. However, the change in the molecular weight averages with PETA and peroxide concentration in the PETA/peroxide reaction system seems non monotonic and it depends on PETA/peroxide relative concentrations. It is found that all the PETA/peroxide modified PPs have smaller  $\bar{M}_n$  and  $\bar{M}_w$  than those of virgin PP but some samples have  $\bar{M}_z$ s similar to that of the virgin PP. It was found that in our system, there may be some broadening in the high molecular weight end in some long chain branched samples such as SPT510, SPT530 and SPT1030.

Finally, experimental result suggests that there is a certain relationship between the inverse MFI and  $\bar{M}_w$  for linear polypropylenes. However, this does not apply for their long chain branched counterparts.

## CHAPTER 6

### APPARENT ELONGATIONAL VISCOSITY AND FLOW ACTIVATION ENERGY

#### 6.1 Apparent Elongational Viscosity of the Whole Polymers

##### 6.1.1 Introduction

Elongational flow is important in polymer processing, such as melt spinning, extrusion coating, blow moulding, and thermoforming, and different methods to characterize the elongational properties of polymers have been explored. Generally, five main approaches (Brydson, 1981) may be identified: a) constant stress measurements, b) constant strain rate measurements, c) constant force measurements, d) continuous drawing of a spinning threadline, and e) Cogswell's method.

The nature of Cogswell's method (Cogswell, 1972) is to use convergent flow regimes in a capillary rheometer to evaluate the apparent elongational viscosity of a polymer. In this method, the elongational viscosity is estimated from the entrance pressure loss, which can be taken as the Bagley end corrections for simplicity. Hence, the apparent elongational rate ( $\dot{\epsilon}$ ) and elongational viscosity ( $\eta_e$ ) can be calculated as:

$$\dot{\epsilon} = \frac{4(\dot{\gamma}_A)^2 \eta_A}{3(n+1)\Delta P_{ent}} \quad (6-1)$$

$$\eta_e(\dot{\epsilon}) = \frac{9(n+1)^2(\Delta P_{ent})^2}{32\eta_A(\dot{\gamma}_A)^2} \quad (6-2)$$

where  $n$ ,  $\eta_a$  and  $\dot{\gamma}_A$  are the power-law index, apparent shear viscosity and apparent shear rate



respectively. The  $\Delta P_{ent}$  is the entrance pressure drop which is calculated using the equation:

$$\Delta P_{ent} = 2n_b \tau_w \quad (6-3)$$

where  $n_b$  is the Bagley correction as calculated from plots of the total pressure drop versus  $L/R$  of the capillary die (Bagley plot), and  $\tau_w$  is the wall shear stress.

Cogswell's method is relatively simple and allows a quick estimation of the apparent elongational viscosity. Shroff et al. (1977) found that such a convergent flow analysis gives quick and reliable information on the elongational flow of melts in a wide range of strain rates and temperatures. Laun et al. (1989) compared the Cogswell analysis with directly measured steady-state elongational viscosities of low density polyethylene (LDPE), high density polyethylene (HDPE) and polystyrene (PS). They found that the converging flow viscosities lie in the right order of magnitude with conventional measurements for all the samples investigated. This agreement is very good at high elongational rates (approximately above  $0.1s^{-1}$ , depending on polymers).

Bersted (1993) reexamined Cogswell's method by relaxing two assumptions which were made during the derivation of this method, namely those of a power-law fluid in shearing flow and a constant elongational viscosity above the orifice. It was concluded that Cogswell's method can provide an accurate and relatively routine method of measuring elongational viscosity in molten polymers, since there is a good agreement between the results of the modified converging flow analysis with conventional elongational measurements over a large range of rates. In summary, Cogswell's method has the following advantages: a) the use of standard capillary rheometers designed for shear flow studies, b) the ability of studies at high elongational rates, c) rapid and reproducible results, and d) application over a wide temperature range.

Little data is available about the elongational flow properties of either linear or

branched PP melts although the shear flow properties of linear PPs have been studied in great detail. Ishizuka et al. (1980) used an improved elongational rheometer to study the elongational viscosity of PP melt at a constant elongational strain rate. Lanfray et al. (1990) studied the elongational properties of a series of six PPs and two polystyrene samples, while Ghijssels et al. (1994) studied the melt strength of linear PP and controlled-rheology PPs using uniaxial tensile experiments. It was found that for conventional linear PPs, the weight average molecular weight ( $\bar{M}_w$ ) is the only structural parameter governing the melt strength.

Long chain branches (LCB) have a significant effect on elongational property and hence on the melt strength of polymers. The melt strength of linear PP can be enhanced by the introduction of long chain branches on the PP backbone. The irradiation method has been one of the approaches (Chapter 2) and it was found that the branched PP had a pronounced strain-hardening behaviour and a higher extensional viscosity than conventional linear PPs (Scheve et al., 1990; Bradley et al., 1991). Hingmann et al. (1994) also studied branched PPs which were produced by crosslinking agents (the reaction system and production process were not disclosed), and found that long chain branched PP shows a maximum in the steady-state elongational viscosity and pronounced strain hardening.

In contrast to PP, there are many thorough investigations about the effect of LCB on the elongational flow behaviour of polyethylenes. For example, La Mantia et al. (1986) studied the influence of LCB on the elongational behaviour of polyethylenes and found that the strain-hardening effect increases with the number of branch points and the elongational viscosity tends to increase with LCB level. It should be noted that although LCB can cause strain hardening behaviour of polymer melts, it has been found that the presence of a high molecular weight tail in polymers can also give rise to strain hardening in elongational flows and thus might result in an enhanced melt strength. This has been observed for both linear PPs (Minoshima et al., 1980) and linear polyethylenes (Linster et al., 1986). For the effect of polydispersity values on the extensional properties, Münstedt and Laun (1981) examined

the degree of extension thickening and tensile viscosity curves for four high density polyethylene resins with polydispersity values between 9 and 13. They concluded that the polydispersity index is not a useful guide to the shape of the tensile viscosity curve, because small differences in the high end of the molecular weight distributions that have little impact on the polydispersity value can have an important effect on the extensional flow properties.

Finally, although the quantities of macrogels in our system are small and hence their effects are assumed to be negligible, it is instructive to elucidate the effects of this kind of solid fillers on the viscosity and elasticity of polymers. The inclusion of a solid filler in a polymer leads, as a rule, to a reduction of the ability of the polymer to undergo rubbery deformations and hence represses the viscoelasticity of the polymer. The die swell and entrance corrections, which are associated with the elastic energy stored in polymers during their capillary flow, will be decreased when a rigid filler is included in a polymer (Newman et al., 1965, Agarwal et al., 1978). Thus, the elongational viscosity will be decreased as the polymer is filled with rigid spherical particles (Nicodemo et al., 1975). In contrast to this, it will lead to the growth of the viscosity if one measures it in shear. The effect of rigid sphere fillers is to increase the viscosity by an amount proportional to the volume fraction of the filler particles regardless of their sizes, which can be expressed by the Einstein equation:

$$\eta = (1 + 2.5\phi)\eta_s \quad (6-4)$$

where  $\eta$  is the viscosity of a suspension;  $\eta_s$  is the viscosity of the polymer and  $\phi$  is the volume content of the solid filler. From the macrogel contents in Chapter 4, it can be estimated that with the maximum macrogel content, the increase in shear viscosity caused by the insolubles is indistinguishable from the experimental error which could be up to 9%.

### 6.1.2 Experimental

Evaluation of the apparent elongational viscosities using Cogswell's method was

performed at 210°C for virgin PP, Montell branched PP, peroxide degraded PPs and PETA/peroxide modified whole polymers. Steady-state shear viscosities were determined at eight shear rates (50, 100, 200, 400, 600, 800, 1000, 1500 s<sup>-1</sup>) with a Kayeness Galaxy V capillary rheometer. Five different dies having L/D ratios of 1.2, 4.7, 10, 20 and 40 respectively were employed except for the case of Montell PP, where severe melt fracture occurred for the die of L/D = 1.2 and hence only the four other dies were used. The diameter and entrance angle of all the dies were 0.03" and 90° respectively. Bagley end corrections were determined in the usual manner by plotting the total pressure loss obtained at a given apparent wall shear rate versus the L/R ratios of the dies.

### 6.1.3 Results and Discussion

The molecular parameters of the samples studied are summarized in Table 6.1. Figs. 6-1 to 6-10 show the Bagley plots for virgin PP, Montell PP, some samples in the 50 ppm peroxide series and all the samples in the 100 ppm peroxide series at eight apparent shear rate levels.

The Bagley correction values obtained are shown in Figs. 6-11 to 6-15 as a function of shear rate. It can be seen that for linear PPs, Bagley corrections increase with  $\bar{M}_w$  and polydispersity values. The Montell branched PP sample has the highest values for Bagley correction, which is probably due to its high weight average molecular weight since its LCB level is not the highest. All the samples in the 50 ppm peroxide series show higher values than those of virgin PP and 50PP over the whole shear rates examined, indicating that the elastic behaviour of PP has been enhanced after the modification. The samples SPT510 and SPT530 show much higher values among the samples in this series. Considering the  $\bar{M}_w$  and  $\bar{M}_z$  of these samples, the enhancement of the elastic behaviour of their melts is definitely due to the introduction of long chain branching since the order in the Bagley correction values

**TABLE 6.1 Summary of Molecular Parameters of the Samples**

Sample	$\bar{M}_n$	$\bar{M}_w$	$\bar{M}_z$	$\bar{M}_w/\bar{M}_n$	$g'$	$\lambda$	$n_w$
Montell PP	81,500	371,800	1,217,800	4.56	0.885	0.006	0.159
Virgin PP	50,600	272,200	1,003,100	5.38	0.896	0	0
50PP	49,500	266,100	935,400	5.38	0.956	0	0
100PP	46,400	237,300	835,000	5.12	0.941	0	0
150PP	45,500	217,300	689,500	4.78	0.967	0	0
200PP	43,800	197,400	636,500	4.51	1.040	0	0
400PP	41,800	186,900	542,300	4.47	0.912	0	0
600PP	37,800	154,300	448,700	4.09	0.990	0	0
SPT505	32,200	175,300	614,500	5.45	0.966	0.007	0.088
SPT510	38,100	188,100	712,500	4.94	0.779	0.017	0.229
SPT520	40,500	212,200	809,200	5.24	0.876	0.009	0.136
SPT530	41,800	227,300	1,093,500	5.43	0.812	0.012	0.195
SPT1005	50,600	262,000	949,800	5.18	0.878	0.015	0.281
SPT1010	45,300	222,800	901,700	4.92	0.761	0.022	0.350
SPT1020	48,500	213,500	794,700	4.40	0.756	0.051	0.778
SPT1030	40,700	205,100	1,004,300	5.04	0.794	0.026	0.381
SPT1505	23,900	119,900	463,700	5.01	1.060	0.001	0.009
SPT1510	24,600	146,500	545,600	5.96	0.888	0.035	0.366
SPT1530	35,300	182,300	654,000	5.17	0.956	0.026	0.338
SPT2005	22,200	82,300	262,400	3.70	1.077	0.006	0.035
SPT2010	36,400	138,900	428,700	3.82	0.967	0.008	0.079
SPT2020	34,000	135,300	409,300	3.97	1.008	0.009	0.087
SPT2030	31,100	93,700	280,200	3.01	0.917	0.006	0.040

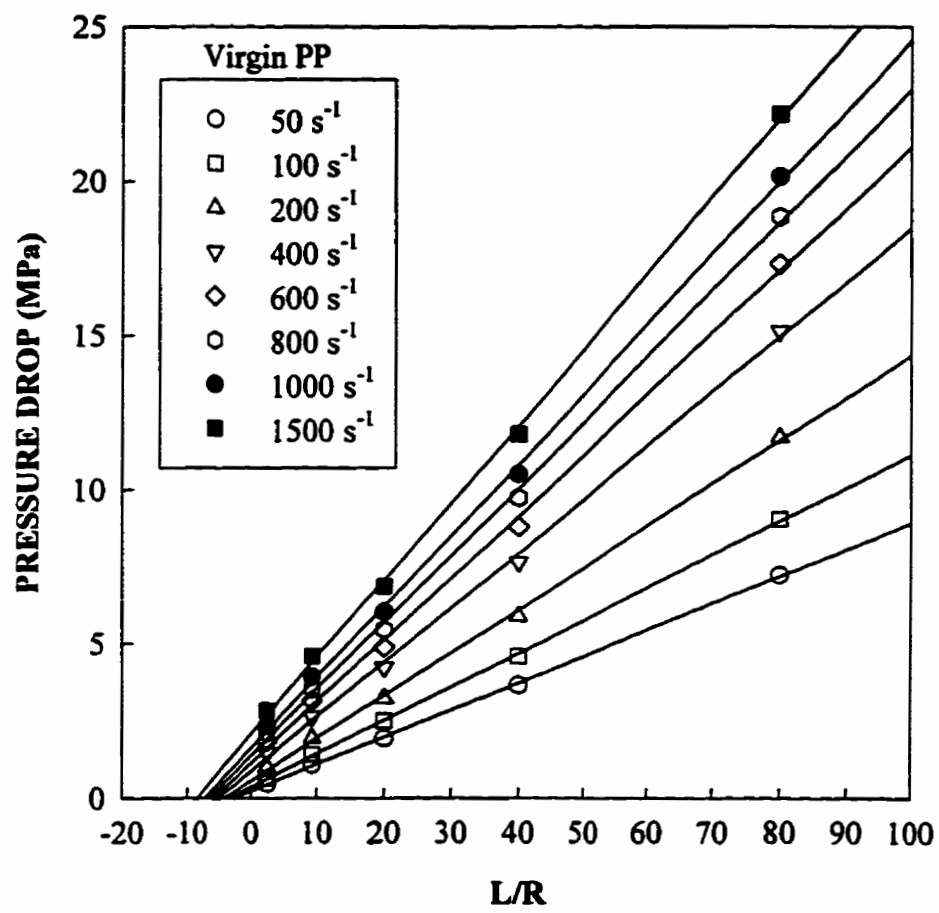


Fig. 6-1 Bagley plot of virgin PP.

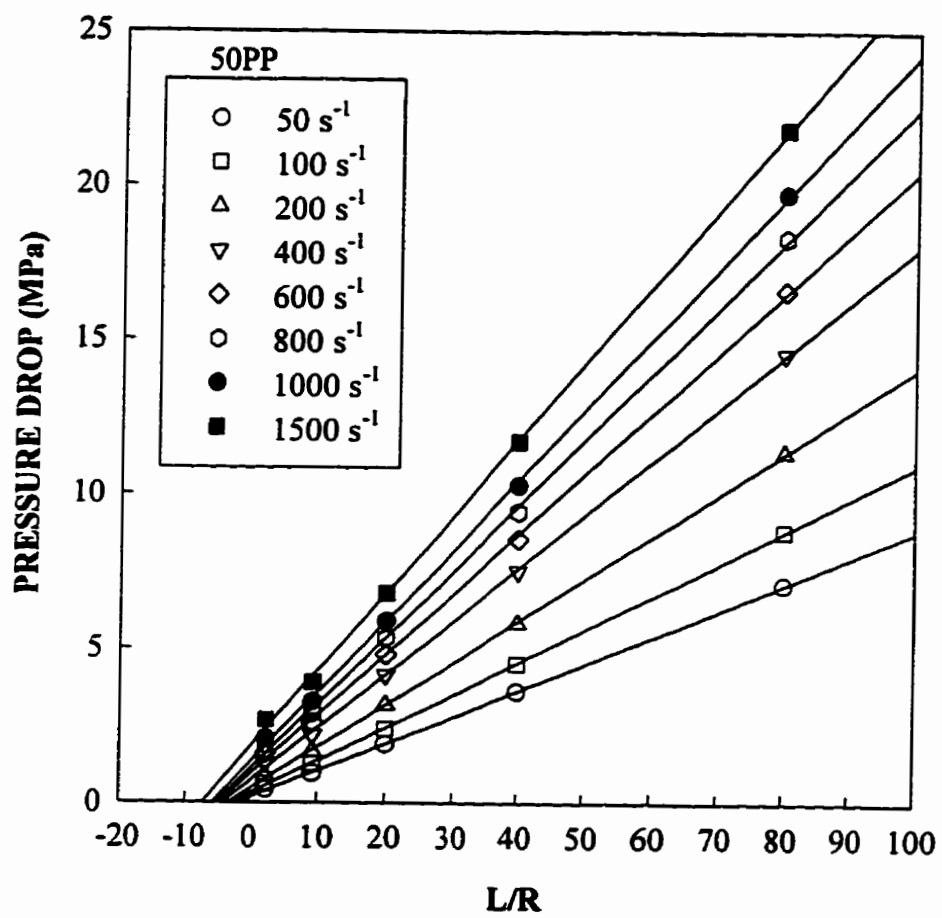


Fig. 6-2 Bagley plot of 50PP (produced with 50 ppm L101).

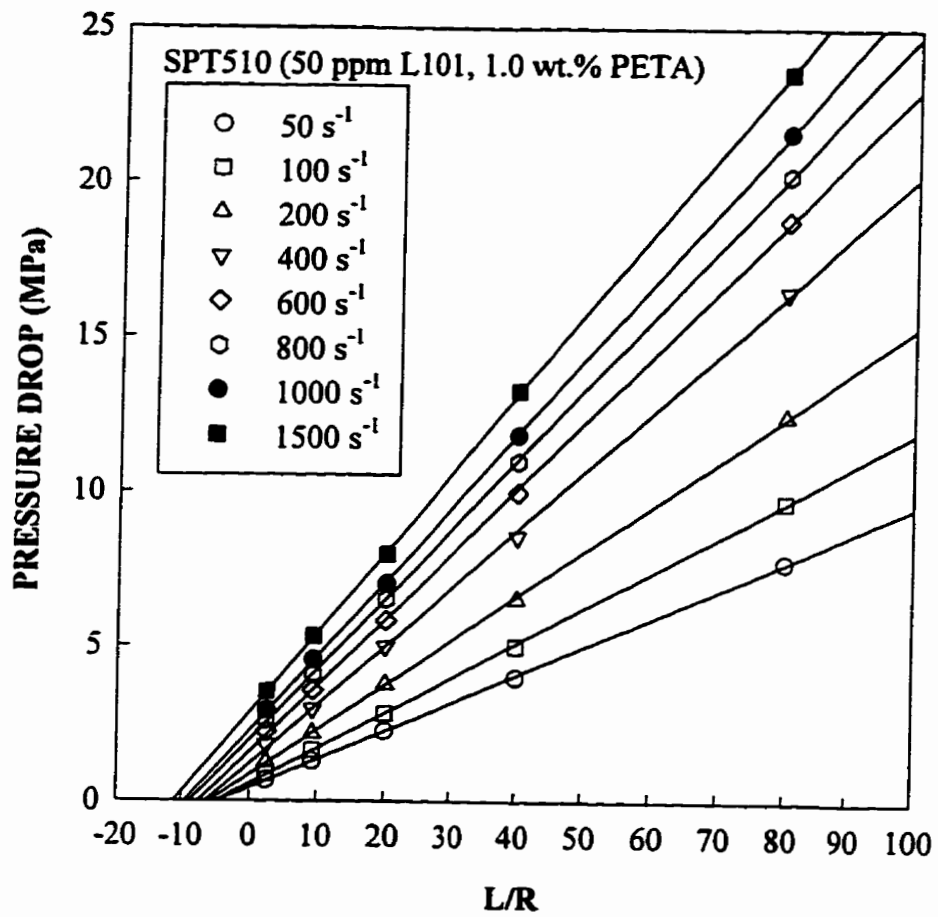


Fig. 6-3 Bagley plot of SPT510 (produced with 50 ppm L101 and 1.0 wt.% PETA).



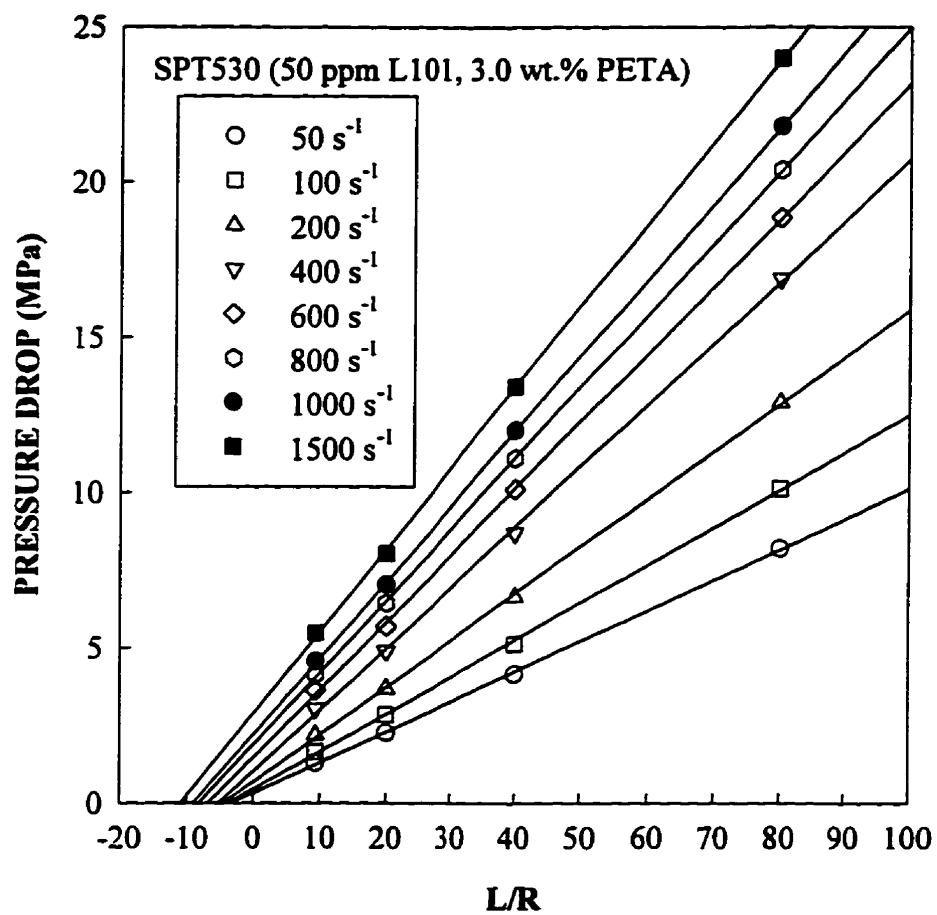


Fig. 6-4 Bagley plot of SPT530 (produced with 50 ppm L101 and 3.0 wt.% PETA).

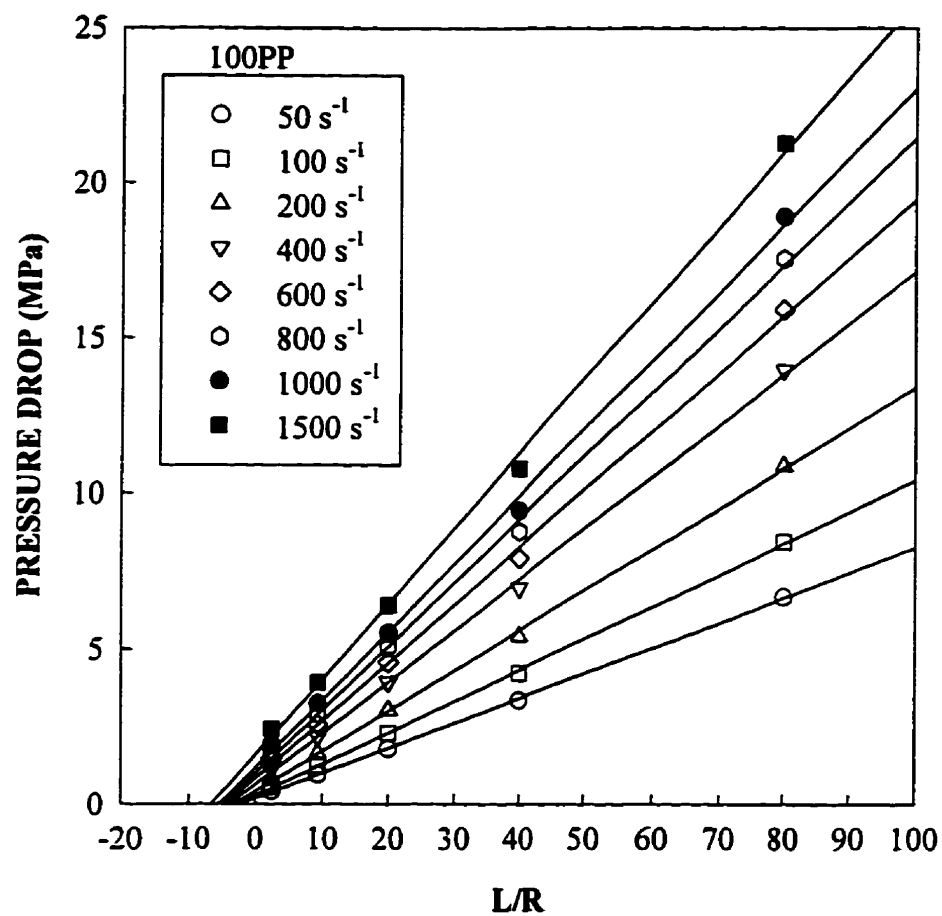


Fig. 6-5 Bagley plot of 100PP (degraded with 100 ppm L101).

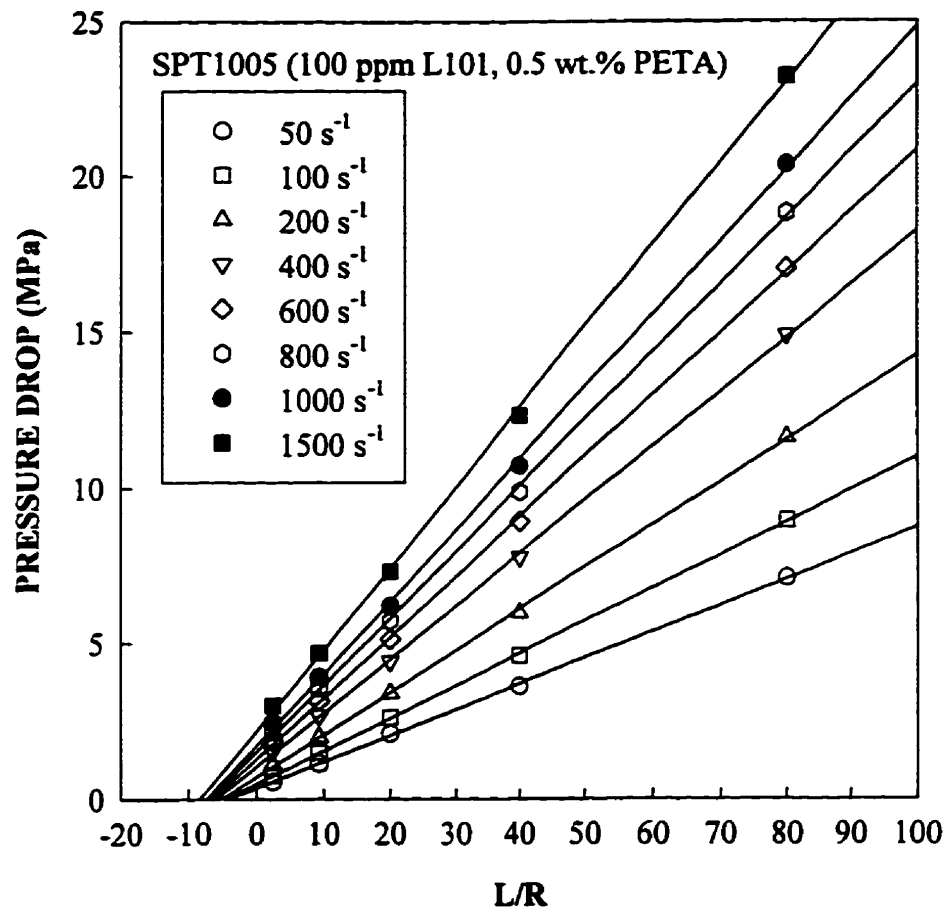


Fig. 6-6 Bagley plot of SPT1005 (produced with 100 ppm L101 and 0.5 wt.% PETA).

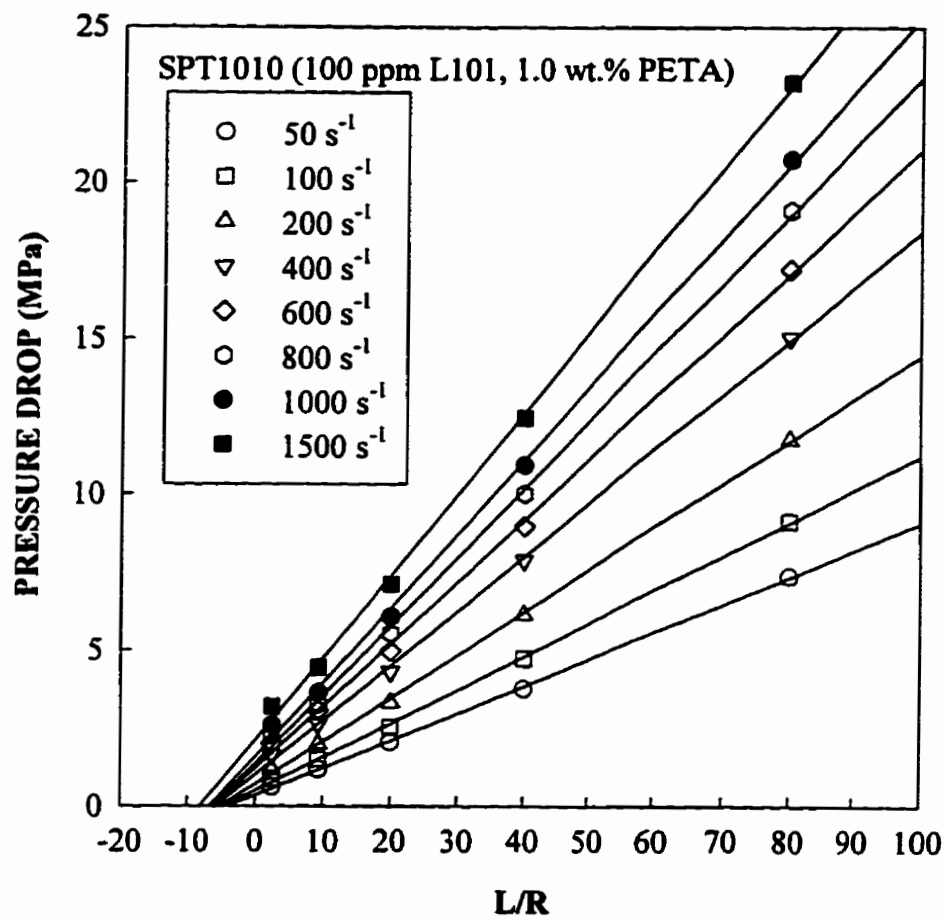


Fig. 6-7

Bagley plot of SPT1010 (produced with 100 ppm L101 and 1.0 wt.% PETA).

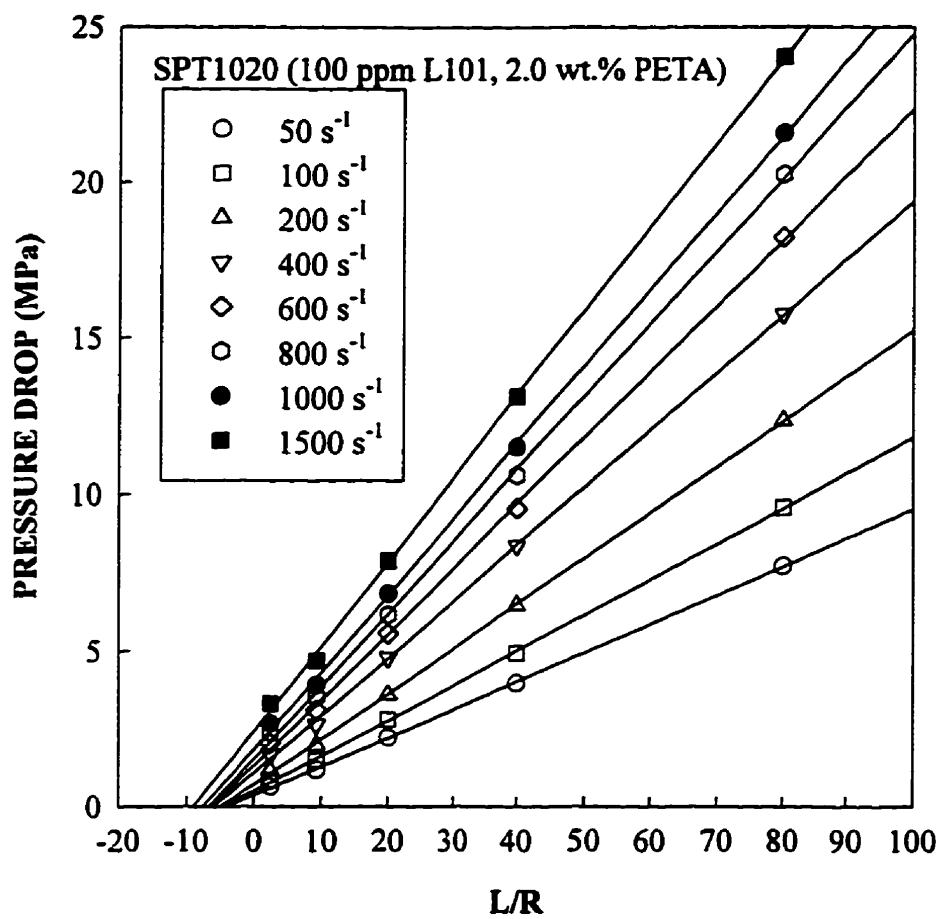


Fig. 6-8 Bagley plot of SPT1020 (produced with 100 ppm L101 and 2.0 wt.% PETA).

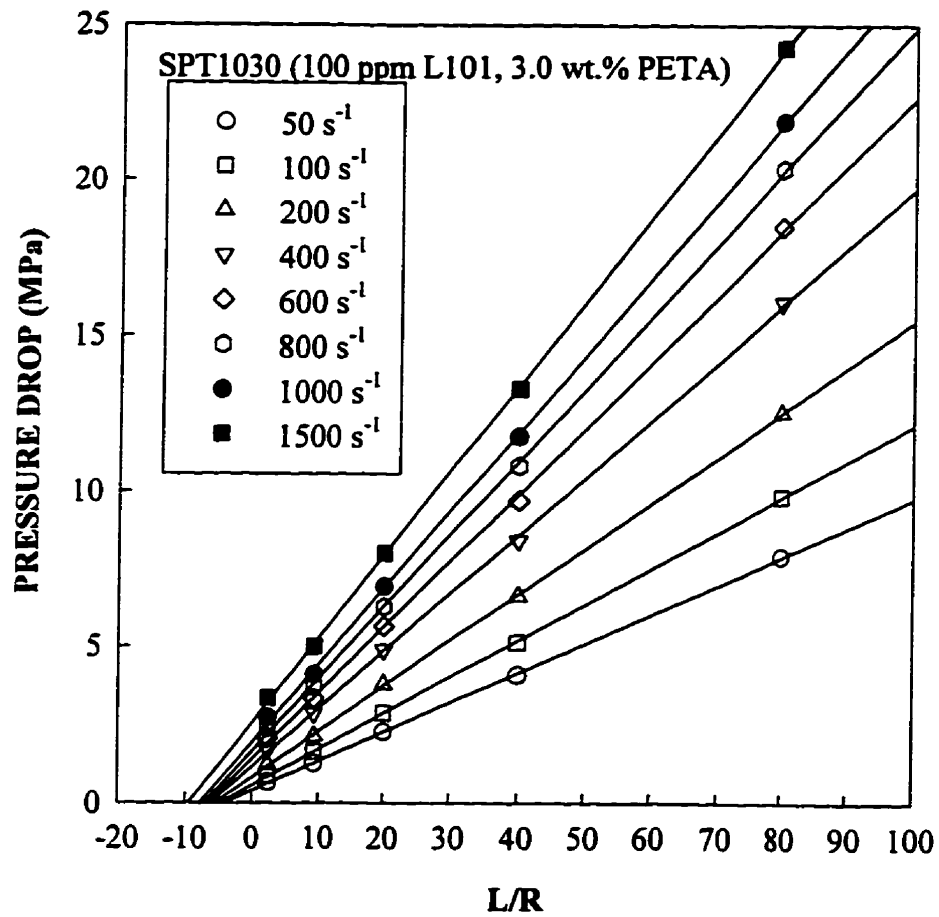


Fig. 6-9 Bagley plot of SPT1030 (produced with 100 ppm L101 and 3.0 wt.% PETA).

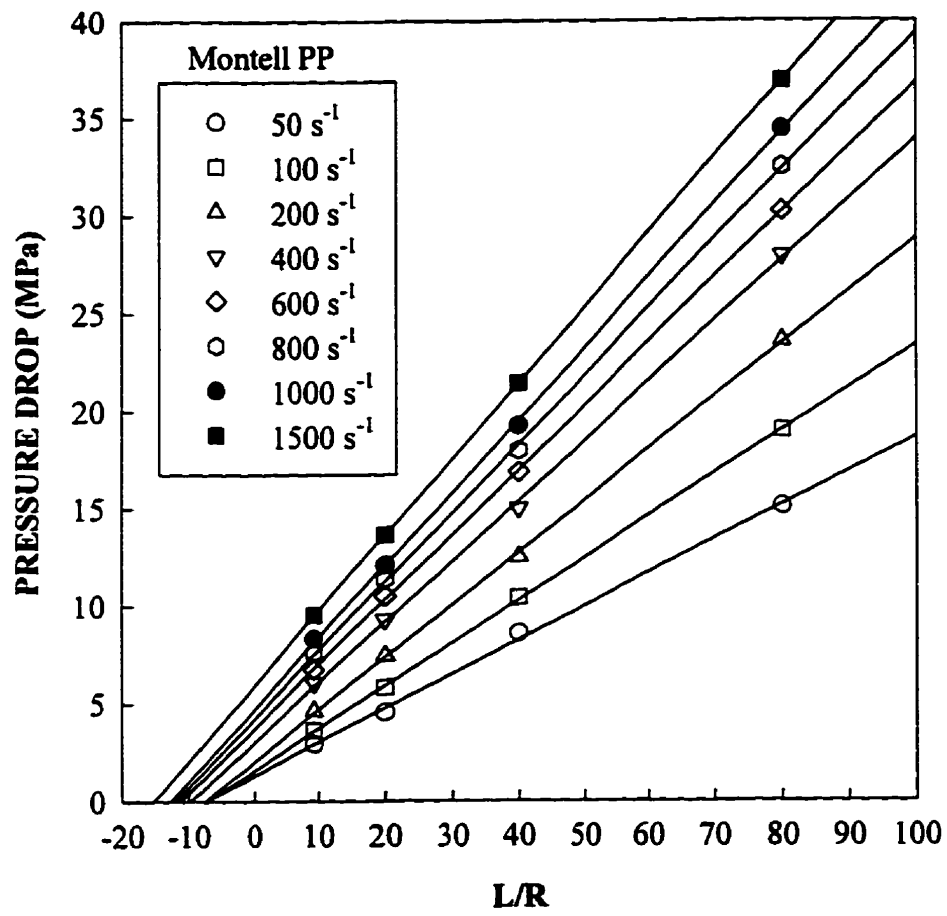


Fig. 6-10 Bagley plot of Montell branched PP.

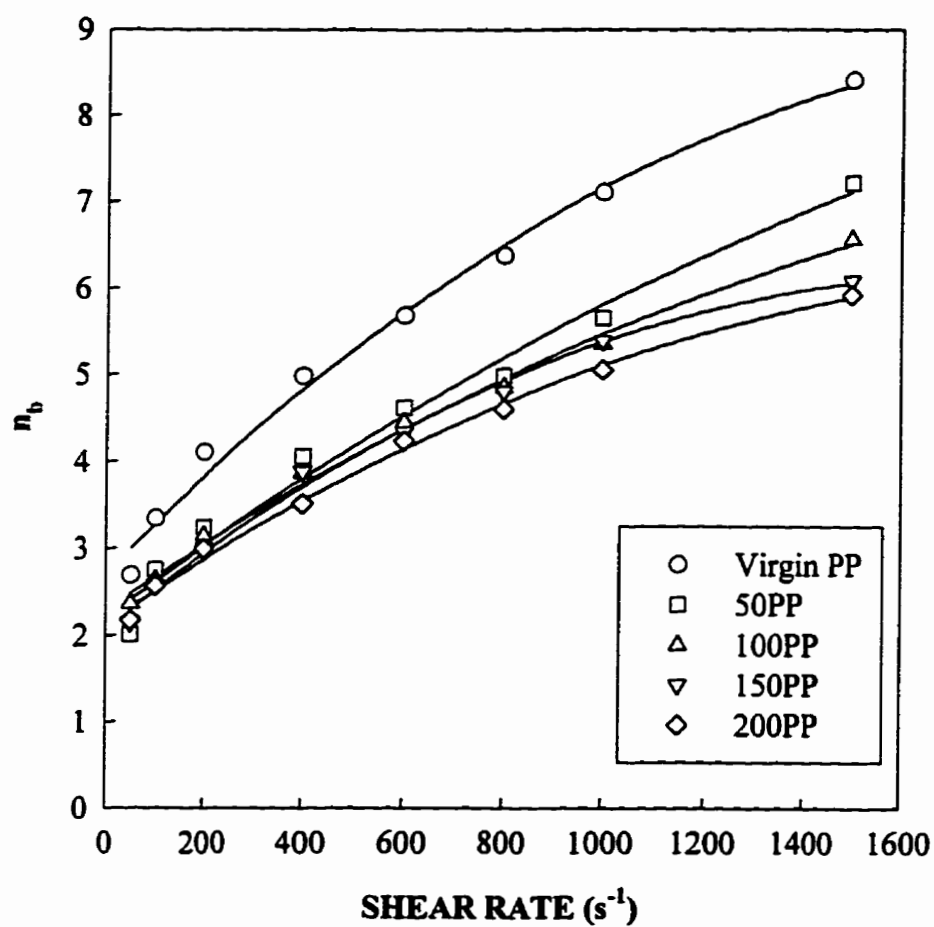


Fig. 6-11 Bagley correction coefficient of virgin PP and Degraded PPs.



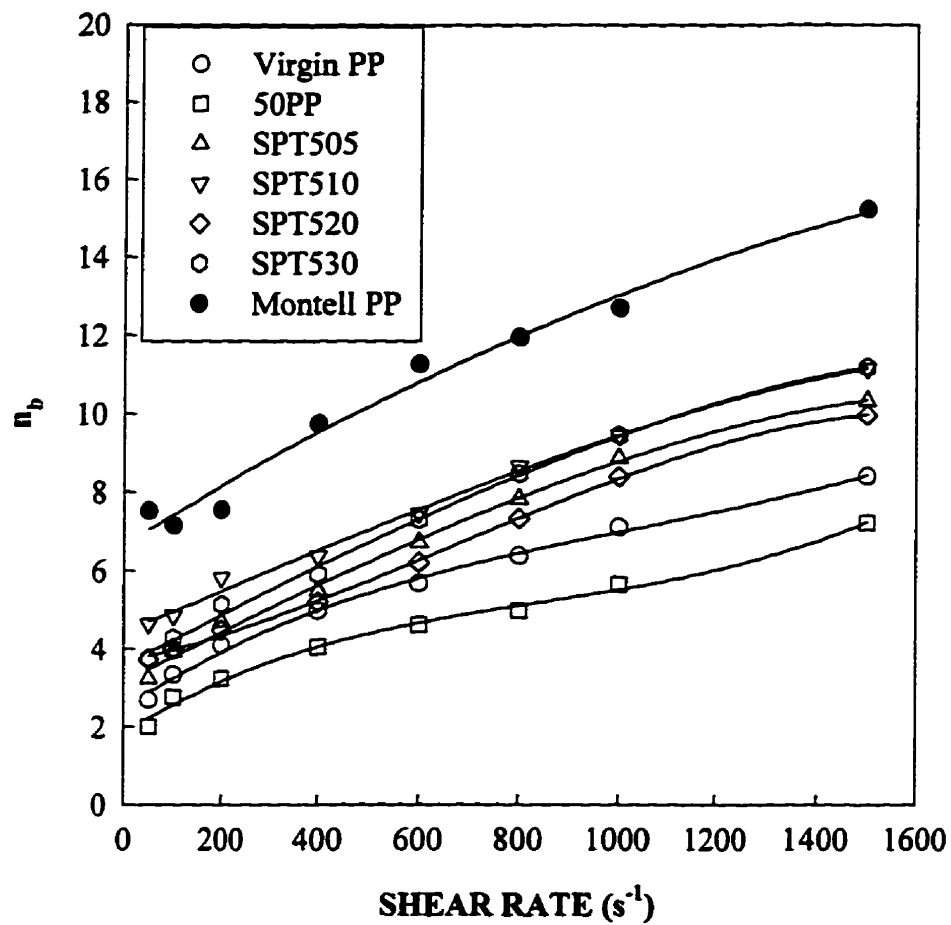


Fig. 6-12 Bagley correction coefficient of virgin PP, Montell PP and the samples in the 50 ppm peroxide series.

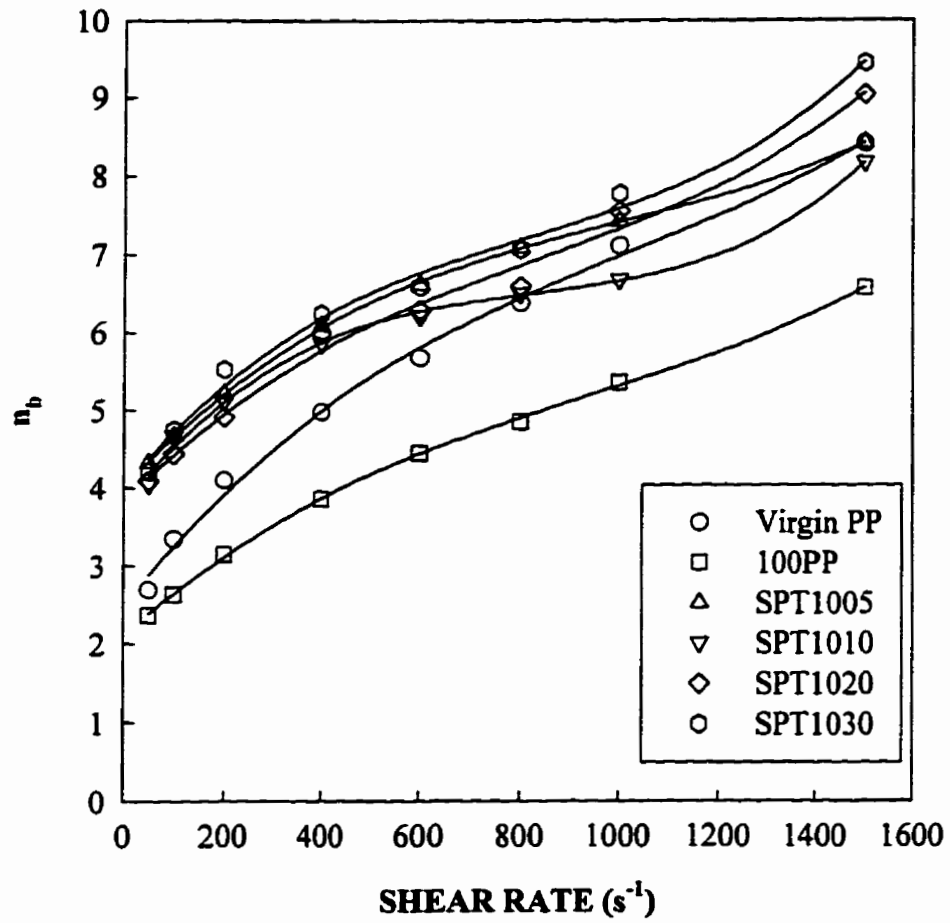


Fig. 6-13 Bagley correction coefficient of the samples in the 100 ppm peroxide series.

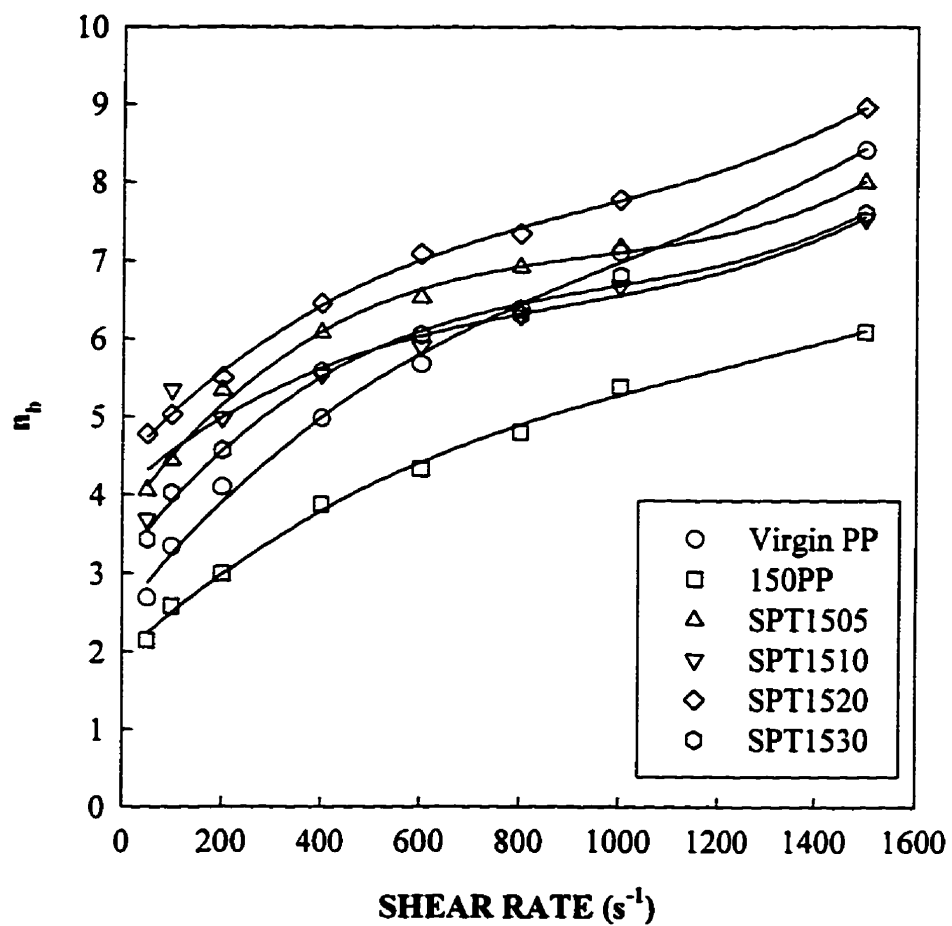


Fig. 6-14 Bagley correction coefficient of the samples in the 150 ppm peroxide series.

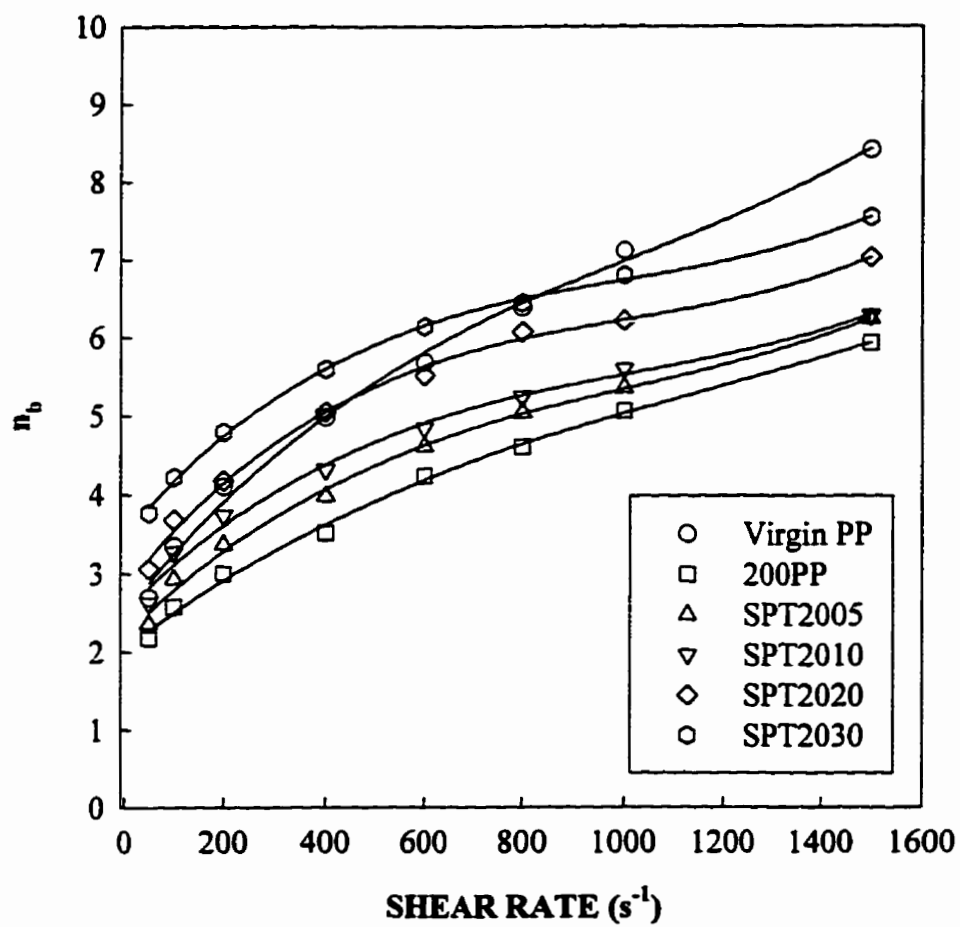


Fig. 6-15 Bagley correction coefficient of the samples in the 200 ppm peroxide series.

are generally in agreement with the LCB levels of these samples. The samples in 100 ppm peroxide series exhibit similar elastic behaviour enhancement and they have similar values in the lower shear rate region. In the 150 and 200 ppm series, the samples SPT1520 and SPT2030 show the highest Bagley corrections among the samples in their corresponding series. However, most of the samples in these two series show lower values than that of virgin PP. It can be seen that generally, the PETA/peroxide modified PPs show higher values than the corresponding degraded PPs in their series, even for the samples of 200 ppm series. Comparing the  $\bar{M}_w$  and  $\bar{M}_z$  of these samples, it is concluded that the increase of Bagley correction values originates from the introduction of branching.

The  $\eta_e$ s were calculated using equations (6-1) and (6-2) and the results are shown in Figs. 6-16 to 6-21. It can be seen that the  $\eta_e$  measurements show similar tendencies as those of the Bagley correction curves. Fig.6-16 shows the  $\eta_e$ s of the virgin and degraded PPs. Three distinct levels of the elongational viscosities are observed in Fig. 6-16 for these linear PPs. Virgin PP has the highest value and the degraded PPs with the peroxide levels of 50, 100, 150 and 200 ppm show lower values than that of virgin PP. It can be seen that these four samples exhibit similar values. The samples produced with 400, 600, 800 and 1000 ppm peroxide levels have much lower elongational viscosities. This monotonic decrease in  $\eta_e$  with decreasing  $\bar{M}_w$  suggests that there is no evidence of long chain branching of PP when Lupersol 101 was used alone under the present reaction conditions. This is also consistent with their LCB levels estimated. The current result also suggests that for the elongational viscosities of linear PPs,  $\bar{M}_w$  or  $\bar{M}_z$  may be the dominant factor since some of them have similar polydispersity values yet have different elongational viscosities. This observation is also in agreement with the result by Ghijssels et al. (1994), who found that the  $\bar{M}_w$  is the only structural parameter governing the melt strength of conventional linear PP and controlled rheology PPs. Montell PP shows much higher apparent elongational viscosity (Fig. 6-17).

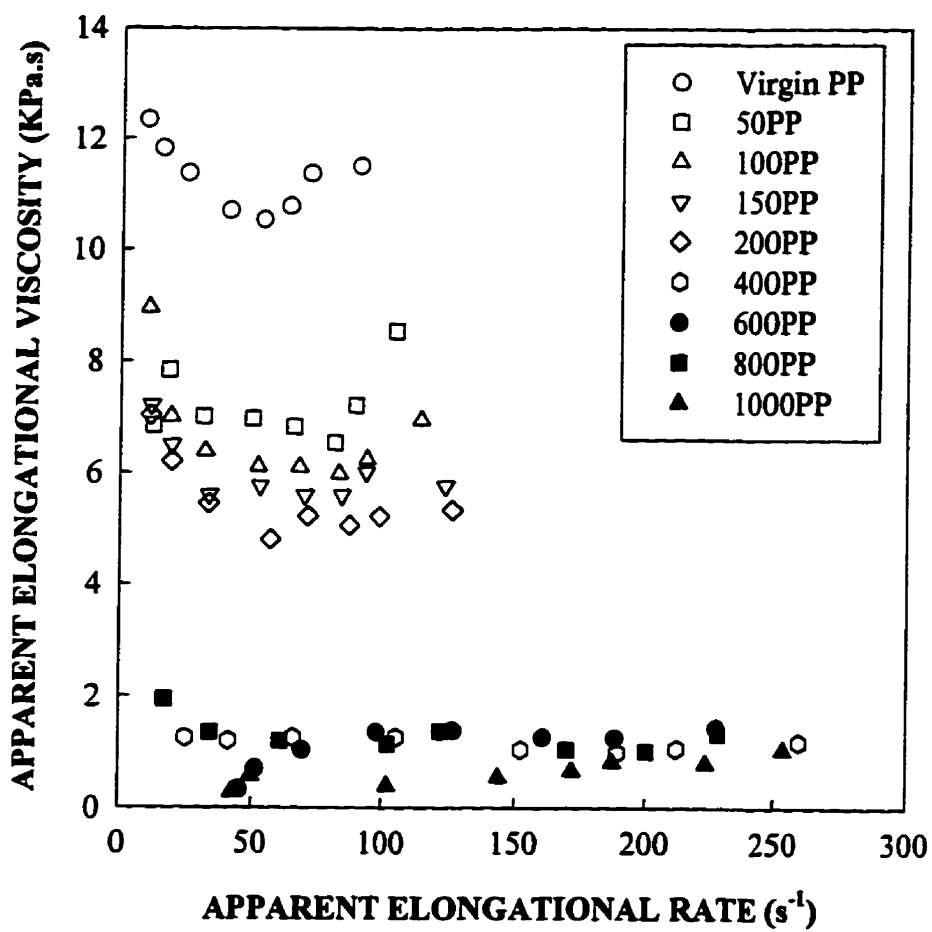


Fig. 6-16 Apparent elongational viscosity of virgin PP and a series of degraded PPs.

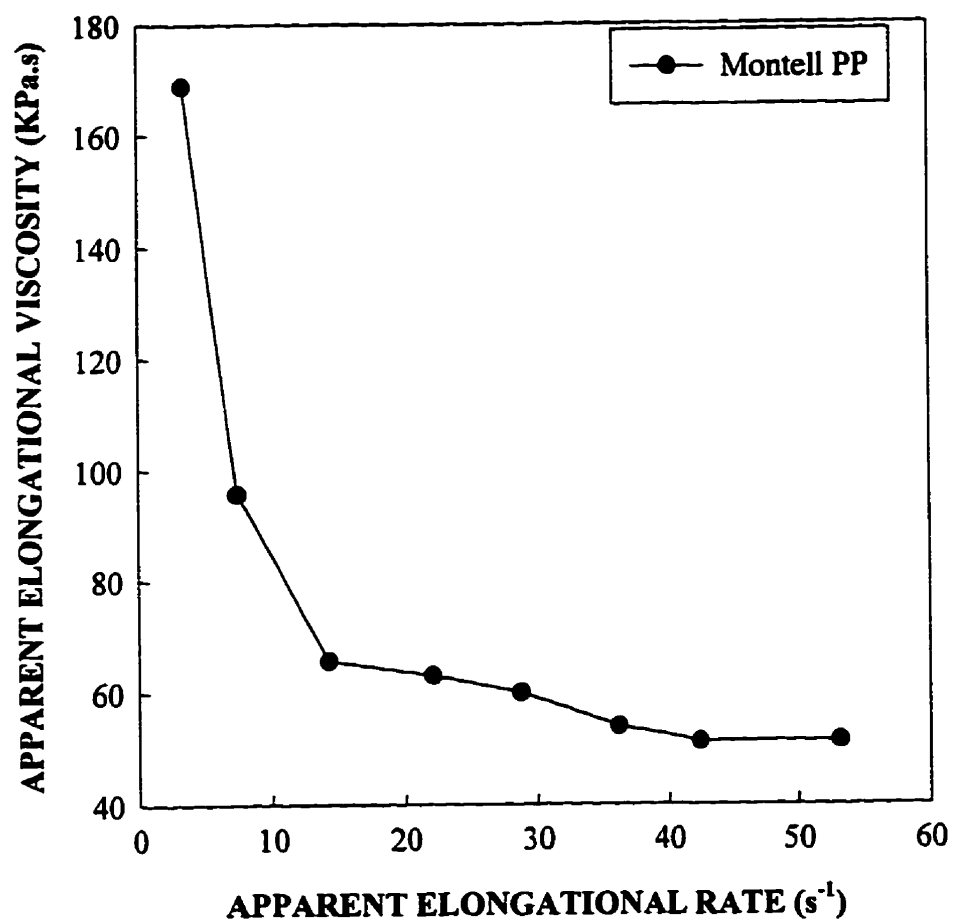


Fig. 6-17 Apparent elongational viscosity of Montell PP.

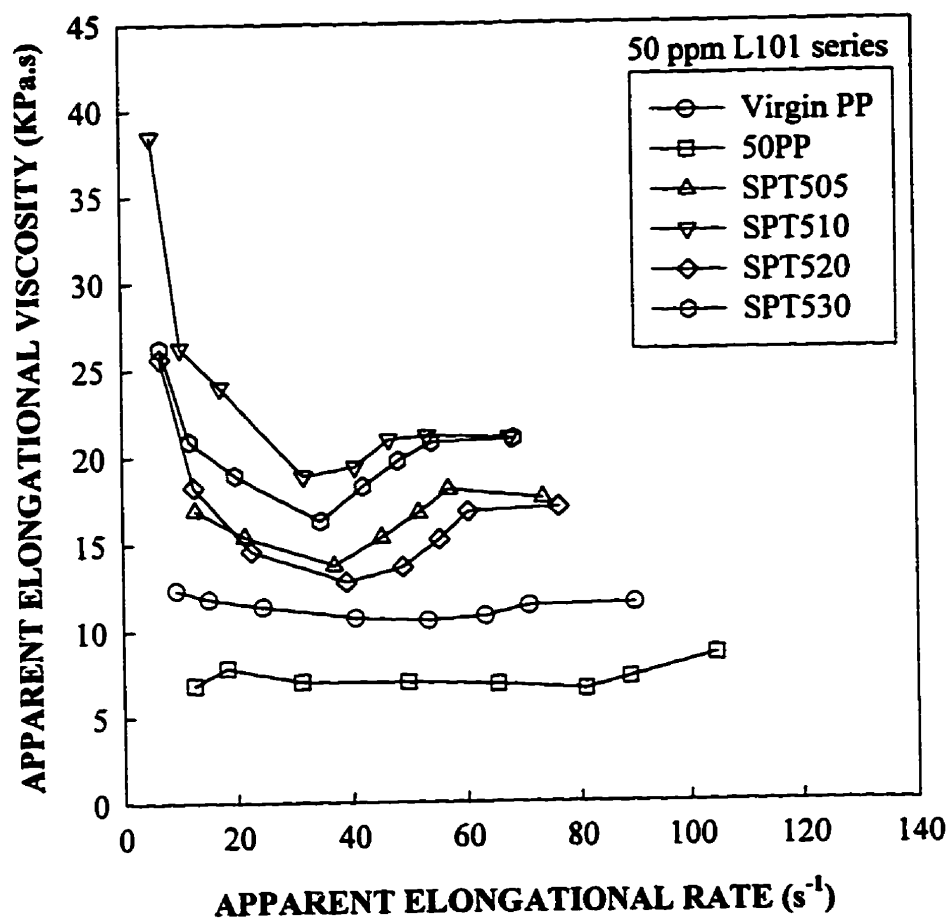


Fig. 6-18 Apparent elongational viscosity of the samples in 50 ppm peroxide series.



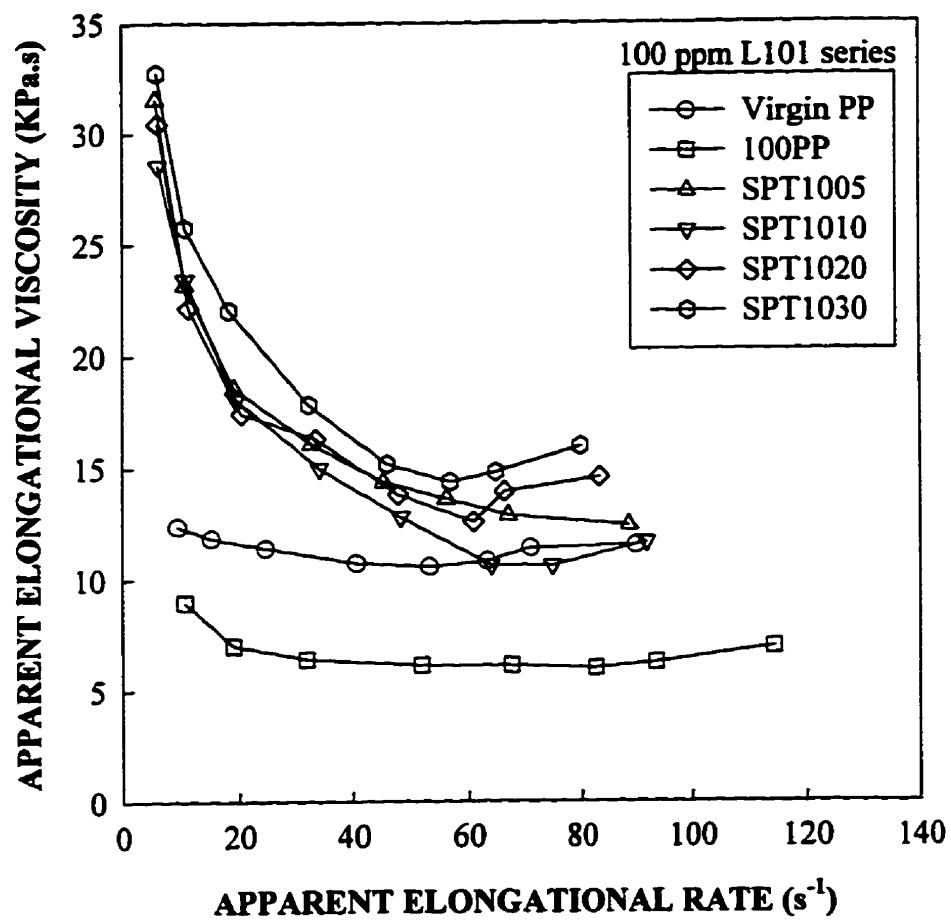


Fig. 6-19 Apparent elongational viscosity of the samples in 100 ppm peroxide series.

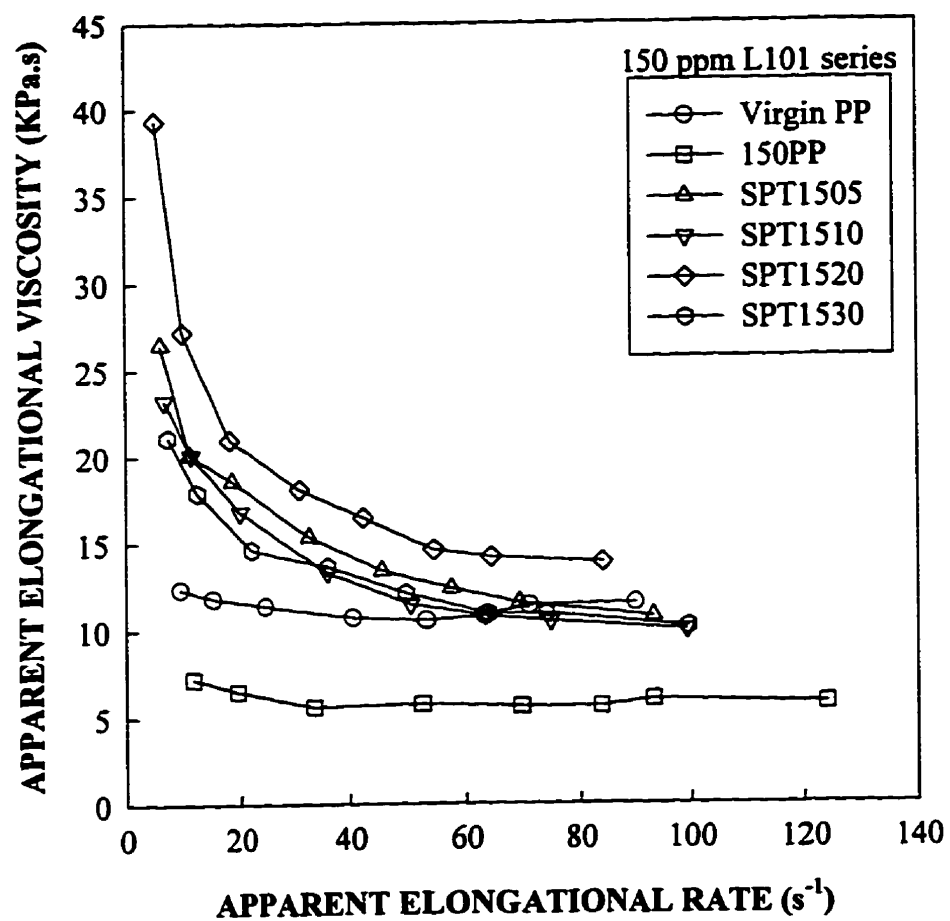


Fig. 6-20 Apparent elongational viscosity of the samples in 150 ppm peroxide series.

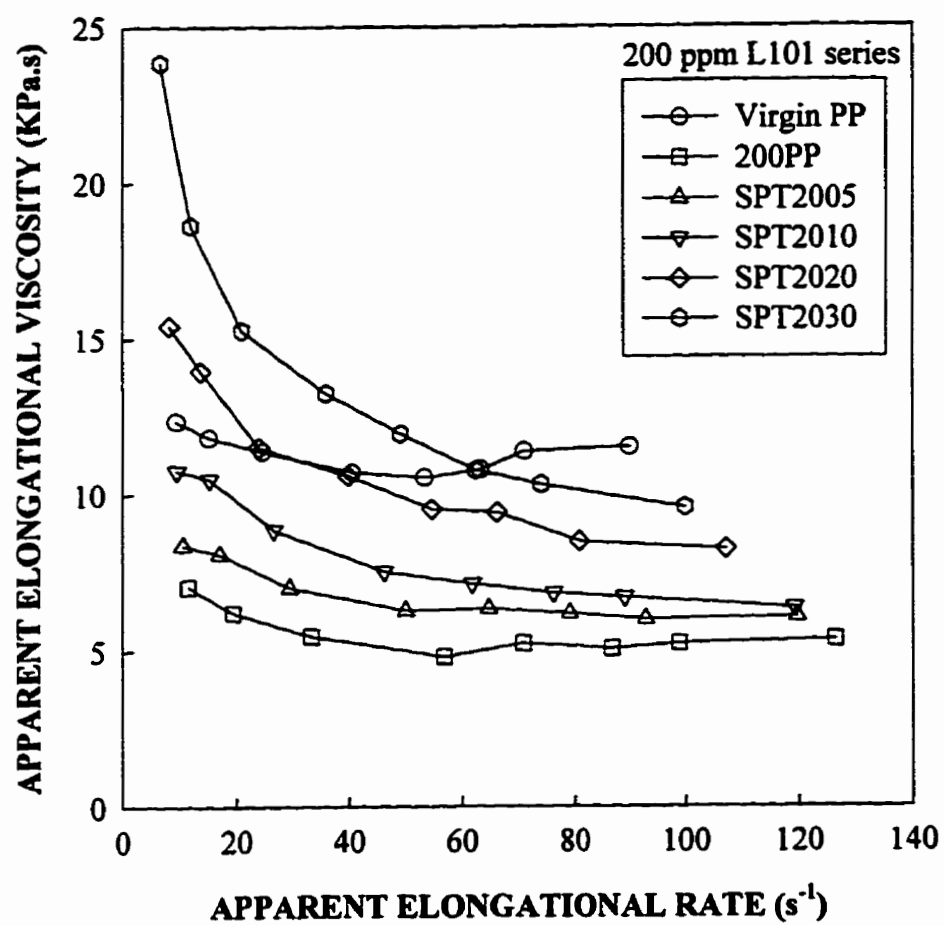


Fig. 6-21 Apparent elongational viscosity of the samples in 200 ppm peroxide series.

Since it has a very low LCB level and a much higher  $\bar{M}_w$  than the other polymers examined, two factors may be responsible for its high  $\eta_e$ : a) its high  $\bar{M}_w$ , and b) the branches are very long although it has a low level of LCB. This may imply that a virgin PP with high molecular weight should be used in reactive extrusion in order to retain a high molecular weight while the branches are being introduced. Meanwhile, the degradation of PP should also be reduced during the reactive extrusion process. These factors may further increase greatly the melt strength of the PETA/peroxide modified PPs.

Fig. 6-18 shows the elongational viscosities of the PETA/peroxide modified samples in the 50 ppm peroxide series. It can be seen that all the PETA/peroxide modified samples show higher  $\eta_e$ s than those of virgin PP and 50PP over the whole elongational rates examined. These modified PPs also seem to have higher tensile resistance than virgin PP even at high elongational rates, i.e., stretch thickening. It is noted that the increase in elongational viscosity does not have a monotonic relationship with respect to the PETA concentration, or with  $\bar{M}_w$  and  $\bar{M}_z$ , while an agreement between the apparent elongational viscosity and the average branches per weight average molecule (or LCB/1000C and branching index) is observed. This leads to the conclusion that the enhancement of elongational viscosity is due to the existence of long chain branching.

Fig. 6-19 shows the results for the samples in the 100 ppm peroxide series. Similarly to the 50 ppm series, all the modified PPs have higher elongational viscosities than those of the virgin PP and 100PP. Some of the samples seem to have melt stretch thickening behaviour at high elongational rates. It is noted that SPT1005, SPT1010, SPT1020 and SPT1030 have similar elongational viscosities, which corresponds to their relatively high average branches per weight average molecule (or LCB/ 1000C and branching index, except for SPT1005).

The results of 50 and 100 ppm series indicate that the apparent elongational viscosity

measurements for whole polymers agree very well with the long chain branching levels evaluated by GPC for sols. This suggests that in our systems, there is no significant difference between the molecular parameters of the whole polymers and their sols and this may be due to the low macrogel amount in these whole polymers. It also implies that the Zimm-Stockmayer relation (Zimm and Stockmayer, 1949) may apply to the current branched/lightly-crosslinked PP (see Chapter 7) systems to a certain quantitative extent.

Figs. 6-20 and 6-21 show the results of 150 and 200 ppm peroxide series. In the 150 ppm peroxide series, all the samples have higher values at low elongational rates. Unlike the samples in 50 and 100 ppm series, most of the samples show elongational thinning behaviours over the elongational rates examined. The sample SPT1530, though it shows higher values at high elongational rates, has no tendency of stretch thickening. In the 200 ppm peroxide series, it can be seen that elongational viscosity increases with increasing PETA concentration, or roughly with the average branches per weight average molecule. Only the sample produced using 3 wt.% PETA (SPT2030) shows higher elongational viscosity within the low elongational rate region. Most of the PETA/peroxide modified samples in this series show lower elongational viscosities than virgin PP and no stretch thickening behaviour is found in this series.

For the samples in 150 and 200 ppm series, the LCB frequencies evaluated by GPC (Chapter 5) suggest that the branches appear mainly in the relatively low molecular weight region, which agrees roughly with their  $\eta_e$  values. It is also noted that many samples in 150 ppm series still show higher  $\eta_e$ s than that of virgin PP, implying that there are some branching in these materials and hence for PETA/peroxide modified PPs, the LCB frequency in the relatively low molecular weight region is not totally fallacious. This also applies to the samples in the 200 ppm series.

It seems that the stretch thickening behaviour might be strongly related to the existence of a significant level of LCB. In the 150 and 200 ppm peroxide series, e.g., no

stretch thickening behaviour is found since generally these polymers have very low LCB levels, or the LCB is relatively short. Instead, stretch thickening is observed in most of the samples of 50 and 100 ppm series since most of these polymers have high LCB levels. The non-monotonic change of the elongational viscosity with respect to PETA and peroxide concentrations indicates that there is an optimum PETA/peroxide relative concentration to enhance the branching reactions. It seems certain that too high peroxide levels will be unfavourable to the enhancement of elongational viscosity. The elongational viscosity measurement seems more sensitive than GPC technique to the low level of branching, as in the cases of 150 and 200 ppm peroxide series.

## 6.2 Viscous Flow Activation Energy

### 6.2.1 Introduction

The concept of the flow activation energy is of fundamental importance in the activation theory of liquid flow. Its experimental determination is of great interest as well the relationship between the activation energy and the structure of polymers. Flow activation energy is determined as the slope of the straight line that represents the dependence of  $\log(\text{viscosity})$  on the inverse of temperature. This Arrhenius-type relationship is as follows:

$$\eta = B \times \exp\left(\frac{E_a}{RT}\right) \quad (6-5)$$

where  $E_a$  is the zero-shear flow activation energy, B is a constant, R is the gas constant, and T is the absolute temperature.

Unlike low-molecular weight compounds, the flow of a polymer chain becomes segmental. It has been proposed (Porter et al., 1968; Vinogradov et al., 1980) that for polymers of sufficiently high molecular weight,  $E_a$  is no longer dependent on molecular weight. It may, thus, be concluded that  $E_a$  of polymers does not depend on their molecular

weight distribution, at least if they do not contain noticeable amounts of low-molecular-weight fractions. The value of  $E_a$  for a polymer is affected by factors that determine the flexibility and interactions of macromolecules, primarily by the microstructure of the chain, the content of polar groups and the regularly or randomly distributed branched chains.

The previous discussion on the temperature dependence of viscosity is concerned with Newtonian viscosity. The apparent viscosity ( $\eta_a$ ) of a polymer is a function not only of temperature but also of the shear rate  $\dot{\gamma}$  or shear stress  $\tau$ . In this case, the temperature dependence of viscosity may be treated by assuming a constant shear rate ( $\dot{\gamma}$ ) or stress ( $\tau$ ) condition. Thus, the quantities of  $E_{\dot{\gamma}}$  (flow activation energy at constant shear rate) and  $E_{\tau}$  (flow activation energy at constant shear stress) may depend on the shear rate or shear stress respectively, at which both are calculated. It has been found that  $E_{\tau}$  is usually larger than  $E_{\dot{\gamma}}$  for polymer melts (Bestul and Belcher, 1953). However, both quantities certainly coincide in the region of Newtonian flow, where the activation energy is independent of the shear stress or shear rate.

The PP flow activation energy for the zero-shear viscosity has been reported to be  $9.56 \pm 0.48$  Kcal/mol (Nielsen, 1977) and 10.52 Kcal/mol (Hingmann et al., 1994). Scheve et al. (1990) have also found that the long chain branched PPs have higher flow activation energies (14.8 and 17.2 kcal/mol) than that of linear PP (13.3 kcal/mol). Although not much literature data were found about the difference between the flow activation energies of linear and branched PPs, there are a lot of data about those of linear and branched polyethylenes, or other polyolefins. Tung (1960) determined zero-shear viscosities at different temperatures and found that the flow activation energy is 7.5 kcal/mol and 14.6 kcal/mol for HDPE and LDPE, respectively. He also used a 1-butene/ethylene copolymer fraction having similar density to that of HDPE and a degree of long chain branching similar to that of LDPE. It was found that the  $E_a$  for this copolymer is the same as that for HDPE. It was, therefore,

concluded that the difference in  $E_a$  between LDPE and HDPE is attributed to the LCB in LDPE rather than short-chain branches. In the work of Schott et al. (1961), the zero-shear activation energies were found to be 11.6-12.7 kcal./mol and 7.0 kcal./mol for LDPE and HDPE, respectively. It was also found that  $E_\tau$  for LDPEs decreases with increasing  $\tau$  whereas  $E_\tau$  for HDPE is almost independent of  $\tau$ . However,  $E_{\dot{\gamma}}$ s for both LDPE and HDPE decrease with increasing shear rate. Sabia (1964) found that for both LDPE and HDPE, a sharp drop in  $E_{\dot{\gamma}}$  with increasing shear rate is observed compared to the zero-shear value. Two significant differences in the melt flow activation energies between HDPE and LDPE were also noticed: first, LDPE has much larger values at fixed shear stress (11.0-13.62 kcal./mol) than HDPE (5.74-8.60 kcal./mol); second,  $E_\tau$ s of LDPE decrease with increasing shear stress, whereas those of HDPE are almost independent of shear stress. The samples of HDPE included ones having ethyl branches whose branching frequency was comparable to that of LDPE. It was, therefore, concluded that the observed differences in the activation energies are attributable to the long branches in LDPE.

Porter et al. (1968) reviewed studies on the flow activation energies of branched polyethylene. It was concluded that the flow activation energies for branched polyethylenes depend on shear stress and all linear polymers exhibit a flow activation independent of stress even well into the shear region for non-Newtonian flow. Short chain branches contribute at most 2 kcal./mol to the activation energy at zero shear and cannot be completely responsible for the large increase in the  $E_a$  of a branched polyethylene compared with that of a linear one. It was proposed that long chain branching may be responsible for this increase.

Combs et al. (1969) studied the rheological properties of polyolefins and found that  $E_\tau$  and melt viscosity increase with increasing the number of short-chain branches (0-10 carbon atoms in side chain). They also found that for PP, the  $E_\tau$  seems to increase as the molecular weight increases (9.9-17.8 kcal/mol) and  $E_{\dot{\gamma}}$  decreases with increasing apparent



shear rate. Raju et al. (1979) showed that the flow activation energy for star-branched hydrogenated polybutadienes is primarily a function of branch length. Romanini et al. (1980) found that contrary to the constant activation energy for linear polyethylene which is close to 6 kcal/mol, long-chain branched LDPE has a higher  $E_a$  and its  $E_a$  in some cases, decreases on increasing the shear stress. Bersted (1985) also noticed that low levels of long chain branching in polyethylene increase both flow activation energy and viscosity at low rates and the flow activation energy increases with the branching level. Laun (1987) has also suggested that long chain branches are responsible for the high flow activation energy of LDPE compared to HDPE, and that a growing number of the branches increases the flow activation energy. This conclusion was drawn based on the following flow activation energy values: 7 kcal/mol for HDPE, 7.9 kcal/mol for LLDPE, 12.9 kcal/mol for a long chain branched LDPE melt with 15  $\text{CH}_3$ -end groups per 1000 C-atoms, 14.3 kcal/mol for the one with 30  $\text{CH}_3$ -end groups per 1000 C-atoms.

In summary, it has been well agreed by many researchers that long chain branches, even at very low levels, will always increase the viscous flow activation energy (both  $E_a$  and  $E_v$ ). With increasing shear rate,  $E_v$ 's for both linear and branched polymers are decreased while with increasing shear stress,  $E_a$ 's for long chain branched polymers seem to be decreased whereas those for linear polymers seem to be independent of shear stress.

### 6.2.2 Experimental

The steady-state shear viscosities were determined for most of the modified whole polymers at 190, 200, 210, 220, 230°C by means of a Kayeness Galaxy V capillary rheometer using a manual operating mode. A die with inlet angle of 90°,  $L/D=40$  and  $D=0.03$ " was used. By applying the Arrhenius equation (6-5) to the flow curves, flow activation energies were obtained either at constant apparent shear rate or at constant apparent shear stress.

### 6.2.3 Results and Discussion

Table 6.2 shows the flow activation energies of the samples at a constant apparent shear rate of  $50 \text{ s}^{-1}$ . It can be seen that all the samples, either high or low molecular weight, linear or branched, exhibit similar and low flow activation energies at a constant shear rate ( $E_{\dot{\gamma}}$ ). Some of the degraded PPs such as 1000PP show a slightly higher  $E_{\dot{\gamma}}$ s than other samples. Obviously this is contrary to our understanding of their molecular structures. One reason for this is that these different polymers evaluated at the same apparent shear rate (Rabinowitch correction was applied), are actually subjected to different shear stresses. Another reason may be that the  $E_{\dot{\gamma}}$  of PP is small and this can be seen from our results.

Figs. 6-22 to 6-25 show typical plots between the shear viscosity and the inverse of temperature for virgin PP, Montell PP and some modified samples evaluated at constant shear stresses. Table 6.3 summarizes the flow activation energies at constant shear stresses ( $E_{\tau}$ ) for the polymers examined. The experimental error of flow activation energy is about  $\pm 0.5 \text{ Kcal/mol}$ . The flow activation energies at a shear stress of 40 KPa are plotted versus the estimated long chain branches per weight average molecule (Fig. 6-26).

It can be seen that for linear PPs,  $E_{\tau}$  remains relatively constant up to the  $\bar{M}_w$  of 154,300 (600PP) and  $E_{\tau}$  seems to decrease with increasing shear stress. After certain molecular weight,  $E_{\tau}$  seems to decrease with decreasing molecular weight. This agrees with the results of Combs et al. (1969) and is also consistent with the proposition that for polymers of sufficiently high molecular weight  $E_{\tau}$  is no longer dependent on molecular weight (Porter et al., 1968; Vinogradov et al., 1980). It can be seen that Montell PP has much higher  $E_{\tau}$ s than any other PPs over the shear stresses examined. The explanation so far is that this may be due to the existence of LCB in Montell PP since the molecular weight dependence of  $E_{\tau}$  is not known up to the very high molecular weight.

Generally, the PETA/peroxide modified polymers show higher  $E_{\tau}$ s than linear PPs

**TABLE 6.2** Flow Activation Energy at a Constant Apparent Shear Rate ( $50 \text{ s}^{-1}$ )

Sample	$E_{\dot{\gamma}}$ (Kcal/mol)
PP	4.24
50PP	4.28
100PP	4.21
150PP	4.55
200PP	5.11
400PP	5.73
600PP	6.08
800PP	6.04
1000PP	6.95
Montell PP	4.03
SPT505	4.52
SPT510	4.28
SPT520	3.39
SPT530	3.66
SPT1005	4.62
SPT1010	4.20
SPT1020	4.07
SPT1030	3.62
SPT2005	4.98
SPT2010	4.96
SPT2020	4.51
SPT2030	4.17

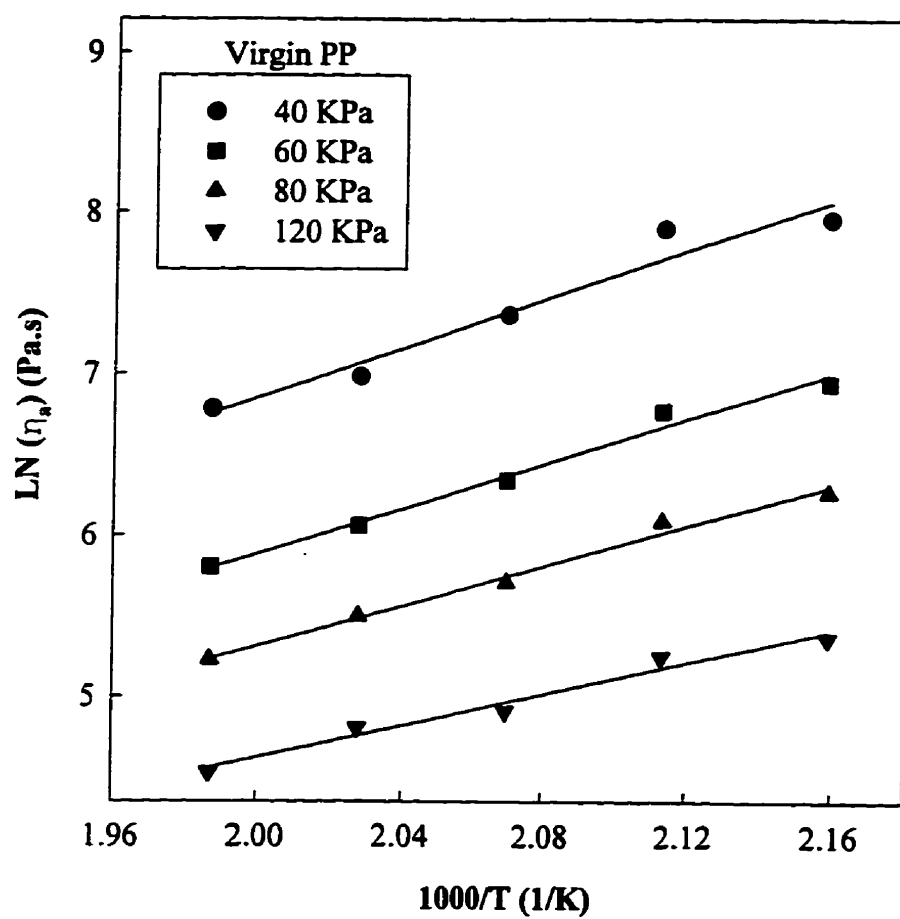


Fig. 6-22 Relationship between the  $\eta$  and  $1/T$  of virgin PP at different shear stresses.

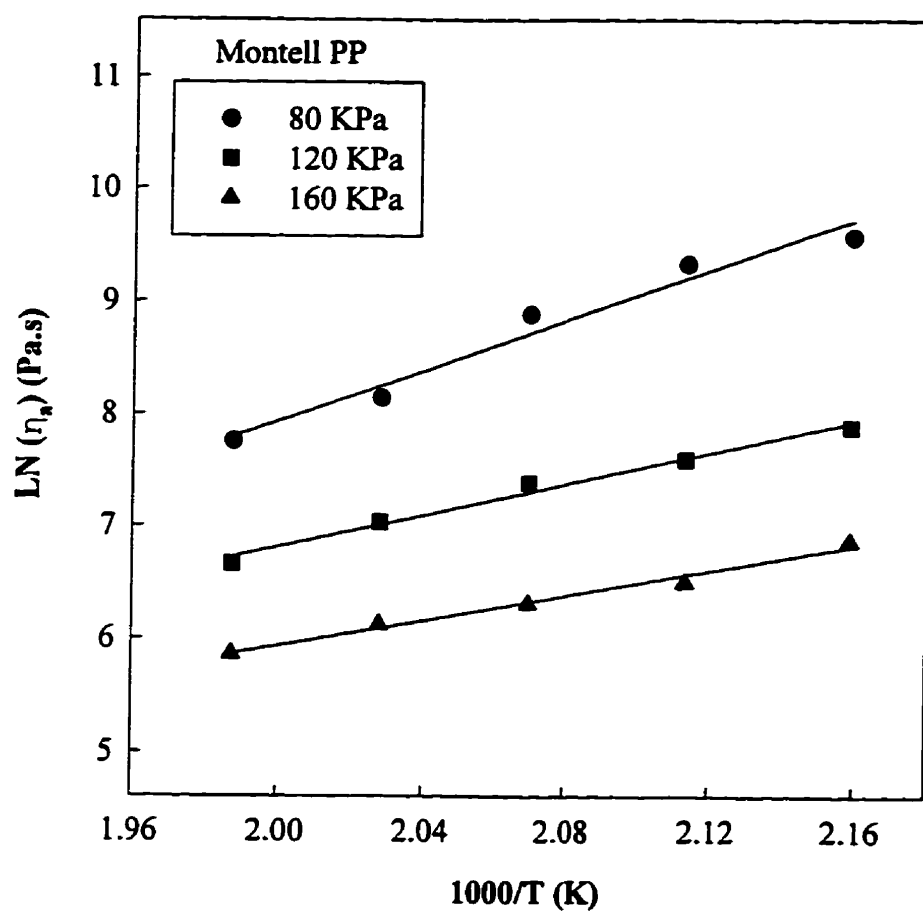


Fig. 6-23 Relationship between the  $\eta$  and  $1/T$  of Montell PP at different shear stresses.

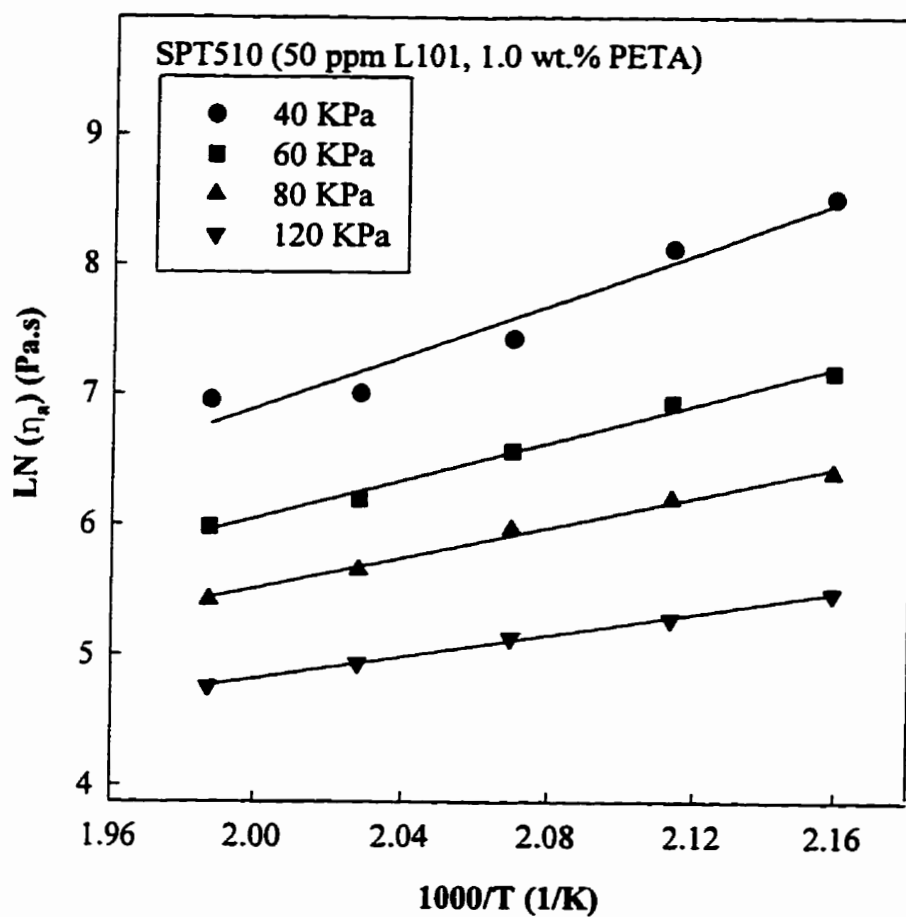


Fig. 6-24 Relationship between the  $\eta$  and  $1/T$  of SPT510 at different shear stresses.

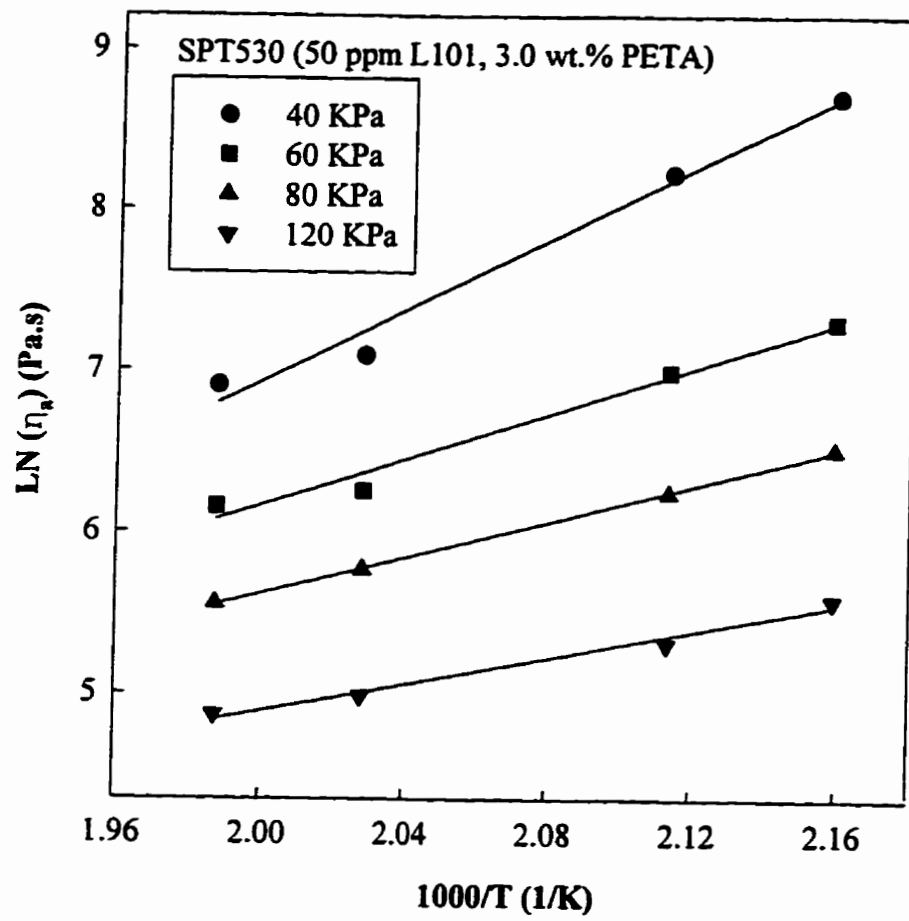


Fig. 6-25 Relationship between the  $\eta$  and  $1/T$  of SPT530 at different shear stresses.

**TABLE 6.3 Flow Activation Energy (Kcal/mol) at Constant Apparent Shear Stresses**

Sample	40 (KPa)	60 (KPa)	80 (KPa)	120 (KPa)
Virgin PP	15.11	13.88	12.40	9.81
50PP	--	13.90	11.67	9.16
100PP	--	12.06	11.25	9.74
200PP	15.22	12.89	11.52	9.89
400PP	15.49	12.24	10.54	8.77
600PP	14.06	11.42	9.76	7.56
800PP	12.28	10.19	9.01	7.83
1000PP	12.53	--	8.66	7.25
Montell PP*	--	--	22.26	13.97
SPT505	19.56	14.43	11.61	8.75
SPT510	19.68	14.43	11.56	8.25
SPT520	16.72	13.29	11.00	7.87
SPT530	19.67	14.06	11.10	8.21
SPT1005	16.24	13.37	11.71	9.73
SPT1010	16.51	13.48	11.66	9.45
SPT1020	--	13.37	13.73	10.76
SPT1030	17.97	12.18	11.03	8.91
SPT2005	14.72	12.12	10.77	9.31
SPT2010	17.73	12.22	10.14	8.89
SPT2020	18.43	12.74	10.63	9.39
SPT2030	16.17	13.72	10.93	9.39

\* The  $E_a$  of Montell PP at the  $\tau_a$  of 160 (KPa) is 11.07 (Kcal/mol)



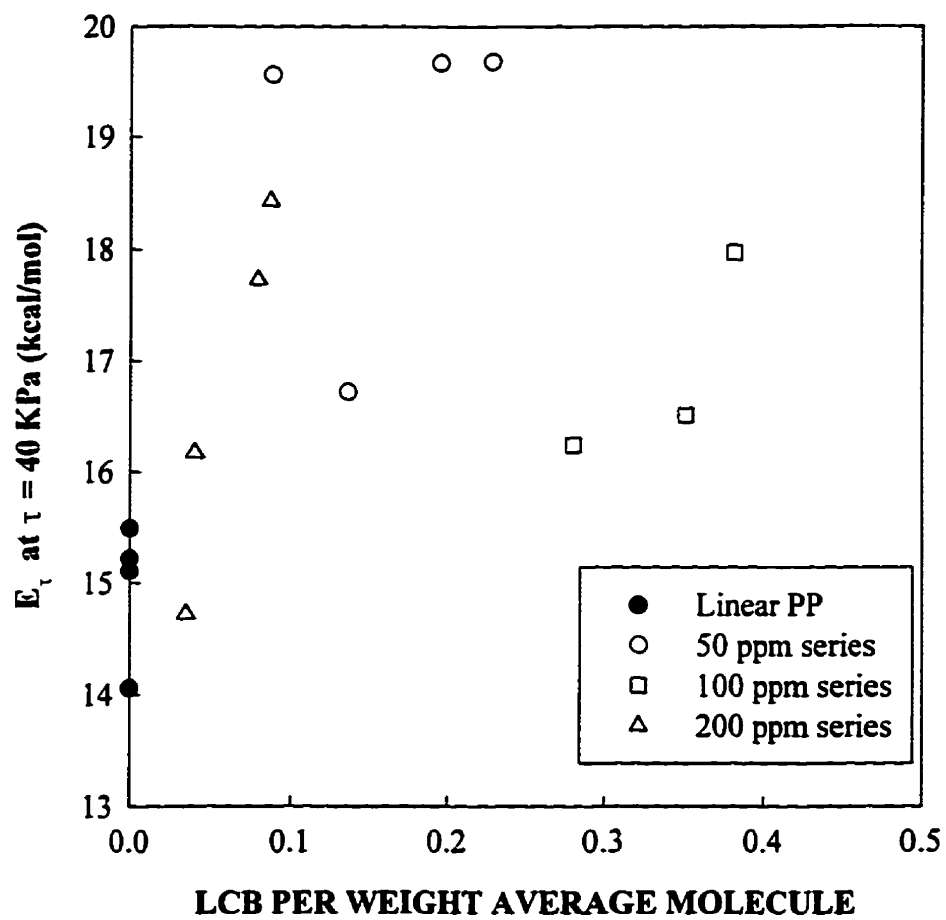


Fig. 6-26 Relationship between the  $E_{\tau}$  (at 40 KPa) and the long chain branches per weight average molecule.

at low shear stress. Similar to linear PPs, the  $E_{\tau}$  of branched PPs also decreases with increasing shear stress and hence there is no significant difference between them at high shear stress. This suggests that  $E_{\tau}$  of linear and branched PP differs significantly only within the region which is close to or at the terminal region.

In Fig. 6-26, roughly the flow activation energy increases with the LCB level and this increase in  $E_{\tau}$  is attributed to the existence of long chain branching.

### 6.3 Conclusions

The apparent elongational viscosity of linear PP can be enhanced greatly by reactive extrusion using PETA and peroxide. The samples in 50 and 100 ppm peroxide series show the highest increase and most of them exhibit stretch thickening behaviour. For these long chain branched PPs, the apparent elongational viscosity measurements are in good agreement with the LCB levels estimated by GPC. This suggests that in our systems, there is no significant difference between the molecular parameters of the whole polymers and their sols. It seems that the Zimm-Stockmayer relation may apply to the current branched/lightly-crosslinked PP systems to a certain quantitative extent.

The flow activation energy at constant shear stress of linear and branched PP is dependent on the shear stress and both decrease with increasing shear stress. The  $E_{\tau}$  of linear PP shows a molecular weight dependence up to a certain value. Montell PP shows a much higher  $E_{\tau}$  than other PPs. The PETA/peroxide modified PPs produced by current reactive extrusion show higher  $E_{\tau}$ s than linear PPs at the low shear stress, which is attributed to the long chain branching.

## CHAPTER 7

### THERMAL PROPERTIES OF THE SOLS

#### 7.1 Simultaneous Thermogravimetric Analysis (TGA) and Differential Thermal Analysis (DTA)

##### 7.1.1 Introduction

Many types of degradation processes are known (Reich et al., 1971) such as: a) thermal degradation, b) oxidative degradation, c) mechanical degradation, d) radiation degradation, e) chemical degradation, and f) biological degradation. In the degradation of polyolefins, structure, morphology, presence of stabilizers, and type of environment are the most relevant factors. It should be pointed out that morphology can have an effect only if the polymer remains crystalline at very high temperatures. Practically, this is not the case for polypropylene or polyethylene. The prime agent affecting deterioration of olefin polymers is oxidative degradation. However, a complete elucidation of the oxidation reactions occurring in polymer systems requires a rather complete knowledge of the mechanisms by which specific reactions take place and often this information is difficult to obtain.

Thermal degradation of polyolefins occurs at elevated temperatures in the absence of oxygen, i.e., in vacuum or inert gases. The structure of a polymer affects greatly its resistance to thermal degradation. For example, polypropylene is less resistant to thermal degradation than linear polyethylene due to the presence of reactive tertiary carbon atoms. Similarly, the thermal decomposition rate of branched polyethylene is higher than that of linear polyethylene again due to the presence of tertiary carbon atoms at chain branches. The greater the branching, the greater the rate of decomposition. The effect appears to be relatively independent of molecular weight, and it has been concluded that the number and length of branches are more critical for establishing decomposition patterns than size of the

molecule (Conley, 1970). Thermal degradation can be roughly divided into two general categories, i.e., random chain scission and depolymerization. Depending on its structure, a polymer may decompose preferentially at reactive sites along the polymer chain, i.e., via depolymerization (such as polystyrene, polyisobutylene) or it may assume a random breakdown process (such as all aliphatic olefin polymers except for polyisobutylene). Little monomer is formed during thermal degradation of all other aliphatic olefin polymers.

The thermal degradation of PP may be described by: a) the thermal random dissociation of a covalent bond into two macroradicals preferentially at the tertiary carbon atoms, which can be considered as a random chain scission initiation, b) the disproportionation of the macroradicals and the intermolecular/intramolecular transfers preferentially to the tertiary hydrogen atoms, and c) termination through the recombination of two macroradicals. In our PETA/peroxide modified polymers, the recombinations result in the elimination of some of the tertiary hydrogen atoms on PP backbone and the formation of lightly crosslinked (intermolecular/intramolecular) structures. The changes in molecular structures should be reflected in the resistance to thermal degradation of the modified PPs.

### **7.1.2 Experimental**

Thermogravimetric experiments were carried out using a SDT 2960 Simultaneous DTA-TGA (TA Instruments) at a heating rate of 20°C with a helium flow rate of 120 cc/min. Experiments were carried out from 40°C to 700°C. The reference material was Al<sub>2</sub>O<sub>3</sub> and the sample weights were from 5 to 6 mg. The purified sols of the samples produced in Chapter 4 (including Montell branched PP) were used and no stabilizer was added.

### **7.1.3 Results and Discussion**

Decomposition temperature data for the modified PPs from both TGA and DTA are summarized in Table 7.1. The TGA curves for the virgin PP, the degraded PPs and Montell

**TABLE 7.1 Decomposition Temperatures of the Modified PPs**

Sample	Material Description	T <sub>d</sub> (°C) from TGA	T <sub>d</sub> (°C) from DTA
Virgin PP	---	430.45	432.45
50PP	50 ppm L101	432.33	430.99
100PP	100 ppm L101	432.57	430.57
150PP	150 ppm L101	437.53	432.86
200PP	200 ppm L101	435.58	433.58
400PP	400 ppm L101	436.70	434.69
Montell PP	---	437.44	434.76
SPT505	50 ppm L101, 0.5 wt.% PETA	437.02	435.02
SPT510	50 ppm L101, 1.0 wt.% PETA	431.48	430.81
SPT520	50 ppm L101, 2.0 wt.% PETA	435.69	435.02
SPT530	50 ppm L101, 3.0 wt.% PETA	436.62	434.61
SPT1005	100 ppm L101, 0.5 wt.% PETA	436.21	434.21
SPT1010	100 ppm L101, 1.0 wt.% PETA	435.82	433.15
SPT1020	100 ppm L101, 2.0 wt.% PETA	435.80	432.46
SPT1030	100 ppm L101, 3.0 wt.% PETA	437.78	435.78
SPT1505	150 ppm L101, 0.5 wt.% PETA	435.15	432.48
SPT1510	150 ppm L101, 1.0 wt.% PETA	436.17	433.50
SPT1520	150 ppm L101, 2.0 wt.% PETA	435.07	431.06
SPT1530	150 ppm L101, 3.0 wt.% PETA	436.53	433.65
SPT2005	200 ppm L101, 0.5 wt.% PETA	437.02	433.68
SPT2010	200 ppm L101, 1.0 wt.% PETA	440.39	438.38
SPT2020	200 ppm L101, 2.0 wt.% PETA	435.39	434.05
SPT2030	200 ppm L101, 3.0 wt.% PETA	437.43	436.10

branched PP are shown in Fig. 7-1. Except for the  $T_m$  (melting temperature) and  $T_d$ , nothing new was found in the DTA curves and hence they are not shown here. The decomposition temperatures obtained are reasonable since it has been found that PP undergoes extensive thermal degradation between 400 to 455°C in vacuum (Reich et al., 1971). The temperature range of TGA curves also seem consistent with this observation. In Fig. 7-1, it can be seen that generally with decreasing molecular weight of linear PPs (shorter chains), the rate of thermal decomposition or thermal decomposition temperature decreases. However, molecular weight shows no significant effect after the chain length has been shortened to some extent. The above behaviour may be due to the higher probability of decomposition for longer PP chains. It is interesting to note that the Montell branched PP has the highest resistance to thermal decomposition among the samples shown in Fig. 7-1. This behaviour may be due to the limited diffusion or mobility of the radicals or products caused by the high local melt viscosity (Jellinek, 1978), due to the much higher molecular weight of Montell PP.

The TGA curves of the sols of the PETA/peroxide modified samples are shown in Figs. 7-2 to 7-5. It seems that the thermal stabilities of these samples are all higher than that of virgin PP or similar to those of the peroxide degraded PPs. It can also be seen that generally the thermal stability increases with increasing PETA concentration. It is also noted that the sample SPT510, which has the highest LCB level among the 50 ppm series, shows a minimum  $T_d$  in this series (see Table 7-1 and Fig. 7-2). This result seems consistent with observations on linear and branched polyethylenes (Conley, 1970).

Reactive modification of PP with PETA/peroxide may result in two structural changes: a) the removal of tertiary hydrogen atoms and this might reduce the chance of intermolecular/intramolecular transfers; however, this effect may be little since the number of the tertiary hydrogen atoms removed could be small, b) the crosslinking of PP chains and this may have two effects to thermal stability of polymers. On one hand, the introduction of branches will form quaternary carbon atoms which are thermally less stable than tertiary ones

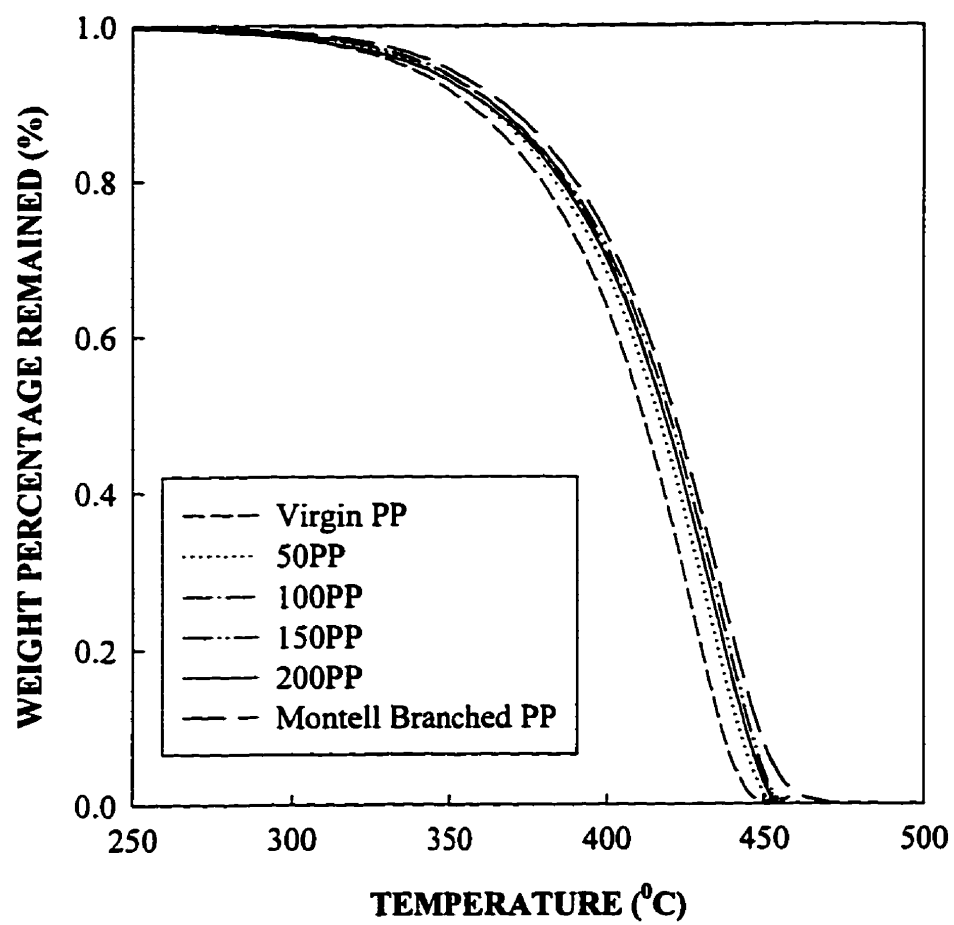


Fig. 7-1 Thermogravimetric analyses of virgin PP, peroxide-degraded PPs and Montell Branched PP.

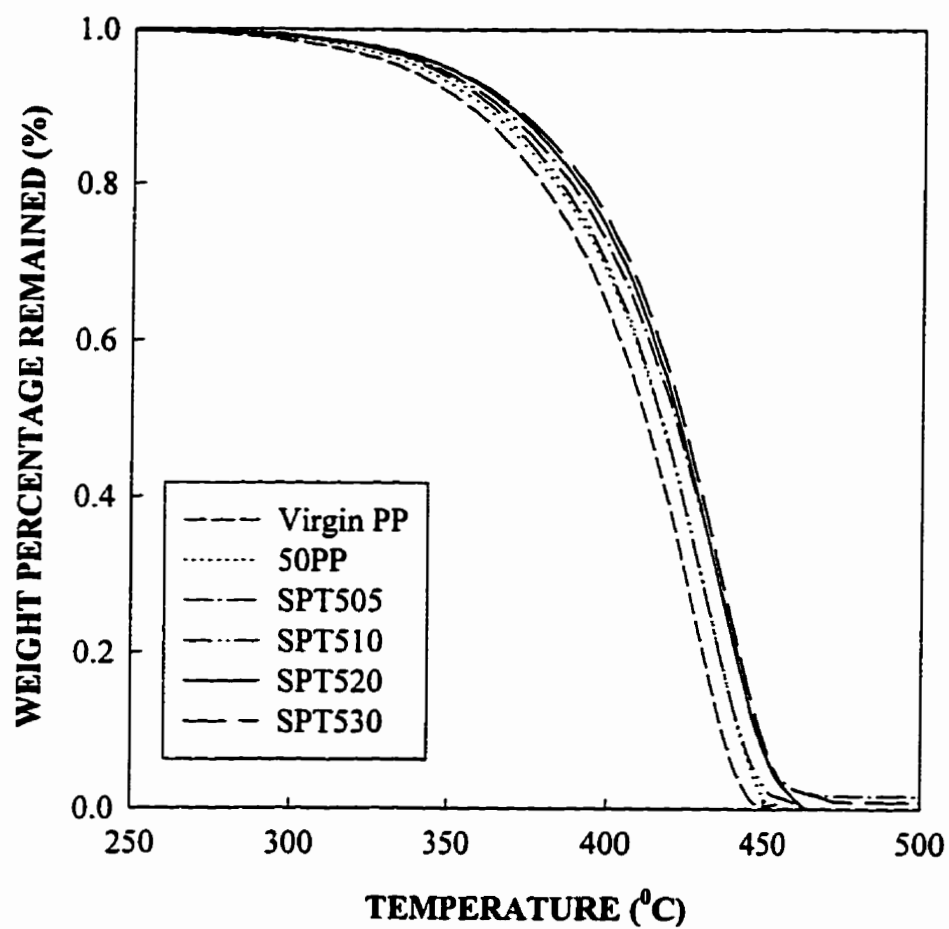


Fig. 7-2 Thermogravimetric analyses of the sols from PETA/peroxide modified PPs (50 ppm L101 series).



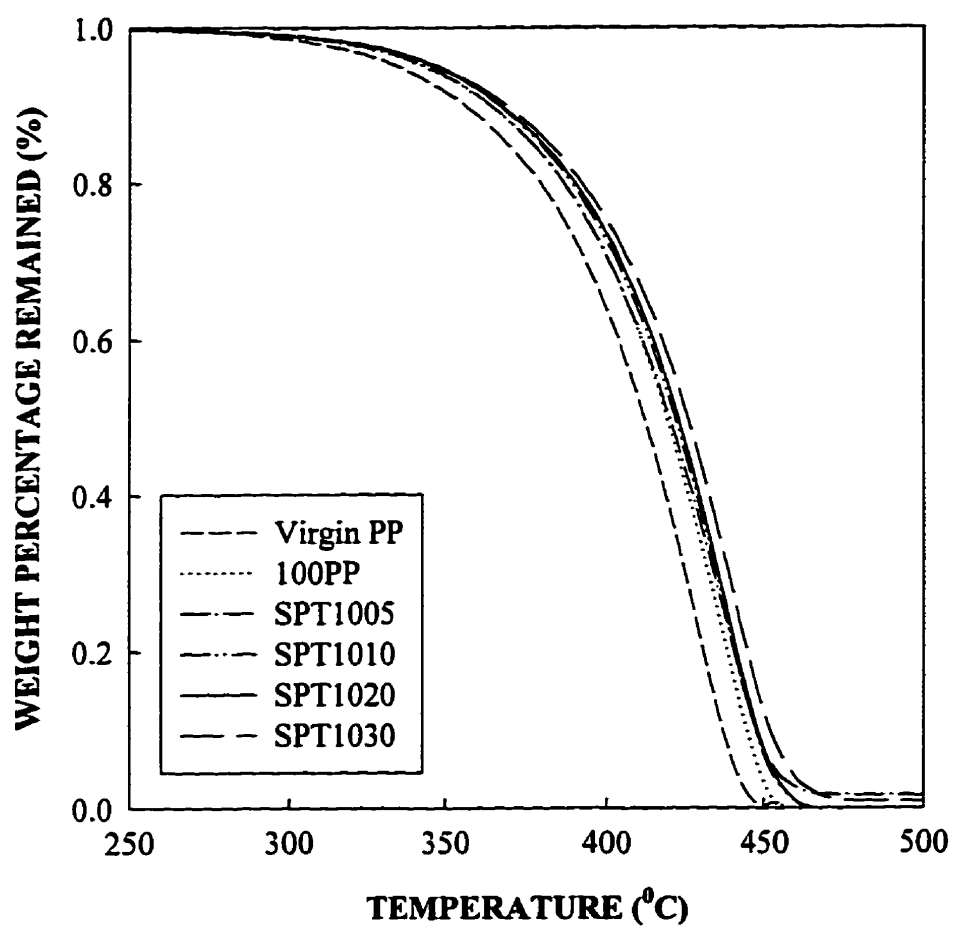


Fig. 7-3 Thermogravimetric analyses of the sols from PETA/peroxide modified PPs (100 ppm L101 series).

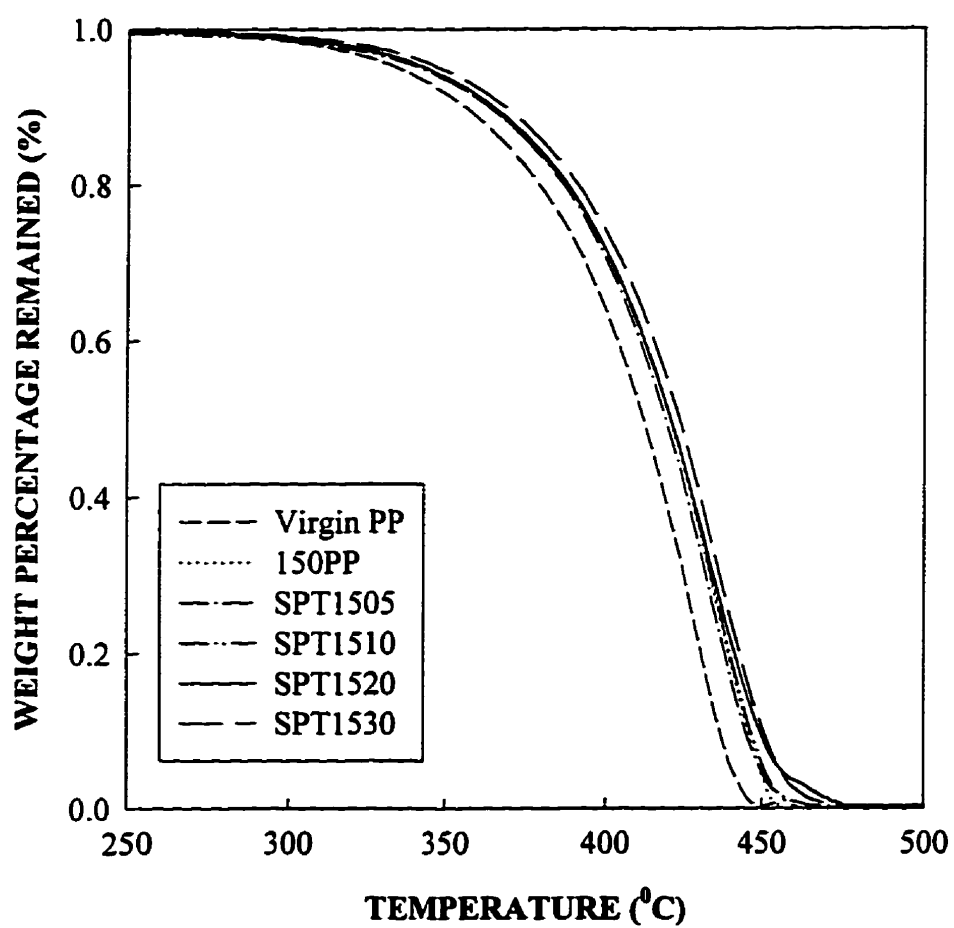


Fig. 7-4 Thermogravimetric analyses of the sols from PETA/peroxide modified PPs (150 ppm L101 series).

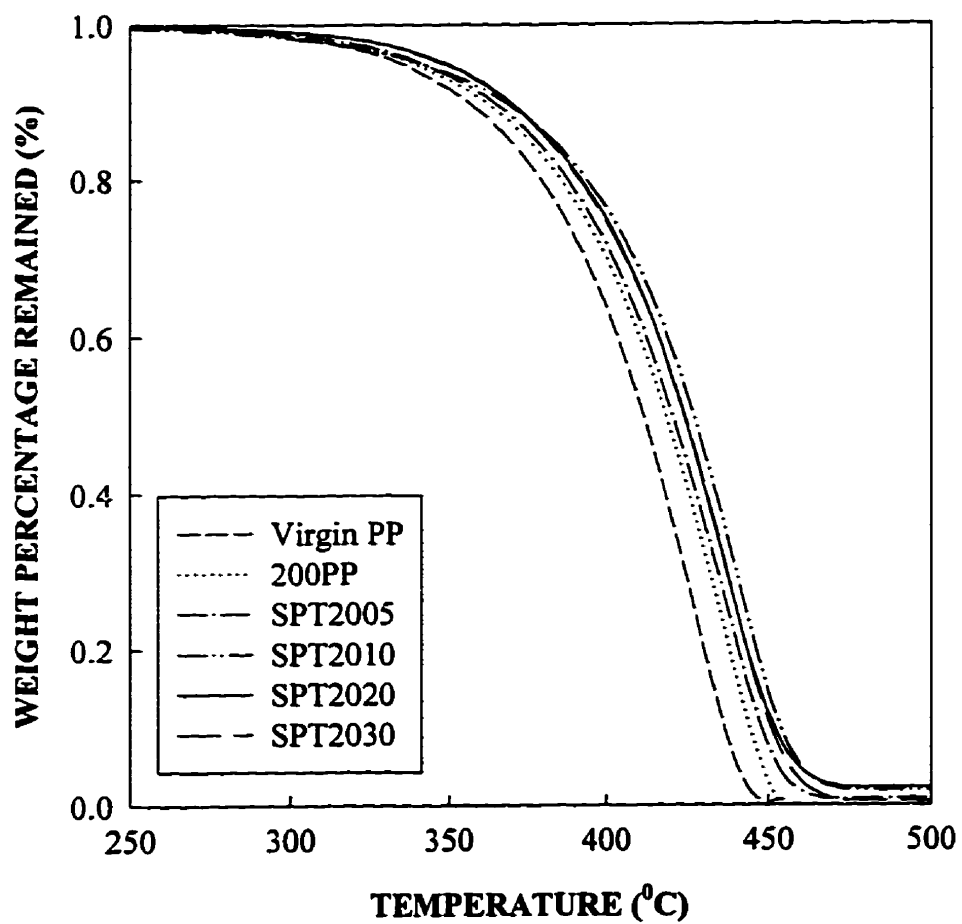


Fig. 7-5 Thermogravimetric analyses of the sols from PETA/peroxide modified PPs (200 ppm L101 series).

and may lower the thermal stability of a polymer. It has been found that in some cases, even the crosslinking will lower the thermal stability of polymers because of the presence of weaker structures such as tertiary or quaternary carbon atoms absent in non-crosslinking polymers (Igarashi et al., 1964). On the other hand, crosslinking will reduce the mobility of chain segments and it is believed that this is the main reason for the increase in thermal stability of the PETA/peroxide modified PPs. Of course, the C-C bond dissociation itself (dissociation energy = 288.9 kJ/mol for C-C bond in PP; Allen, 1983) is not affected much by this hindrance of chain segment movement. However, when the free movement of two macroradicals formed by bond dissociation is hindered due to chemical bond formation, the chance for their immediate recombination may appreciably increase and the effective rate of macroradical production decreases. A decrease in the apparent rate of scission may be expected for crosslinked polymers.

Therefore, besides the branched structures suggested by GPC-viscometry, apparent elongational viscosity and flow activation energy, TGA results further imply that PETA/peroxide modified PPs also have intermolecular and/or intramolecular crosslinked molecular structures, which differ from those of some branched polymers such as commercial low density polyethylenes.

The decomposition temperatures ( $T_d$ ) from both TGA and DTA are plotted versus the long chain branches per weight average molecule for PETA/peroxide modified PPs (Figs. 7-6 and 7-7). Although the  $T_d$  seems to decrease with LCB level in the 50 ppm series (Figs. 7-6 and 7-7) and probably in the 100 ppm series (Fig. 7-7), overall, there is no clear relationship between the decomposition temperatures and the LCB per weight average molecule for the four peroxide series. This is not surprising since thermal stabilities are affected by both branching level and crosslinks. However, the information evaluated by GPC-viscometry only reflects the LCB levels. This situation also applies to the correlations of LCB per weight average molecule with  $T_m$ ,  $T_c$  and  $(T_m - T_c)$  in the next section.

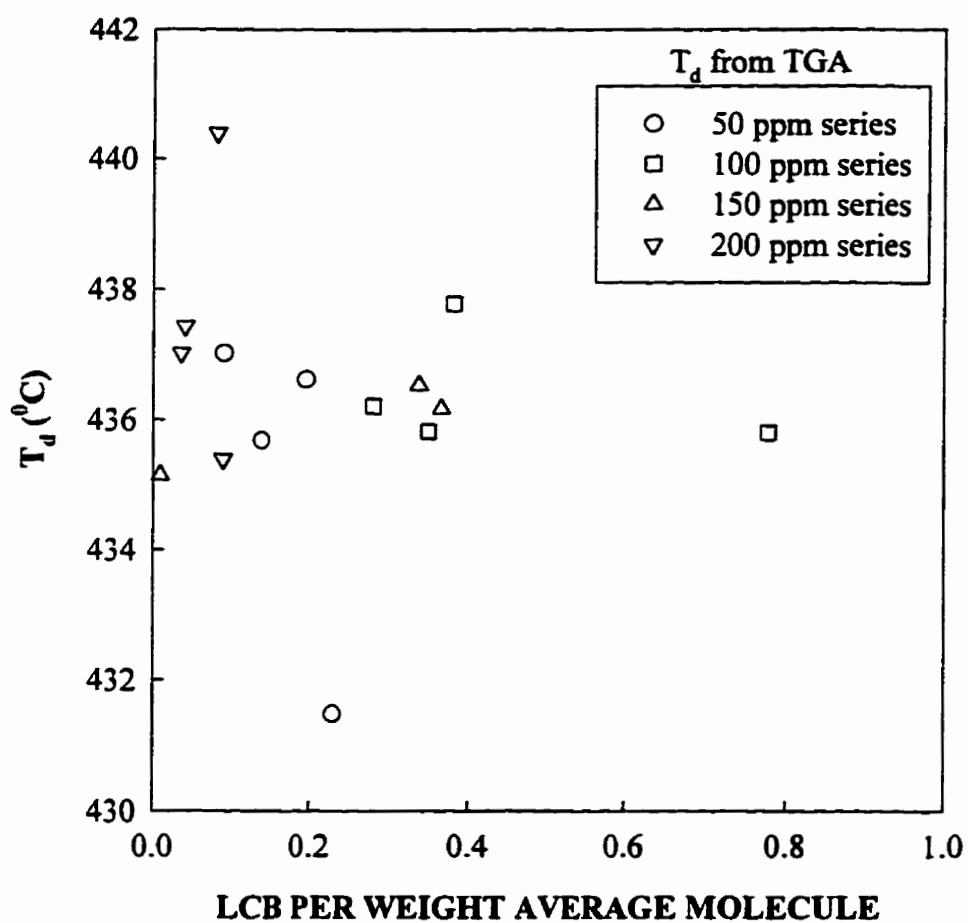


Fig. 7-6 Plot of the decomposition temperature ( $T_d$ ) from TGA versus LCB per weight average molecule for PETA/peroxide modified PPs.

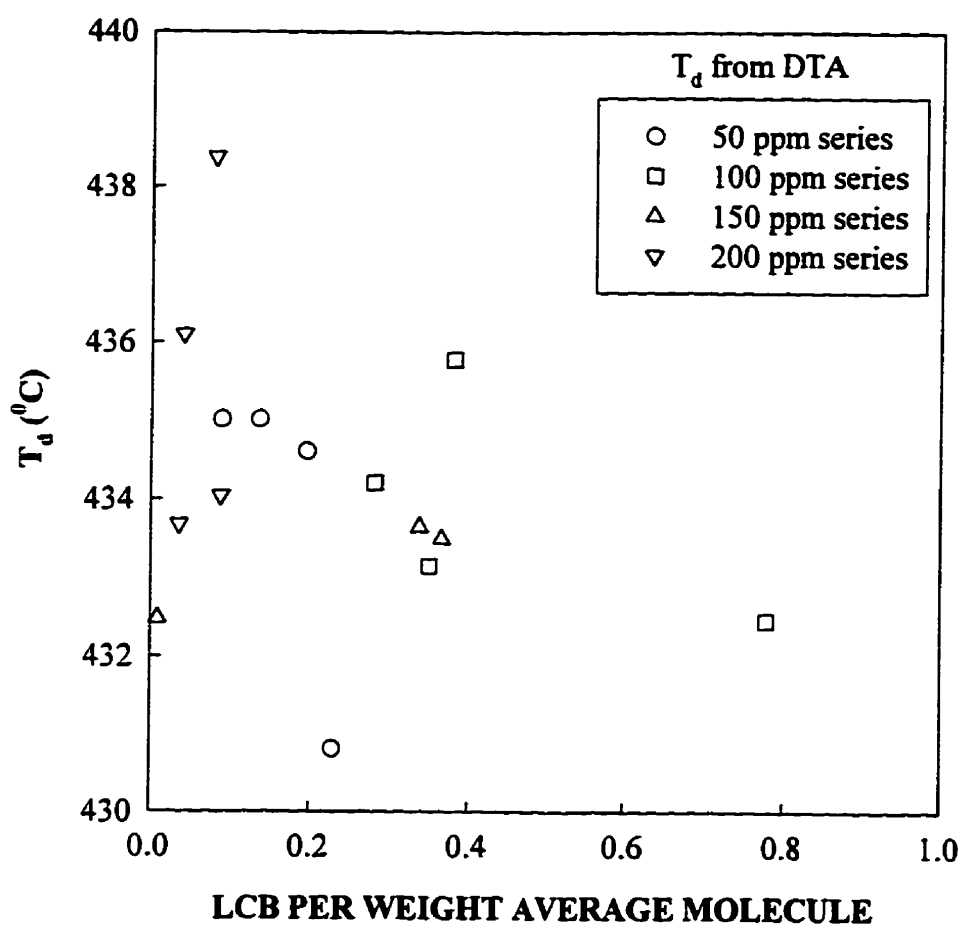


Fig. 7-7 Plot of the decomposition temperature ( $T_d$ ) from DTA versus LCB per weight average molecule for PETA/peroxide modified PPs.

## **7.2 Differential Scanning Calorimetry (DSC)**

### **7.2.1 Introduction**

In the PETA/peroxide modified system, degradation, recombination and grafting reactions may take place simultaneously. These reactions will result in the changes of the following molecular factors: (a) molecular weight and its distribution, (b) chain irregularity due to branching/crosslinking, grafting of PETA and/or binding of peroxide radicals to the polymer chain. These microstructural differences will affect the crystallization behaviour of the sols of the modified PPs. Generally, for a given polymer and at a given crystallization temperature, the degree of crystallinity depends on the molecular weight and the structural regularity of the chain (Mark et al., 1993). For homopolymers, at higher molecular weight and hence melt viscosity, the ease of crystallization decreases and thus the final extent of crystallization is reduced. Thus, the level of crystallinity is relatively high at the lower molecular weights and then decreases monotonically with increasing molecular weights until a limiting value is reached. The crystallinity level is further reduced by the introduction of noncrystallizing structural units into the chains such as branching. Meanwhile,  $T_m$  decreases due to the introduction of chain defects (chain ends, crosslinks, branching points and non-isotactic sequences) which would act as a second component in the system.

### **7.2.2 Experimental**

Thermal analyses of the purified sols prepared in Chapter 4 were carried out on a TA Instruments thermoanalyzer equipped with a 2920 differential scanning calorimetric (DSC) cell under a helium environment. The DSC was calibrated with indium as a standard and no stabilizer was added to the samples measured. Specimens were scanned from  $-60^{\circ}\text{C}$  to  $200^{\circ}\text{C}$ , held at  $200^{\circ}\text{C}$  for three minutes, and then cooled to  $40^{\circ}\text{C}$ . The heating and cooling rates were  $20^{\circ}\text{C}/\text{min}$  and the same sample weight ( $4.12 \pm 0.02$  mg) was used throughout the DSC experiments. For all the experiments, the first heating/cooling cycle was used to condition

the samples and hence only the data of the second cycle are reported here. The information obtained consists of (a) the heat of fusion ( $\Delta H_m$ ), (b) the melting temperature ( $T_m$ ), (c) the crystallization temperature ( $T_c$ ), (d) the crystallization enthalpy ( $\Delta H_c$ ), and (e) the degree of undercooling ( $T_m - T_c$ ).

### 7.2.3 Results and Discussion

The fusion and crystallization curves are shown in Figs. 7-8 to 7-17 for the sols of the modified PPs (peroxide degraded and PETA/peroxide modified) and Montell PP, and data are summarized in Table 7.2.

Figs. 7-8 and 7-9 present the melting and crystallization curves for linear PPs (virgin PP, some of peroxide degraded PPs) and Montell branched PP. For the sake of clarity, the samples of 400PP and 600PP are not included. It can be seen that virgin PP shows a doublet melting endotherm and this has been attributed to the possible coexistence of the  $\alpha$  and  $\beta$  form crystals or due to the proceeded perfection of crystal structures by recrystallization (Chapter 4). The variation in  $T_m$  and  $T_c$  are about  $0.20^\circ\text{C}$  and  $0.55^\circ\text{C}$  respectively on the repeated DSC measurement of virgin PP and it is assumed that this experimental error is valid to other samples examined. Due to the difficulties in baseline estimation, the variation in fusion enthalpy can be up to 10%. It can be seen that the  $T_m$  is initially increased with decreasing molecular weight and then becomes relatively constant. This suggests that for linear PPs,  $T_m$  is not strongly dependent on the molecular weight (MW) after MW is decreased to some extent. With decreasing MW, generally  $T_c$  is increased and there is a decrease in the degree of undercooling ( $T_m - T_c$ ). Montell branched PP shows a similar  $T_m$  to that of virgin PP but lower than those of the degraded PPs. However, its  $T_c$  is much higher than those of the linear materials and the degree of undercooling is much lower.

The fusion and crystallization curves of the PETA/peroxide modified samples are shown in Figs. 7-10 to 7-17. In the 50 ppm peroxide series, it can be seen that with increasing



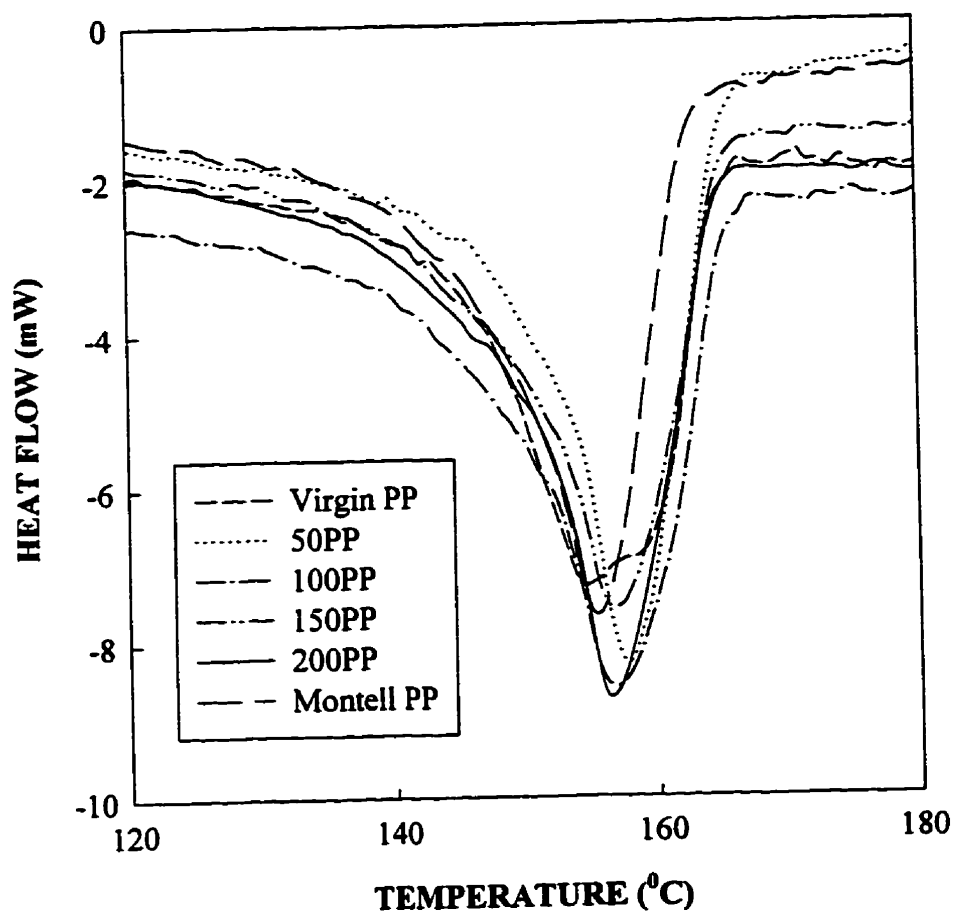


Fig. 7-8 Melting endotherms of linear PPs and Montell branched PP.

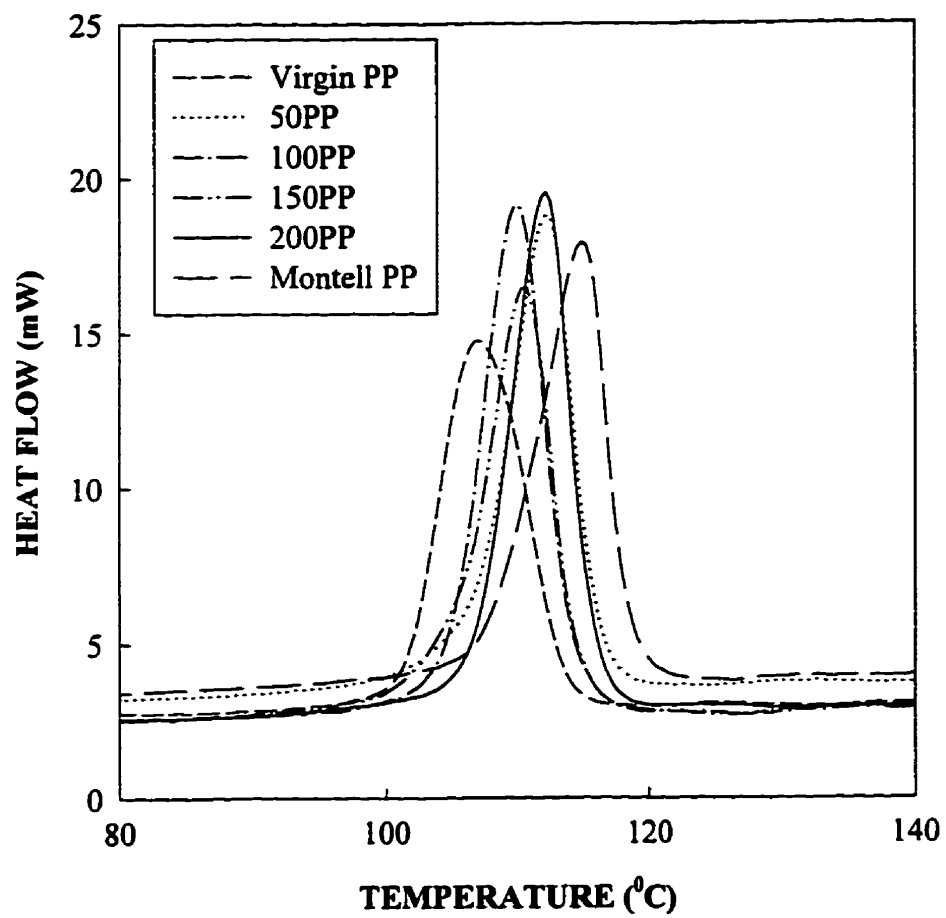


Fig. 7-9 Crystallization exotherms of linear PPs and Montell branched PP.

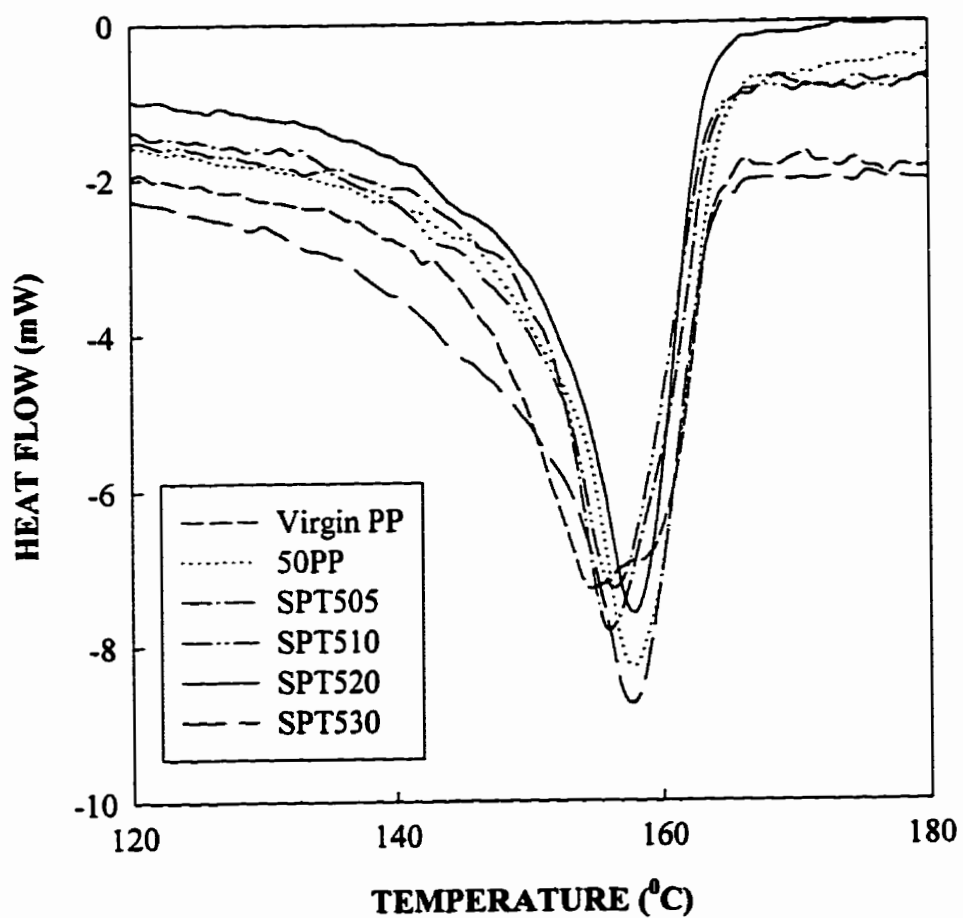


Fig. 7-10 Melting endotherms of the sols of PETA/peroxide modified PPs (50 ppm L101 series).

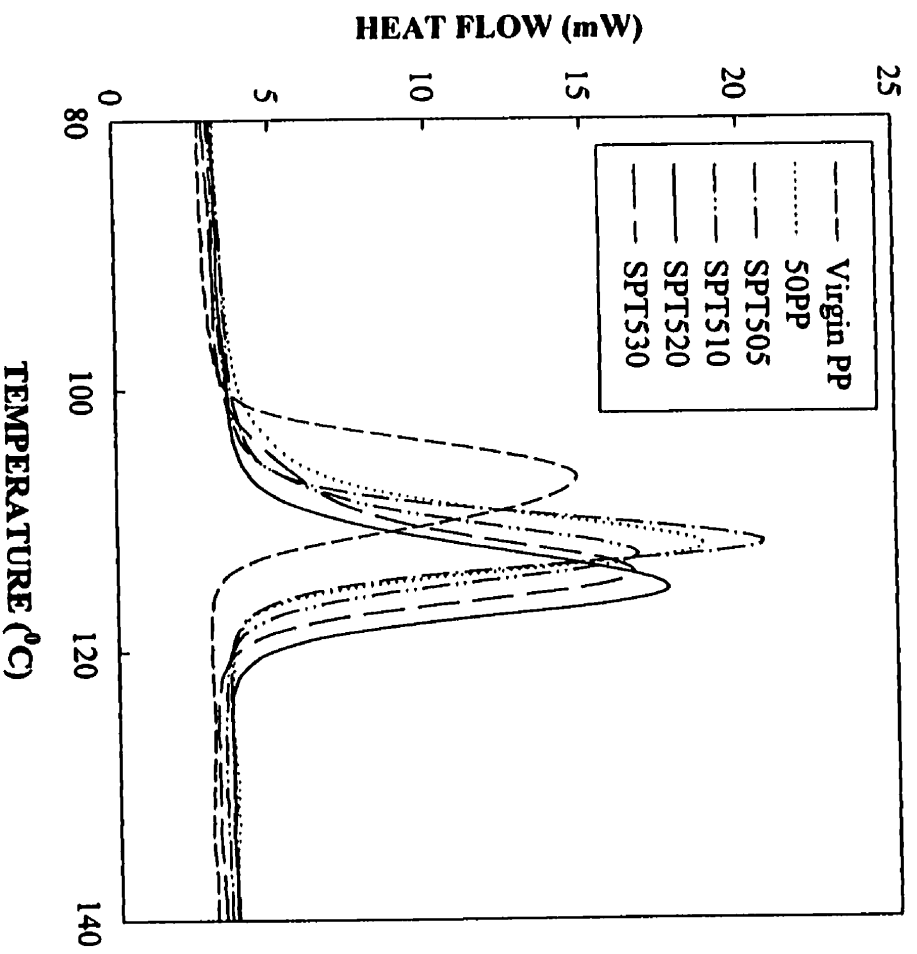


Fig. 7-11 Crystallization exotherms of the sols of PETA/peroxide modified PPs (50 ppm L101 series).

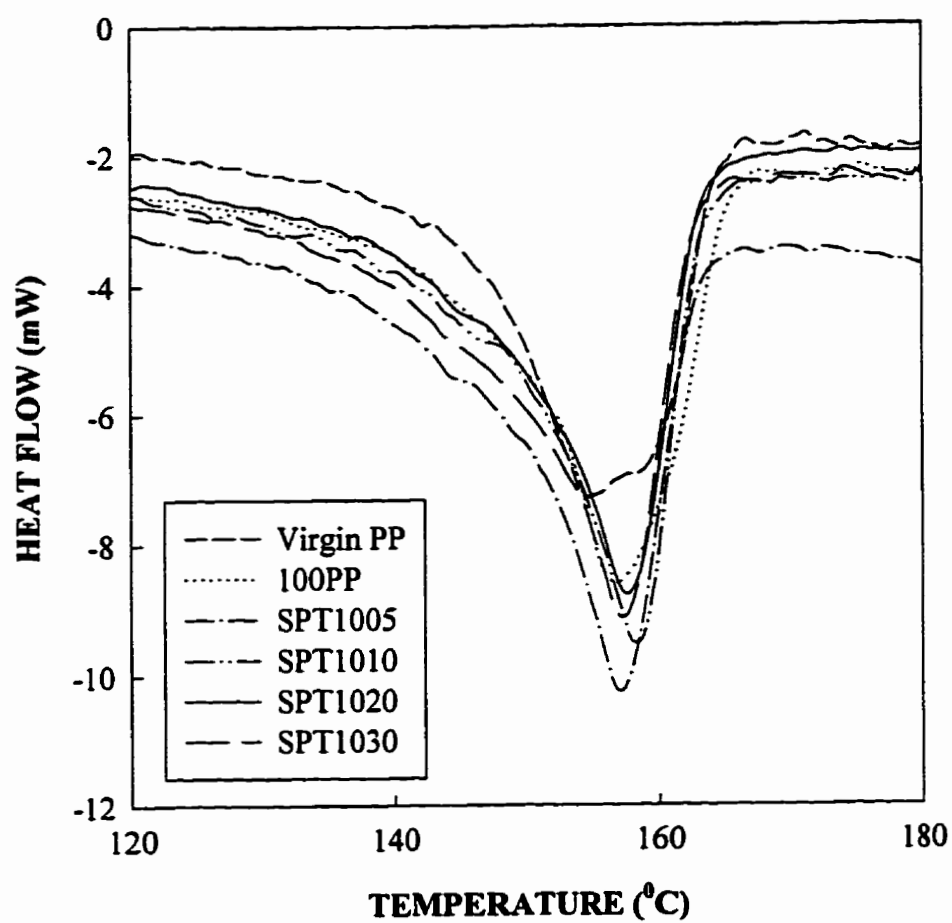


Fig. 7-12 Melting endotherms of the sols of PETA/peroxide modified PPs (100 ppm L101series).

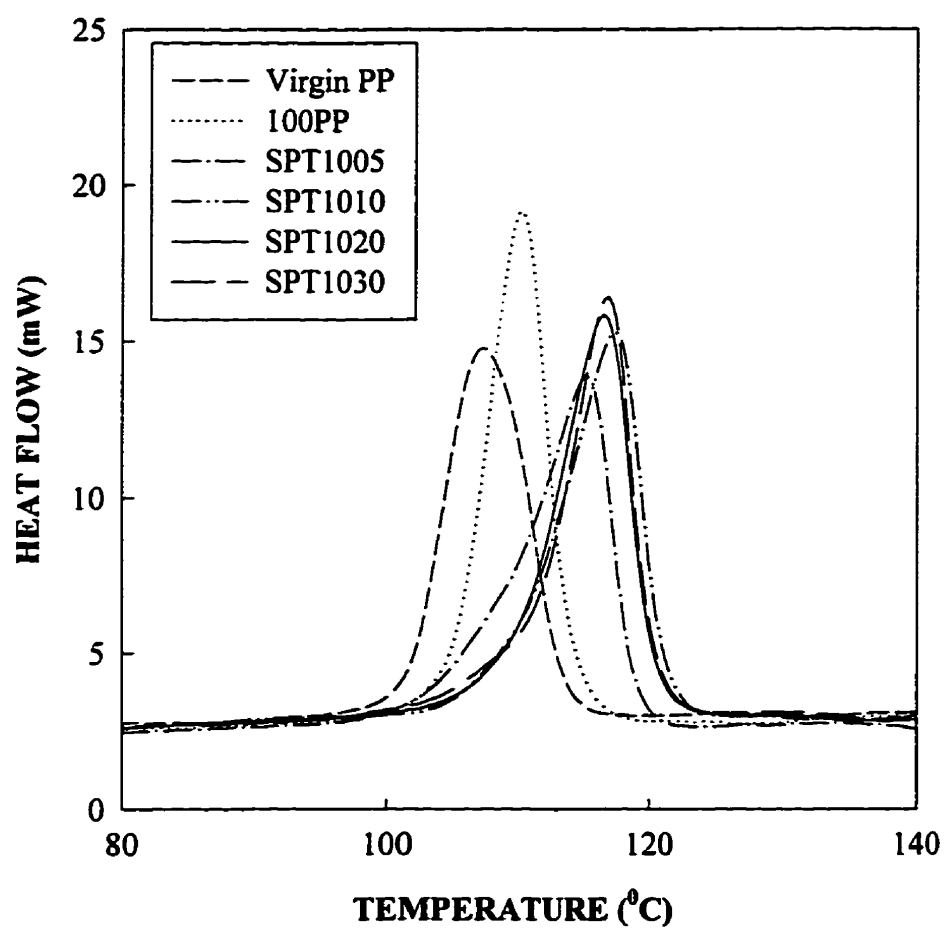


Fig. 7-13 Crystallization exotherms of the sols of PETA/peroxide modified PPs (100 ppm L101 series).

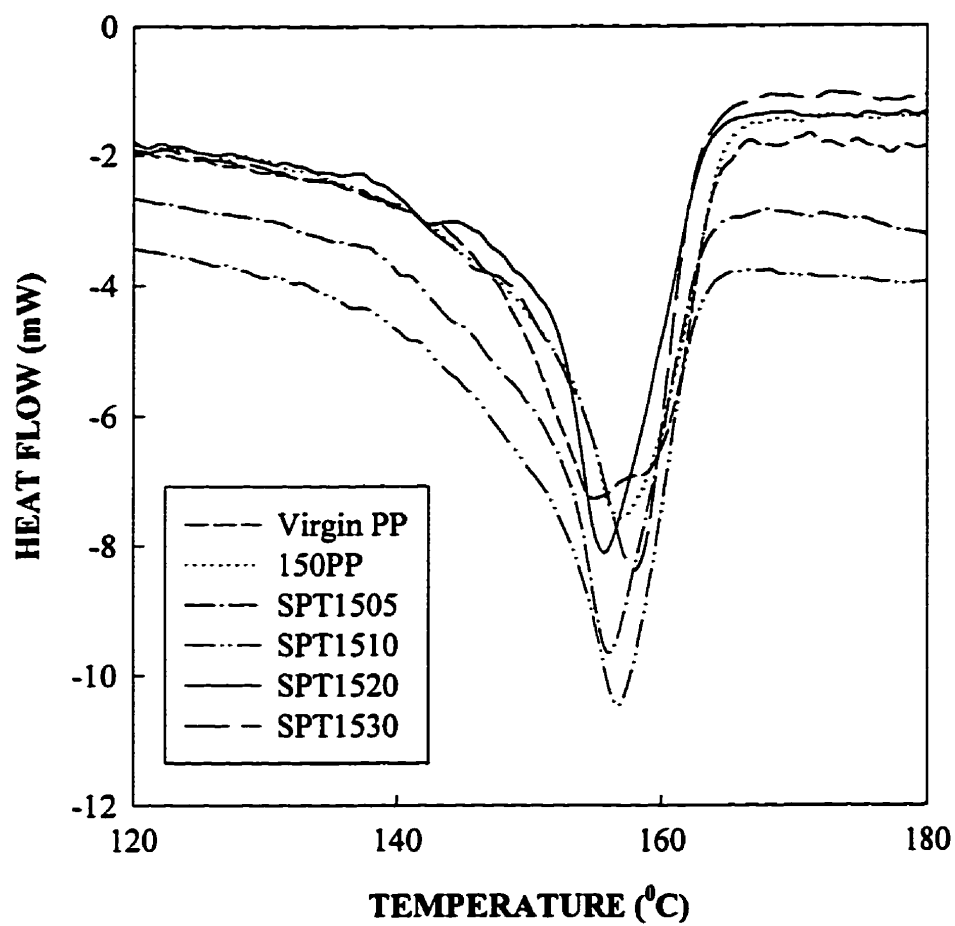


Fig. 7-14 Melting endotherms of the sols of PETA/peroxide modified PPs (150 ppm L101series).

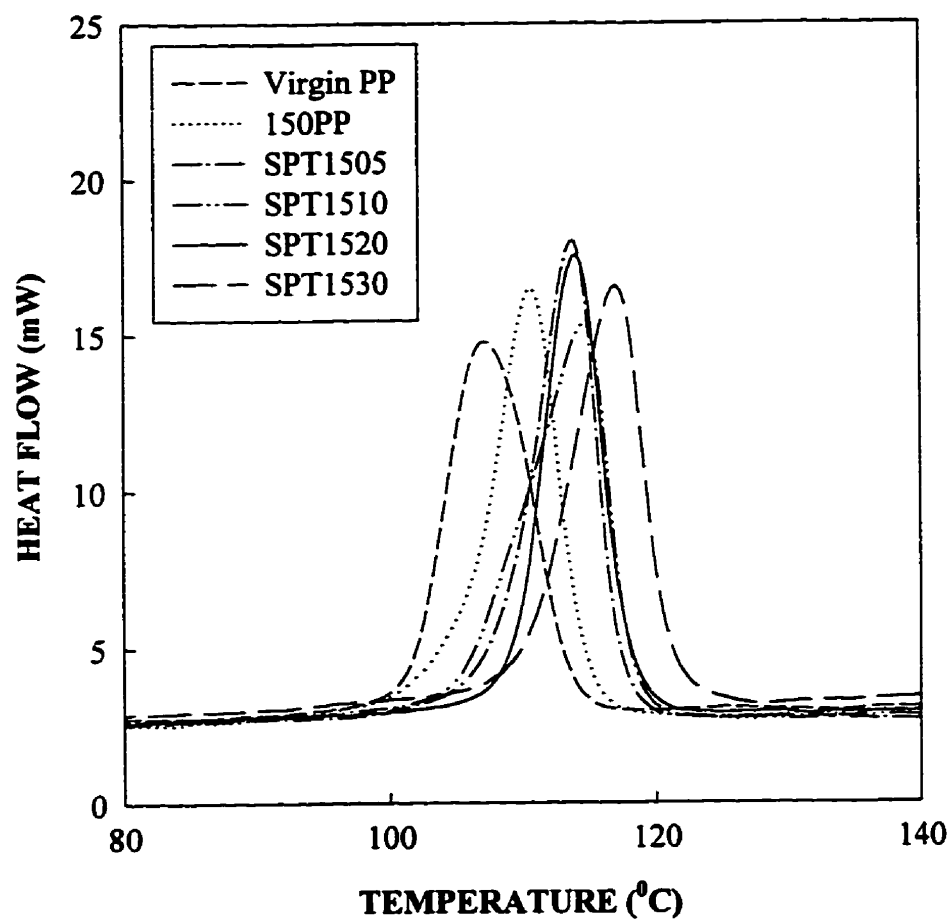


Fig. 7-15 Crystallization exotherms of the sols of PETA/peroxide modified PPs (150 ppm L101 series).



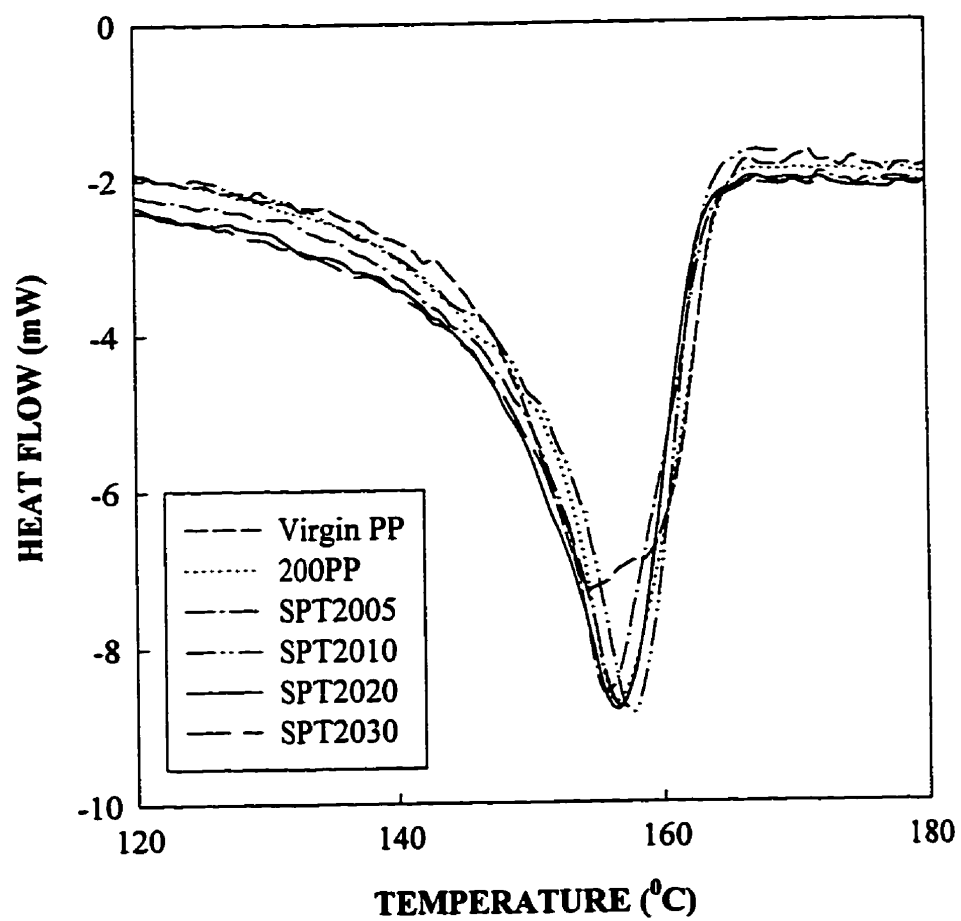


Fig. 7-16 Melting endotherms of the sols of PETA/peroxide modified PPs (200 ppm L101series).

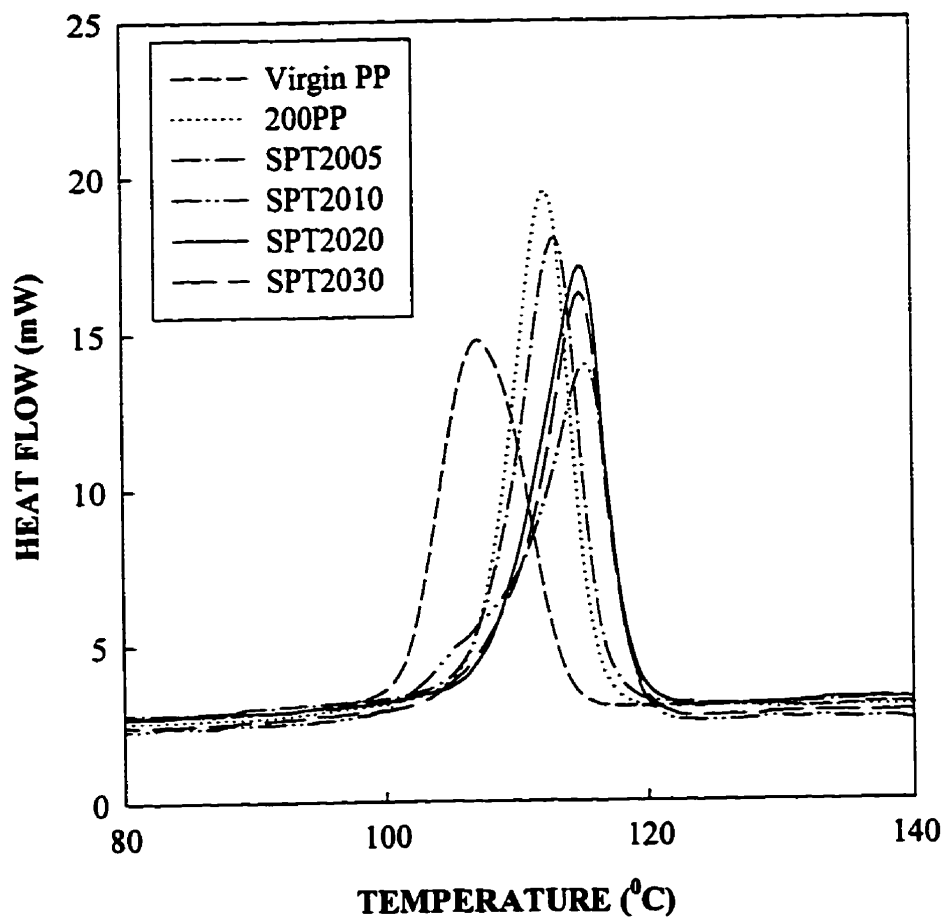


Fig. 7-17 Crystallization exotherms of the sols of PETA/peroxide modified PPs (200 ppm L101 series).

**TABLE 7.2 DSC Results For the Sols of the Modified PPs**

Sample	$T_m$ ( $^{\circ}\text{C}$ )	$\Delta H_m$ (J/g)	$T_c$ ( $^{\circ}\text{C}$ )	$\Delta H_c$ (J/g)	$T_m - T_c$ ( $^{\circ}\text{C}$ )
Virgin PP	154.61, 158.14	84.48	107.04	72.21	47.57
50PP	157.73	102.80	112.13	76.49	45.60
100PP	156.85	95.30	110.06	72.99	46.79
150PP	156.74	84.16	110.63	69.94	46.11
200PP	156.24	83.30	112.09	74.20	44.15
400PP	156.33	83.10	113.00	72.17	43.33
600PP	156.60	85.34	111.36	72.22	45.24
Montell PP	155.46	101.30	114.79	73.70	40.67
SPT505	155.92	92.76	111.85	69.89	44.07
SPT510	156.47	98.79	112.87	66.67	43.60
SPT520	157.85	104.51	115.44	75.41	42.41
SPT530	157.71	94.04	114.26	74.50	43.45
SPT1005	157.10	77.79	115.03	69.33	42.07
SPT1010	158.38	102.80	117.37	72.80	41.01
SPT1020	157.59	98.06	116.44	71.03	41.15
SPT1030	157.38	97.23	116.81	74.43	40.57
SPT1505	155.74	65.47	113.47	72.59	42.27
SPT1510	156.71	65.11	114.40	73.77	42.31
SPT1530	158.01	103.8	117.02	72.30	40.99
SPT2005	155.24	83.30	112.09	74.20	43.15
SPT2010	156.96	92.78	115.24	73.51	41.72
SPT2020	156.46	91.42	114.75	72.19	41.71
SPT2030	156.59	93.99	114.79	72.19	41.80

PETA concentration, the  $T_m$  is decreased initially and then increased to values comparable with that of degraded PP (50PP). For  $T_c$ , generally it increases with increasing PETA concentration and at high PETA concentration the  $T_c$  is higher than those of the linear PPs. Similar tendencies of  $T_m$ ,  $T_c$  and degree of undercooling with respect to PETA concentration are observed in the samples of 100, 150 and 200 ppm peroxide series. It is, hence, concluded that generally, the branched/crosslinked PPs show similar to or even higher melting temperatures than those of linear PPs under the current thermal conditions examined.  $T_m$  increases initially with increasing PETA concentration and then becomes relatively constant. The PETA/peroxide modified samples usually have higher  $T_c$ , especially at higher PETA level, and they have lower degree of undercooling than those of linear PPs. It can be seen that the samples in the 100 ppm series seem to show higher  $T_m$ s,  $T_c$ s and lower degree of undercooling than other comparable materials examined. It seems that  $T_m$ ,  $T_c$  and degree of undercooling are dependent more on the molecular structures (crosslinking or branching in our cases) of the polymers than on the molecular weight. The DSC results also suggest that besides the positive long chain branching effect on the rheological properties, the crosslinking points introduced by reactive extrusion, may act as a nucleating agent for PP crystallization and hence decrease the degree of undercooling at a fixed heating and cooling rate. This is another positive factor in terms of reducing the cycle time for processing.

Figs. 7-18 to 7-20 show the plots of the melting temperature ( $T_m$ ), crystallization temperature ( $T_c$ ) and degree of undercooling ( $T_m - T_c$ ) versus the long chain branches per weight average molecule for these PETA/peroxide modified PPs. It can be seen that roughly,  $T_m$  and  $T_c$  for these branched/crosslinked PPs increase with increasing long chain branches per weight average molecule while the degree of undercooling ( $T_m - T_c$ ) decreases. These results can be supported by the fact that the samples in 100 ppm series, which have higher LCB levels than most of the samples examined, generally have the highest  $T_c$  and ( $T_m - T_c$ ) than those of other comparable samples in other series. The increase of  $T_m$  with LCB level

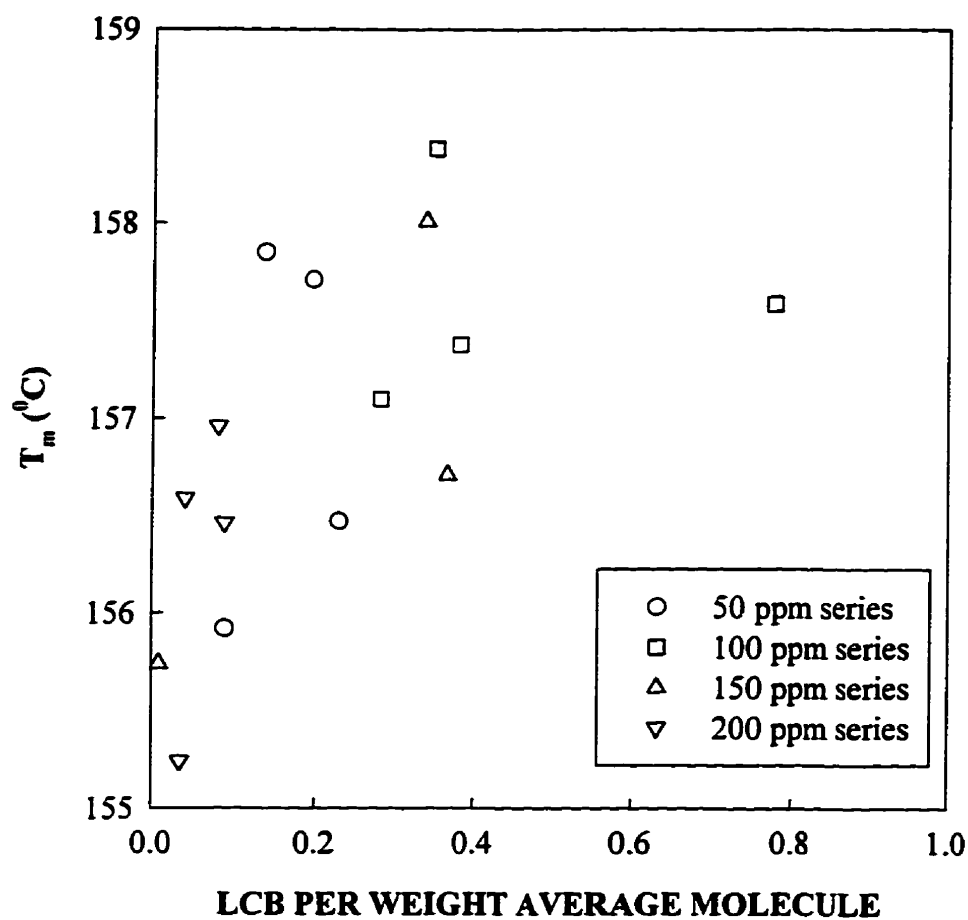


Fig. 7-18 Plot of the melting temperature ( $T_m$ ) versus LCB per weight average molecule for the PETA/peroxide modified PPs.

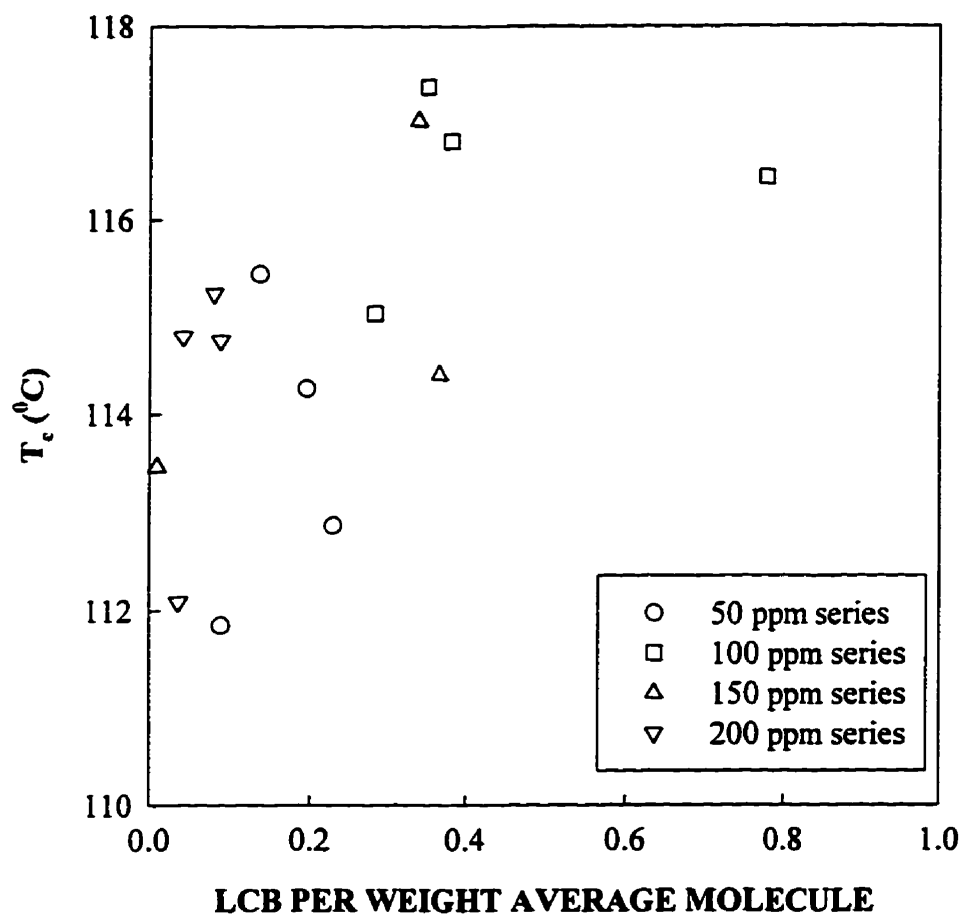


Fig. 7-19 Plot of the crystallization temperature ( $T_c$ ) versus LCB per weight average molecule for the PETA/peroxide modified PPs.

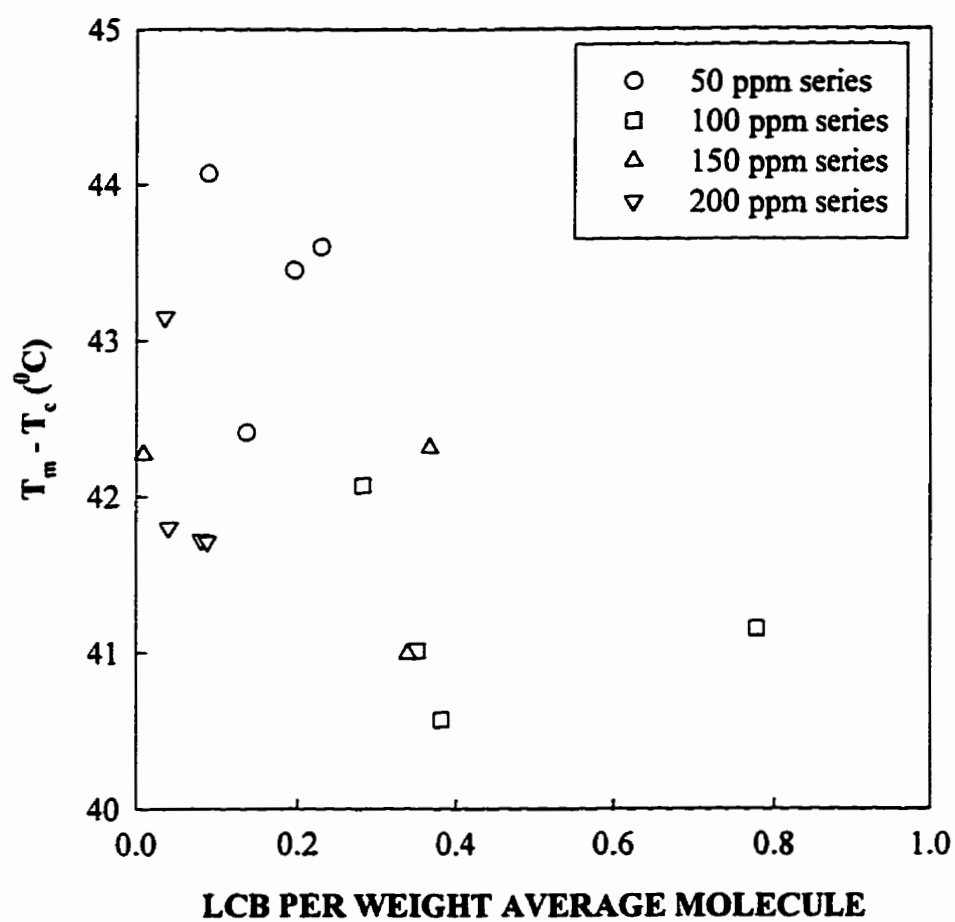


Fig. 7-20 Plot of the degree of undercooling ( $T_m - T_c$ ) versus LCB per weight average molecule for the PETA/peroxide modified PPs.

in this work is different from what has been observed for conventional random branched polymers such as polyethylenes. This may be attributed to the unique molecular structures of the branched/crosslinked PPs produced.

### 7.3 Concluding Remarks

Besides the branched structures suggested by GPC-viscometry, apparent elongational viscosity and flow activation energy, TGA results further imply that PETA/peroxide modified PPs may also have intermolecular and/or intramolecular crosslinked molecular structures, due to their higher thermal stabilities than that of virgin PP. This situation differs from that of some branched polymers such as commercial low density polyethylenes. The poor correlation between the decomposition temperatures and the LCB per weight average molecule may be attributed to the unique branched/crosslinked molecular structures of the modified PPs produced.

Generally, the branched/crosslinked PPs exhibit melting temperatures similar to those of linear PPs under the current thermal conditions examined.  $T_m$  increases initially with increasing PETA concentration and then becomes relatively constant. The PETA/peroxide modified samples usually have higher  $T_c$ , especially at higher PETA level, and they have lower degree of undercooling than those of linear PPs. Roughly, melting and crystallization temperatures for these branched/crosslinked PPs increase with increasing LCB per weight average molecule while the degree of undercooling ( $T_m - T_c$ ) decreases.



## CHAPTER 8

### LINEAR VISCOELASTIC PROPERTIES

#### 8.1 Introduction

From a structural point of view, it is generally understood that the different rheological properties are the consequences of different large-scale molecular structures existing in materials, i.e., molecular weight (MW), molecular weight distribution (MWD) and molecular architectures such as long chain branching (LCB). Apart from its use as an indicator of relative breadth of MWD, there have been some exploitations of rheology as a structural tool trying to define resin structures, particularly the nature and degree of LCB. Significant progress has been made in elucidating the effects of molecular architecture upon the rheological behaviour of certain model polymer systems which contain well-defined branch frequency, branch length, and narrow MWD (Rocheffort et al., 1979; Rachapudy et al., 1979; Raju et al., 1979). However, it should be noted that the molecular architecture and hence, the viscoelastic properties of many commercial branched polymers may not be well represented by these model systems.

Elucidation of the effects of molecular branching upon the melt viscosity and elasticity of polymers has been difficult. One of the difficulties is to define in a quantitative manner the variation in the types and distributions of branches existing in most polymers. Another difficulty is to separate the effects of MWD from those of branching. It is, therefore, instructive to elucidate the effects of MWD on the melt viscosity and melt elasticity of the polymers for systems of similar weight average molecular weight ( $\bar{M}_w$ ) and molecular architecture. The analysis of MWD is based upon the concept that the low shear rate viscosity (or low frequency moduli) reveals relaxation processes of the larger molecules whereas the high shear rate viscosity (or high frequency moduli) is dominated by relaxation

processes associated with the smaller molecules and segments of larger molecules. For example, studies on polyethylene indicate that the low shear rate viscosities of broad MWD samples are higher than those of narrow MWD samples. However, the high shear rate viscosity decreases as MWD broadens, leading to crossovers in the shear viscosity-shear rate curves for samples of varying MWD (Guillet et al., 1965; Chartoff et al., 1969). Similar results have been obtained for polystyrene (Thomas et al., 1969).

Branching has an effect on polymer melt viscosity. Bueche (1964) has attempted to theoretically explain this effect and predicted that there would be a reduction in melt viscosity. However, it was also shown by experiments that branched polymers may have higher viscosity than linear polymers of the same molecular weight at very low rates of deformation. For example, Kraus and Gruver (1965) studied the relationship between the branch architecture and shear rate dependent viscosity of polybutadiene. The major feature of this relationship is that the zero-shear rate Newtonian viscosity ( $\eta_0$ ) of a polymer having branches of molecular weight  $M_b$ , less than 3-4 times  $M_c$ , is less than that of a linear polymer of similar  $\bar{M}_w$ . For cases in which  $M_b$  of the branched system exceeds 3-4 times  $M_c$ , the  $\eta_0$  of the branched polymer exceeds that of the linear polymer ( $\eta_0$  enhancement). A further observation was that the high shear rate non-Newtonian viscosities of the branched systems were lower than those of their linear counterparts, even though viscosity enhancement was observed at low shear rates. The extensive work of Graessley and co-workers (Rocheffort et al., 1979; Rachapudy et al., 1979; Raju et al., 1979) with monodisperse linear and star polybutadienes and their hydrogenated products supports the earlier observations by Kraus and Gruver (1965). Similar rheological behaviours have also been observed for branched and linear polyethylene of similar molecular weight. For polyethylenes, generally branched low density polyethylene (LDPE) materials have greatly diminished melt viscosities relative to the linear high density polyethylene (HDPE) at constant weight average molecular weight. However, dramatic viscosity enhancement at low shear rates ( $\eta_0$  enhancement) has also been

observed (Mendelson et al., 1970; Wild et al., 1976; Graessley et al., 1977 ) when LCB is present at low concentrations and for high molecular weights. Therefore, branching can either increase or decrease zero shear rate viscosity ( $\eta_0$ ), depending on the length of the branches. LCB usually increases the shear viscosity at low shear rates, but decreases the viscosity at high shear rates.

Branching can also have an effect on viscoelastic properties of polymers. For example, Folt (1969) found that the relative degree of long chain branching in polybutadiene and polyisoprene could be assessed by the magnitude of stress oscillation encountered in capillary flow measurements: the magnitude of the stress oscillation decreased with increasing long chain branching. Nakajima et al. (1982) found that the concentration dependence of viscoelastic properties was significantly affected by the presence of long branches. Long chain branched polymers not only produced different shift factors in the concentration superposition but also deviated from the master curve at semidilute concentration.

One of the empirical methods to compare the differences in viscoelastic behaviour resulting from variations in LCB is to construct a modified Cole-Cole plot (Harrell and Nakajima, 1984). The authors prepared a series of ethylene-propylene copolymer samples in which the degree of branching was systematically varied. Then, a logarithmic Cole-Cole plot, in which  $G'$  is plotted against  $G''$ , was used for analysis of molecular architecture. The generated Cole-Cole plot can reflect the fact that the relative value of  $G'$  over that of  $G''$  at low frequencies is affected by MWD and more significantly by the presence of long chain branching. It is found that a single, molecular weight independent Cole-Cole plot is formed within the high moduli region for a series of linear elastomers having similar MWDs, but different molecular weights. Other representations have also been used to compare the elastic properties in a relative sense. Rochefort et al. (1979) plotted  $J'(\omega)$  versus  $G'(\omega)$  to show the viscoelastic difference of linear and model star-branched polymers. Shroff and Mavridis

(1994) used the representation of  $\tan\delta$  versus complex modulus  $G^*$  which is sensitive to the differences in polydispersity.

In this chapter, the polydispersity of linear PPs is also attempted to be correlated with the ones determined by two rheological techniques (rheological PI and Modsep). For linear PPs, Zeichner and Patel (1981) have proposed a polydispersity index derived from frequency data in linear viscoelastic region. This polydispersity index, or rheological PI, is defined as:

$$PI = \frac{10^5(Pa)}{G_c} \quad (8-1)$$

where  $G_c$  is the crossover modulus. It has been found that there is good correlation between PI and the  $\bar{M}_w/\bar{M}_n$  from GPC data for polypropylenes.

Recently Yoo (1993) proposed the use of the "Modulus Separation" (Modsep) to characterize polydispersity of linear PP. In this method, the distance between the  $G'$  and  $G''$  curves is measured at a constant modulus, namely, 1,000, 500, or 100 Pa, depending on the resin melt flow index. The modulus separation is defined as:

$$Modsep = \frac{\omega'}{\omega''} \quad (8-2)$$

where  $\omega' = \omega$  (@ $G' = 1000, 500, \text{ or } 100 \text{ Pa}$ ) and  $\omega'' = \omega$  (@ $G'' = 1000, 500, \text{ or } 100 \text{ Pa}$ ).

## 8.2 Experiments

Dynamic viscoelastic experiments were carried out with Rheometrics Mechanical Spectrometer RMS-605 using a parallel plate geometry (12.5 mm diameter and 2 mm thickness) at 210°C over the angular frequency range of  $10^{-1}$  to  $10^2 \text{ s}^{-1}$ . Some samples were re-measured over the range of  $10^{-2}$  to  $10^2 \text{ rad/s}$ . The whole modified PPs (contained 1 wt.% Irganox 1010 prior to reactive extrusion) produced from reactive extrusion experiments in

Chapter 4 (stage 2) were used directly and no further stabilizer was added. The variation in the data of the duplicated samples was about 4%. It was decided that there was negligible degradation during the measurements since comparable results could be obtained from consecutive runs on the same sample at the temperatures ranging from 200 to 230°C. The region of linear viscoelastic response was determined by strain sweep (1-25% strain) at an angular frequency of 1 rad/s. It was found that for all the samples examined in this experiment, a 15% strain was well within the linear response region, which is also consistent with the recommendation by Shang (1993). Thus, the frequency sweeps were carried out at a 15% strain for all the samples. The obtained information were complex viscosity  $\eta^*$ , storage modulus  $G'$ , loss modulus  $G''$ , loss tangent  $\tan\delta$  and dynamic storage compliance  $J'$ . The data reported in the tables represent the average values of two measurements.

### 8.3 Results and Discussion

#### 8.3.1 Complex Viscosity ( $\eta^*$ ) and the Relationship Between $\eta_0$ and $\bar{M}_w$

Fig. 8-1 shows the complex viscosities for six linear PPs, which include the virgin PP and five peroxide degraded PPs, as well as the Montell PP. The  $\bar{M}_w$ s of these polymers can be found in Chapter 5. It can be seen that the  $\eta^*$  is reduced monotonically with increasing peroxide concentration or decreasing  $\bar{M}_w$ .

The  $\eta^*$ s of the PETA/peroxide modified PPs are shown in Figs. 8-2 to 8-5. At low frequencies,  $\eta^*$  increases with increasing PETA concentration at all peroxide levels and the order of the magnitude in  $\eta^*$  is similar to that in the previous MFI measurements (Chapter 4). It is also noted that generally  $\eta^*$  drops with increasing peroxide concentrations at constant PETA levels, suggesting the increased degradation by peroxide radicals even with the presence of a crosslinking agent.

Since the Cox-Merz rule (Cox et al., 1958) applies to both linear and branched PP

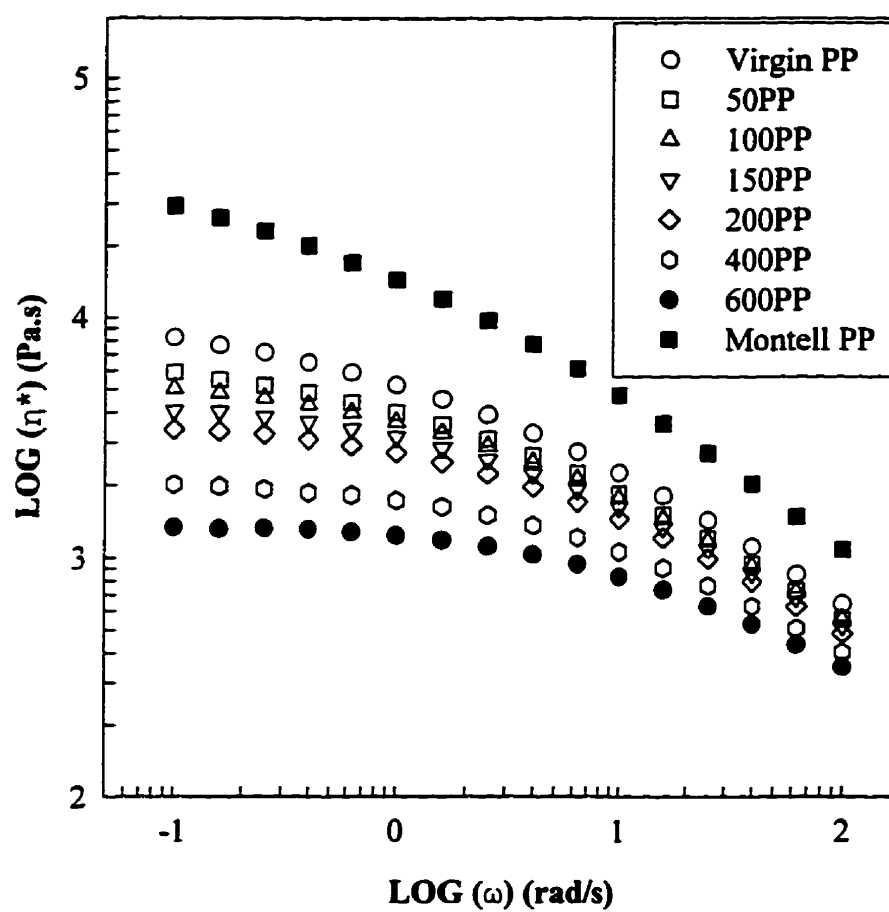


Fig. 8-1 Complex viscosities of virgin PP, peroxide-degraded PPs and Montell PP.

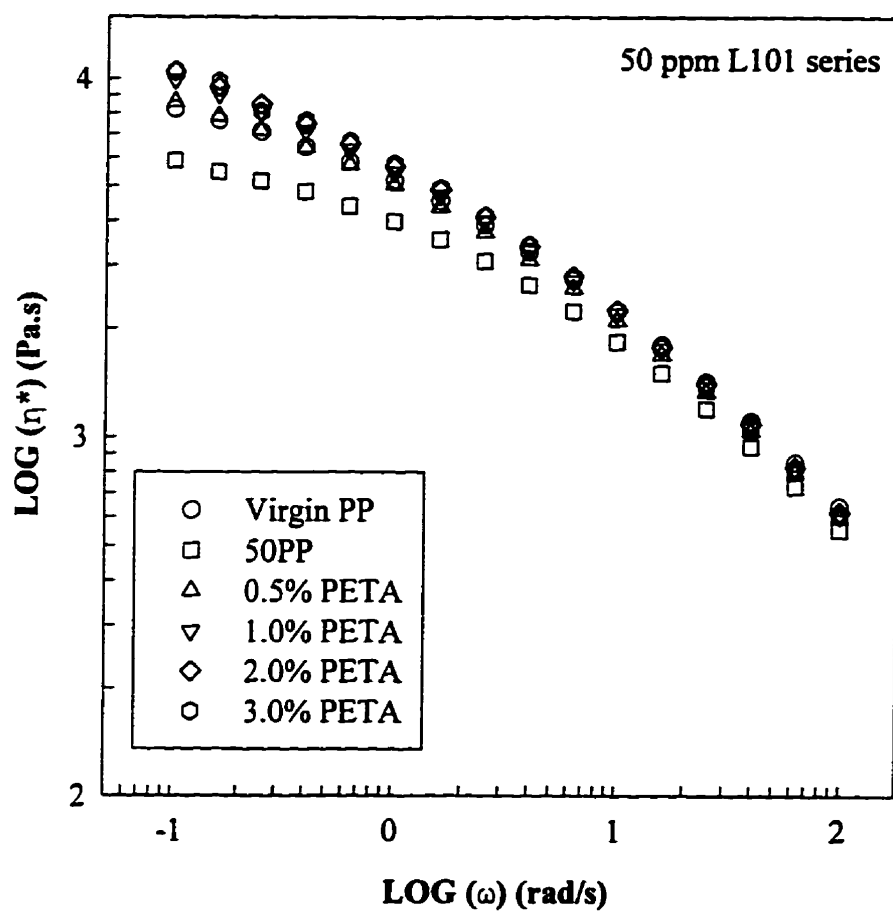


Fig. 8-2 Effects of the PETA and peroxide concentrations on the complex viscosities of the products (50 ppm L101 series).

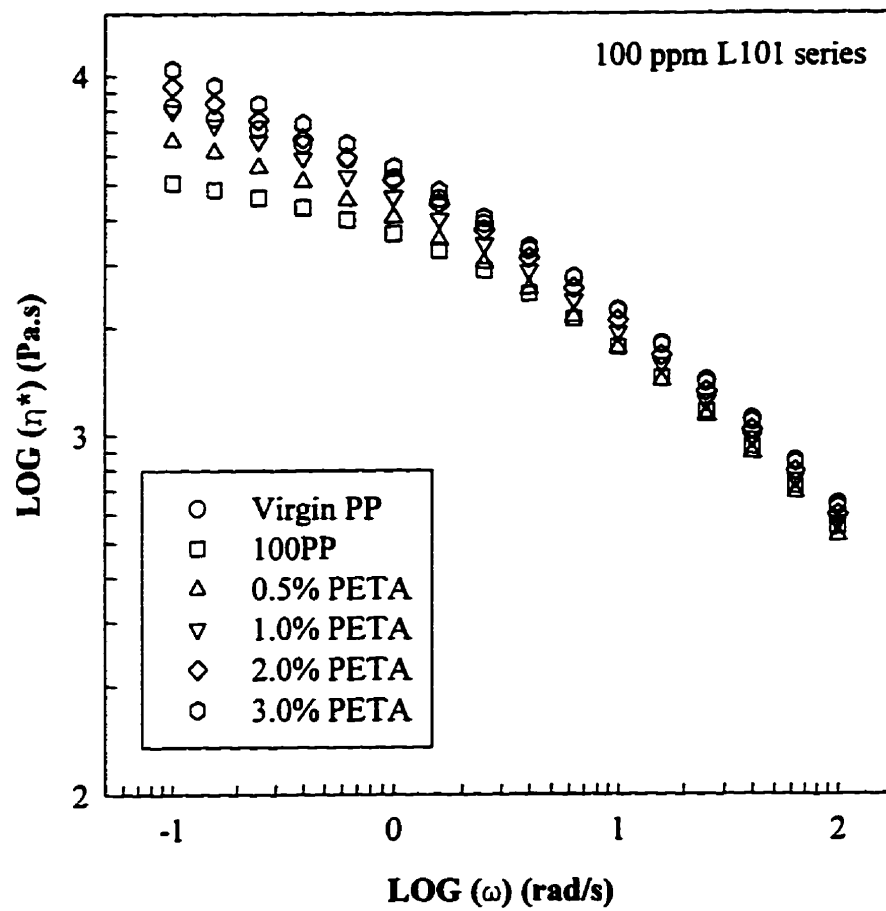


Fig. 8-3 Effects of the PETA and peroxide concentrations on the complex viscosities of the products (100 ppm L101 series).



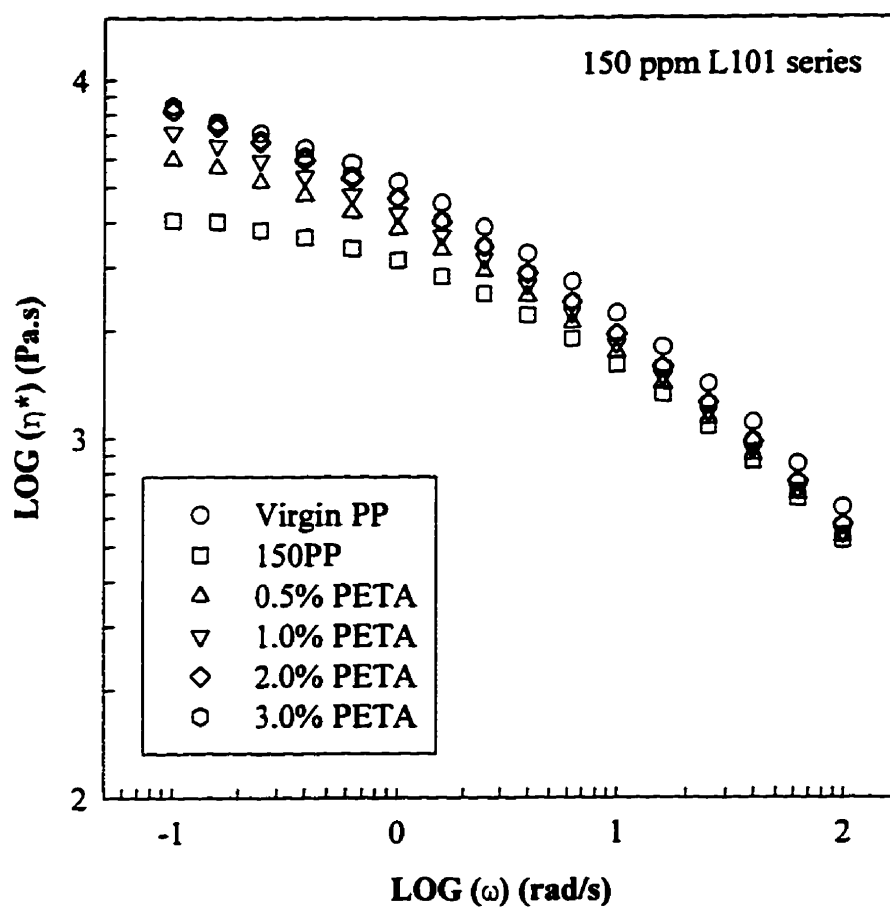


Fig. 8-4 Effects of the PETA and peroxide concentrations on the complex viscosities of the products (150 ppm L101 series).

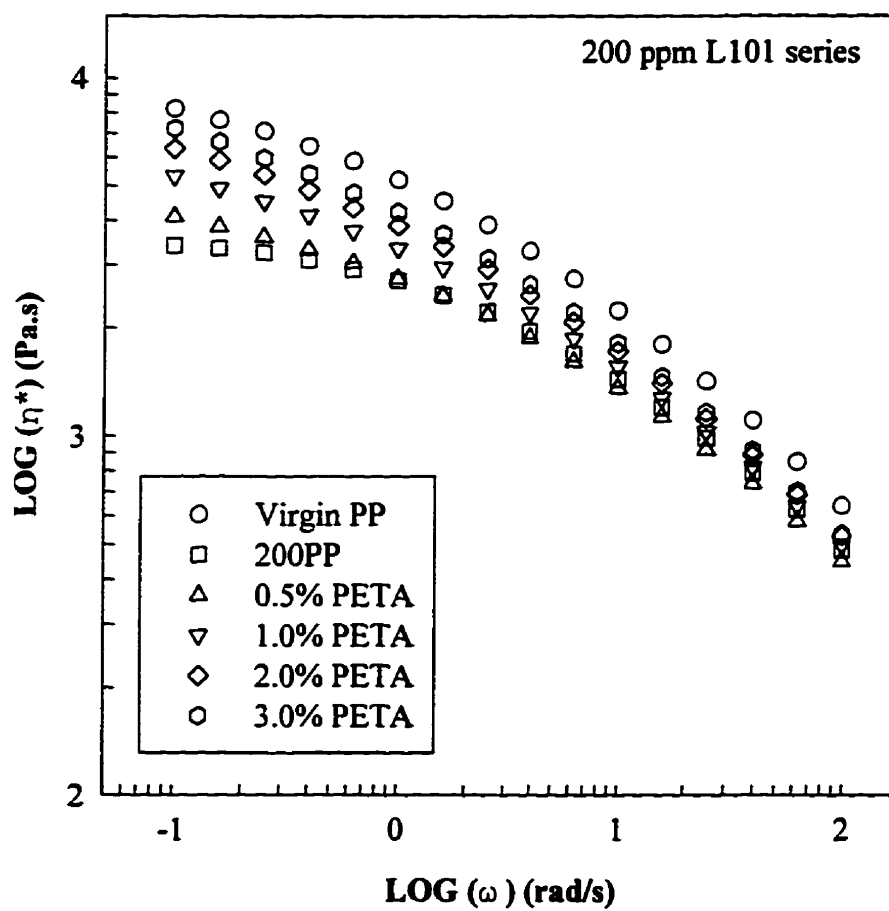


Fig. 8-5 Effects of the PETA and peroxide concentrations on the complex viscosities of the products (200 ppm L101 series).

melts (Hingmann et al., 1994), the zero-shear rate viscosity ( $\eta_0$ ) for all the samples were estimated with both the Ellis (1960) and Bueche (1958) model using a built-in program in the RMS and the results are tabulated in Tables 8.1 and 8.2. It can be seen that for linear PP,  $\eta_0$  is decreased with decreasing  $\bar{M}_w$ . Many of the PETA/peroxide modified PPs have higher  $\eta_0$ s than that of virgin PP though they show lower  $\bar{M}_w$ . As shown below, the Bueche model seems to give a higher and more reasonable estimation of  $\eta_0$  than the Ellis model.

It has been known that for nearly all of the linear monodisperse polymers, the relationship  $\eta_0$  and  $\bar{M}_w$  is of the form:

$$\eta_0 = K\bar{M}_w^\alpha \quad (8-3)$$

Up to a critical molecular weight ( $M_c$ ), the relationship is linear, i.e.,  $\alpha = 1$ . Above  $M_c$  the dependence of  $\eta_0$  on  $\bar{M}_w$  is much greater and  $\alpha$  is found to be in the range 3.4 - 3.5.

For linear polydisperse PPs, Ghijssels et al. (1994) found the exponent to be 3.57 at 190°C, which is higher than the expected value. In our system, the  $\eta_0$  is plotted as a function of  $\bar{M}_w$  (from Chapter 5) for linear and PETA/peroxide modified PPs (Figs. 8-6 and 8-7). It can be seen that the data from virgin PP and all peroxide degraded PPs form a single line, with a slope of about 3.22 ( $\eta_0$  estimated from the Ellis model) and 3.49 ( $\eta_0$  estimated from the Bueche model) respectively. The former slope is somewhat lower than the expected value (about 3.4), but the latter slope is very close. Hence, the current results suggest that virgin PP and peroxide degraded PPs are all linear polymers. The results also imply that the Bueche model seems to give the more reasonable estimation of  $\eta_0$  in terms of the expected relationship between  $\eta_0$  and  $\bar{M}_w$ .

In Figs. 8-6 and 8-7, it is noted that the data for Montell PP is on or very close to the regression interval of the regression line for linear PPs at a 95% confidence level. One may also argue that there is no data for linear PP at higher molecular weight, which may affect

**TABLE 8.1  $\eta_0$  Estimated by Ellis Model**

Sample	$\eta_0$ (KPa.s)	Sample	$\eta_0$ (KPa.s)	Sample	$\eta_0$ (KPa.s)
Montell PP	38.503	SPT505	10.594	SPT1505	7.021
Virgin PP	9.43	SPT510	12.166	SPT1510	8.966
50PP	6.911	SPT520	13.600	SPT1520	10.409
100PP	5568	SPT530	13.431	SPT1530	10.985
150PP	4.448	SPT1005	8.518	SPT2005	4.899
200PP	3.738	SPT1010	10.724	SPT2010	6.283
400PP	2.121	SPT1020	12.431	SPT2020	8.403
600PP	1.397	SPT1030	13.866	SPT2030	9.527

**TABLE 8.2  $\eta_0$  Estimated by Bueche Model**

Sample	$\eta_0$ (KPa.s)	Sample	$\eta_0$ (KPa.s)	Sample	$\eta_0$ (KPa.s)
Montell PP	56.064	SPT505	16.096	SPT1505	8.092
Virgin PP	11.200	SPT510	17.522	SPT1510	13.790
50PP	8.138	SPT520	19.764	SPT1520	14.483
100PP	6.244	SPT530	19.043	SPT1530	15.678
150PP	4.849	SPT1005	12.562	SPT2005	5.944
200PP	4.004	SPT1010	14.947	SPT2010	8.088
400PP	2.206	SPT1020	18.038	SPT2020	12.037
600PP	1.428	SPT1030	20.586	SPT2030	13.178

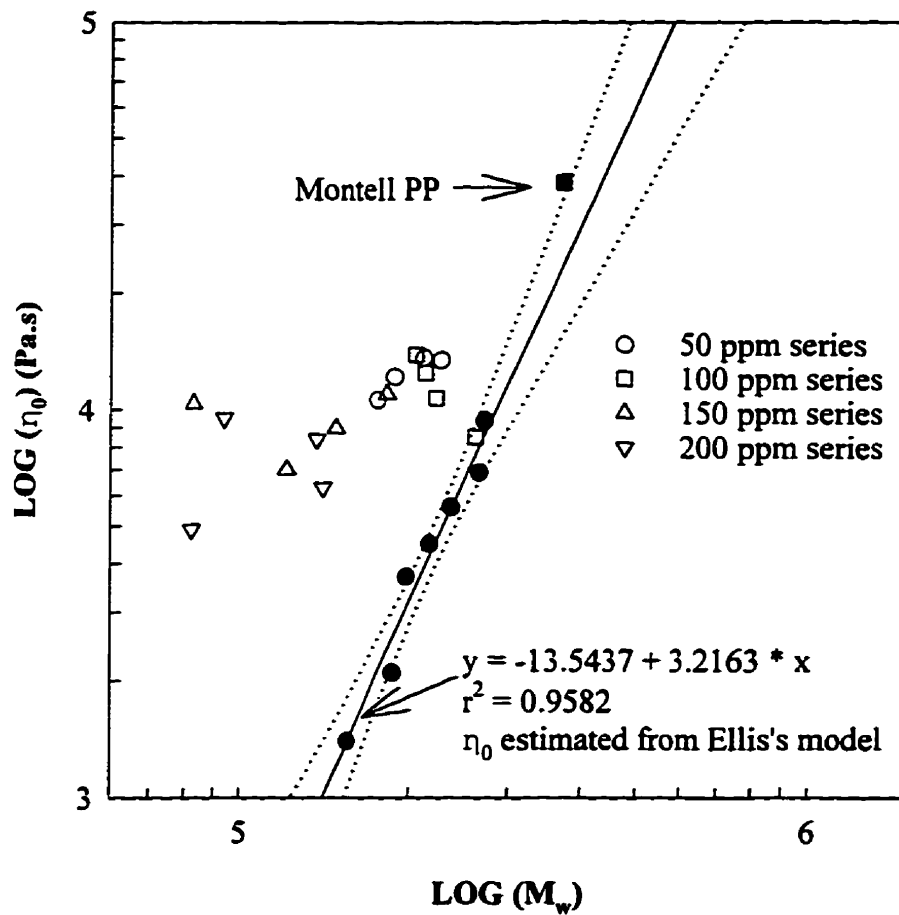


Fig. 8-6 The relationship between the  $\eta_0$  (estimated by Ellis model) and  $\bar{M}_w$  of virgin PP, peroxide degraded PPs, Montell PP and PETA/peroxide modified PPs (solid line: the regression line for linear PPs; dashed lines: the regression interval at a 95% confidence level).

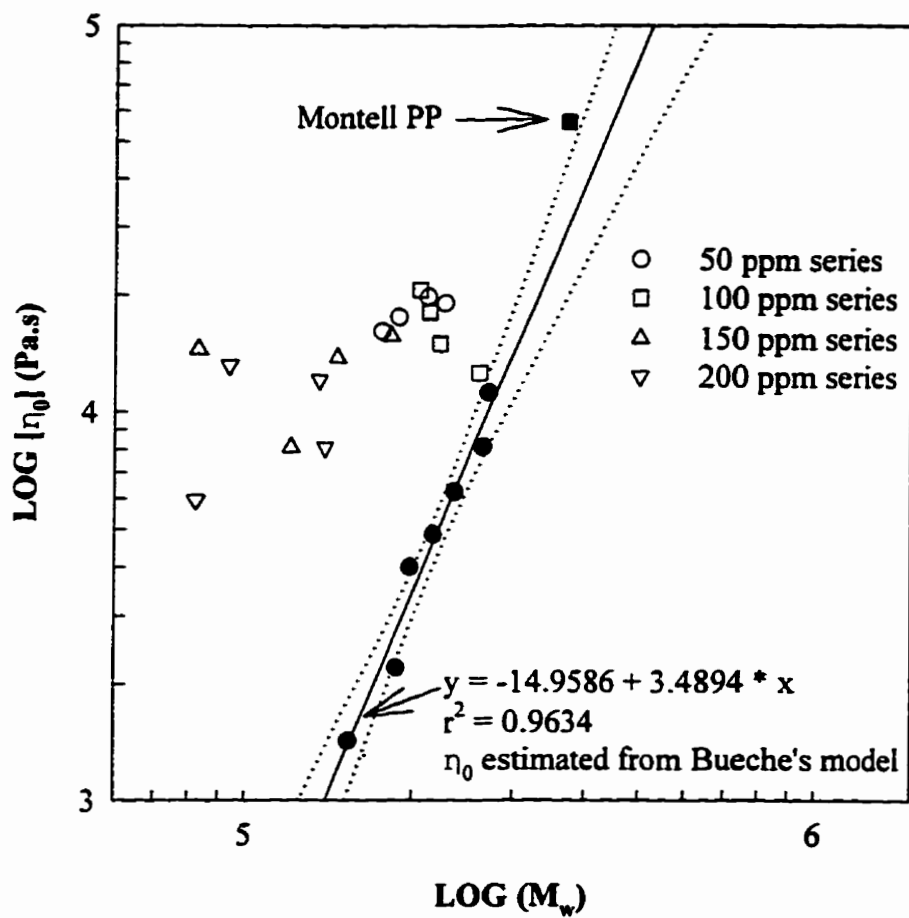


Fig. 8-7 The relationship between the  $\eta_0$  (estimated by Bueche model) and  $\bar{M}_w$  of virgin PP, peroxide degraded PPs, Montell PP and PETA/peroxide modified PPs (solid line: the regression line for linear PPs; dashed lines: the regression interval at a 95% confidence level).

the regression. At this stage, there is no strong evidence to conclude that the relationship between the  $\eta_0$  and  $\bar{M}_w$  of Montell PP is different from that of the linear PP. This appears to further support the LCB frequency results and the resultant speculation in Chapter 5, that Montell PP might be a polymer with low level of LCB. It is found that the  $\eta_0$  of PETA/peroxide modified PP is considerably larger than the equivalent linear PP at a similar  $\bar{M}_w$ , implying that the long chain branched molecular structures exist in these modified PPs. The  $\eta_0$  enhancement can also be inferred from the fact that at low frequencies, many of the PETA/peroxide modified PPs have significantly higher  $\eta^*$ s than that of virgin PP.

It can be found that the data points for the 150 and 200 ppm L101 series also lie far from the regression line represented by the linear PP. Recall the GPC characterizations on the samples of these two series, where it was found difficult to distinguish the samples in these two series from linear PPs. The current results indicate that rheological measurements are more sensitive to the branched structures than the GPC technique. Another interesting behaviour is that a higher viscosity enhancement at a higher molecular weight, is not observed in Figs. 8-6 or 8-7. However, this kind of behaviour is usually found for either randomly branched or star branched polymers (Masuda, et al., 1972; Rachapudy et al., 1979). At this stage, it is not clear whether or not this is due to the coexistence of the branched and lightly crosslinked structures in our materials.

### 8.3.2 Storage Modulus ( $G'$ ), Loss Modulus ( $G''$ ) and Various Correlations

Figs. 8-8 and 8-9 show the frequency dependencies of  $G'$  and  $G''$  of a series of linear PPs and Montell PP. As expected, the increased degradation reaction has a monotonic reducing effect on both the  $G'$  and  $G''$  of linear PP. The moduli of linear PPs with higher  $\bar{M}_w$  seem to have smaller frequency dependencies, suggesting a slower relaxation of longer polymer chains. The  $\bar{M}_w$  plays a dominant role in determining the magnitude of moduli of

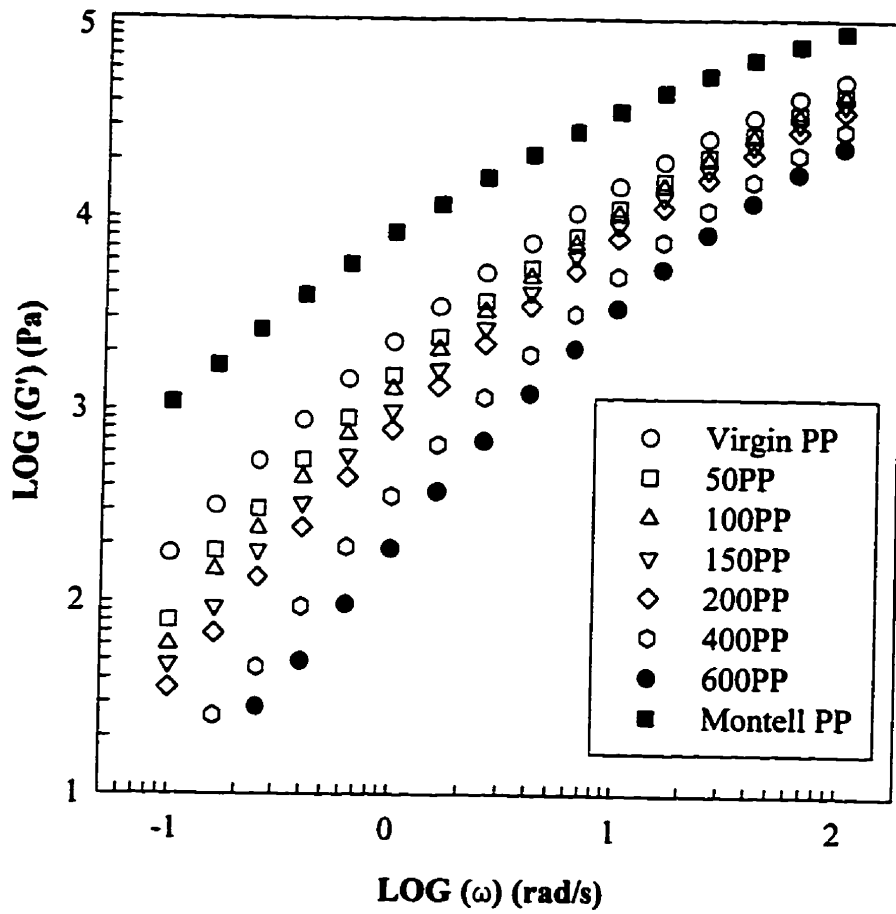


Fig. 8-8 Storage moduli of virgin PP, peroxide degraded PPs and Montell PP.



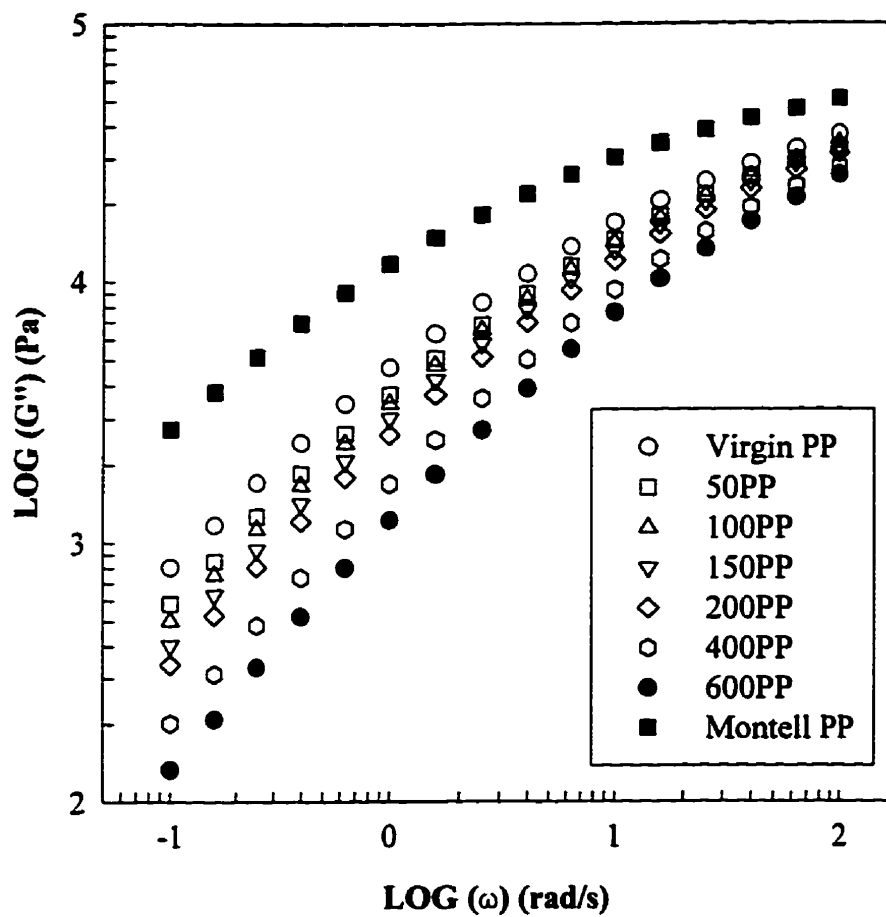


Fig. 8-9 Loss moduli of virgin PP, peroxide degraded PPs and Montell PP.

linear PPs since some of the linear PPs (such as virgin PP and 50PP) have very similar MWDs as indicated by GPC (Chapter 5), yet exhibit distinct moduli curves. It can be seen that Montell PP shows much higher moduli than the other materials.

Figs. 8-10 to 8-17 show the frequency dependencies of the  $G'$  and  $G''$  of PETA/peroxide modified PPs. Generally,  $G'$  and  $G''$  increase with increasing PETA concentration and decrease with increasing peroxide level. For all the samples in 50 and 100 ppm L101 series, very similar values of  $G'$  and  $G''$  with those of virgin PP were observed at high frequencies. It has been known that relatively short chain segments are involved in the relaxations at high frequency and the effects of local chain structure may become important in this region. Hence, the current results suggest that when very low concentrations of PETA and peroxide are used, the structure of short chain segments of PP are not altered greatly after the reactive extrusion. However, large scale molecular structures (molecular weight, molecular weight distribution and extent of long chain branching) of PP are altered during reactive extrusion since the  $G''$  and  $G'$  at low and intermediate frequencies are different from those of virgin PP. These large-scale structural changes have also been confirmed by the GPC measurements (Chapter 5). Thus, it is possible to change the large scale molecular structures while retaining the structures of short chain segments by using very low peroxide and PETA concentrations. The peroxide level appears to be the dominant factor in this case. When higher peroxide concentrations are used, both the local chain structure and the large scale parameters of PP may be changed since at high and low frequencies, the samples in the 150 and 200 ppm L101 series exhibit significantly different moduli from those of virgin PP. For the samples at the same peroxide level, however, their local chain structures may not be significantly different since they all show similar moduli at high frequencies.

In Figs. 8-10 and 8-12, it can be seen that the  $G'$ 's at low frequencies for the samples in 50 and 100 ppm L101 series are much higher than that of virgin PP. This is certainly due to the existence of LCB in these PETA/peroxide modified PPs since they all have  $\bar{M}_w$ 's lower

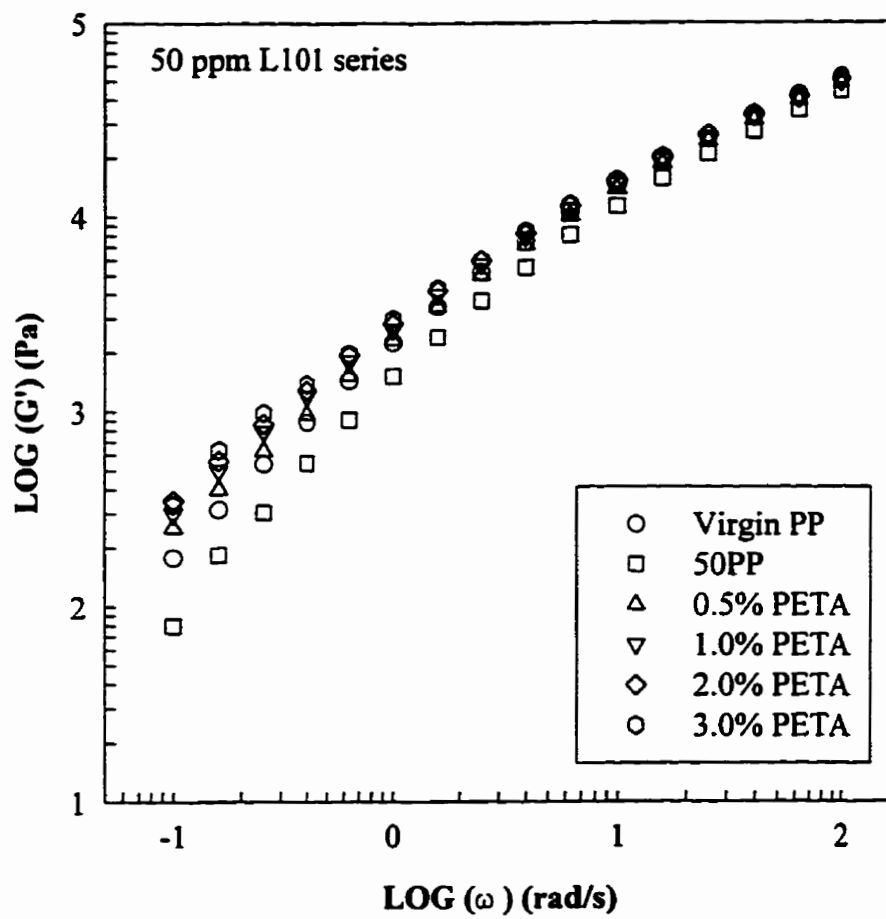


Fig. 8-10 Effects of the PETA and peroxide concentrations on the storage moduli of the products (50 ppm L101 series).

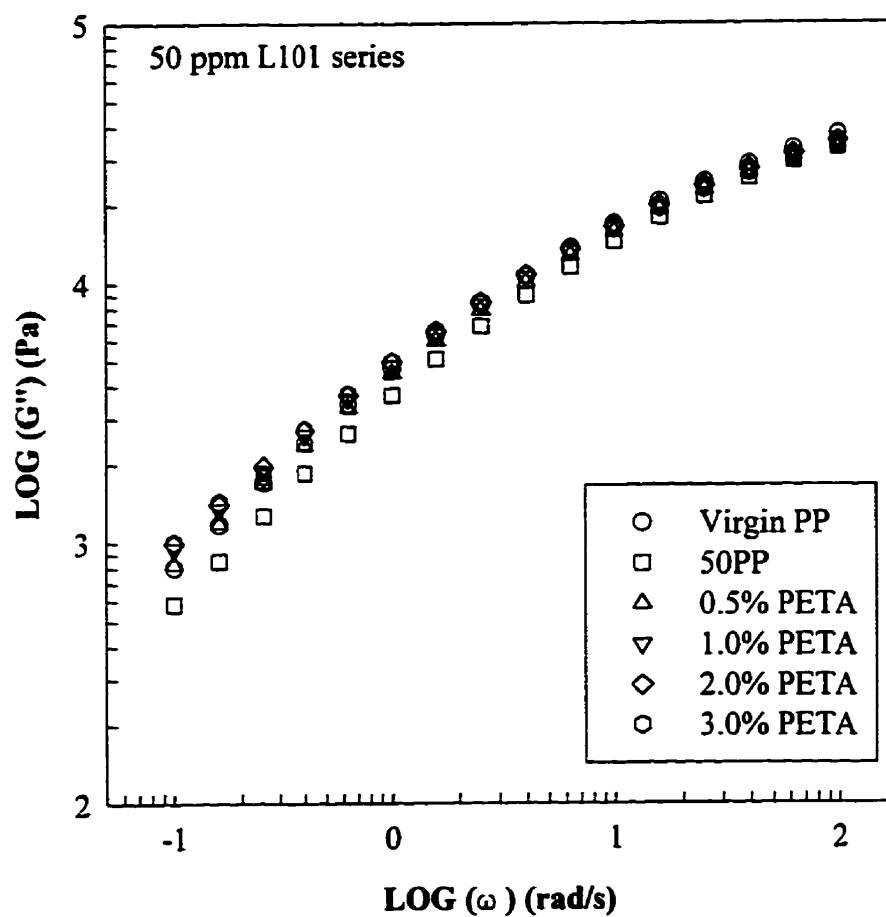


Fig. 8-11 Effects of the PETA and peroxide concentrations on the loss moduli of the products (50 ppm L101 series).

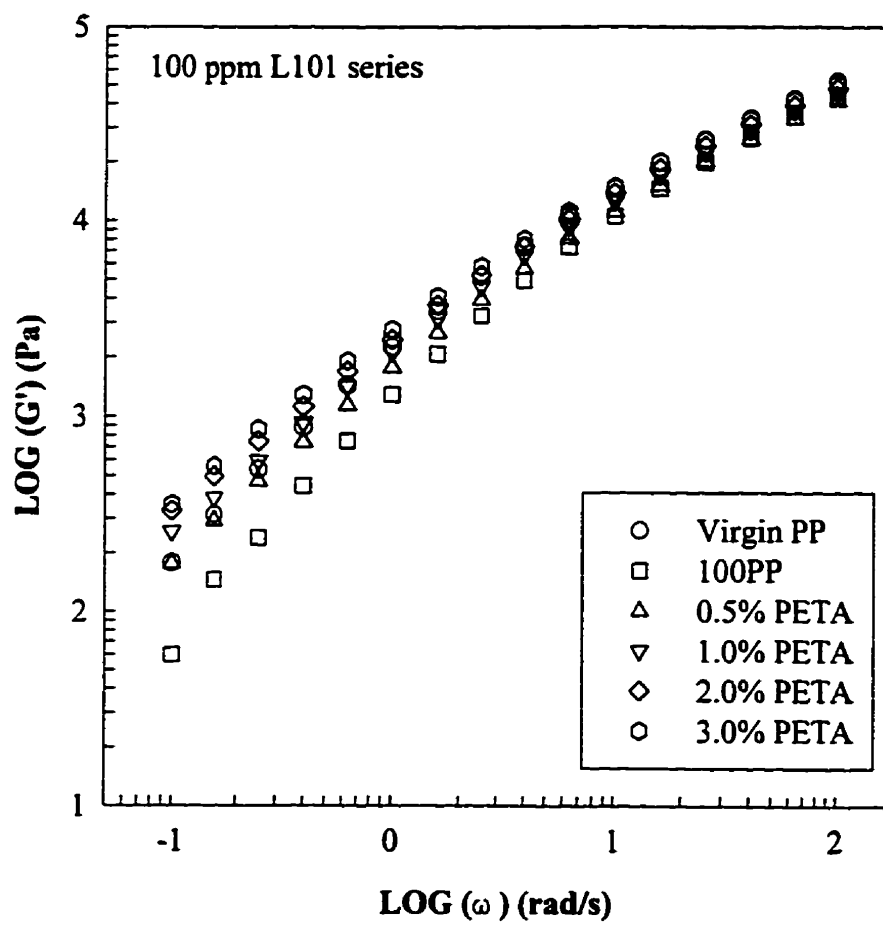


Fig. 8-12 Effects of the PETA and peroxide concentrations on the storage moduli of the products (100 ppm L101 series).

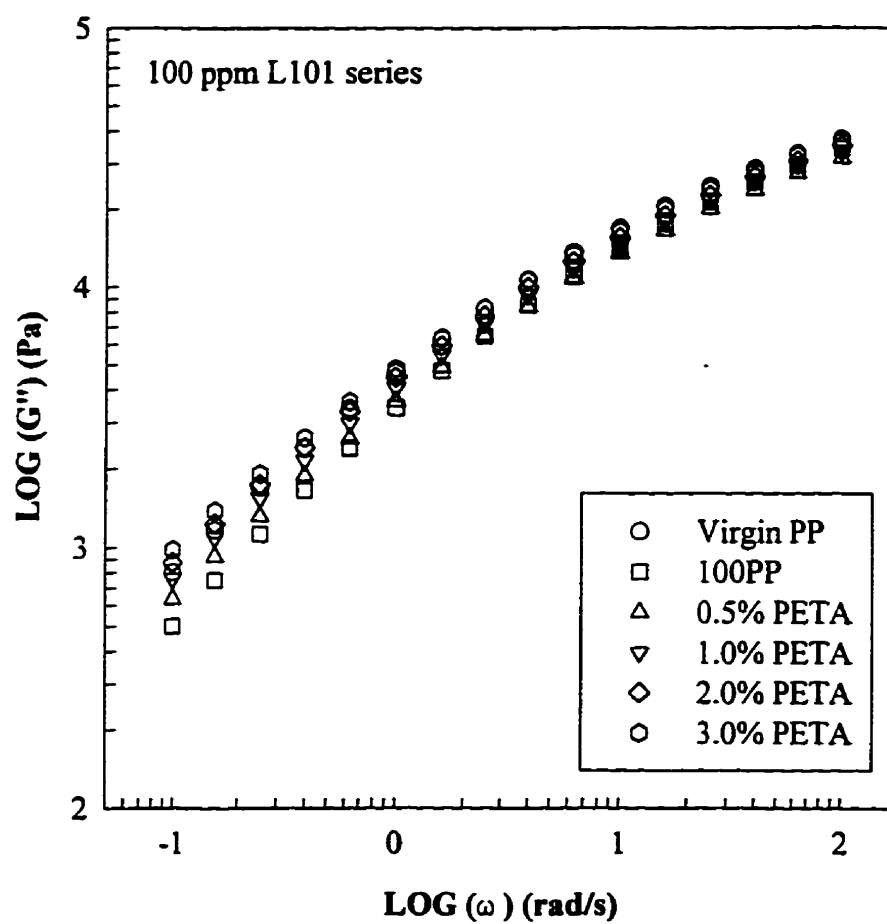


Fig. 8-13 Effects of the PETA and peroxide concentrations on the loss moduli of the products (100 ppm L101 series).

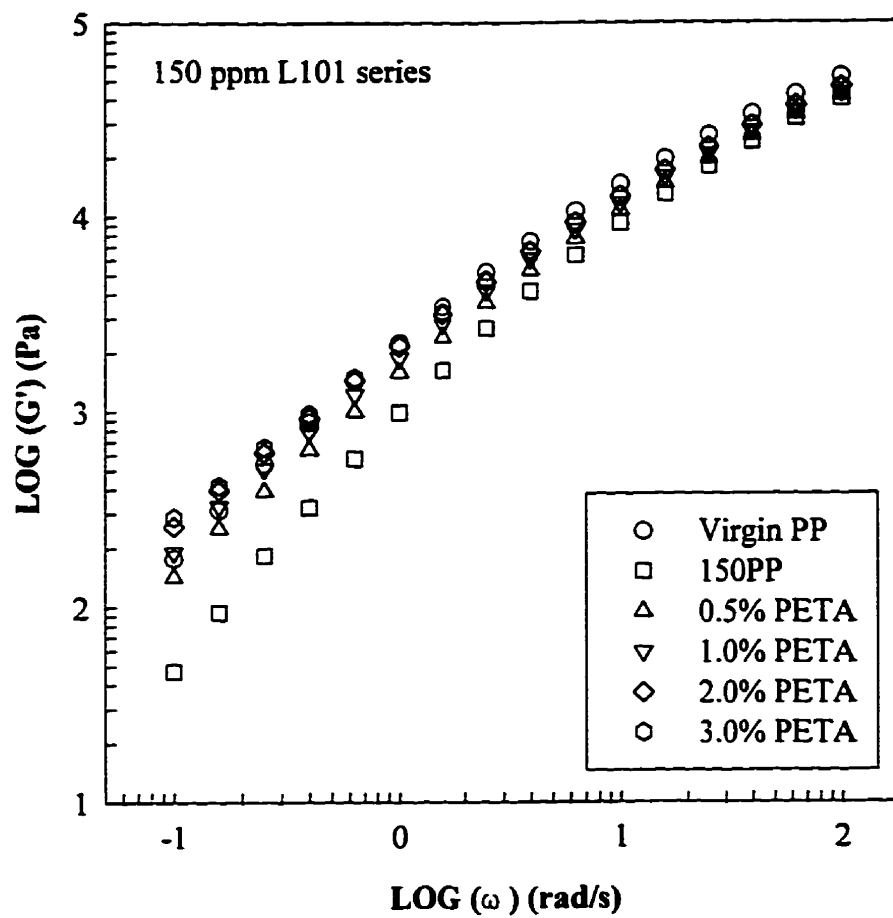


Fig. 8-14 Effects of the PETA and peroxide concentrations on the storage moduli of the products (150 ppm L101 series).

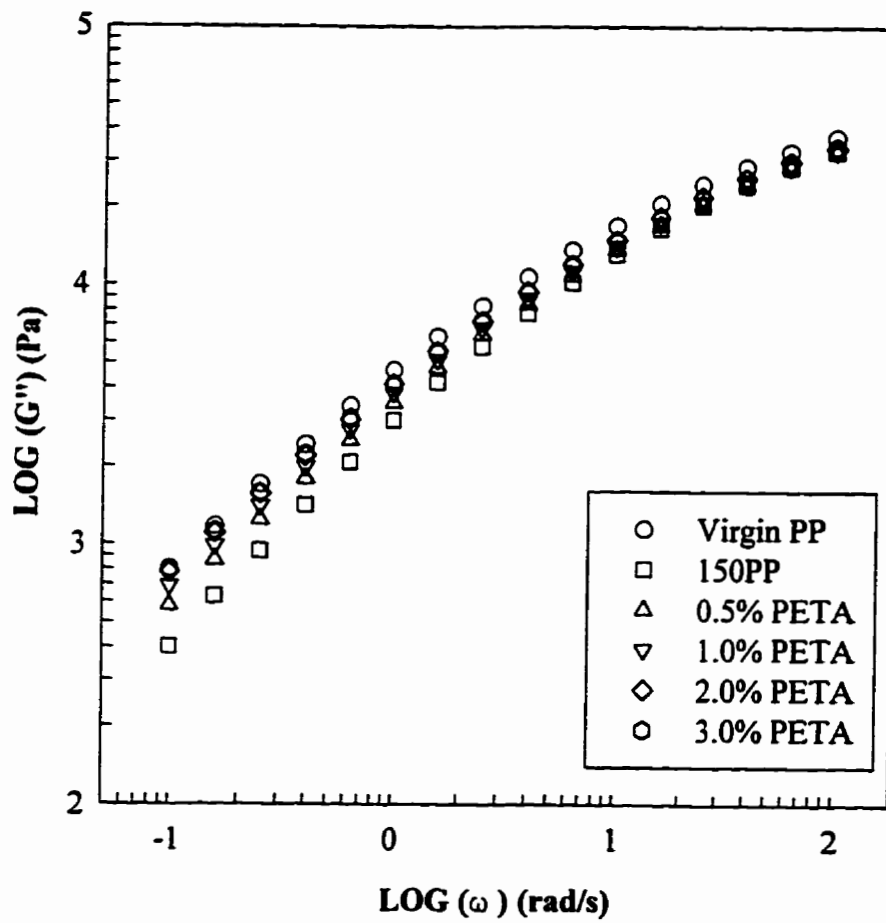


Fig. 8-15 Effects of the PETA and peroxide concentrations on the loss moduli of the products (150 ppm L101 series).



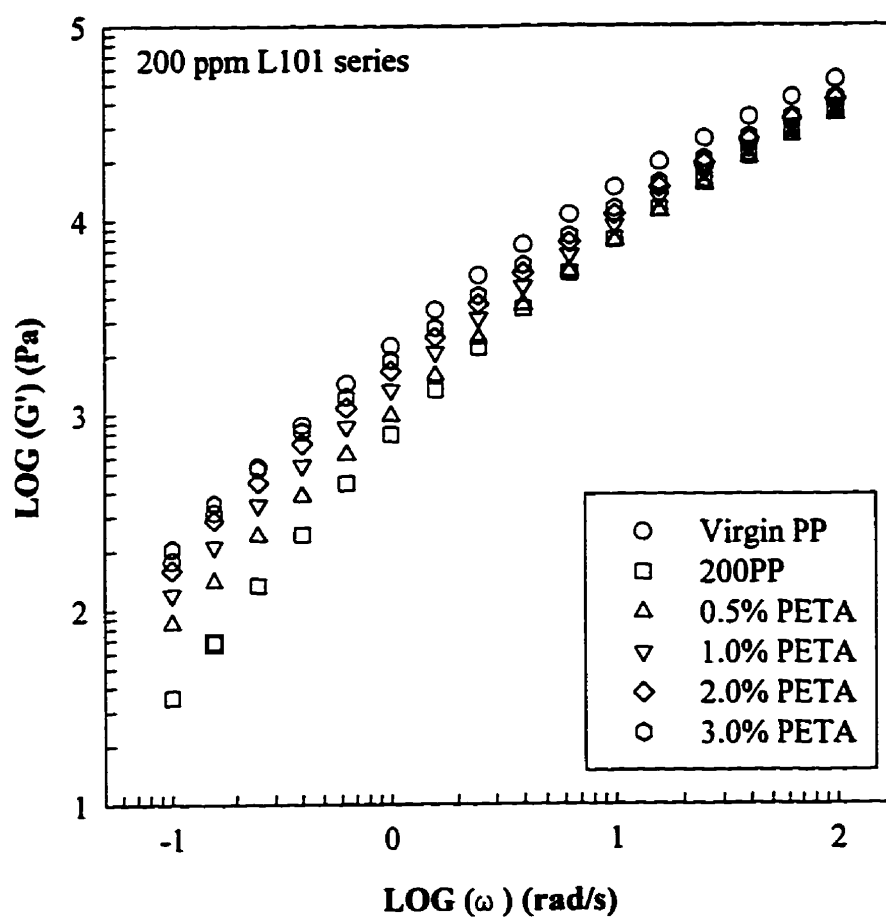


Fig. 8-16 Effects of the PETA and peroxide concentrations on the storage moduli of the products (200 ppm L101 series).

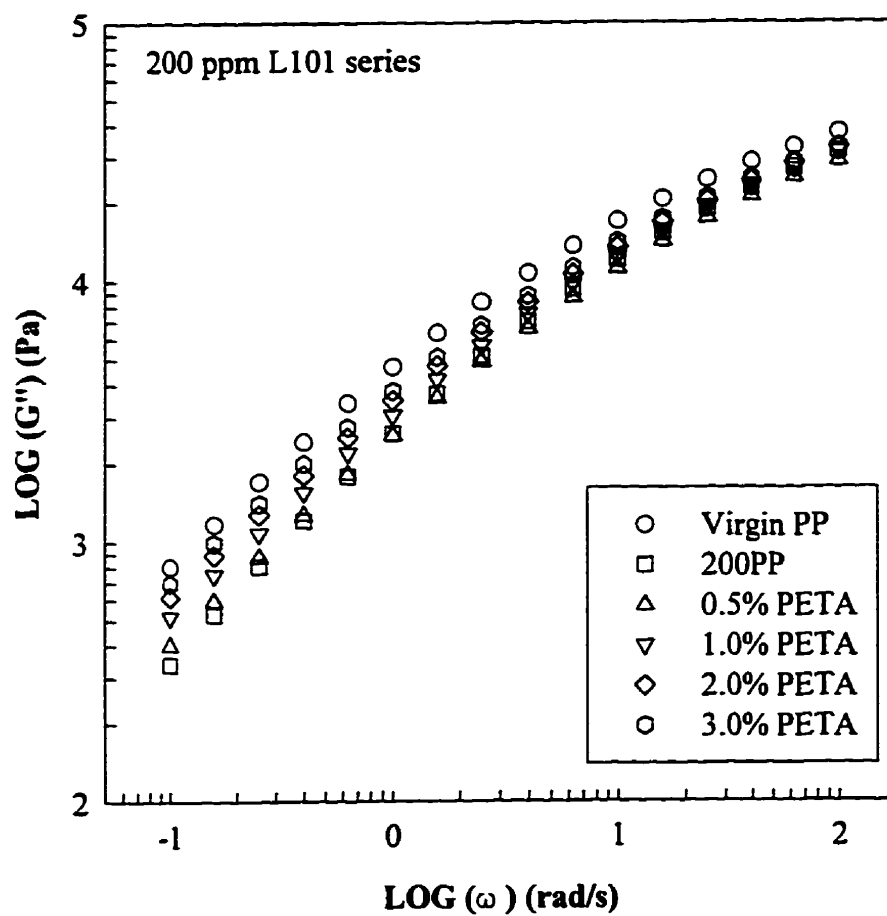


Fig. 8-17 Effects of the PETA and peroxide concentrations on the loss moduli of the products (200 ppm L101 series).

than that of virgin PP and many of their MWDs are not significantly different. Another reason is that no significant high molecular weight tail was found in these modified polymers (Chapter 5). The enhancement of the storage modulus at low frequencies has been observed in both star branched (Raju et al., 1979) and randomly branched polymers (Wild et al., 1976). Note that there is no such behaviour for linear PP when both MW and MWD are changed. As a result of the increase in  $G'$ , these samples also have larger dynamic storage compliance at low frequencies, which will be seen in section 8.3.5. The enhancement of  $G'$  at low frequencies due to branching can also be seen for most of the samples in 150 ppm L101 series (SPT1510, SPT1520 and SPT1530) and the sample SPT2030 (in Figs. 8-14 and 8-16), even though they have much lower  $\bar{M}_w$ s and narrower MWDs. Note that in Figs. 8-15 and 8-17, these four samples show similar or even lower loss moduli than that of virgin PP. The increase of  $G'$  at low  $\omega$  has been confirmed when some of the samples were re-run within the frequency range of 0.01 to 100 rad/s. Hence, the current results indicate that after the introduction of branching, more elastic energy can be stored while undergoing the sinusoidal deformation.

The moduli of PETA/peroxide modified PPs have weaker frequency dependencies than those of virgin PP, implying a slower relaxation of polymer chains caused by LCB. For monodisperse polymers, the expected slopes of the  $G'$  and  $G''$  curves at the terminal zones will be 2 ( $G' \propto \omega^2$ ) and 1 ( $G'' \propto \omega$ ) respectively. Deviations from these two values, i.e., smaller slope values, indicate the broadening of MWD and the existence of LCB (if any). Owing to the limited range of low frequency examined, none of our materials reaches the expected limiting behaviour. As an approximation, the slopes of  $G'$  and  $G''$  at low  $\omega$  can reflect these deviations. Thus, these slopes are calculated and summarized in Tables 8.3 and 8.4. For linear PP, indeed there are tendencies of the slopes of  $G'$  and  $G''$  to drift from the expected values of 2 and 1 respectively, when the MWD is broadened. Note that the slope of  $G''$  for 600PP has a very high value of 0.99. The slopes for the PETA/peroxide modified

**TABLE 8.3 Slopes of  $G'$  of Modified PPs at Low Frequencies**

Sample	Slope	Sample	Slope	Sample	Slope
Montell PP	0.95	SPT505	0.99	SPT1505	1.10
Virgin PP	1.20	SPT510	1.05	SPT1510	1.06
50PP	1.45	SPT520	0.98	SPT1520	0.94
100PP	1.51	SPT530	1.17	SPT1530	0.90
150PP	1.47	SPT1005	1.06	SPT2005	1.12
200PP	1.44	SPT1010	0.92	SPT2010	1.15
400PP	1.47	SPT1020	0.89	SPT2020	1.12
600PP	1.25	SPT1030	0.96	SPT2030	1.03

**TABLE 8.4 Slopes of  $G''$  of Modified PPs at Low Frequencies**

Sample	Slope	Sample	Slope	Sample	Slope
Montell PP	0.69	SPT505	0.78	SPT1505	0.83
Virgin PP	0.82	SPT510	0.74	SPT1510	0.78
50PP	0.84	SPT520	0.74	SPT1520	0.76
100PP	0.88	SPT530	0.63	SPT1530	0.75
150PP	0.92	SPT1005	0.80	SPT2005	0.84
200PP	0.94	SPT1010	0.77	SPT2010	0.80
400PP	0.94	SPT1020	0.75	SPT2020	0.79
600PP	0.99	SPT1030	0.73	SPT2030	0.76

deviate from the terminal slopes of  $G'$  and  $G''$ , which are attributed to the introduction of LCB since they can not be completely explained by the changes in MWD. Roughly, there is a tendency that the slopes become smaller with increasing extent of LCB and this is more evident from  $G''$  data.

To further verify the effect of LCB, relaxation time constants of the PPs are calculated using the Convected Maxwell model in which the relaxation constant ( $\lambda$ ), is defined as:

$$G' = \frac{\eta_0 \lambda \omega^2}{1 + \lambda^2 \omega^2} \quad (8-4)$$

where  $G'$  is storage modulus,  $\eta_0$  is zero-shear rate viscosity and  $\omega$  is frequency. As an approximation,  $\lambda$  was calculated by taking the  $G'$  at the frequency of  $0.1 \text{ s}^{-1}$ . The estimated relaxation time constants are listed in Table 8.5. It can be seen that the long chain branched PPs have longer relaxation time than linear virgin PP.

The crossover frequency ( $\omega_c$ ), crossover modulus ( $G_c$ ) and rheological polydispersity (PI) are summarized in Tables 8.6, 8.7 and 8.8 respectively. For linear polymers, it has been known that  $\omega_c$  is inversely proportional to the molecular weights of polymers. The  $\omega_c$  and  $\bar{M}_w$  for both linear and branched PPs are plotted in Fig. 8-18. For linear PP, there is an excellent correlation between these two parameters ( $r^2 = 0.95$ ):

$$\text{LOG}(\bar{M}_w) = 5.8522 - 0.3150 \times \text{LOG}(\omega_c) \quad (8-5)$$

Yoo (1993) also proposed a similar correlation which, however, contains another term for crossover modulus ( $G_c$ ). It seems that in our case, the  $\omega_c$  alone is sufficient to establish this relationship. In Fig. 8-18, the dashed lines represent the regression intervals of the regression line for linear PPs at the 95% confidence level. Generally the data for branched PPs lie far from this regression line and the of branched PP has a weaker dependence on  $\omega_c$ . The data

**TABLE 8.5 Relaxation Time Constant ( $\lambda$ ) of Polypropylenes**

Sample	$\lambda$ (s)	Sample	$\lambda$ (s)	Sample	$\lambda$ (s)
Montell PP	3.09	SPT505	2.54	SPT1505	2.13
Virgin PP	1.96	SPT510	2.64	SPT1510	2.24
50PP	1.17	SPT520	2.76	SPT1520	2.68
100PP	1.07	SPT530	2.75	SPT1530	2.83
150PP	1.06	SPT1005	2.17	SPT2005	1.80
200PP	0.97	SPT1010	2.56	SPT2010	1.99
400PP	--	SPT1020	2.89	SPT2020	1.98
600PP	0.67	SPT1030	2.75	SPT2030	2.27

**TABLE 8.6 Cross-over Frequency ( $\omega_c$ ) of Modified PPs (rad/s)**

Sample	$\omega_c$ (rad/s)	Sample	$\omega_c$ (rad/s)	Sample	$\omega_c$ (rad/s)
Montell PP	4.33	SPT505	18.72	SPT1505	30.24
Virgin PP	19.6	SPT510	16.55	SPT1510	24.26
50PP	26.87	SPT520	15.25	SPT1520	21.48
100PP	33.28	SPT530	14.04	SPT1530	21.06
150PP	41.02	SPT1005	24.53	SPT2005	44.28
200PP	49.18	SPT1010	20.81	SPT2010	36.95
400PP	86.32	SPT1020	17.87	SPT2020	28.88
600PP	115.30 <sup>1</sup>	SPT1030	16.29	SPT2030	26.53

1: Estimated by curve-fitting with 5th order polynomial

**TABLE 8.7 Cross-over Modulus ( $G_c$ ) of Modified PPs**

Sample	$G_c$ (KPa)	Sample	$G_c$ (KPa)	Sample	$G_c$ (KPa)
Montell PP	23.2	SPT505	22.0	SPT1505	23.5
Virgin PP	23.2	SPT510	19.7	SPT1510	24.8
50PP	23.4	SPT520	23.2	SPT1520	23.4
100PP	26.3	SPT530	21.4	SPT1530	23.1
150PP	24.8	SPT1005	24.3	SPT2005	23.5
200PP	26.9	SPT1010	22.0	SPT2010	25.7
400PP	29.6	SPT1020	22.4	SPT2020	23.3
600PP	26.9 <sup>1</sup>	SPT1030	20.5	SPT2030	22.8

1: Estimated by curve-fitting with 5th order polynomial

**TABLE 8.8 Polydispersity Index (PI) of Modified PPs**

Sample	PI	Sample	PI	Sample	PI
Montell PP	4.31	SPT505	4.56	SPT1505	4.24
Virgin PP	4.30	SPT510	5.09	SPT1510	3.99
50PP	4.28	SPT520	4.32	SPT1520	4.28
100PP	3.80	SPT530	4.69	SPT1530	4.34
150PP	4.04	SPT1005	4.12	SPT2005	4.25
200PP	3.72	SPT1010	4.31	SPT2010	3.90
400PP	3.38	SPT1020	4.73	SPT2020	4.29
600PP	3.62 <sup>1</sup>	SPT1030	4.87	SPT2030	4.40

1: Estimated by curve-fitting with 5th order polynomial

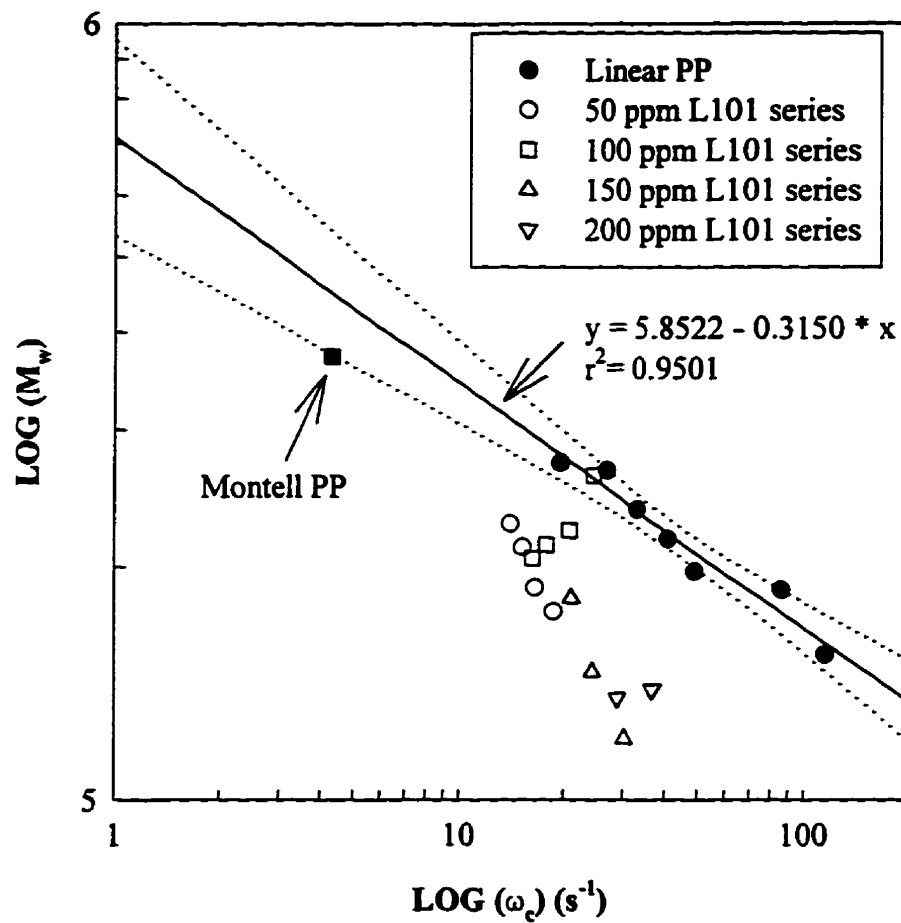


Fig. 8-18 Correlation between the crossover frequency  $\omega_c$  and weight average molecular weight for virgin PP, peroxide degraded PPs, Montell PP and PETA/peroxide modified PPs (solid line: the regression line for linear PPs; dashed lines: the regression interval at a 95% confidence level).



point for the Montell PP is on the regression interval and this further supports the previous speculation.

Table 8.9 summarizes the PDI (from GPC), PI (by crossover modulus technique), and Modsep (at 1000 Pa and 500 Pa) for linear PPs. Fig. 8-19 shows the relationship between

**Table 8.9 Polydispersity Measures of Modified PPs**

Polymer	$\bar{M}_w/\bar{M}_n$ from GPC	PI	Modsep @1000 Pa	Modsep @ 500 Pa
virgin PP	5.38	4.30	3.33	5.83
50PP	5.38	4.28	3.48	1.76
100PP	5.12	3.80	3.43	9.80
150PP	4.78	4.04	3.79	3.19
200PP	4.51	3.72	3.77	3.97
400PP	4.47	3.38	3.79	4.50
600PP	4.09	3.62	3.89	6.73

the PDI and PI for both linear and branched PP. For linear PP, the correlation is found as follows ( $r^2 = 0.6796$ ):

$$PI = 1.1138 + 0.5735 \times \frac{\bar{M}_w}{\bar{M}_n} \quad (8-6)$$

It can be seen that most of the data for branched PP deviate significantly from the regression line for linear PP. This may be another indication of branching since it has been known that rheological PI may come from two sources: MWD and LCB (Mavridis and Shroff, 1993). In the case of high density polyethylene (HDPE), increasing long chain branching results in

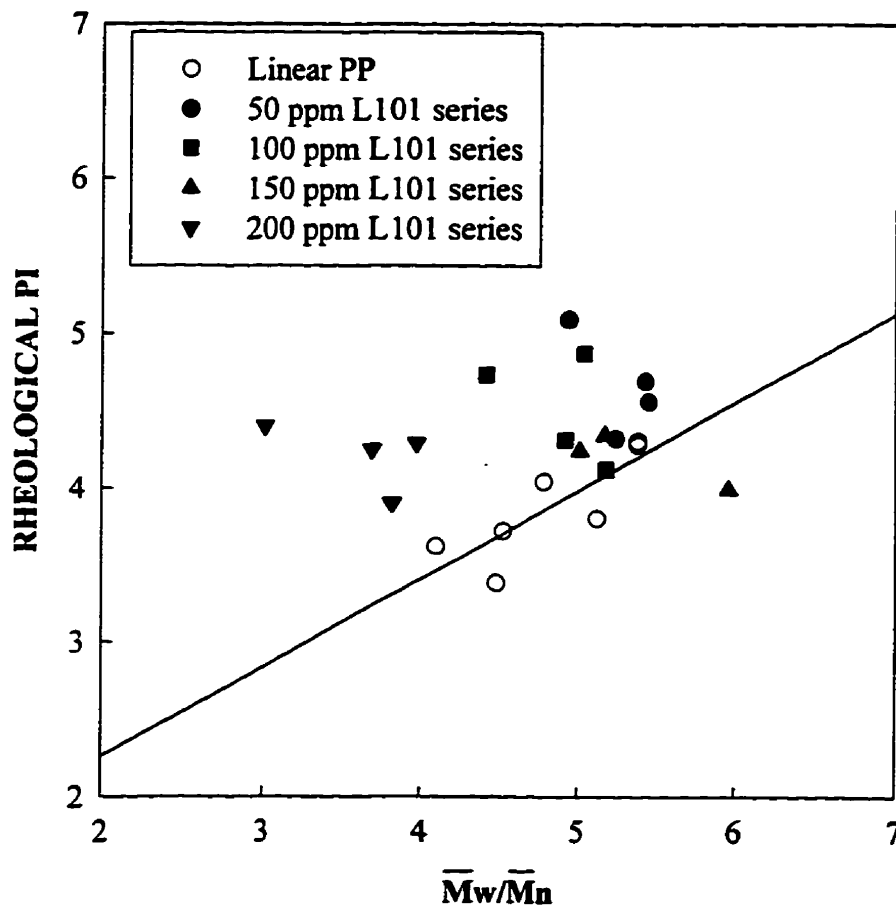


Fig. 8-19 Correlation between the rheological PI and polydispersity by GPC for virgin PP, peroxide degraded PPs, Montell PP and PETA/peroxide modified PPs.

an increase of rheological polydispersity (Mavridis and Shroff, 1993). For the PETA/peroxide modified PPs, the rheological PI is plotted versus the long chain branches per weight average molecule ( $n_w$ ) in Fig. 8-20. Overall, there is no clear correlation between these two parameters. It can still be seen, however, that roughly the increase in  $n_w$  leads to an increase in rheological PI in the 50 and 100 ppm peroxide series. Indeed, SPT510 and SPT1030 in our system have the highest rheological PI, which correspond to relatively high  $n_w$  and apparent elongational viscosity.

For linear PPs, the correlation between the PDI from GPC and Modsep at 1000 Pa (Fig. 8-21) is ( $r^2 = 0.8654$ ):

$$Modsep@1000Pa = 5.6374 - 0.4146 \times \frac{\bar{M}_w}{\bar{M}_n} \quad (8-7)$$

While it is found that Modsep at 500 Pa does not be correlated well with PDI data. Also, the correlation between rheological PI and Modsep at 1000 Pa (Fig. 8-22) is poor ( $r^2 = 0.4841$ ):

$$Modsep@1000Pa = 5.3678 - 0.4458 \times PI \quad (8-8)$$

### 8.3.3 Modified Cole-Cole Plot

Figs. 8-23 to 8-27 show the modified Cole-Cole plots for linear virgin PP, peroxide degraded PPs (linear), Montell PP and PETA/peroxide modified PPs (branched). Within the high moduli region, the data from both linear PP, branched PP and Montell PP form one single curve. Thus, the curve in the high moduli region is independent of large scale molecular structures (MW, MWD and LCB). The result is similar to that observed by Harrell and Nakajima (1984). This is not surprising since it has been justified that any measure derived from rheological data in such a way that the relaxation time is eliminated and only moduli are involved will be independent of molecular weight (Shroff and Mavridis, 1994)

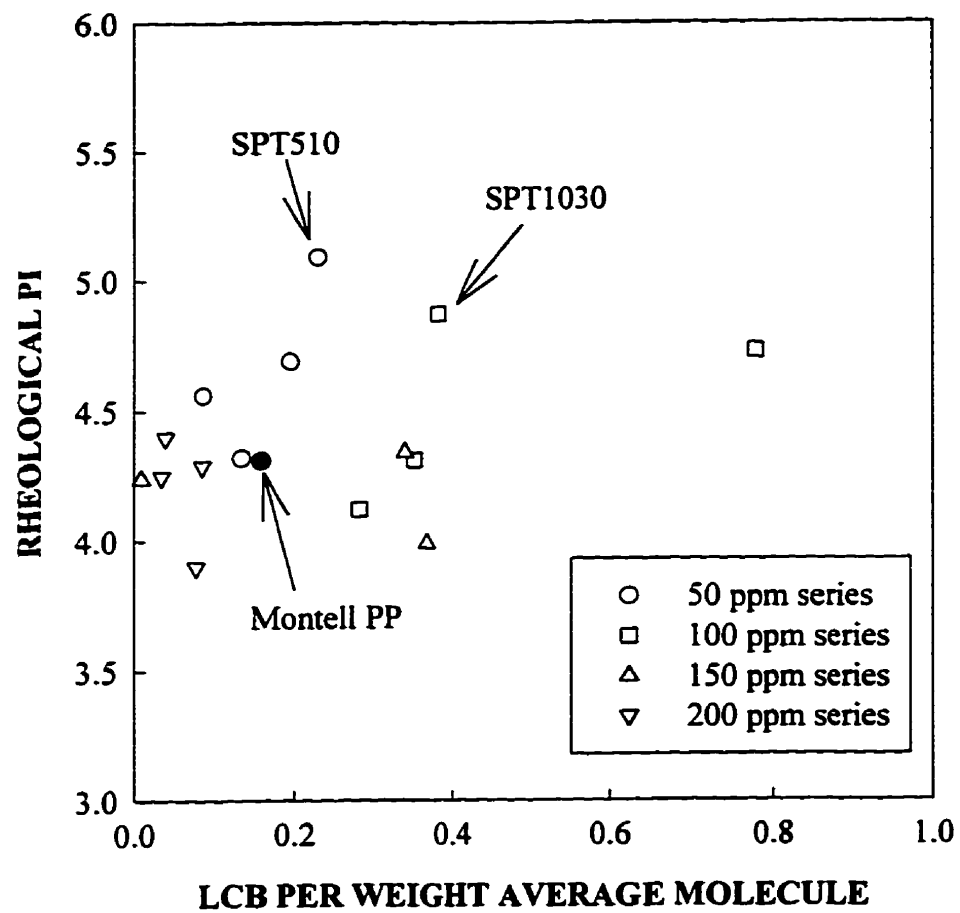


Fig. 8-20 Correlation between the rheological PI and LCB per weight average molecule for PETA/peroxide modified PPs.

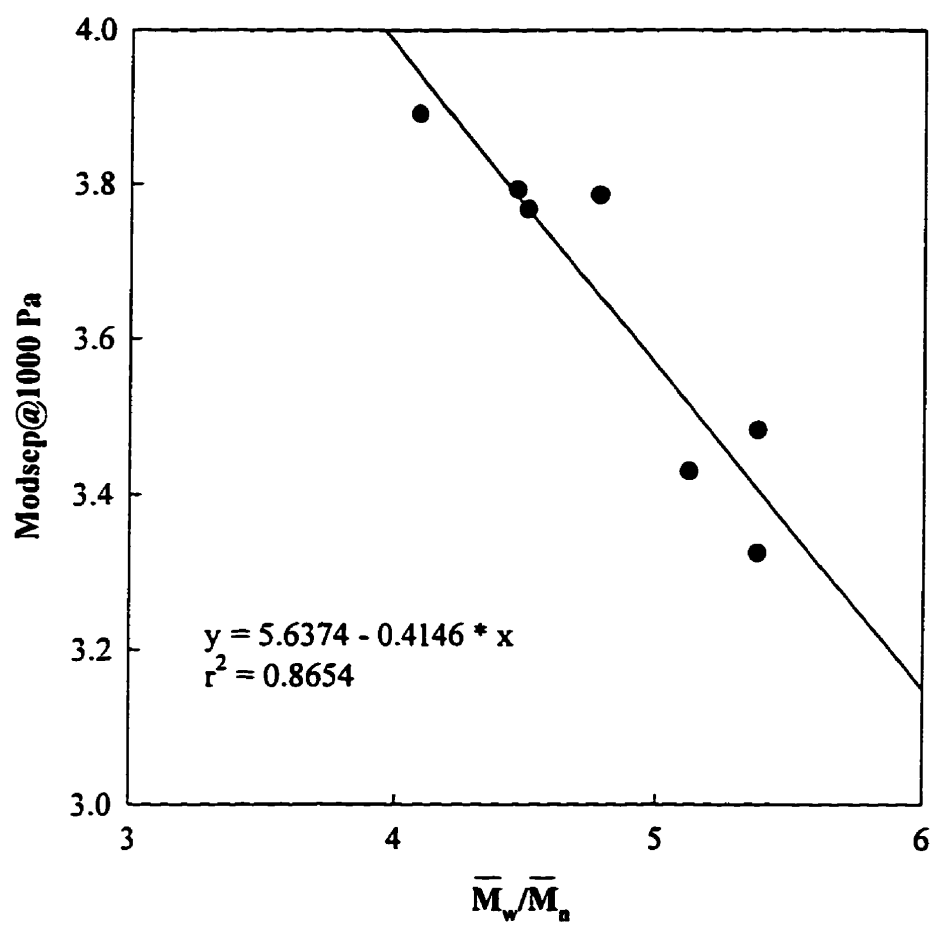


Fig. 8-21 Correlation between the Modsep at 1000 Pa and polydispersity by GPC for linear PP.

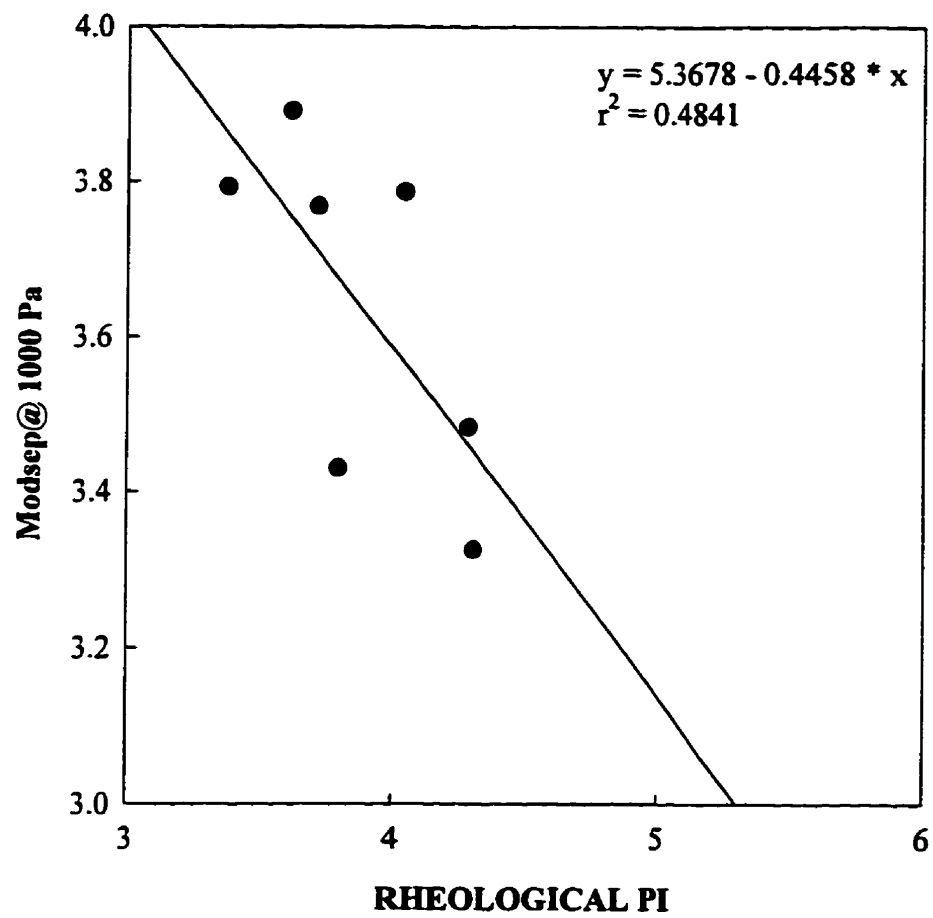


Fig. 8-22 Correlation between the Modsep at 1000 Pa and rheological PI for linear PP.

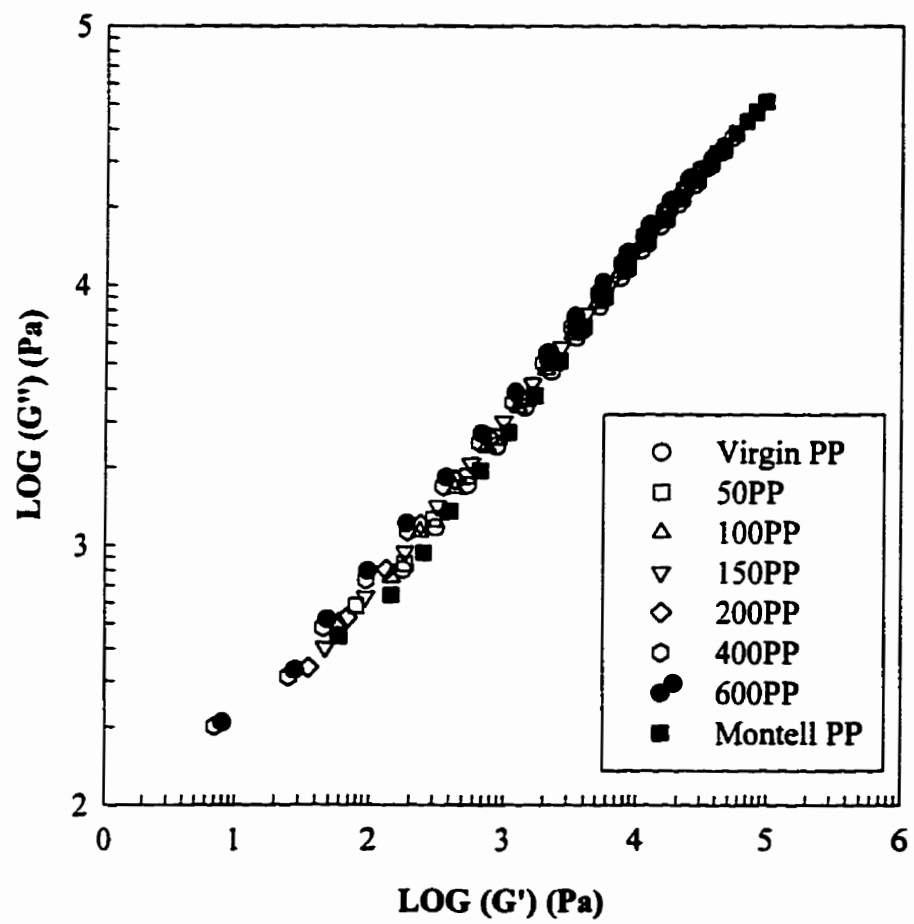


Fig. 8-23 Modified Cole-Cole plots of virgin, peroxide degraded and Montell PP.

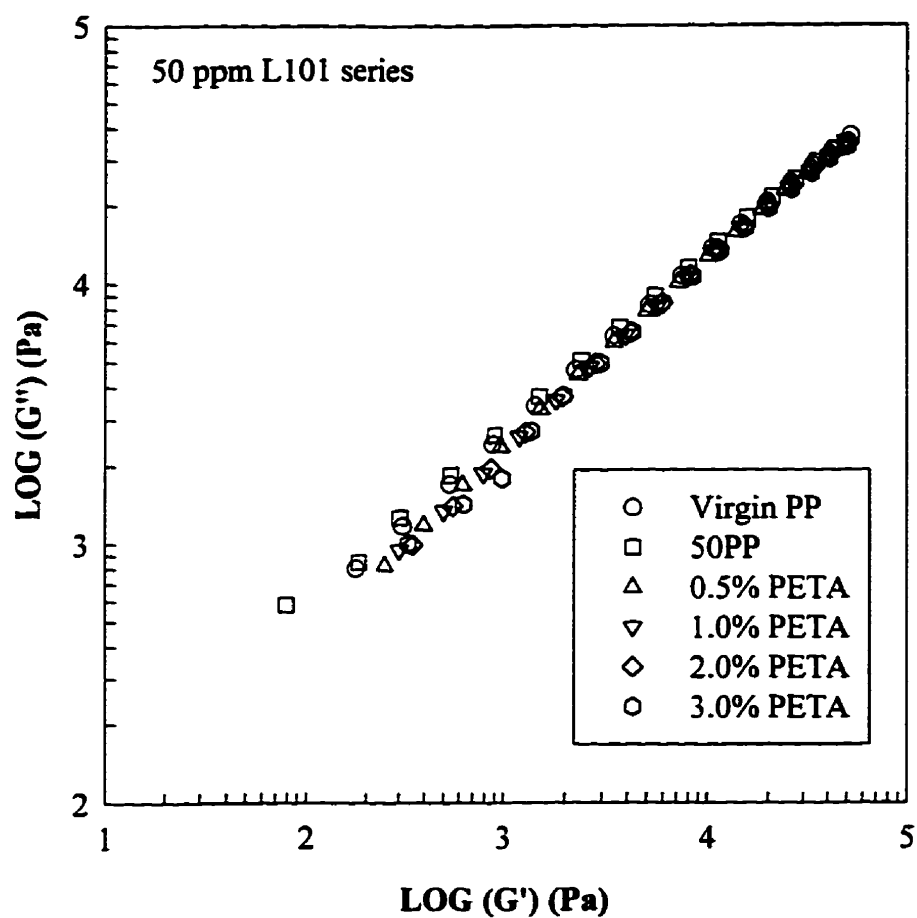


Fig. 8-24 Modified Cole-Cole plots of the PETA/peroxide modified PPs (50 ppm L101 series).



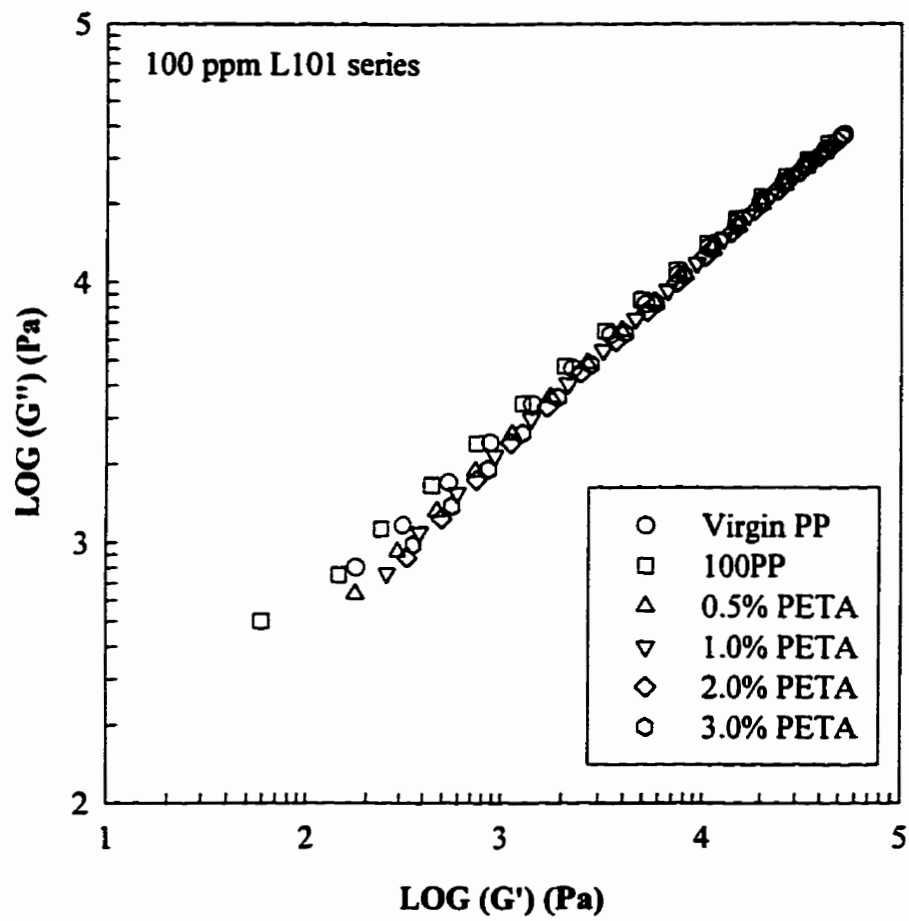


Fig. 8-25 Modified Cole-Cole plots of the PETA/peroxide modified PPs (100 ppm L101 series).

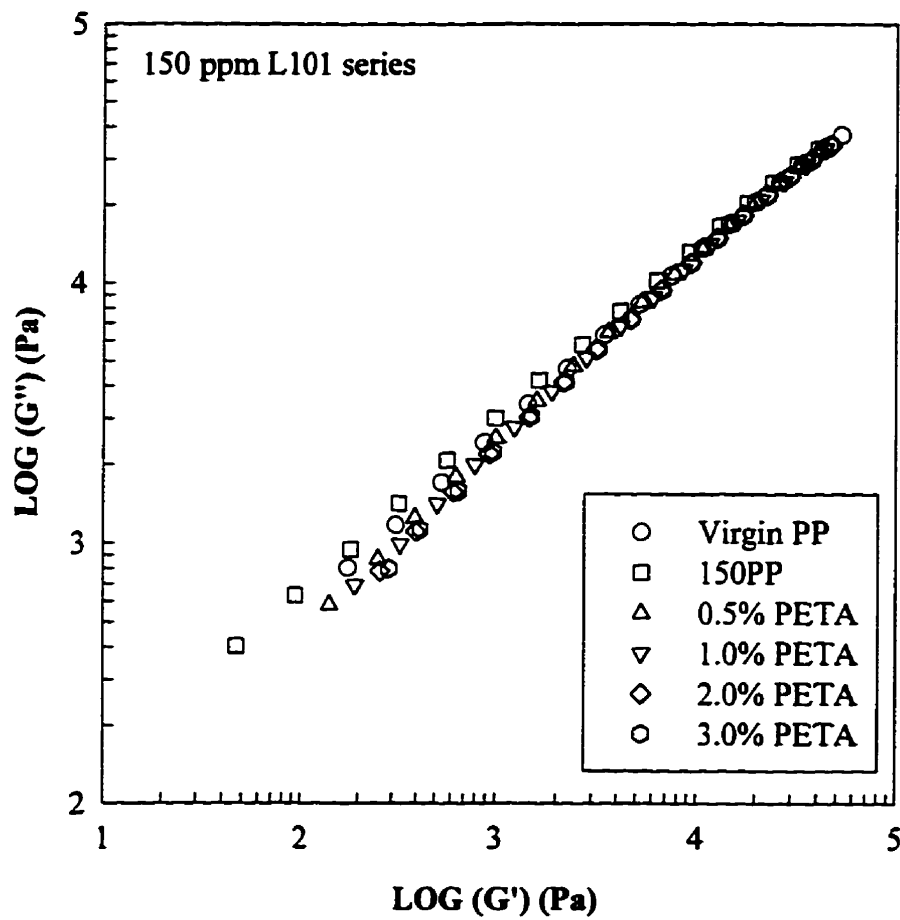


Fig. 8-26 Modified Cole-Cole plots of the PETA/peroxide modified PPs (150 ppm L101 series).

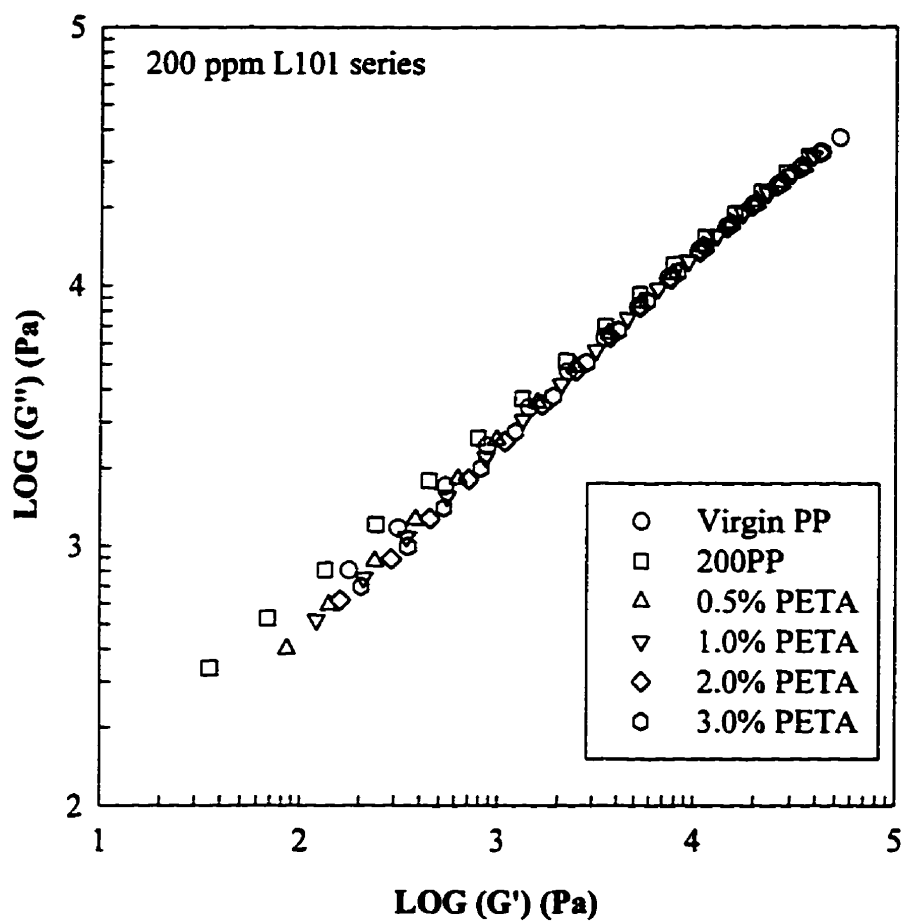


Fig. 8-27 Modified Cole-Cole plots of the PETA/peroxide modified PPs (200 ppm L101 series).

and this is the case of the modified Cole-Cole plot. From the molecular structure point of view, the high moduli region at high frequencies is related to the relaxation of short range segments, which may not be altered greatly by reactive extrusion due to the low peroxide and PETA concentrations used. It is also noted that in the work of Harrel et al. (1984), the single curve was obtained by varying the MW of linear polymers while keeping their MWDs and molecular structure invariant. In our system, the molecular weight, MWD and molecular architecture are all varying and this seems to support the structural point of view.

The rule of forming a single curve seems to break up at lower moduli region for most of the samples. The results of linear PPs and Montell PP are shown in Fig. 8-23. Within the whole moduli range examined, the data of 50PP and 100PP can be virtually reduced to one single curve with that of virgin PP. The Cole-Cole plot curves of linear PPs are shifting monotonically downwards with increasing PDI. Hence, for linear PPs, the broadening of MWD will shift the Cole-Cole plot to higher values of  $G'$  at constant values of  $G''$ . It can be seen that the curve of Montell PP is drifting further downwards, which is attributed to the existence of branching since this can not be explained by molecular weight distribution. However, the extent of LCB must be very low as it can be inferred from the results below.

Figs. 8-24 to 8-27 show the results of PETA/peroxide modified PPs. Within the low moduli region, all these plots lie under that of linear virgin PP, indicating that branching will shift the Cole-Cole plot to higher values of  $G'$  at constant values of  $G''$ . The reason why the existence of LCB is the dominant factor for this drifting comes from the fact that, some of the branched PPs have very similar MWD values (by GPC) to that of virgin PP yet their data lie far from it. It follows that for branched PPs, this distance (the data points from that of virgin PP at a low  $G'$ ) seems to reflect the extent of branching, at least qualitatively. This is supported by the following observation. At comparable  $G'$ , these distances for 50 and 100 ppm L101 series are larger than those for 150 and 200 ppm series, with 100 ppm series having the largest values. Again, this is well consistent with the LCB evaluation and apparent

elongational viscosity measurements. Note that this distance for Montell PP is much smaller even though it has a much higher  $\bar{M}_w$ . This fact certainly supports the justification that the modified Cole-Cole is independent of molecular weight and implies its very low level of LCB. This analysis is consistent with the GPC result.

Although the existence of LCB may be inferred roughly from the modified Cole-Cole plots, their low sensitivities to the degree of branching can still be seen in our system, since it is hard to distinguish these branched polymers within the same peroxide series. This may be caused by the current low frequency limit examined, or the difference in the extents of LCB is very small. Thus, more representations are shown below in order to look for the ones which are more sensitive to the change in molecular structures.

#### 8.3.4 Loss Tangent Versus Frequency ( $\tan\delta - \omega$ ) and Loss Tangent Versus Complex Modulus ( $\tan\delta - G^*$ )

The loss tangent,  $\tan\delta = G''/G'$ , is a measure of the ratio of energy lost to energy stored in a cyclic deformation. Fig. 8-28 shows the logarithmic plots of  $\tan\delta$  versus  $\omega$  for the virgin PP, peroxide degraded PPs and Montell PP. The  $\tan\delta$  is decreased with increasing molecular weight and the broadening of MWD, indicating the increasing ability to store elastic energy. With the changes, the  $\tan\delta$  is also more sensitive to  $\omega$ . Note that the  $\tan\delta$  of Montell PP is much lower than those of linear PPs.

Figs. 8-29 to 8-32 show the  $\tan\delta - \omega$  plots for the PETA/peroxide modified PPs, which reveal the distinct difference between them and linear PPs. It can be found that most of these samples have lower  $\tan\delta$  than that of virgin PP, suggesting the higher ability for storing elastic energy. This is attributed to branching as inferred from the information of their MW and MWD. However, some samples such as SPT1505, SPT2005 and SPT2010, seem to have higher  $\tan\delta$  than that of virgin PP. The reason for this is that besides the effects of LCB and MWD, the representation of  $\tan\delta$  versus  $\omega$  is also dependent on molecular weight and this

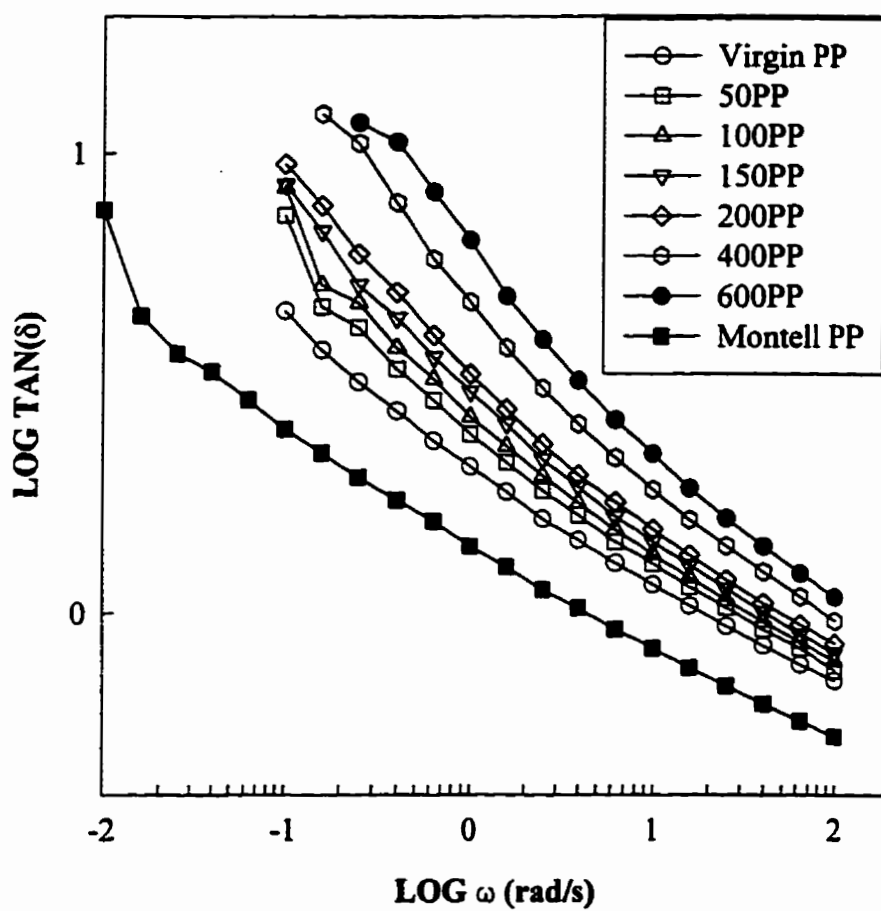


Fig. 8-28 The representations of loss tangent versus frequency ( $\tan\delta-\omega$ ) for virgin PP, peroxide degraded PPs and Montell PP.

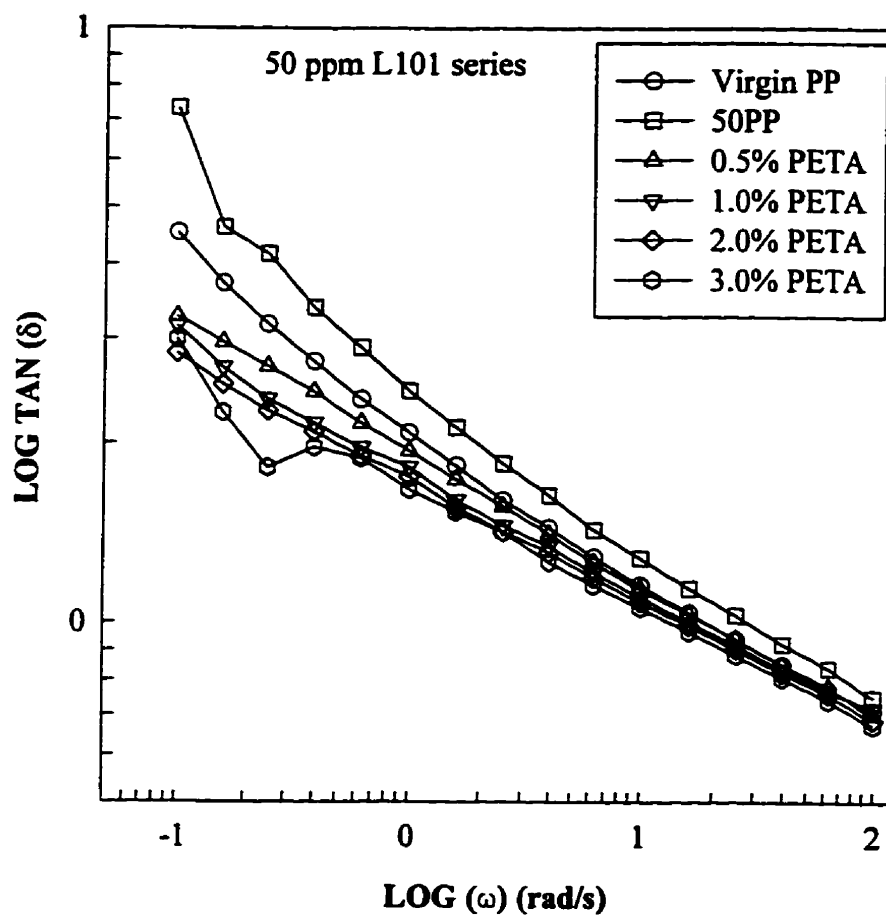


Fig. 8-29 The representations of loss tangent versus frequency ( $\tan\delta-\omega$ ) for the PETA/peroxide modified PPs (50 ppm L101 series).

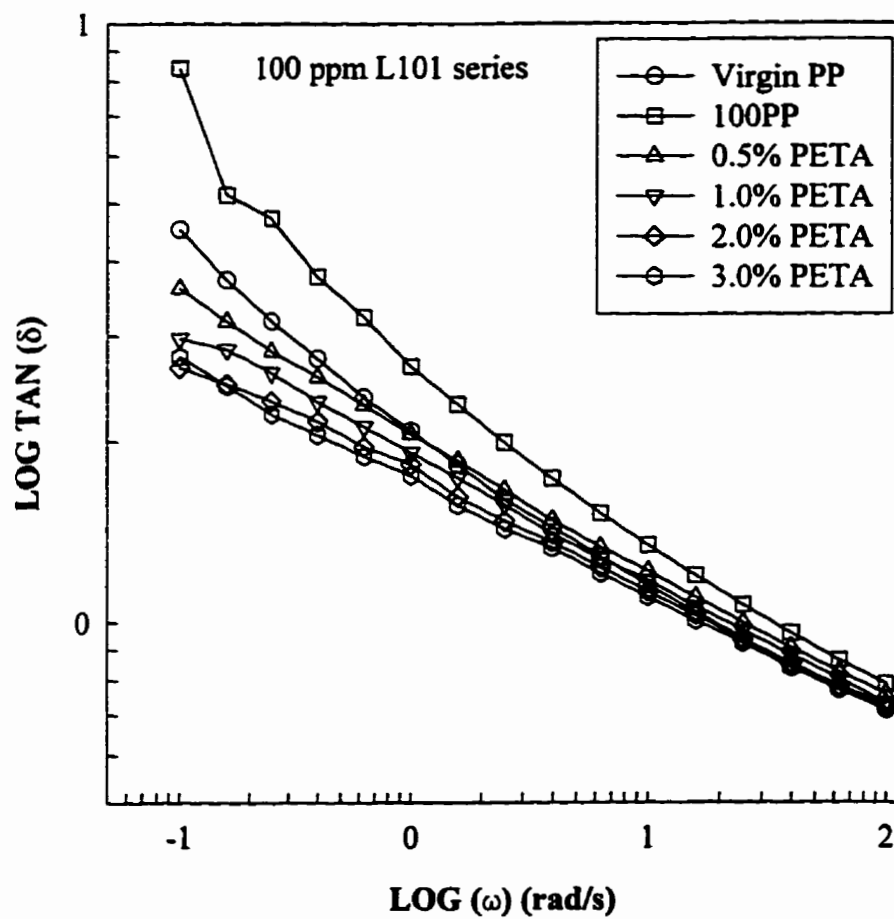


Fig. 8-30 The representations of loss tangent versus frequency ( $\tan\delta-\omega$ ) for the PETA/peroxide modified PPs (100 ppm L101 series).



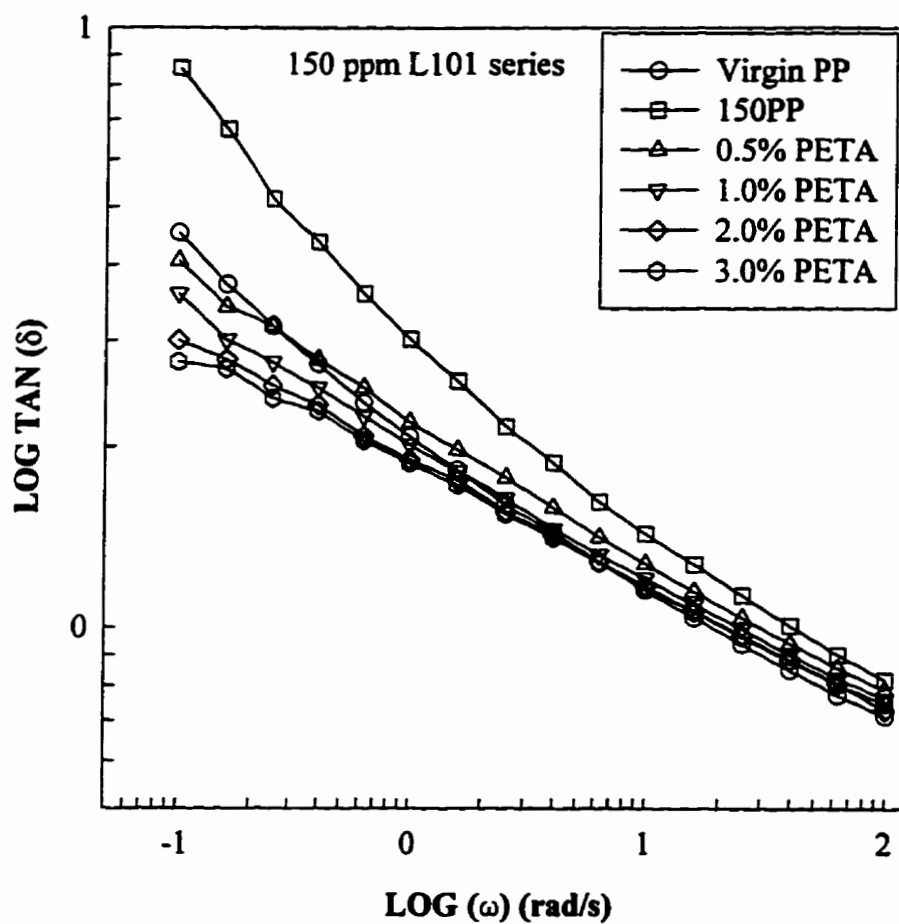


Fig. 8-31 The representations of loss tangent versus frequency ( $\tan\delta-\omega$ ) for the PETA/peroxide modified PPs (150 ppm L101 series).

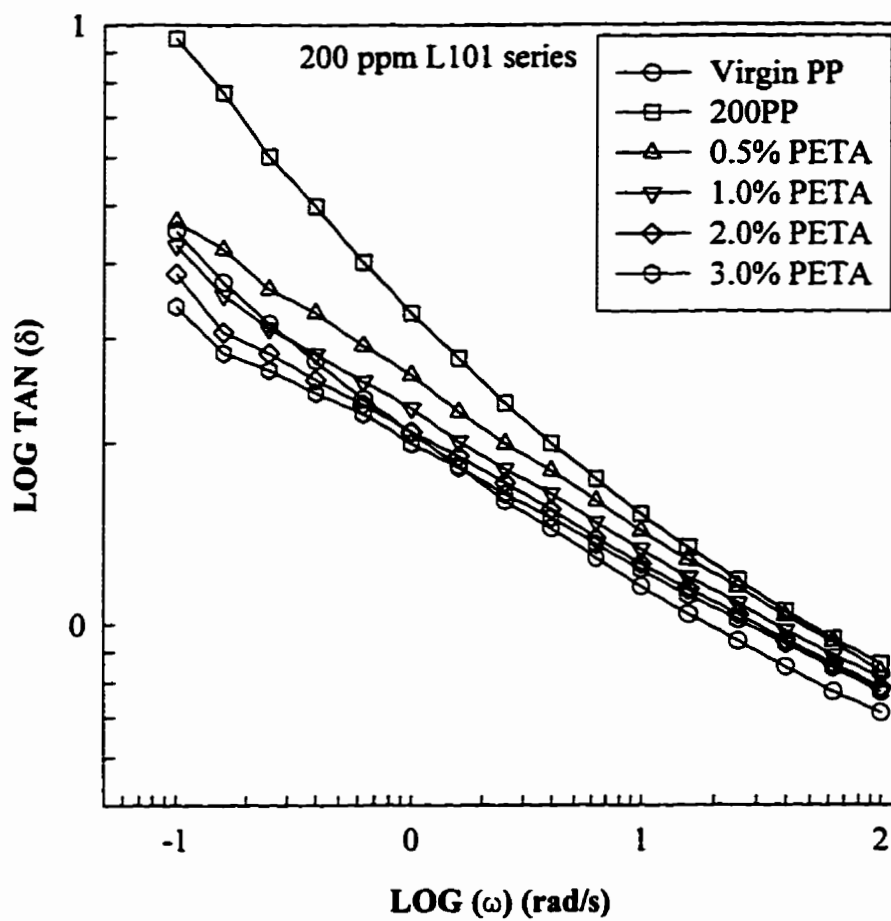


Fig. 8-32 The representations of loss tangent versus frequency ( $\tan\delta-\omega$ ) for the PETA/peroxide modified PPs (200 ppm L101 series).

can be supported by observing the position of the curve for Montell PP.

As suggested by Shroff and Mavridis (1994), the plot of  $\tan\delta$  versus  $G^*$  ( $G^* = [G'^2 + G''^2]^{1/2}$ ) is independent of molecular weight and sensitive to the differences in polydispersity. It should be pointed out that in our system, effects are due both MWD and LCB. The plots are shown in Figs. 8-33 to 8-37. As one compares Fig. 8-23 with Fig. 8-33 for the linear PPs and Montell PP, it seems that the  $\tan\delta$ - $G^*$  representation has a better discrimination sensitivity than the Modified Cole-Cole plot. Similar improvements are also observed in the other corresponding plots. For linear PPs, the curve is drifting upwards with increasing PDI and indicates that the broadening of MWD will shift the curve to lower values of  $\tan\delta$  at constant values of  $G^*$ . Similar to the observation in the modified Cole-Cole plot, it can be inferred that the existence of LCB is the dominant factor for this drifting. For example, the SPT505 (very low concentrations of PETA and peroxide) and virgin PP have very similar PDI values. However, they show two distinct curves at low  $G^*$ . Again, the independence of the molecular weight for this type of representation can be inferred from the curve position of Montell PP and its high weight average molecular weight. However, the moduli at lower  $\omega$  are still needed to differentiate the samples at the same peroxide levels.

### 8.3.5 Dynamic Storage Compliance versus Storage Modulus ( $J'$ - $G'$ )

The dynamic storage compliance  $J'(\omega) = G'(\omega)/[G'(\omega)^2 + G''(\omega)^2]$ , defined as the strain in a sinusoidal deformation in phase with the stress divided by the stress, is also a measure of the energy stored and recovered per cycle. Rochefort et al. (1979) plotted  $J'(\omega)$  versus  $G'(\omega)$  to show the viscoelastic difference of linear and model star-branched polymers. The reason for this plotting is that the storage modulus  $G'(\omega)$  is a monotonic function of  $\omega$  and is a more convenient plotting variable than  $\omega$  since, when temperature-frequency superposition is obeyed, Plots of  $J'(\omega)$  versus  $G'(\omega)$  should be practically independent of temperature. Similar plots are constructed for our samples in Figs. 8-38 to 8-42. Again, it can

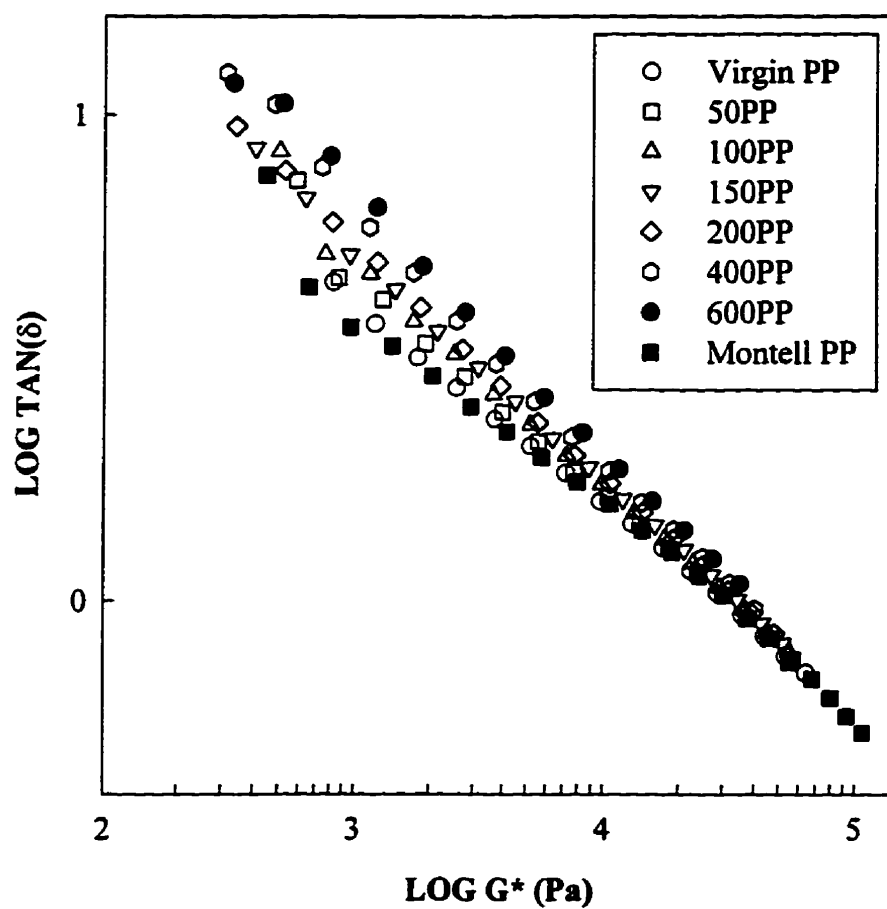


Fig. 8-33 The representations of loss tangent versus complex modulus ( $\tan\delta$ - $G^*$ ) for virgin PP, peroxide degraded PPs and Montell PP.

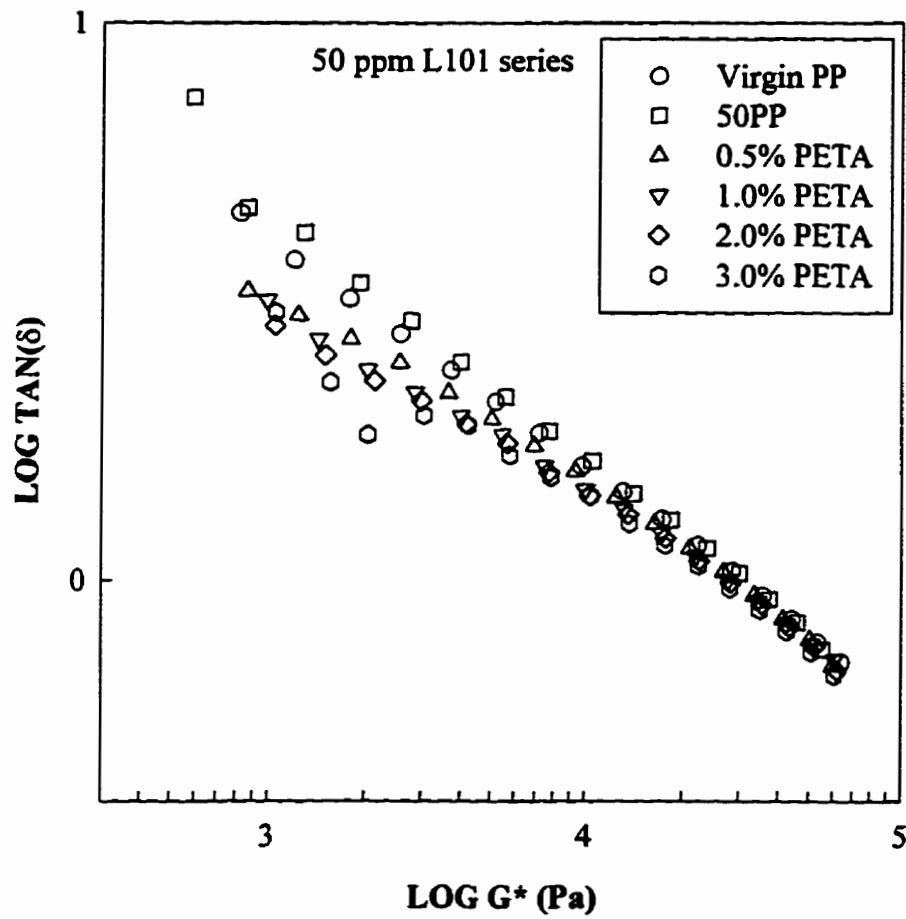


Fig. 8-34 The representations of loss tangent versus complex modulus ( $\tan\delta$ - $G^*$ ) for the PETA/peroxide modified PPs (50 ppm L101 series).

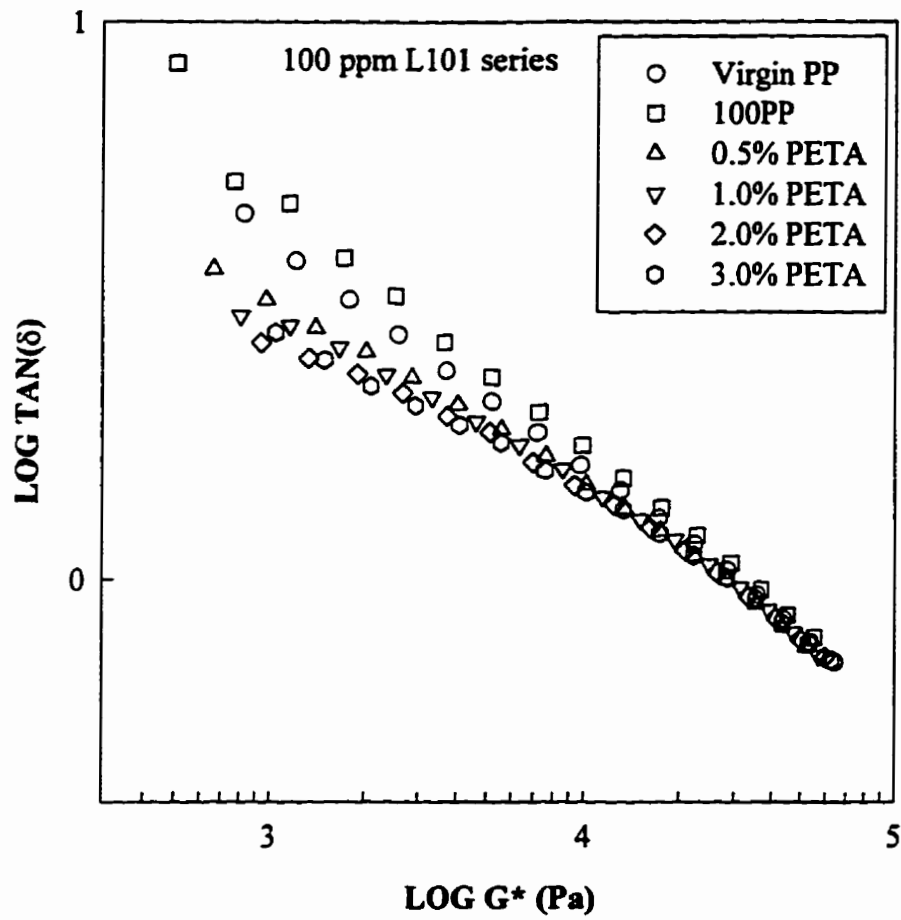


Fig. 8-35 The representations of loss tangent versus complex modulus ( $\tan\delta$ - $G^*$ ) for the PETA/peroxide modified PPs (100 ppm L101 series).

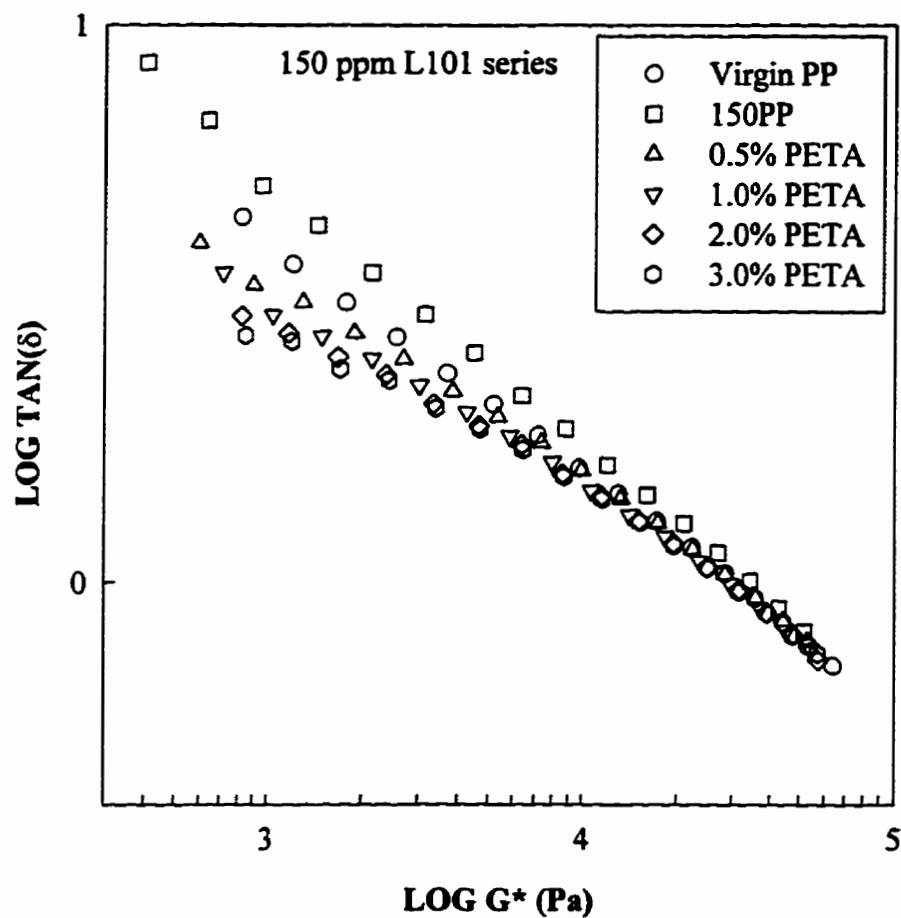


Fig. 8-36 The representations of loss tangent versus complex modulus ( $\tan\delta$ - $G^*$ ) for the PETA/peroxide modified PPs (150 ppm L101 series).

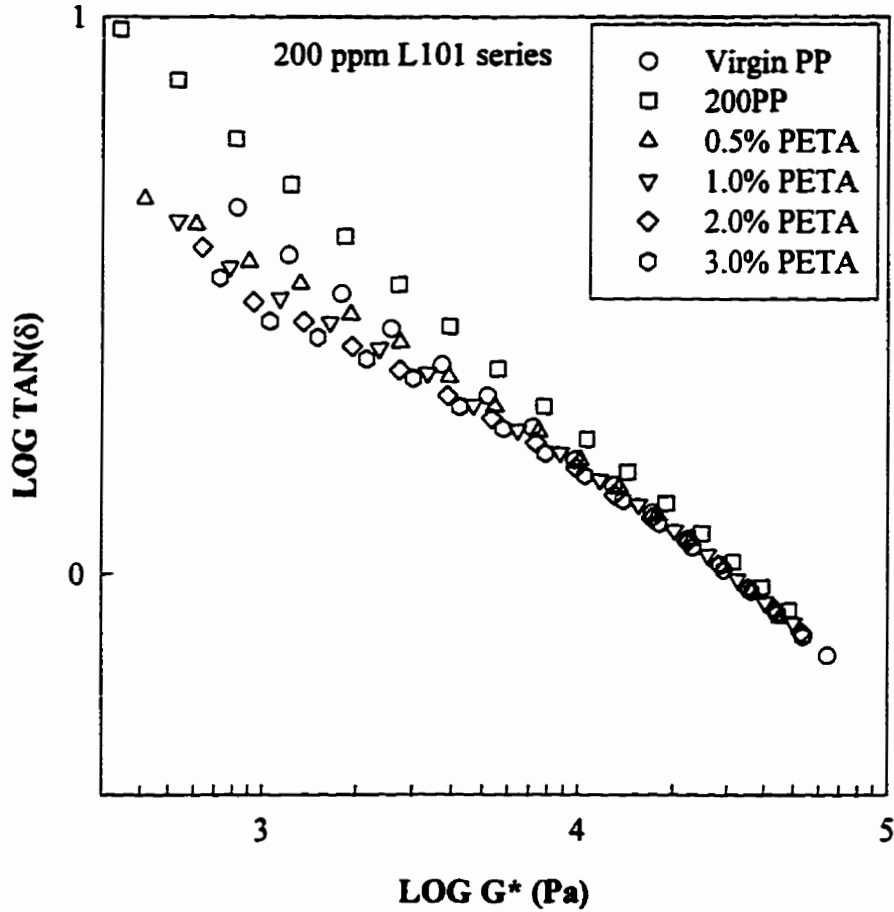


Fig. 8-37 The representations of loss tangent versus complex modulus ( $\tan\delta$ - $G^*$ ) for the PETA/peroxide modified PPs (200 ppm L101 series).



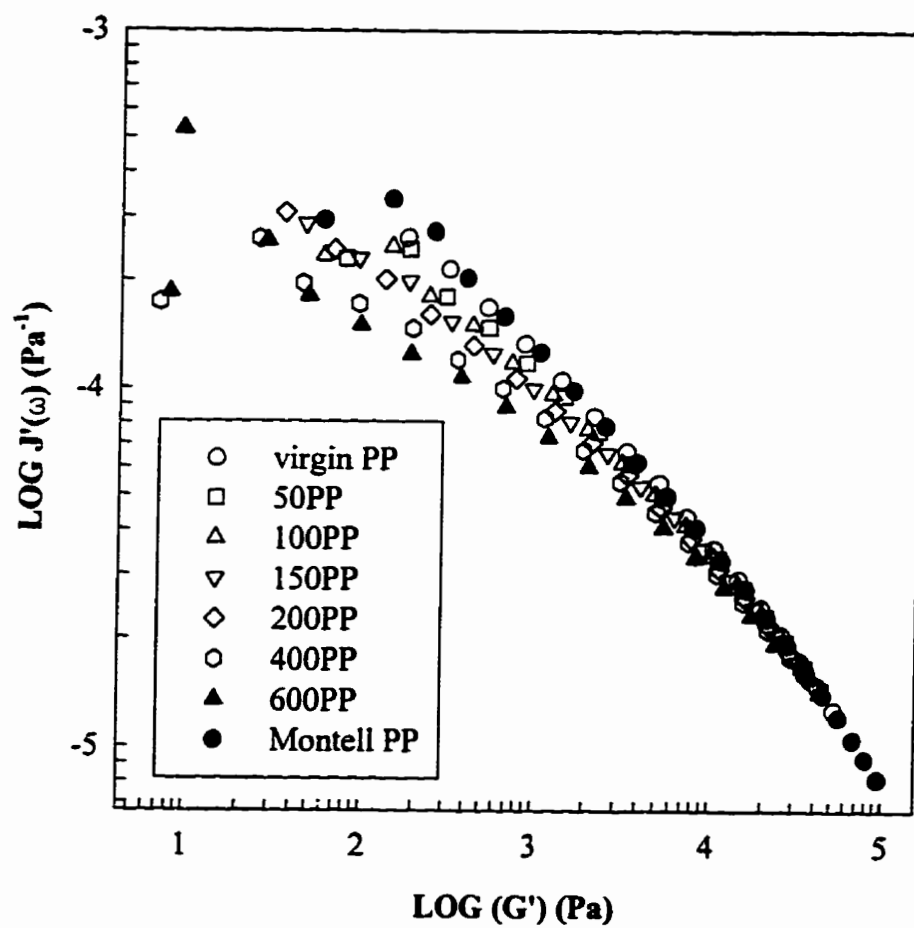


Fig. 8-38 The representations of storage compliance versus storage modulus ( $J'$ - $G'$ ) for virgin PP, peroxide degraded PPs and Montell PP.

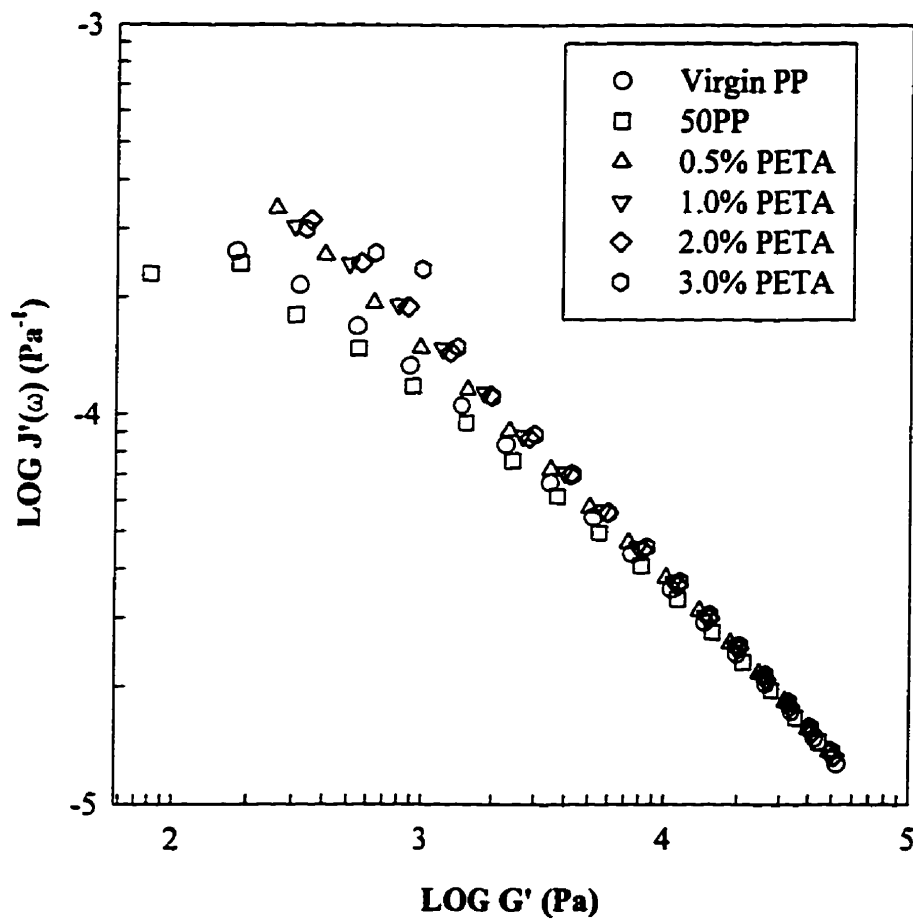


Fig. 8-39 The representations of storage compliance versus storage modulus ( $J'$ - $G'$ ) for the PETA/peroxide modified PPs (50 ppm L101 series).

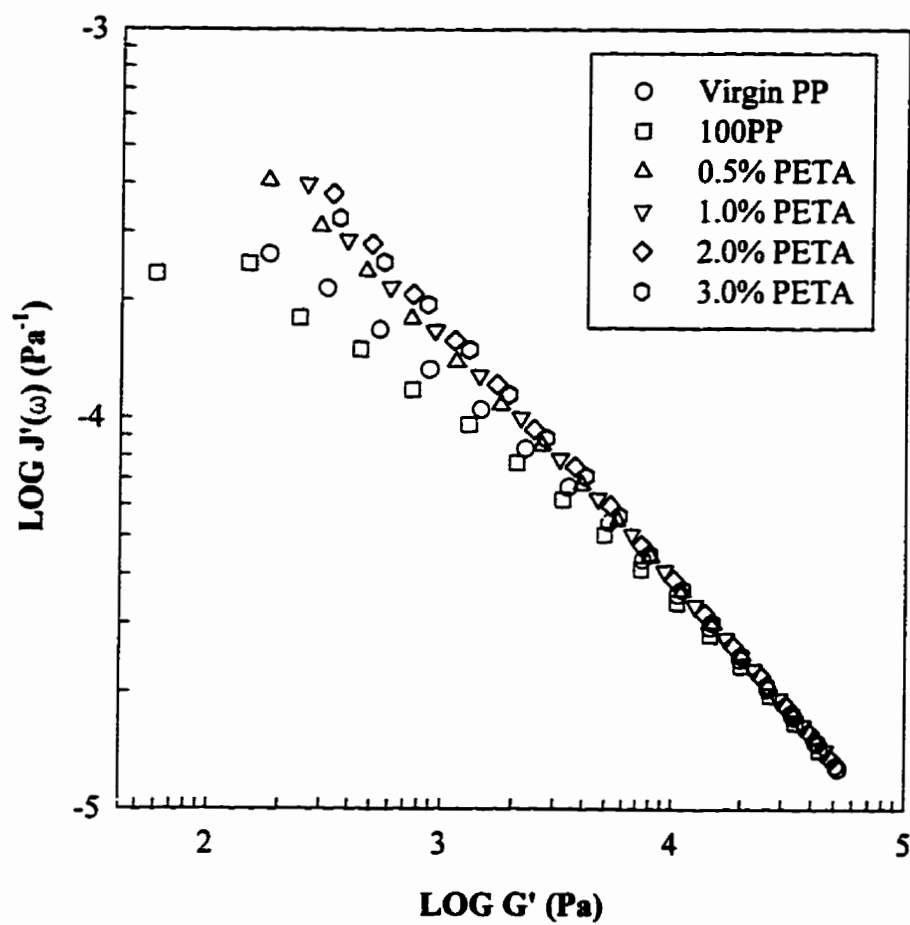


Fig. 8-40 The representations of storage compliance versus storage modulus ( $J'$ - $G'$ ) for the PETA/peroxide modified PPs (100 ppm L101 series).

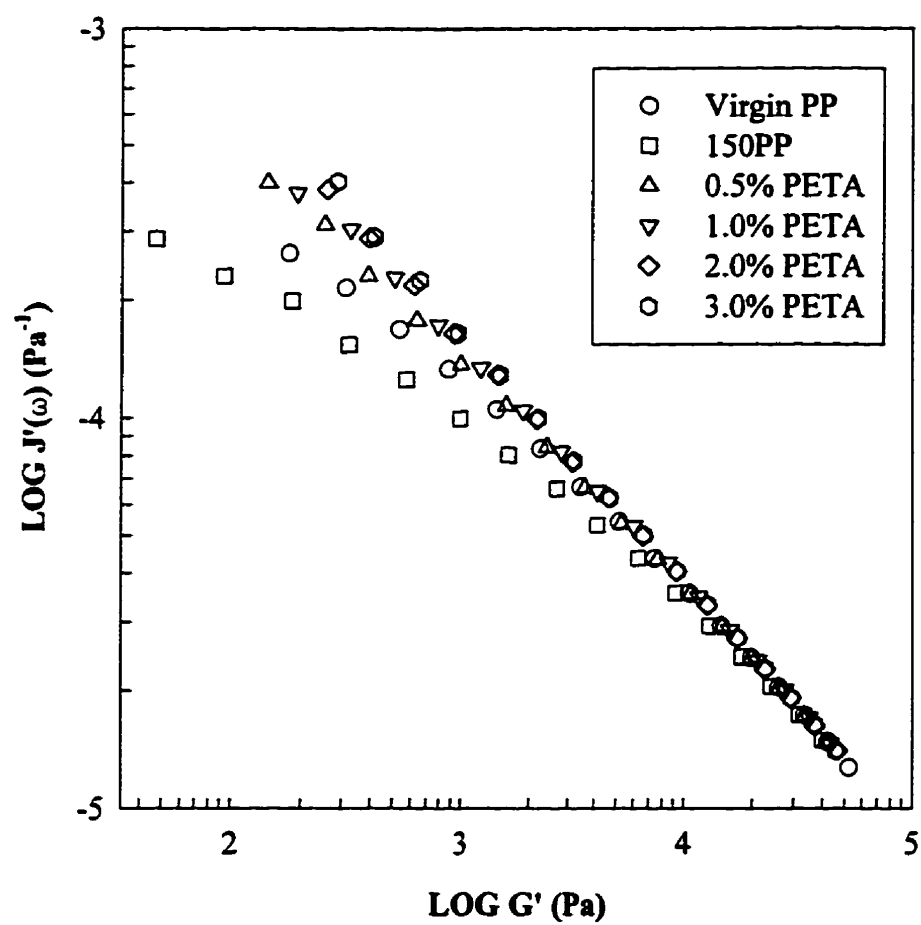


Fig. 8-41 The representations of storage compliance versus storage modulus ( $J'$ - $G'$ ) for the PETA/peroxide modified PPs (150 ppm L101 series).

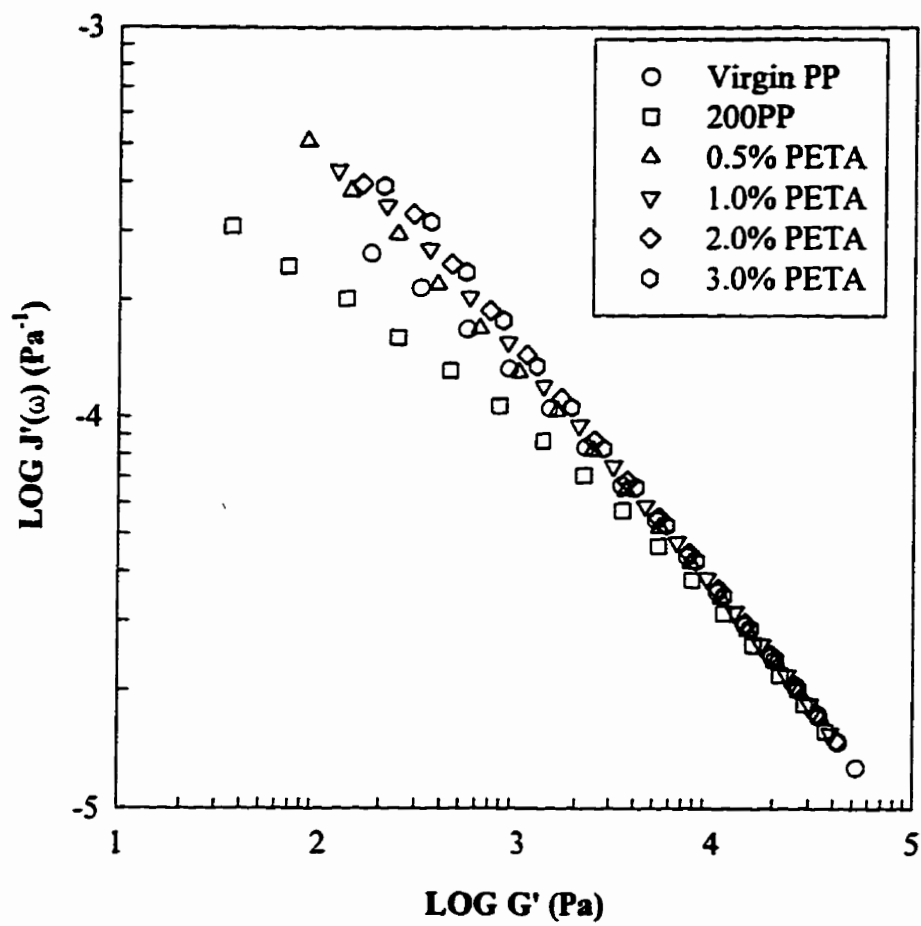


Fig. 8-42 The representations of storage compliance versus storage modulus ( $J'$ - $G'$ ) for the PETA/peroxide modified PPs (200 ppm L101 series).

be observed that the plot is independent of molecular weight. Its discrimination sensitivity is better than that of the modified Cole-Cole plot and similar to that of the  $\tan\delta$ - $G^*$  representation. With increasing PDI, linear PP has a larger storage compliance at a constant low storage modulus. From the MWD data, it can be inferred that for branched PP, branching is the predominant factor in determining the position of the curve. Generally, the storage compliance at a constant low storage modulus will be increased with increasing the extent of branching.

#### 8.4 Conclusions

Most of PETA/peroxide modified PPs show higher  $\eta_0$ s than that of linear virgin PP though they exhibit lower  $\bar{M}_w$ s, which suggests the existence of long chain branching in these polymers. For linear PPs, the relationship between the  $\eta_0$  and  $\bar{M}_w$  can be described by the general equation for linear polymers. It is found that the  $\eta_0$ s of all PETA/peroxide modified PPs are considerably larger than the equivalent linear PPs at a similar  $\bar{M}_w$ , further suggesting that the long chain branches exist in these polymers. The relationship between the  $\eta_0$  and  $\bar{M}_w$  of Montell PP is not significantly different from that of linear PP.

The  $G$ 's at low frequencies of many of these modified PPs are larger than that of virgin PP, which is caused by long chain branching. The slower relaxations of these branched polymers are indicated by both the smaller slopes of  $G'$  and  $G''$  curves at low frequencies and larger relaxation constants estimated. All these significant differences from the rheological properties of linear PPs can not be completely explained by using only their MW and MWD data, suggesting that the PETA/peroxide modified PPs are long chain branched polymers. For PETA/peroxide modified PPs, the structure of short chain segments of PP may not be altered greatly when very low concentrations of PETA and peroxide were used.

A single modified Cole-Cole curve can be formed within the high moduli region,

which is independent of molecular weight (MW), molecular weight distribution (MWD) and molecular architecture. Within the low moduli region, the modified Cole-Cole plot is still independent of molecular weight. For linear PPs, the broadening of MWD will shift the plot to higher  $G'$  at a constant  $G''$ . For branched PPs in our system, long chain branching (LCB) is found to be the dominant factor for this shifting. Roughly, the increasing extent of LCB will shift the plot to higher  $G'$  storage modulus at a constant  $G''$ . The increase in the long chain branches per weight average molecule ( $n_w$ ) seems to result in an increase in rheological polydispersity in the most branched materials in our system.

Although the representation of loss tangent ( $\tan\delta$ ) versus frequency ( $\omega$ ) may reflect the rheological change caused by MWD and LCB, it is also dependent on molecular weight. Thus, this representation is not unique to the change of molecular architecture. Similar to the modified Cole-Cole plot, the one of loss tangent ( $\tan\delta$ ) versus complex modulus ( $G^*$ ) is independent of molecular weight but has a better discrimination sensitivity than the former. For linear PPs, the broadening of MWD shifts the curve to lower values of  $\tan\delta$  at constant values of  $G^*$ . For branched PPs in our system, the existence of LCB is the dominant factor for this drifting. The increase of branching will shift the curve to lower values of  $\tan\delta$  at constant values of  $G^*$ . The representation of storage compliance ( $J'$ ) versus storage modulus ( $G'$ ) has very similar characteristics to the one of  $\tan\delta$  vs.  $G^*$ .

The three representations shown are all sensitive to the existence of LCB, i.e., having high sensitivity to distinguish branched PP from linear ones. However, for better discrimination sensitivity to the differences among branched PPs, lower moduli, i.e., lower angular frequency data should be considered. Finally, the linear viscoelastic properties in our system are in agreement with other results in terms of the effect of LCB.

## **CHAPTER 9**

### **CONCLUSIONS AND RECOMMENDATIONS**

Long chain branched polypropylenes have been produced by reactive extrusion (REX) and the thermal, rheological and molecular properties of the modified PPs have been fully characterized. For the long chain branched samples, it is found that there is good agreement among the results from GPC, thermal properties, apparent elongational viscosity, flow activation energy, and linear viscoelastic properties.

Two reaction routes have been used in this work. In the first route, model branched polypropylenes were produced by the reaction of acrylic acid grafted PP with hexadecylamine in solution and REX. It was found that the attachment of the alkyl chains lowers the glass transition, melting and crystallization temperatures of PP, and increases the moduli and shear viscosity. However, the branch length introduced is relatively short in terms of the long chain branching (LCB) concept.

In the second reaction route, the possibility of producing long chain branched PP was explored through the reactions of a commercial linear PP with a polyfunctional monomer (PETA) and a peroxide (Lupersol 101) by REX in two stages. Preliminary experiments were carried out in the first stage, using an unstabilized linear PP with relatively high concentrations of peroxide (200, 600, and 1000 ppm) and PETA (0-5 wt.%). From the shear viscosity enhancement, FTIR spectra and thermal properties of the products, it was inferred that branching structures may exist in these modified PPs.

Based on the results of stage 1, REX experiments were carried out in the second stage, using stabilized linear PP with very low concentrations of peroxide (50 - 200 ppm) and PETA (0 - 3%wt.). Soxhlet extraction shows that most of these products have low levels of macrogels. DSC results indicate that the majority of macrogel formed during REX in stage



2 is PETA homopolymer. The coexistence of crosslinking structures was suggested by the higher thermal stability of the sols from these PETA/peroxide modified PPs, compared to that of virgin PP. The high melting points of the macrogels also imply that the crosslinking density in the sols of the PETA/peroxide modified PPs is low. Generally, the sols from the PETA/peroxide modified PPs have higher melting and crystallization temperatures than those of linear PPs. The thermal behaviours of branched/lightly crosslinked PPs seem different from those of randomly branched PPs.

Long chain branching information has been obtained using a high temperature GPC. From the combined results of average  $g'$ ,  $[\eta]$ ,  $\lambda$  and  $n_w$  of the whole GPC samples, the viscosity law plot,  $g'$  distribution, long chain branching frequency per 1000 C ( $\lambda$ ), GPC analysis determines that there is virtually no long chain branching in virgin linear PP and peroxide-degraded PPs. For the long chain branched PP produced in our work, the average LCB frequency for the whole sample is estimated to be from 0.01 to 0.05 LCB/1000C, which corresponds to about 0.2 to 0.8 branches per weight average molecule. The commercial branched PP from Montell has a much higher  $\bar{M}_w$  than those of all the samples in our system and may contain a low LCB level.

The molecular weight averages in peroxide-degraded polypropylenes decrease with increasing peroxide concentration. However, the change in the molecular weight averages with PETA and peroxide concentration in the PETA/peroxide reaction system seems nonmonotonic and it depends on PETA/peroxide relative concentrations. It is found that all the PETA/peroxide modified PPs have smaller  $\bar{M}_n$  and  $\bar{M}_w$  than those of the virgin PP but some samples have  $\bar{M}_z$ s similar to that of the virgin PP. There is some broadening in the high molecular weight end in some long chain branched samples. Experimental results also suggest that there is a certain relationship between the inverse MFI and  $\bar{M}_w$  for linear polypropylenes. However, this does not apply for their long chain branched counterparts.

The results of apparent elongational viscosity and flow activation energy seem consistent with the GPC results. Most of the PETA/peroxide modified PPs produced in the second stage have higher flow activation energies at constant shear stresses and higher elongational viscosities than linear PPs, which has been attributed to the existence of LCB.

Linear viscoelastic properties of the branched PPs produced, are also in agreement with the GPC and apparent elongational viscosity results. The  $\eta_0$ s of all PETA/peroxide modified PPs are considerably larger than the equivalent linear PPs at a similar  $\bar{M}_w$ , suggesting the existence of LCB in these polymers. For linear PPs, the relationship between the  $\eta_0$  and  $\bar{M}_w$  can be described by the general equation for linear polymers but this is not the case for branched PPs. It is found that the relationship between the  $\eta_0$  and  $\bar{M}_w$  of Montell branched PP is not significantly different from that of linear PP.

The G's at low frequencies of many of these modified PPs are larger than that of virgin PP, which is caused by long chain branching. These branched polymers also show slower relaxations, which are indicated by the smaller slopes of G' and G'' curves at low frequencies, and larger relaxation constants. The increase in the  $n_w$  (long chain branches per weight average molecule) seems to result in an increase in rheological polydispersity in the most branched materials of our system.

Three molecular-weight-independent representations, i.e., modified Cole-Cole plot, plots of loss tangent ( $\tan\delta$ ) versus complex modulus ( $G^*$ ) and storage compliance ( $J'$ ) versus storage modulus ( $G'$ ), have been constructed in order to detect the effects of MWD and LCB. In the case of modified Cole-Cole plot, for linear PPs, the broadening of MWD will shift the plot to higher G' at a constant G''. For branched PPs in our system, LCB is found to be the dominant factor for this shifting. Roughly, the increasing extent of LCB will shift the plot to higher G' storage modulus at a constant G''.

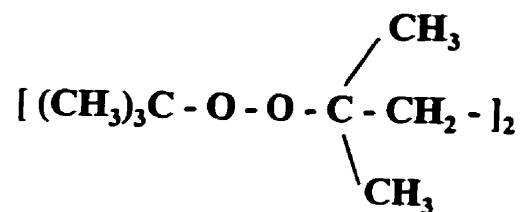
The representation of loss tangent ( $\tan\delta$ ) versus complex modulus ( $G^*$ ) seems to

have a better discrimination sensitivity than the modified Cole-Cole plot. For linear PPs, the broadening of MWD shifts the curve to lower values of  $\tan\delta$  at constant values of  $G^*$ . For branched PPs in our system, the existence of LCB is the dominant factor for this drifting. The increase of branching will shift the curve to lower values of  $\tan\delta$  at constant values of  $G^*$ . The plot of storage compliance ( $J'$ ) versus storage modulus ( $G'$ ) has very similar characteristics to the one of  $\tan\delta$  vs.  $G^*$ . For these three representations, however, lower angular frequency data should be considered for better discrimination sensitivity to the differences among branched PPs. Experimental results also indicate that GPC may not be as sensitive as the rheological measurements in terms of the sensitivity to differentiate linear and branched polymers.

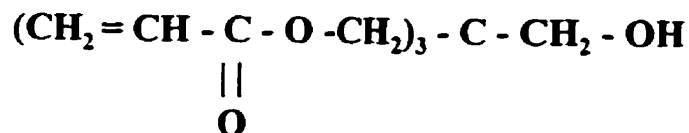
Future experiments can be carried out at a lower REX temperature (170-180°C) which is slightly higher than the melting temperature of linear PP, in order to further minimize degradation and increase the chance to form long chain branches. A higher molecular-weight virgin PP should be used. It is expected that the elongational viscosity of the modified PP can be further enhanced remarkably by satisfying these two conditions. Other combinations of polyfunctional monomers and peroxides can also be tried, such as a peroxide with a longer half life of decomposition. Steady-state elongational viscosity and strain hardening behaviour can be measured using an elongational rheometer. Linear viscoelastic properties at a broader frequency range (from  $10^3$  to  $10^5$  rad/s) should be obtained in order to differentiate better between the branching features among the modified PPs and estimate the plateau modulus. This could be achieved by using the time-temperature superposition principle. Dynamic mechanical properties can be measured in order to determine the effects of crosslinking and long chain branching. The sols can be fractionated and then analyzed in order to reduce the effect of molecular weight distribution.

APPENDIX A

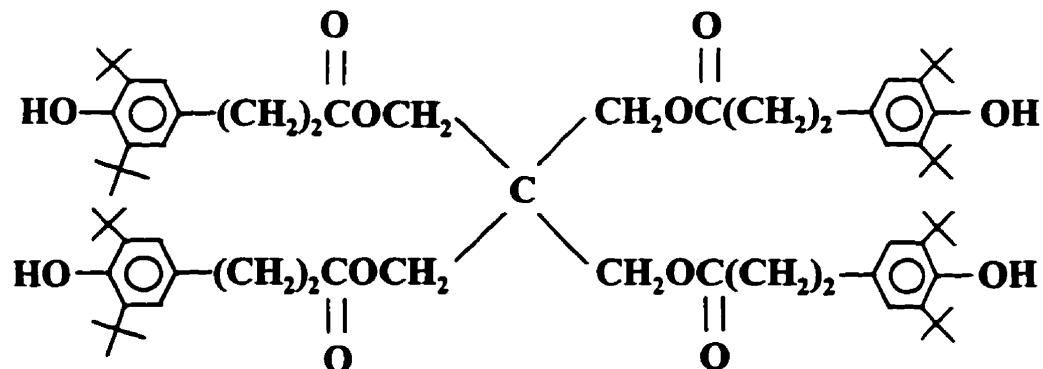
CHEMICAL STRUCTURES OF LUPERSOL 101, PENTAERYTHRITOL  
TRIACRYLATE AND IRGANOX 1010



Lupersol 101



Pentaerythritol Triacrylate (PETA)



Irganox 1010

## APPENDIX B

### Molecular Weight Averages and Mark-Houwink Constants (K and $\alpha$ ) Measured by GPC for Virgin PP and Peroxide-degraded PPs

For PP homopolymers, a wide range of K is described between  $10^{-4}$  to  $7.4 \times 10^{-4}$  dl/g, while a value of the  $\alpha$  exponent was proposed between 0.5 to 0.8, with a mean value in the range of 0.7 to 0.75 (Karger-Kocsis, 1995). Different values of K and  $\alpha$  were used by different authors for linear polypropylene, even when using the same temperature and same kind of solvent. For example, at 135°C and by using 1,2,4-trichlorobenzene (TCB), a K value of  $1.90 \times 10^{-4}$  dl/g and a  $\alpha$  value of 0.725 were used by Lederer et al. (1994), while a K value of  $1.50 \times 10^{-4}$  dl/g and a  $\alpha$  value of 0.757 were used by DeNicola et al. (1992). The average molecular weight averages, branching index, intrinsic viscosity, K and  $\alpha$  for virgin PP, 100PP and other peroxide-degraded PPs in this thesis are summarized as follows. The K and  $\alpha$  values were obtained within the good data region. The m is the mean and the  $\sigma$  is one standard deviation. The average values of K and  $\alpha$  seems relatively reasonable within the range of literature data reported.

#### 1. Molecular Parameters of Virgin PP

Sample	$M_n$ $\times 10^2$	$M_w$ $\times 10^2$	$M_w/M_n$	$M_z$ $\times 10^2$	$g'$	$[\eta]$ (dl/g)	K (dl/g) $\times 10^{-4}$	$\alpha$
1	518	2,797	5.40	10,359	0.896	1.4689	2.26	0.725
2	494	2,647	5.36	9,703	0.895	1.5780	0.79	0.809
average	506	2,722	5.38	10,031	0.896	1.5234	1.52	0.767

## APPENDIX B (continued)

## 2. Molecular Parameters of 100PP

Sample	$M_n$ $\times 10^2$	$M_w$ $\times 10^2$	$M_w/M_n$	$M_z$ $\times 10^2$	$g'$	$[\eta]$ (dl/g)	$K$ (dl/g) $\times 10^{-4}$	$\alpha$
1	461	2,380	5.17	8,087	0.998	1.2088	14.6	0.557
2	459	2,363	5.05	8,558	0.914	1.3105	2.75	0.711
3	471	2,376	4.78	8,406	0.911	1.2499	2.44	0.713
m	464	2,373	5.12	8,350	0.941	1.2564	6.60	0.661
$\pm \sigma$	$\pm 6$	$\pm 9$	$\pm 0.06$	$\pm 240$	$\pm 0.049$	$\pm 0.0512$	$\pm 6.93$	$\pm 0.090$

3. Summary of  $K$  and  $\alpha$  for Virgin PP and Peroxide Degraded PPs

Sample	$K$ (dl/g) $\times 10^{-4}$	$\alpha$
Virgin PP-1	2.26	0.725
Virgin PP-2	0.79	0.809
50PP	5.45	0.640
100PP-1	14.6	0.557
100PP-2	2.75	0.711
100PP-3	2.44	0.713
150PP	7.83	0.621
200PP	3.51	0.488
400PP	2.09	0.719
600PP	9.77	0.600
m $\pm \sigma$	$5.15 \pm 4.35$	$0.658 \pm 0.095$

## REFERENCES

- Abramowicz, M. A. and Hallden-Abberton, M. P., "Reactive Extrusion- An Alternative to Reactor Polymerization", *Abstracts of Papers of the American Chemical Society*, Vol. 203, April, pp. 15, Tech. (1992)
- Agarwal, P. K., Bagley, E. B., and Hill, C. T., "Viscosity, Modulus and Die Swell of Glass Bead Filled Polystyrene-Acrylonitrile Copolymer", *Polym. Eng. Sci.*, 18, 282(1978)
- Allen, N. S., ed., "Degradation and Stabilization of Polyolefins", Applied Science Publ., New York, 1983, p. 72
- Armat, R. and Moet, A., "Morphological origin of toughness in polyethylene-nylon-6 blends", *Polymer*, 34(5), 977(1993)
- Bagley, E. B., "The Separation of Elastic and Viscous effects in Polymer Flow", *Trans.Soc.Rheol.*, 5, 355(1961)
- Benoit, H. C., Grubisic, Z., Rempp, P., Decker, D., and Zilliox, J. G., *J. Chem. Phys.*, 63, 1507(1966)
- Berry, G.C., "Thermodynamic and Conformational Properties of Polystyrene. III Dilute Solution Studies on Branched Polymers", *J. Polym. Sci.*, A2, 9, 687(1971)
- Bershtein, V. A. and Egorov, V. M., *Differential Scanning Calorimetry of Polymers: Physics, Chemistry, Analysis, Technology*, Ellis Horwood, Great Britain, 1994
- Bersted, B. H., "On the Effects of Very low Levels of Long Chain Branching on Rheological Behaviour in Polyethylene", *J. Appl. Polym. Sci.*, Vol.30, 3751(1985)
- Bersted, B. H., "Refinement of the Converging Flow Method of Measuring Extensional Viscosity in Polymers", *Polym. Eng. Sci.*, 33(16), 1079(1993)
- Bestul, A. B. and Belcher, H. V., "Temperature Coefficients of Non-Newtonian Viscosity at Fixed Shearing Stress and at Fixed Rate of Shear", *J. Polym. Phys.*, 24, 696(1953)
- Billiani, J. and Lederer, K., "Polypropylene Characterization by High Temperature SEC

- Coupled with LALLS", *J. Liquid Chromatography*, 13(15), 3013(1990)
- Borsig, E., Fiedlerová, A., and Lazár, M., "Efficiency of Chemical Cross-Linking of Polypropylene", *Macromol. Sci.-Chem.*, A16(2), 513(1981)
- Borsig, E., Fiedlová, A., Rychlá, L. And Lazár, M., "Crosslinking of Polypropylene-Polyethylene Blends by Peroxide and the Effect of Pentaerythritol Tetraallyl Ether", *J. Appl. Polym. Sc.*, 7, 467(1989)
- Borsig, E., Čapla, M., Fiedlová, A. and Lazár, M., "Cross-linking of Polypropylene Using a System Consisting of Peroxide and Thiourea or Its Derivatives", *Polym. Commun.*, 31(7), 293(1990)
- Borsig, E., Malcherová, E. and Lazár, M., "Cross-linking of Atactic Polypropylene by the System Peroxide-Pentaerythritol Tetraallyl Ether", *Polym. Int.*, 30(3), 367-370(1993)
- Bowmer, T. N. and O'Donnell, J. H., "Nature of the side chain branches in low density polyethylene: volatile products from gamma radiolysis", *Polymer*, 18, 1033(1977)
- Bradley, M. B. and Phillips, E. M., "Novel Polypropylenes for Foaming on Conventional Equipment", *Plastics Engineering*, March, 82(1991)
- Brady, J. M. and Thomas, E. L., "Effect of Short-chain Branching on the Morphology of LLDPE-Oriented Thin Films", *J. Polym. Sci.: Part B: Polymer Physics*, 26, 2385(1988)
- Bremner, T., Cook, D. G. and Rudin, A., "Melt Flow Index Values and Molecular Weight Distributions of Commercial Thermoplastics" *J. Appl. Polym. Sci.*, 41, 1617(1990)
- Brown, S. Bruce, Chapter 4 in "Reactive Extrusion: Principles and Practice", edited by Xanthos, M., Hanser, New York (1992)
- Brydson, J. A., *Flow Properties of Polymer Melts*, 2nd ed., George Godwin Limited, 1981
- Bueche, F. and Harding, S. W., "A New Absolute Molecular Weight For Linear Polymers", *J. Polym. Sci.*, 32, 177(1958)
- Bueche, F., "Viscosity of Molten Branched Polymers and Their Concentrated Solutions",



- J. Chem. Phys.*, 40, 484(1964)
- Bugada, D. C. and Rudin, A., "Branching in Low Density Polyethylene by  $^{13}\text{C}$ -NMR", *Eur. Polym. J.*, 23(10), 809(1987)
- Carr, M. E., Kim, S., Yoon, K. J. and Stanley, K. D., "Graft-Polymerization of Cationic Methacrylate, Acrylamide, and Acrylonitrile Monomers onto Starch by Reactive Extrusion", *Cereal Chemistry*, 69(1), 70(1992)
- Chang, F. C. and Hwu, Y. C., "Styrene Maleic Anhydride and Styrene Glycidyl Methacrylate Copolymers as In Situ Reactive Compatibilizers of Polystyrene/Nylon 6,6 Blends", *Polym. Eng. Sci.*, 31(21), 1509(Mid-November, 1991)
- Channell, A. D. and Clutton, E. Q., "The effects of short chain branching and molecular weight on the impact fracture toughness of polyethylene", *Polymer*, 33(19), 4109(1992)
- Chapiro, A., *Radiation Chemistry of Polymeric Systems*, Wiley, New York, 1962. Chap.IX.
- Chartoff, R. P. and Maxwell, B., "Dynamic Mechanical Properties of Polymer Melts: The Dependence of Viscoelastic Properties on Molecular Weight Distribution", *Polym. Eng. Sci.*, 9, 159(1969)
- Chen, C., Nguyen, K. T., Sanschagrin, B., and Piché, L., "Characterization of Controlled-Degradation Polypropylene", *ANTEC 94*, San Francisco, May 1-5, Vol.1, 2041 (1994)
- Cheng, S.Z.D., Janimak, J. J. and Rodriguez, J., Chapter 2: Crystalline structures of polypropylene homo- and copolymers, in *Polypropylene: Structure, blends and composites*. Edited by Karger-Kocsis, J., Chapman & Hall, London, 1995
- Chen, L., Hu, G. H., Lindt, J. T., "Acceleration of Chemical Reaction in Reactive Extrusion Accompanied by Devolatilization", *ANTEC '96*, p.295
- Chiang, W.Y. and Yang, W.D., "Polypropylene Composites. I. Studies of the Effect of Grafting of Acrylic Acid and Silane Coupling Agent on the Performance of

- Polypropylene Mica Composites", *J. Appl. Polym. Sci.*, 35, 807(1988)
- Chodák, I. and Lazár, M., "Effect of the Type of Radical Initiator on Cross-linking of Polypropylene", *Die Angew. Makromol.Chem.*, 106, 153(1982)
- Chodák, I. and Zimányová, E., "The Effect of Temperature on Peroxide Initiated Cross-linking of Polypropylene", *Eur. Polym. J.*, 20(1), 81(1984)
- Chodák, I. and Lazár, M., "Peroxide-Initiated Cross-linking of Polypropylene in the Presence of P-Benzoquinone", *J. Appl. Polym. Sci.*, 32(6), 5431(1986a)
- Chodák, I. and Matisovarychla, L., "Thermo-oxidative Stability of Crosslinked Polypropylene", *Polym. Degra. Stab.*, 16(3), 213(1986b)
- Chodák, I., Lazár, M. and Čapla, M., "Cross-linking of Polypropylene Initiated by Peroxide in the Presence of Thiourea as a Coagent", *J. Polym. Sci.: Part A, Polym. Chem.*, 29(4), 581(1991)
- Cogswell, F. N., "Converging Flow of Polymer Melts in Extrusion Dies", *Polym. Eng. Sci.*, 12(1), 64(1972)
- Colthup, N. B., Daly, L. H. and Wiberley, S. E., "Introduction to Infrared and Raman Spectroscopy", 3rd Edition, Academic Press, Inc., 1990
- Combs, R. L., Slonaker, D. F. and Jr. Coover, H. W., "Effects of Molecular Weight Distribution and Branching on Rheological Properties on Polyolefin Melts", *J. Appl. Polym. Sci.*, 13, 519(1969)
- Conley, R. T., *Thermal Stability of Polymers*, Vol.1, Marcel Dekker Inc., New York, 1970
- Coudray, S., Pascault, J.P., and Taha, M., "Acrylated polyurethanes by reactive extrusion", *Polymer Bulletin*, 32, 605(1994)
- Cox, W. P. and Merz, E. H., "Correlation of Dynamic and Steady Flow Viscosity", *J. Polym. Sci.*, 28, 619(1958)
- Dagli, S. S., Xanthos, M. and Biesenberger, J. A., "Blends of Nylon-6 and Polypropylene

- with Potential Applications in Recycling - Effects of Reactive Extrusion Variables on Blend Characteristics", *ACS Symposium Series*, Vol. 513, 241(1992)
- De Candia, F., Romano, G., Vittonia, V. and Chodák, I., "Drawing Behaviour of Crosslinked Isotactic Polypropylene", *Colloid. Polym. Sci.*, 268(7), 625(1990)
- Defoor, F., Groeninckx, G., Schouterden, P. and Van der Heijden, B., "Molecular, thermal and morphological characterization of narrowly branched fractions of 1-octene linear low density polyethylene: 1. Molecular and thermal characterization", *Polymer*, 33(18), 3878(1992a)
- Defoor, F., Groeninckx, G., Schouterden, P. and Van der Heijden, B., "Molecular, thermal and morphological characterization of narrowly branched fractions of 1-octene linear low-density polyethylene: 2. Study of the lamellar morphology by transmission electron microscopy", *Polymer*, 33(24), 5186(1992b)
- DeNicola, A. J., Galambos, A. F. and Wolkowicz, M. D., *Polymeric Materials Science and Engineering*, Vol. 67, Fall Meeting 1992, Washington, DC, USA, p.106
- Dharmarajan, N. and Datta, S., "Toughening styrene maleic anhydride copolymers with functionalized ethylene propylene rubbers", *Polymer*, 33(18), 3848(1992)
- Dickie, B. D. and Koopmans, R. J., "Long-Chain Branching Determination in Irradiated Linear Low-Density Polyethylene", *J. Polym. Sci.: Part C: Polym. Lett.*, 28, 193(1990)
- Doi, Y. and Keii, T., "Synthesis of "Living" Polyolefins with Soluble Ziegler-Natta Catalysts and Application to Block Copolymerization", *Adv. Polym. Sci.*, 73/74, 201(1986)
- Donabedian, D. H., Gross, R. A. and McCarthy, S. P., "Pullulan Plasticization and Reactive Extrusion", *Abstracts of Papers of the American Chemical Society*, Vol. 204, August, pp.160, PMSE, 1992
- Drott, E. E. and Mendelson, R. A., "Determination of Polymer Branching with Gel-Permeation Chromatography. I. Theory", *J. Polym. Sci.*, Part A-2, 8, 1361(1970)

- Ellis, S. B., in *Deformation, Strain and Flow*, M. Reiner, Ed., Interscience, New York, 1960
- Folt, V. L., "The Effects of Mechanical Degradation on Rheological Properties of Elastomers", *Rubber Chem. Technol.*, 42, 1294(1969)
- Foreman, J. A., Klinger, K. A. and Wolkowicz, M., "Thermal analysis and rheology of modified polypropylenes", *American Laboratory*, January, 19(1996)
- Fujimoto, T., Narukawa, H. and Nagasawa, M., "Viscoelastic Properties of Comb-Shaped Polystyrenes", *Macromolecules*, 3,57(1970)
- Ganzeveld, K. J. and Janssen, L.P.B.M., "The Grafting of Maleic Anhydride on High Density Polyethylene in an Extruder", *Polym. Eng. Sci.*, 32(7), 467(1992)
- Ganzeveld, K. J. and Janssen, L.P.B.M., "Role of Mixing and Rheology in Reactive Extrusion", *Ind. Eng. Chem. Res.*, 33, 2398(1994)
- Gaylord, N. G., and Mishra, M. K., "Nondegradative Reaction of Maleic Anhydride and Molten Polypropylene in the Presence of Peroxide", *J. Polym. Sci.: Polym. Letters Ed.*, 21, 23(1983)
- Ghijssels, A. and Clippeleir, J. De, "Melt Strength Behaviour of Polypropylenes", *Intern. Polym. Proc.*, IX(3), 252(1994)
- Gohil, R. M. & Phillips, P. J., "Crystallinity in chemically crosslinked low density polyethylenes: 3. Morphology of the XLPE-2 system", *Polymer*, 27, 1687(1986)
- Graessley, W. W., "Effect of Long Branches on the Flow Properties of Polymers", *Accts. Chem. Res.*, 10, 332(1977)
- Grinsphun, V., Rudin, A., Russel, K. E., Scammell, M. V., "Long-Chain Branching Indices from Size-Exclusion Chromatography of Polyethylenes", *J. Polym. Sci., Polym. Lett. Ed.*, 24, 1171(1986)
- Guillet, J. E., Combs, R. L., Slonaker, D. F., Weemes, D. A. and Coover, Jr., H. W., "Effects of Molecular Weight Distribution and Branching on Rheological Parameters of Polyethylene Melts. Part I. Unfractionated Polymers", *J. Appl. Polym. Sci.*, 8,

757(1965)

- Hagberg, C. G. and Dickerson, J. L., "Innovative Products From Post Consumer Nylon Carpet Via Reactive Extrusion", *ANTEC '96*, p.288
- Hallden-Abberton, M. P., Bortnick, N. M., Cohen, L. A., Freed, W. T. and Fromuth, H. C., US Patent 4,727,117, Rohm and Haas (1988)
- Halldenabberton, M.P., "Reactive Extrusion Imidization of Acrylic Polymers", *Abstracts of Papers of the American Chemical Society*, Vol. 202, August, pp.179, PMSE, 1991
- Han, C. D. and Villamizar, C. A., "Effects of Molecular Weight Distribution and Long-Chain Branching on the Viscoelastic Properties of High- and Low-Density Polyethylene Melts", *J. Appl. Polym. Sci.*, 22, 1677(1978)
- Haney, M. A., Johnston, D. W. and Clampitt, B. H., "Investigation of Short-Chain Branches in Polyethylene by Pyrolysis-GCMS", *Macromolecules*, 16, 1775(1983)
- Harrell, E. R. and Nakajima, N., "Modified Cole-Cole Plot Based on Viscoelastic properties for Characterizing Molecular Architecture of Elastomers", *J. Appl. Polym. Sci.*, 29, 995(1984)
- Hert, M. and Strazielle, C., *Makromol. Chem.*, 184, 135(1983)
- Hert, M., "Tough thermoplastic polyesters by reactive extrusion with epoxy-containing copolymers", *Die Angewandte Makromolekulare Chemie*, 196, 89(1992)
- Hingmann, R. and Marczinke, B. L., "Shear and Elongational Flow Properties of Polypropylene Melts", *J. Rheol.*, 38(3), 573(1994)
- Hlouskova, Z., Tino, J. and Borsig, E., "Study of Crosslinked i-Polypropylene by Spin Probe Methods", *Polym. Commun.*, 25(4), 112(1984)
- Hornsby, P. R., Tung, J. F. and Tarverdi, K., "Characterization of Polyamide 6 Made by Reactive Extrusion. I. Synthesis and Characterization of the Properties", *J. Appl. Polym. Sci.*, 53, 891(1994a)
- Hornsby, P. R. and Tung, J. F., "Characterization of Polyamide 6 Made by Reactive

- Extrusion. II. Analysis of Microstructure", *J. Appl. Polym. Sci.*, 54, 899(1994b)
- Huang, Y. L. and Brown, N., "The Dependence of Butyl Branch Density on Slow Crack Growth in Polyethylene: Kinetics", *J. Polym. Sci., Part B: Polymer Physics*, 28, 2007(1990)
- Igarashi, S., Mita, I. and Kambe, H., "Thermogravimetric Analysis of the Effect of Ionizing Radiation on thermal Stability of Polyethylene", *J. Appl. Polym. Sci.*, 8, 1455(1964)
- Ishizuka, O. and Koyama, K., "Elongational Viscosity at a Constant Elongational strain Rate of Polypropylene Melt", *Polymer*, 21, 164(1980)
- Jacoby, P., Bersted, B. H., Kissel, W. J., and Smith, C. E., "Studies on the  $\beta$ -Crystalline Form of Isotactic Polypropylene", *J. Polym. Sci.: Part B: Polym. Phys.*, 24, 461(1986)
- Jellinek, H.H.G., *Aspects of Degradation and Stabilization of Polymers*, Elsevier Scientific Publishing Company, New York, 1978
- Jurkiewicz, A., Pislewski, N. and Kunert, K. A., "NMR Investigation of Segmental Mobility in Chemically Crosslinked Polypropylene", *J. Macromol. Sci.-Chem.*, A18(4), 511(1982)
- Kao, Y. H. and Phillips, P. J., "Crystallinity in chemically crosslinked low density polyethylenes: 1. Structural and fusion studies", *Polymer*, 27, 1669(1986)
- Karger-Kocsis, J., editor, "Polypropylene: Structure, blends and composites", published in 1995, Chapman & Hall, London
- Kim, K. J. and Kim, B. K., "Crosslinking of HDPE during Reactive Extrusion: Rheology, Thermal, and Mechanical Properties", *J. Appl. Polym. Sci.*, 48, 981(1993)
- Kim, B. K. and Kim, K. J., "Cross-Linking of Polypropylene by Peroxide and Multifunctional Monomer During reactive Extrusion", *Adv. Polym. Tech.*, 12(3), 263(1993)
- Kim, B. K. and Choi, C. H., "Reactive Extrusion of Polyolefin Ternary Blends", *J. Appl. Polym. Sci.*, 60, 2199(1996)

- Kimura, K., Katoh, T. and McCarthy, S. P., "Compatibilization of PET/EVOH Blends by Reactive Extrusion", *ANTEC '96*, p.2626
- Kopchik, R.M., U.S.P. 4,246,374, Rohm and Haas (1981)
- Kraus, G. and Gruver, J. T., "Rheological Properties of Multichain Polybutadienes", *J. Polym. Sci.*, A3, 105(1965)
- Kunert, K. A., Chodák, I., Ranachowski, J. and Pislewski, N., "Comparison of NMR investigation of chemically crosslinked polyethylene and polypropylene", *Polym. Bull.*, (Berlin), 3(8-9), 449(1980)
- Kunert, K. A., "Comparison of Static Mechanical Properties of Crosslinked Polypropylene and Polyethylene", *J. Polym. Sci., Polym. Lett. Ed.*, 19(10), 479(1981a)
- Kunert, K.A., Ranachowski, J., Chodák, I., Soszynska, H. and Pislewski, N., "Physico mechanical investigation of crosslinked polypropylene", *Polymer*, 22(12),1677(1981b)
- Kunert, K. A., "Comparison of Storage Moduli of Chemically Crosslinked Polyethylene and Polypropylene", *J. Polym. Sci., Polym. lett. ed.*, 20(1), 53(1982)
- Kunert, K. A., Jurkiewicz, A. and Pislewski, N., "The Investigation of Chemically Crosslinked Polypropylene by Spin-lattice Relaxation Time", *J. Polym. Sci., Polym. Chem. Ed.*,21(4), 1195(1983)
- Kye, H. and White, J. L., "Simulation of Reactive Extrusion: Polymerization of Caprolactam in a Modular Corotating Twin Screw Extruder", *ANTEC '96*, p.309
- La Mantia, F.P., Valenza, A., and Acierno, D., *Polym. Bull.*, 15, 381(1986)
- Lambra, M. and Seadan, M., "Interfacial Grafting and Cross-linking by Free Radical Reactions in Polymer Blends", *Polym. Eng. Sci.*, 32(22), 1687(November 1992)
- Lanfray, Y. and Marin, G., "The Effect of Molecular Weight Distribution on the Elongational Properties of Linear Polymers", *Rheol. Acta*, 29, 390(1990)
- Laun, H. M., "Orientation of macromolecules and elastic deformations in polymer melts.

- Influence of molecular structure on the reptation of molecules", *Progress in Colloid & Polymer Science*, 75, 111(1987)
- Laun, H. M. and Schuch, H., "Transient Elongational Viscosities and Drawability of Polymer Melts", *J. Rheol.*, 33(1), 119(1989)
- Lecacheux, D., Lesec, J., and Quivoron, C., "High-Temperature Coupling of High-Speed GPC with Continuous Viscometry. I. Long-Chain Branching in Polyethylene", *J. Appl. Polym. Sci.*, 27, 4867(1982)
- Lederer, K, Beytollahi-Amtmann, I., and Billiani, J., "Determination and Correction of Peak Broadening in Size Exclusion Chromatography of Controlled Rheology Polypropylene", *J. Appl. Polym. Sci.*, 54, 47(1994)
- Liang, Z. and Williams, H. L., "Dynamic Mechanical Properties of Polypropylene-Polyamide Blends: Effect of Compatibilization", *J. Appl. Polym. Sci.*, 44, 699(1992)
- Linster, J. J. and Meissner, J., "Melt elongation and structure of linear polyethylene (HDPE)", *Polymer Bulletin*, 16, 187(1986)
- Liu, N. C. and Baker, W. E., "Reactive Polymers for Blend Compatibilization". *Advan. Polym. Tech.*, 11(4), 249(1992a)
- Liu, T. M. and Baker, W. E., "The Effect of the Length of the Short Chain Branch on the Impact Properties of Linear Low Density Polyethylene", *Polym. Eng. Sci.*, 32(14). 944(1992b)
- Lovell, P.A., in *Comprehensive Polymer Science*, ed. by Allen, G., Pergamon Press, Oxford, 1989, Vol. 1, Chapter 9
- Lu, M., Collier, J. R., and Collier, B. J., "Reactive Extrusion of Polypropylene", *ANTEC '96*, p.277
- Maier, C. and Lambla, M., "Esterification in Reactive Extrusion", *Polym. Eng. Sci.*, 35(15), 1197(1995a)
- Maier, C. and Lambla, M., "Grafting Fast Blue BB onto Maleated EPR Using Reactive



- Extrusion", *Angewandte Makromolekulare Chemie*, Vol. 231, September, 145(1995b)
- Mavridis, H. and Shroff, R., "Appraisal of a Molecular Weight Distribution-to-Rheology Conversion Scheme for Linear Polyethylenes", *J. Appl. Polym. Sci.*, 49, 299(1993)
- Meira, B. H., *Modern Methods of Polymer Characterization*, ed. by Barth, H. G. and Mays, J. W., John Wiley and Sons, New York, 1991, Chapter 2
- Mark, J. E., Eisenberg, A., Graessley, W. W., Mandelkern, L., Samulski, E. T., Koenig, J. L. and Wignall, G. D., "Physical properties of Polymers", 2nd Ed., ACS, Washington DC, 1993
- Masuda, T., Nakagawa, Y., Ohta, Y. and Onogi, S., "Viscoelastic Properties of Concentrated Solutions of Randomly Branched Polystyrenes", *Polym. J.*, 3, 92(1972)
- Mead, D. W., "Evolution of the Molecular Weight Distribution and Linear Viscoelastic Rheological Properties During the Reactive Extrusion of Polypropylene", *J. Appl. Polym. Sci.*, 57, 151(1995)
- Meares, P., "Polymers: Structure and Bulk properties", D. Van Nostrand Company Ltd., London, 1965
- Mendelson, R. A., Bowles, W. A. and Finger, F. L., "Effect of Molecular Structure on Polyethylene Melt Rheology. I. Low-Shear Behaviour", *J. Polym. Sci., Part A2*, 8, 105(1970)
- Michaeli, W., Höcker, H., Berghaus, U. and Frings, W., "Reactive Extrusion of Styrene Polymers", *J. Appl. Polym. Sci.*, 48, 871(1993)
- Michaeli, W., Grefenstein, A., and Berghaus, U., "Twin-Screw Extruders for Reactive Extrusion", *Polym. Eng. Sci.*, 35(19), 1485(1995)
- Minoshima, W., White, J. L., Spruiell, J. E., "Experimental Investigation of the Influence of Molecular Weight Distribution on the Rheological Properties of Polypropylene melts", *Polym. Eng. Sci.*, 20, 1166(1980)
- Mirabella Jr., F. M. and Wild, L., *ACS Adv. Chem. Ser.*, 227, C.D. Craver, and T. Provder,

- eds., 23(1990)
- Münstedt, H. and Laun, H. M., "Elongational Properties and Molecular Structure of Polyethylene Melts", *Rheol. Acta*, 20(3), 211(1981)
- Nakajima, N., "Processability of Raw Elastomers and its Relation to Deformational and Failure Behaviour", *Polym. Eng. Sci.*, 19, 215(1979)
- Nakajima, N. and Harrell, E. R., "Effect of Extending Oil on Viscoelastic Behavior of Elastomers", *J. Rheol.*, 26, 427(1982)
- Nakanishi, K. and Solomon, P. H., "Infrared Absorption Spectroscopy", 2nd Edition, Holden-Day, Inc., 1977
- Nedkov, E., Stoyanov, A. and Kretev, V., "Morphology of Gamma-Irradiated Polypropylene gels Crystallized from Xylene Solution. 1. Optical Microscopy and sols", *Radiat. Phys. Chem.*, 37(2), 299(1991a)
- Nedkov, E., Stoyanov, A. and Kretev, V., "Morphology of Gamma-irradiated Polypropylene gels crystallized from Xylene Solution. 2. Kinetics of Melting and Crystallization", *Radiat. Phys. Chem.*, 37(2), 305(1991b)
- Newman, S. and Trementozzi, Q. A., "Barus Effect in Filled Polymer Melts", *J. Appl. Polym. Sci.*, 9, 3071(1965)
- Nicodemo, L., De Cindio, B., and Nicolais, L., "Elongational Viscosity of Microbead Suspensions", *Polym. Eng. Sci.*, 15, 679(1975)
- Nielsen, L. E., *Polymer Rheology*, Marcel Dekker, New York, 1977
- Nishio, T., Suzuki, Y., Kojima, K. and Kakugo, M., "Morphology of Maleic Anhydride Grafted Polypropylene and Polyamide Alloy Produced by Reactive Processing", *J. Polym. Eng.*, 10(1-3), 123(1991)
- Nojiri, A. and Sawasaki, T., "Radiation Cross-linking of Polypropylene", *Radiat. Phys. Chem.*, 26(3), 339-46(1985)
- Nordmeier, E., Lanver, U., and Lechner, M. D., "The Molecular Structure of Low-Density

- Polyethylene. 1. Long-Chain Branching and Solution properties", *Macromolecules*, 23, 1072(1990)
- Odian, G., Lamparella, D. and Canamare, J., "Radiation Effects in Polypropylene and Ethylene Propylene Copolymers", *J. Polym. Sci.: Part C*, 16, 3619(1968)
- Pabedinskas, A. and Cluett, W. R., "Controller Design and Performance Analysis for a Reactive Extrusion Process", *Polym. Eng. Sci.*, 34(7), 585(1994a)
- Pabedinskas, A., Cluett, W. R. and Balke, S. T., "Modelling of Polypropylene Degradation During Reactive Extrusion With Implications for Process Control", *Polym. Eng. Sci.*, 34(7), 598(1994b)
- Padwa, A. R., "Compatibilized Blends of Polyamide-6 and Polyethylene", *Polym. Eng. Sci.*, 32(22), 1703(1992)
- Pang, S. and Rudin, A., "Size-Exclusion Chromatographic Assessment of Long-Chain Branch Frequency in Polyethylenes", Chapter 17 in "Chromatography of Polymers", edited by Provder, T., ACS Symposium Series 521(1993)
- Phillips, P. J. and Kao, Y. H., "Crystallinity in Chemically Crosslinked Low Density Polyethylenes: 2. Crystallization Kinetics", *Polymer*, 27, 1679(1986)
- Polance, R. and Jayaraman, K., "Mixing in Reactive Extrusion of Low-Density Polyethylene Melts: Linear vs. Branched", *Polym. Eng. Sci.*, 35(19), 1535(1995)
- Porter, R. S., Knox, J. P., Johnson, J. F., "On the flow and Activation Energy of Branched Polyethylene Melts", *Trans. Soc. Rheol.*, 12:3, 409(1968)
- Rachapudy, H., Smith, G. G., Raju, V. R. and Graessley, W. W., "Properties of Amorphous and Crystallizable Hydrocarbon Polymers. III. Studies of the Hydrogenation of Polybutadiene", *J. Polym. Sci., Polym. Phys. Ed.*, 17, 1211(1979)
- Raju, V. R., Rachapudy, H., and Graessley, W. W., "Properties of Amorphous and Crystallizable Hydrocarbon Polymers. IV. Melt Rheology of Linear and Star-Branched Hydrogenated Polybutadiene", *J. Polym. Sci.: Polym. Phys. Edition*, 17,

1223(1979)

Ramsey, R., Hahnfeld, J., Pike, W., Welsh, G., Lewis, C., Zawisza, M., Quirk, R., and Carriere, C., "The Effects of Branching, Molecular Weight and Molecular Topology on the Uniaxial Elongational Viscoelastic Properties of Atactic Polystyrene", *ANTEC '96*, p. 1124

Reich, L. And Stivala, S. S, *Elements of Polymer Degradation*, McGraw-Hill Book Company, 1971, p.123

Robinson, A. E., U.S.P. 3, 294, 869(1966)

Rocheftort, W. E., Smith, G. C., Rachapudy, H., Raju, V. R. and Graessley, W. W., "Properties of Amorphous and Crystallizable Hydrocarbon Polymers. II. Rheology of Linear and Star-Branched Polybutadiene", *J. Polym. Sci., Polym. Phys. Ed.*, 17,1197(1979)

Romanini, D., Savadori, A., and Gianotti, G., "Long Chain Branching in Low Density Polyethylene: 2. Rheological Behaviour of the Polymers", *Polymer*, Vol.21, 1092(1980)

Rudin, A., Grinsphun, V., and O'Driscoll, D. F., *J. Liq. Chrom.*, 7, 1809(1984)

Rudin, A., "Molecular Weight Distributions of Olefin Polymers From High Temperature SEC", *IPR Polyolefin Symposium*, Institute for Polymer Research, University of Waterloo, Waterloo, Ontario, Canada, May 25-26, 1993

Sabia, R., "On the Characterization of Non-Newtonian Flow. III", *J. Appl. Polym. Sci.*, Vol.8, 1651(1964)

Salovey, R. and Dammont, F. R., "Irradiation of Polyethylene Oxide and Polypropylene", *J. Polym. Sci.: Part A*, 1, 2155(1963)

Scheve, B.J., Mayfield, J.W. and DeNicola, Jr.,A.J., U.S.P 4,916,198, Himont, 1990

Scheibelhoffer, A. S., Wimolkiasak, A. S., Leonard, B. L., and Chundury, D., *ANTEC '93*, p.629

- Schott, H. and Kaghan, W. S., "Viscous Flow of Molten Polyethylene Resins", *J. Appl. Polym. Sci.*, 5(14), 175(1961)
- Schröder, E., Müller, G. and Arndt, K., *Polymer Characterization*, Hanser Publishers, New York, 1989
- Shang, S. W., "The precise Determination of Polydispersity Index (PI) in Rheological Testing of Polypropylene", *Adv. Polym. Tech.*, 12(4), 389(1993)
- Shiono, T., Kurosawa, H., Soga, K., "Synthesis of carboxyl- and chloro-terminated poly(propylene)s using  $Zn(C_2H_5)_2$  as chain transfer reagent", *Makromol. Chem.*, 193, 2751(1992)
- Shiono, T., Kurosawa, H., Ishida, O. and Soga, K., "Synthesis of Polypropylene Functionalized with Secondary Amino Groups at the Chain Ends", *Macromolecules*, 26, 2085(1993)
- Showaib, E. A. and Moet, A., "Effect of Short Chain Branching on the Viscoelastic Behaviour during Fatigue Fracture of Medium Density Ethylene Copolymers", *Polym. Eng. Sci.*, 35(9),786(1995)
- Shroff, R. N., Cancio, L.V., and Shida, M., "Extensional Flow of Polymer melts", *Trans. Soc. Rheol.*, 21, 429(1977)
- Shroff, R. and Mavridis, H., "Polydispersity Measures from Rheological Data on Polymer Melts", *J. Appl. Polym. Sci.*,
- Song, Z. and Baker, W. E., "Chemical Reactions and Reactivity of Primary, Secondary, and Tertiary Diamines with Acid Functionalized Polymers", *J. Polym. Sci.: Part A, Polym. Chem.*, Vol.30, 1589(1992)
- Spielau, P., Kühnel, W., Klaar, K., Gaspar, B., Weiss, R., Ulb, H., Breitscheidel, H.-U, Klingberg, G., and Fenske, J., US 4,652,326, Dynamit Nobel (1987)
- Sun, Y., Hu, G. and Lambla, M., "Effect of Processing Parameters on the Compatibilization of Polypropylene and Poly(Butylene Terephthalate) Blends by One-Step Reactive

Extrusion", *ANTEC '96*, p.270

Sundararaj, U., Macosko, C. W., Nakayama, A. and Inoue, T., "Milligrams to Kilograms: An Evaluation of Mixers for Reactive Polymer Blending", *Polym. Sci. Eng.*, 35(1), 100(1995)

Suwanda, D., Lew, R. and Balke, S. T., "Reactive Extrusion of Polypropylene II: Degradation Kinetic Modelling", *J. Appl. Polym. Sci.*, 35, 1033(1988)

Suwanda, D., Ph.D. thesis, University of Toronto, 1992.

Suwanda, D. and Balke, S. T., "Combined Reactive Extrusion-Orientation of Polyethylene", *Polym. Eng. Sci.*, 33(8), 455(1993)

Takeda, Y., Keskkula, H. and Paul, D. R., "Effect of polyamide functionality on the morphology and toughness of blends with a functionalized block copolymer", *Polymer*, 33(15), 3173(1992)

Teh, J. W. and Rudin, A., "Compatibilization of a Polystyrene-Polyethylene Blends Through Reactive Processing in a Twin Screw Extruder", *Polym. Eng. Sci.*, 32(22), 1678(1992)

Thitiratsakul, R., M.A.Sc. thesis, University of Toronto (1991)

Thomas, D. P. and Hagan, R. S., "The Influence of Molecular Weight Distribution on Melt Viscosity, Melt Elasticity, Processing Behaviour and Properties of Polystyrene", *Polym. Eng. Sci.*, 9, 164(1969)

Thompson, M. R., Tzoganakis, C. and Rempel, G.L., "Terminal Functionalization via the Alder Ene Reaction", submitted to *Polymer*, 1996

Togo, S., Amagai, A., Kondo Y., and Yamada, T., EPA 268,486, Mitsubishi Gas Chemical (1988)

Todd, D.B., "Consider Reactive Extrusion", *Chemical Engineering Progress*, August, 72(1992)

Tung, L. H., "Melt Viscosity of Polyethylenes at Zero Shear", *J. Polym. Sci.*, 46, 409(1960)

- Turcsanyi, B., "Graft Modification of Polyethylene with N-Vinylimidazole by Reactive Extrusion and Compatibilization of Polyethylene Polypropylene Blends via Imidazole-Carboxyl Interactions", *J. Macromol. Sci. - Pure and Applied Chemistry*, Vol. A32, Iss. S3, 255(1995)
- Tzoganakis, C., Vlachopoulos, J. and Hamielec, A.E., "Production of Controlled-Rheology Polypropylene Resins by Peroxide Promoted Degradation During Extrusion", *Polym. Eng. Sci.*, 28(3), 170(1988a)
- Tzoganakis, C., Ph.D. thesis, University of McMaster, Canada, 1988b
- Usami, T. and Takayama, S., "Identification of Branches in Low-Density Polyethylenes by Fourier Transform Infrared Spectroscopy", *Polym. J.*, 16(10), 731(1984)
- Van Krevelen, D.W., *Properties of Polymers*, 3rd ed., Elsevier Science, Amsterdam, 1990
- Vermeesch, I. M., Groeninckx, G., and Coleman, M. M., "Poly(styrene-co-N-maleimide) Copolymers: Preparation by Reactive Extrusion, Molecular Characterizations by FTIR, and Use in Blends", *Macromolecules*, 26(24), 6643(1993)
- Vermeesch, I. and Groeninckx, G., "Chemical Modification of Poly(styrene-co-maleic anhydride) with Primary A-Alkylamines by Reactive Extrusion", *J. Appl. Polym. Sci.*, 53, 1365(1994)
- Vinogradov, G. V. and Malkin, A.Ya., *Rheology of Polymers*, published in Russian (1977), English translation, Mir Publishers (1980), p.119
- Wang, X.C., *Research Proposal for Ph.D Comprehensive Exam.*, April, 1994
- Wang, X. C., Tzoganakis, C., and Rempel, G. L., "Reactive extrusion of acrylic acid grafted polypropylene with hexadecylamine", *Polym. Eng. Sci.*, 34(23), 1750(1994)
- Wang, X. C., Tzoganakis, C., and Rempel, G. L., "Chemical Modification of Polypropylene with Peroxide/Pentaerythritol Triacrylate by Reactive Extrusion", *J. Appl. Polym. Sci.*, 61, 1395(1996)
- Watanabe, Y. And Hatakeyama, T., "Adhesive Property of Polypropylene Modified With

- Maleic Anhydride by Extrusion Molding", *J. Appl. Polym. Sci.*, 37, 1141(1989)
- Waters 150CV plus Gel Permeation Chromatography, "Viscometer Supplement", 1994a
- Waters 150CV plus Gel Permeation Chromatography, "GPC/V Software: Getting Started Guide", 1994b
- Wild, L., Ranganath, R. and Knobloch, D. C., "Influence of Long-Chain Branching on the Viscoelastic Properties of Low-Density Polyethylenes", *Polym. Eng. Sci.*, 16(12), 811(1976)
- Willis, J. M. and Favis, B. D., "Reactive Processing of Polystyrene-Co-maleic anhydride/Elastomer Blends: Processing-Morphology-Property Relationships", *Polym. Eng. Sci.*, 30(17), 1073(1990)
- Wong, B. and Baker, W. E., "Polypropylene Graft Modified With Glycidyl Methacrylate and Styrene", *ANTEC '96*, p.283
- Wooster, J. J., Parikh, D. R., Sehanobish, K. and Chum, S. P., "The Effects of SCBD and Morphology on the Fracture Toughness of LLDPE Resins", *Polym. Prepr.*, 30, 323(1989)
- Xanthos, M. and Dagli, S.S, "Compatibilization of Polymer Blends by Reactive Processing", *Polym. Eng. Sci.*, 31(13), 929(1991)
- Xanthos, M. (ed.), "Reactive Extrusion: Principles and Practice", Hanser, New York (1992)
- Xanthos, M., "Applications of On-Line Rheometry in Reactive Compounding", *Adv. Polym. Tech.*, 14(3), 207(1995)
- Yang, Z.G. and Lauke, B., "Investigations on the simulation of the Reactive Extrusion of Nylon 6", *J. Appl. Polym. Sci.*, 57, 679(1995)
- Yoo, H. J., "Use of Rheology in Polypropylene Resin Design", *ANTEC'93*, p.3037
- Yong, K. J., Carr, M. E., and Bagley, E. B., "Reactive Extrusion vs. Batch Preparation of Starch-g-Polyacrylonitrile", *J. Appl. Polym. Sci.*, 45, 1093(1992)
- Yoon, L. K., Choi, C. H., and Kim, B. K., "Reactive Extrusion of PP/Natural Rubber



- Blends", *J. Appl. Polym. Sci.*, 56, 239(1995)
- Yu, Y. and Choi, K., "Crystallization Behaviour of the Blends of PET and PBT by Extrusion", *ANTEC '96*, p.305
- Zeichner, G. R., and Patel, P. D., "A Comprehensive Evaluation of Polypropylene Melt Rheology", in Proc. 2nd World Congress Chem. Eng., October 4-9, Montreal. Quebec, Vol. 6 (1981), p.333
- Zimm, B. H. and Kilb, R. W., "Dynamics of Branched Polymer Molecules in Dilute Solution", *J. Polym. Sci.*, 37, 19(1959)
- Zimm, B. H. and Stockmayer, W. H., "The Dimensions of Chain Molecules Containing Branches and Rings", *J. Chem. Phys.*, 17(12), 1301(1949)